

THESE DE DOCTORAT DE

L'UNIVERSITE D'ANGERS
COMUE UNIVERSITE BRETAGNE LOIRE
et
L'UNIVERSITE DE NOTTINGHAM

ECOLE DOCTORALE N° 605
Biologie Santé
Spécialité : «*Science Pharmacologie*»

Par

« Milad POURBAGHI MASOULEH »

« Development of lipid nanocapsules for antiangiogenic treatment of glioblastoma and evaluation of their potential for nose-to-brain drug delivery »

Thèse présentée et soutenue à «Salle de Visioconférence- Institut de Biologie en Santé-CHU»,
le « 25/09/2018 »

Unité de recherche : CRCINA - GLIAD

Thèse N° : 120111

Rapporteurs avant soutenance : **Composition du Jury :**

Dr. Anne SAPIN-MINET
Maître de Conférences HDR, Université de Lorraine, France
Prof. Antony D'EMANUELE
Professor, De Montfort University, the United Kingdom

Dr. Anne SAPIN-MINET, Rapporteur
Maître de Conférences HDR, Université de Lorraine, France
Prof. Antony D'EMANUELE, Rapporteur
Professor, De Montfort University, the United Kingdom
Dr. Martin GARNETT,
Associate Professor, University of Nottingham, the United Kingdom
Prof. Frank BOURY, Examineurs
Professeur de l'Université, Université d'Angers, France
Prof. Philippe MENEI, Directeur de thèse
Professeur de l'Université - Praticien Hospitalier, Université d'Angers,
France
Dr. Snow STOLNIK, Co-directeur de thèse
Associate Professor, University of Nottingham, the United Kingdom

Invité(s) :

Dr. Anne CLAVREUL, Co-encadrant
Ingénieur Hospitalier, CHU d'Angers, France
Dr. Cynthia BOSQUILLON, Co-encadrant
Assistant Professor, University of Nottingham, the United Kingdom

2014-2018

Diplôme : Docteur

Discipline: Biomolécules, Pharmacologie, Thérapeutique

Specialty: Science Pharmacologie

Development of lipid nanocapsules for antiangiogenic treatment of glioblastoma and evaluation of their potential for nose-to-brain drug delivery

Milad POURBAGHI MASOULEH |

Rapporteurs: **Madame Anne SAPIN-MINET, Maître de Conférences HDR, Université de Lorraine, France**
Monsieur Antony D'EMANUELE, Professor, De Montfort University, the United Kingdom

Examineurs: **Monsieur Frank BOURY, Professeur de l'Université, Université d'Angers, France**
Monsieur Martin GARNETT, Associate Professor, University of Nottingham, the United Kingdom

Invité(s): **Madame Anne CLAVREUL, Ingénieur Hospitalier, CHU d'Angers, France, Co-encadrant**
Madame Cynthia BOSQUILLON, Assistant Professor, University of Nottingham, the United Kingdom, Co-encadrant

Directeur de Thèse: **Monsieur Philippe MENEI, Professeur de l'Université - Praticien Hospitalier, Université d'Angers, France**

Co-directeur de Thèse: **Madame Snow STOLNIK, Associate Professor, University of Nottingham, the United Kingdom**

**L'auteur du présent document
vous
autorise à le partager,
reproduire,
distribuer et communiquer selon
les conditions suivantes :**



- Vous devez le citer en l'attribuant de la manière indiquée par l'auteur (mais pas d'une manière qui suggérerait qu'il approuve votre utilisation de l'œuvre).
- Vous n'avez pas le droit d'utiliser ce document à des fins commerciales.
- Vous n'avez pas le droit de le modifier, de le transformer ou de l'adapter.

**Consulter la licence creative commons complète en français :
<http://creativecommons.org/licences/by-nc-nd/2.0/fr/>**

Ces conditions d'utilisation (attribution, pas d'utilisation commerciale, pas de modification) sont symbolisées par les icônes positionnées en pied de page.



RÉSUMÉ

Le glioblastome (GB), tumeur primitive du cerveau, la plus agressive, et la plus fréquente chez l'adulte, présente une prolifération vasculaire importante. Des agents thérapeutiques innovants ciblant à la fois l'angiogenèse et les cellules tumorales sont recherchés, ainsi que des systèmes pour augmenter leur délivrance dans la tumeur cérébrale. Un de ces agents est le sorafénib (SFN), un inhibiteur de tyrosine kinase. Sa mauvaise solubilité aqueuse et ses effets secondaires indésirables limitent son utilisation. Le premier objectif de cette thèse était d'encapsuler cet agent dans des nanocapsules lipidiques (NCL) pour contrer ces inconvénients. Nous avons développé des NCL avec une haute efficacité d'encapsulation du SFN qui inhibaient in vitro l'angiogenèse et la viabilité de la lignée de GB humain U87MG. La délivrance intratumorale de SFN-NCL chez des souris porteuses d'une tumeur intracérébrale U87MG induit une normalisation vasculaire tumorale précoce qui pourrait améliorer l'efficacité de la chimiothérapie et de la radiothérapie. Le second objectif était de définir si la délivrance intranasale de NCL pouvait constituer une voie non-invasive alternative. Nous avons étudié via le transfert d'énergie par résonance de type Förster, le devenir des NCL chargées d'un fluorochrome à travers des monocouches de cellules Calu-3, un modèle de l'épithélium nasal. L'utilisation de NCL augmente le passage du fluorochrome à travers les cellules Calu-3, mais les particules sont rapidement dégradées après leur capture. Ces données mettent en évidence que les NCL sont appropriées pour la délivrance locale du SFN mais doivent être modifiées pour une délivrance intranasale.

Mots-clés: Glioblastome; Systèmes de délivrance; Anti-angiogénique; Nanocapsule lipidique; Intranasal; Barrière épithéliale; FRET; Nanomédecine

ABSTRACT

Glioblastoma (GB), the most aggressive, and the most frequent primary tumor of the brain in adults, present a prominent vascular proliferation. Innovative therapeutic agents targeting both angiogenesis and tumor cells are urgently required, along with competent systems for their delivery to the brain tumor. One such agent is sorafenib (SFN), a tyrosine kinase inhibitor. However, poor aqueous solubility and undesirable side effects limit its clinical application. The first objective of this thesis was to encapsulate this drug inside lipid nanocapsules (LNCs) to overcome these drawbacks. We developed LNCs with a high SFN encapsulation efficiency (> 90%) that inhibited in vitro angiogenesis and the viability of the human U87MG GB cell line. Intratumoral delivery of SFN-LNCs in mice bearing intracerebral U87MG tumors induced early tumor vascular normalization which could be used to improve the efficacy of chemotherapy and radiotherapy in the treatment of GB. The second objective was to define whether intranasal delivery of LNCs could be an alternative non-invasive route. In this regard, we investigated through Förster resonance energy transfer, the fate of dye-loaded LNCs across Calu-3 cell monolayers, a model of the nasal mucosa. We showed that employment of LNCs dramatically increased the delivery of the dye across Calu-3 cell monolayer but they were rapidly degraded after their uptake. These data highlight that LNCs are suitable nanocarriers for the local delivery of SFN but must be redesigned for enhancing their nose-to brain delivery.

Keywords: Glioblastoma; Delivery systems; Anti-angiogenic; Lipid nanocapsules; Intranasal; Epithelial barrier; FRET; Nanomedicine

ENGAGEMENT DE NON PLAGIAT

Je, soussigné(e)
déclare être pleinement conscient(e) que le plagiat de documents ou d'une
partie d'un document publiée sur toutes formes de support, y compris l'internet,
constitue une violation des droits d'auteur ainsi qu'une fraude caractérisée.
En conséquence, je m'engage à citer toutes les sources que j'ai utilisées
pour écrire ce rapport ou mémoire.

signé par l'étudiant(e) le

**Cet engagement de non plagiat doit être signé et joint
à tous les rapports, dossiers, mémoires.**

Présidence de l'université
40 rue de rennes – BP 73532
49035 Angers cedex
Tél. 02 41 96 23 23 | Fax 02 41 96 23 00



Acknowledgements

It is with enormous pleasure and gratitude that I acknowledge the people who have helped me during my entire period of thesis work.

First and foremost, I would like to express my special appreciation and thanks to my thesis supervisors and directors Dr. Anne Clavreul and Prof. Philippe Menei from Université d'Angers (FR), and also Dr. Cynthia Bosquillon and Dr. Snow Stolnik from the University of Nottingham (UK).

I would like to thank especially Prof. Philippe Menei, my thesis director, for accepting me as a member of his team. It was a great pleasure and honor to work on this project under your supervision and learning a lot from your quintessential knowledge of glioblastoma.

I express my deepest gratitude to Dr. Anne Clavreul, my thesis co-director, for her immense support and guidance throughout this project. It was a pleasure working with you and grasping a valuable knowledge about “glioblastoma” from you during the entire period of my thesis. I would like to thank you for supporting my research and for allowing me to grow as a research scientist. Your advice on research as well as on my career has been priceless. During my experimentation whenever I made mistakes, you always encouraged me and were supportive. I am really grateful for that kind of encouragement and support which helped me to learn new things. I do adore your precision and persistence in science and I will always remember this attitude in my future career. Finally, I thank you for the great skills and knowledge I learnt from you. You are a great supervisor and I learnt to be organized and to conduct research in a more structured way. Your contribution towards my success today is highly acknowledged.

I would like to express my sincere gratitude to my thesis co-director Dr. Cynthia Bosquillon from the University of Nottingham (UK), for her continuous support of my Ph.D. study and related research, for her patience, motivation, and immense knowledge, for the stimulating discussions, deep insights and different perspectives she provided for the project.

It is hard to express how grateful I am to be supervised by Dr. Snow Stolnik. I thank Snow for being my thesis director and for believing in me and my abilities and

extending her support in every possible way. Without your scientific, financial and moral support, my project in Nottingham would not have progressed to the current level. I admire your scientific curiosity and our walk-in discussions. Your magnanimity, indeed, propelled me forward by leaps and bounds. To be honest, working under your supervision was an honor and a privilege to say the least. *"I can no other word make but thanks, and thanks, and ever thanks."*

I would like to sincerely thank Dr. Emilie Roger, my scientific advisor from Université d'Angers (FR), who greatly helped me in formulations. I learnt a lot from the fruitful collaboration with you. I am really happy for working with you and I always felt very positive during our conversations. I also would like to appreciate your support in completing our research paper.

I would like to express my gratitude to Dr. Giuseppe Mantovani from University of Nottingham (UK), for his scientific advices and supports during my research in Nottingham.

I also sincerely thank my thesis committee members Dr. Martin Garnett from the University of Nottingham (UK) and Dr. Emilie Allard-Vannier from Université de Tours (FR), for your brilliant comments and suggestions throughout my thesis committee meetings. I really developed myself in understanding thoroughly about the project and overcame major challenges in my research work

I deeply thank *NanoFar*, an Erasmus Mundus Joint Doctorate (EMJD) Program, for funding this project. I thank Prof. Frank Boury, for his hard-work, vision and efforts in creating this wonderful program that allows many students like me to follow our research dreams. I also thank *En avant la vie* organization for funding this project.

I thank Prof. Jean-Pierre Benoit, director of the MINT (Micro et Nanomédecines Biomimétiques, INSERM UMR-S1066), and Prof. Emmanuel Garcion, director of the CRCINA (Centre de Recherche en Cancérologie et Immunologie Nantes-Angers) for allowing me to perform this thesis project work in their laboratories.

I really thank Dr. Claudia Conte, for her generous help and scientific advices during my project in Nottingham. I learn a lot from you and hope we will collaborate more in the near future.

I deeply thank Nolwenn Lautram, Olivier Thomas and Jérôme Bejaud for their scientific and technical support during my project in Université d'Angers (FR).

My sincere gratitude to Masoud, Sahar, little Sophie, Jimmy and Barbara.

Last but not least:

Thank you Edward Milbank.

Thank you Saikrishna Kandalam.

Thank you Katya Sansone.

Thank you Masoud Pourhaghgouy.

Thank you Shubaash ANTHIYA.

Thanks to all my friends who generously supported me during this time.

To my mother, Nargess ...

To my father, Farhad ...

To Mojtaba, To Yalda ...

To my splendid, gorgeous, lovely niece, my topiloo, Rosa

Dedicated to my late aunt, Mary

Table of contents

General Introduction	1
1. Glioblastoma and angiogenesis	2
1.1. Background	2
1.1.1. Epidemiology	2
1.1.2. Histology and molecular biology	2
1.1.3. Clinical presentation and diagnosis	6
1.1.4. Treatment of glioblastoma	7
1.1.4.1. Conventional therapy	7
1.1.4.2. Novel strategies in treatment of glioblastoma	9
1.2. Angiogenesis in glioblastoma	11
1.2.1. Angiogenesis mechanisms	12
1.2.2. Antiangiogenic therapy	14
1.2.3. Sorafenib as an antiangiogenic drug	17
1.2.3.1. Sorafenib in treatment of glioblastoma	18
1.2.3.2. Nanosystems for delivery of sorafenib	21
2. Lipid nanocapsules for drug delivery	22
2.1. Lipid nanocapsule formulation	22
2.2. Physical characteristics of lipid nanocapsules	24
2.3. Therapeutic agent loading and functionalization	26
2.4. Application of lipid nanocapsules in the treatment of glioblastoma	27
3. Nose-to-brain drug delivery	33
3.1. Intranasal administration	34
3.1.1. Macroscopical anatomy of nasal cavity	35
3.1.1.1. Olfactory region	35
3.1.1.2. Respiratory region	36
3.1.1.3. Other pathways	37
3.1.2. In-depth overview of transport across epithelial cells in nasal cavity	37

3.1.2.1. Nasal Mucosa and Mucus	38
3.1.2.2. Paracellular transport between epithelial cells	38
3.1.2.3. Transcellular Transport across epithelial cells	39
3.1.2.4. Axons in olfactory region	39
3.2. In vitro models for nasal permeability studies	40
3.2.1. Artificial membranes	40
3.2.2. Nasal tissue	40
3.2.3. Primary cell cultures	41
3.2.4. Cell lines	42
3.3. Lipid-based nanoformulations for nose-to-brain drug delivery	43
Aims and Objectives	45
Chapter 1: Development and characterization of sorafenib-loaded lipid nanocapsules for the treatment of glioblastoma	48
Chapter 2: Lipid nanocapsule transport across Calu-3 based model of nasal epithelial barrier	72
General Discussion	115
Conclusions and Future Perspectives	128
References	131
Annexes	174

List of figures

Figure 1: Standard and prototypical histopathologic ...	3
Figure 2: Radiographic features of GB ...	7
Figure 3: Schematic representation of radiotherapy plus ...	8
Figure 4: Mostly important pathways for formation of ...	13
Figure 5: Vasculature in normal tissue and tumor tissue ...	14
Figure 6: Normalization of tumor vasculature ...	15
Figure 7: Chemical structure of SFN ...	17
Figure 8: Applied nanocarriers for delivery of SFN ...	22
Figure 9: Preparation of LNC formulation ...	24
Figure 10: Schematic representation of LNC ...	24
Figure 11: The feasibility zone obtained for formation ...	25
Figure 12: Fluorescent microscopy images ...	33
Figure 13: Cellular structure of the olfactory and respiratory mucosa ...	35
Figure 14: Detailed microscopic view of nanoparticles ...	38
Figure 15: The virtual passages of nose-to-brain delivery ...	121
Figure 16: Internalization of LNCs ...	125

List of tables

Table 1: GB molecular subclassifications	4
Table 2: Clinical trials of VEGF/VEGFR targeting	16
Table 3: GB treatment with SFN in clinical trials	20
Table 4: Influence of different factors	23
Table 5: Employment of LNC for the treatment of orthotopic GB model	27
Table 6: Quantity and percentage of SFN associated with the MSCs	125

Abbreviations

ACQ:	Aggregation-Caused Quenching
BBB:	Blood-Brain-Barrier
CED:	Convection-Enhanced Delivery
CNS:	Central Nervous System
CT:	Computed Tomography
DSPE:	1,2-distearoyl-sn-glycero-3-phosphoethanolamine
EGFR:	Epidermal Growth Factor Receptor
FDA:	Food and Drug Administration
FRET:	Förster Resonance Energy Transfer
GB:	Glioblastoma
GRAS:	Generally Recognized As Safe
HLB:	Hydrophilic-Lipophilic Balance
IDH:	Isocitrate Dehydrogenase
LNC:	Lipid Nanocapsule
MGMT:	O ⁶ -Methylguanine DNA Methyltransferase
MIAMI:	Marrow-Isolated Adult Multilineage Inducible
MPS:	Mononuclear Phagocyte System
MRI:	Magnetic Resonance Imaging
MSC:	Mesenchymal Stem Cell
NSC:	Neural Stem Cell
NTA:	Nanoparticle Tracking Analysis
PDI:	Polydispersity Index
PDT:	Photodynamic Therapy
PEG:	Polyethylene Glycol
PFS:	Progression-Free Survival
PFS-6:	Progression-Free Survival at 6 months
P-gp:	P-glycoprotein
PIT:	Phaseinversion Temperature
PS:	Photosensitizing
PTT:	Photothermal Therapy
SFN:	Sorafenib

STAT3: Signal Transducers, Activators Of Transcription Type 3
TAA: Tumorassociated Antigen
TfR: Transferrin Receptor
TKI: Tyrosine Kinase Inhibitor
TMZ: Temozolomide
TPB: Tetraphenyl Borate
WHO: World Health Organization

General Introduction

1. Glioblastoma and angiogenesis

1.1. Background

1.1.1. Epidemiology

Glioblastoma (GB) is the most common and aggressive primary malignant brain tumor in adults, with a poor prognosis [1,2]. It has been estimated that GB count for 12-15% of all brain tumors, and 60-75% of astrocytic tumors [3]. This type of tumor occurs in patients of all genders and races, even though it is more usual amongst Caucasians race. The average age at diagnosis of GB is 64 years of age, and it has shown a clear male predilection, being about 1.6 times more common in males than females [4]. In France, the incidence of this type of tumor is 4.96 cases/100,000 inhabitants/year [5]. In the UK, the reports show that the incidence of GB is 4.64 cases/100,000 inhabitants/year [6].

1.1.2. Histology and molecular biology

The most frequently utilized and widely used classification for malignant gliomas is primarily based on a consensus by the World Health Organization (WHO), which designated GB a WHO grade IV neoplasm. WHO grading was based on GB as a “cytologically malignant, mitotically active, necrosis-prone neoplasm normally related to fast pre- and postoperative disease evolution and deadly outcome [7].” Drawbacks with using the WHO schema consist of lack of ability to account for molecular subtypes, therapeutic responses, or size and region of lesion. In order to overcome these drawbacks numerous researchers, also clinicians supports a molecular evaluating framework which takes into account those evolving comprehension of the sub-atomic pathogenesis of GB.

On histology, gliomas exhibit a number of characteristic namely anaplasia, high levels of mitotic activity, cellular pleomorphism, nuclear atypia, and coagulation necrosis that accompanies microvascular proliferation [8]. Necrosis is the outcome of ischemia resulting from endothelial cell hyperplasia and hypertrophy. There is a hypercellularity present all over the tumor, with atypical mitotic figures, abnormal nuclei, and multinucleated cells. Generally alluded to is the idea of pseudopalisading necrosis, which comprises of tumor cells that seem to encompass centralized necrotic zones. The presence of both necrosis and endothelial proliferation is fundamental for the

histologic diagnosis to be complete, to separate glioblastoma from anaplastic astrocytoma (**Figure 1**).

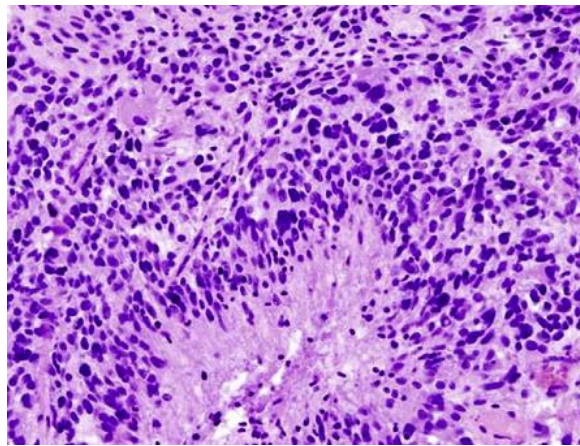


Figure 1: Standard and prototypical histopathologic hematoxylin and eosin stain of glioblastoma. Clearly observed are necrotic foci (pink) encompassed by a pseudopalisading necrosis.

These histologic observations have been being used for quite a long time, and stay imperative in the underlying characterization after biopsy or resection of a tumor. Lately, and importantly, Verhaak and partners [9], categorized a group of high-grade gliomas into four individual types as indicated by genetic and molecular hallmarks in light of genomic variations from the norm found in The Cancer Genome Atlas Network. The specialists utilized the factor analysis technique to incorporate information from GB and ordinary brain tests on three distinctive gene expression platforms. Consensus clustering and further validation at last yielded four subtypes that were named from their signature gene expression: proneural, neural, classic, and mesenchymal (**Table 1**).

Table 1: GB molecular subclassifications

Subtype	Features
Classic	<ul style="list-style-type: none"> - Chromosome 7 amplification - Chromosome 10 loss - EGFR amplifications - Lack of TP53, NF1, PGFRA, or IDH1 mutations - Expression of NES, Notch and Sonic hedgehog signaling pathways
Proneural	<ul style="list-style-type: none"> - PDGFRA alterations - IDH1 mutations - TP53 mutations - Expression of development genes (PDGFRA, NKX2-2, OLIG2, SOX, DCX, DLL3, ASCL1, TCF4) - Developmental disturbances
Neural	<ul style="list-style-type: none"> - Overexpression of neuronal markers (NEFL, GABRA1, SYT1, SLC12A5) - Neuron projection and axon and synaptic transmission disturbances
Mesenchymal	<ul style="list-style-type: none"> - NF1 deletions/mutations - PTEN mutation - Expression of mesenchymal markers (CHI3L1, MET) - Genes of tumor necrosis factor family and NF-kB pathways

Over the past decade, advances in molecular biology have had a significant impact on the diagnosis, classification and even therapeutic management of GB. In GB, several prognostic, diagnostic or predictive markers of tumor chemosensitivity have been identified through molecular biology. The most studied molecular markers, are the isocitrate dehydrogenase (IDH), the methylation of the promoter of O⁶-methylguanine-DNA methyltransferase (MGMT), the epidermal growth factor receptor (EGFR), the 1p/19q co-deletion and the p53.

The mutation of the **IDH** is the most recently identified marker in gliomas [10]. The IDH1 and 2 genes encode the IDH enzyme which participates in the decarboxylation of the isocitrate to α -ketoglutarate. The most frequent mutation in glial tumors is the R132H mutation on the IDH1 gene, which is present in more than 90% of cases and whose identification is feasible in immunohistochemistry using specific antibodies. In addition, the mutation of the IDH2 gene is not frequent.

Diagnostic value: Mutation of the IDH1 gene is present in more than 70% of diffuse gliomas and in only 5% of primary GB. The presence of this mutation is used in current practice to distinguish between secondary GB, developed from a low-grade glial lesion, and de novo GB. [10].

Prognostic value: A factor of prognosis, independent of the histological grade of the tumor [11].

The second marker identified in GB is an epigenetic marker: **methylation of the MGMT promoter** [12]. This epigenetic modification of the MGMT promoter causes a decrease in the production of this protein, which is a molecule that opposes the action of alkylating agents such as temozolomide (TMZ).

Prognostic value: A good prognostic marker of GB regardless of the received treatment [13–15]

Tumor chemosensitivity value: Methylation of the MGMT promoter and therefore the repression of the expression of this protein makes it possible to increase the chemosensitivity of the tumor to the alkylating agents conventionally used in the treatment of GB [16].

The **amplification of EGFR** is common in de novo GB. This amplification leads to structural alterations of the receptor that may have pro-oncogenic properties, such as the variant III of this receptor (EGFRvIII), which is a constitutively active form even in the absence of ligand [17]. The amplification of EGFR remains exceptional in oligodendroglial tumors. The amplification of EGFR, in particular variant VIII, is detectable in immunohistochemistry.

Prognostic value: EGFR amplification has a prognostic value in some patient populations [18].

1p/19q (short arm of chromosome 1 and long arm of chromosome 19) co-deletion is a chromosomal marker. This mutation is associated in 100% of cases with the mutation of the IDH1 gene and in 90% of cases with methylation of the MGMT promoters [19]. This marker is associated with an oligodendroglial histological phenotype and is therefore not found in tumors of the astrocytic line, of which the GB is a part, unless the GB has an oligoendroglial component. It is possible to evaluate the presence of a 1p/19q co-deletion by assaying the expression of internexin α , the overexpression of which is predictive of the presence of a co-deletion with a positive predictive value of 76%.

Diagnostic value: Identification of a 1p/19q co-deletion is a characteristic of the presence of an oligodendroglial contingent with GB [20].

Prognostic value: A good prognostic marker of GB regardless of the received treatment [21].

Tumor chemosensitivity value: Randomized controlled trials have demonstrated an increased therapeutic response in patients with this co-deletion [22].

The **p53 protein** is a transcription factor involved in the regulation of a number of cellular functions such as mitosis or apoptosis. This mutation is not predictive of the therapeutic response or a better prognosis in GB, unlike so-called infiltrating glial tumors of low grades, of which it is a factor of poor prognosis. This mutation is detectable in immunohistochemistry by observing an intranuclear accumulation of the p53 protein [23].

Diagnostic value: A marker of the tumors of the astrocyte line which GB is part of it [24]

Prognostic value: The frequency of p53 immuno-positivity is higher in high-grade patients than that in low-grade category. Immunohistochemical expression of this protein has an effective usefulness in predicting the prognosis in patients with glioma [25].

1.1.3. Clinical presentation and diagnosis

The symptoms and initial clinical presentation of a GB depends on its size and location. Because of the fact that GB can grow rapidly, the most common symptoms are usually caused by increased pressure in the brain [26]. Common presenting symptoms include, slowly progressive neurologic deficit (usually motor weakness), generalized symptoms of increased intracranial pressure (including headaches, nausea and vomiting, and cognitive impairment), seizures, hemiparesis, sensory loss, visual loss and aphasia.

The first step in diagnostic imaging may include a magnetic resonance imaging (MRI) or computed tomography (CT). In the case of MRI, GB enhances with gadolinium contrast and exhibit an irregularly shaped mass with a dense ring of enhancement and hypointense center of necrosis (**Figure 2**). Necrosis is considered as a hallmark feature of GB, and presence of necrosis is necessary for a brain tumor to be classified

as GB based on the WHO system [27]. Ventricular distortion or displacement, hemorrhage and vasogenic edema may also be present on diagnostic imaging [28,29]. In nearly 13% of the patients, GB may appear as multifocal (more than two lesions including leptomeningeal dissemination), distant (second lesion noncontiguous with primary lesion), diffuse disease [29,30].

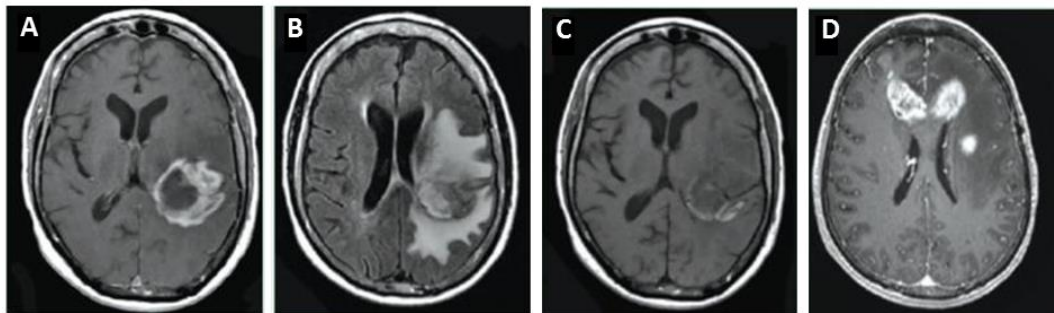


Figure 2: Radiographic features of GB obtained from MRI: (A) T1 post-gadolinium contrast with dense rim enhancement; (B) axial flair showing extensive vasogenic edema resulting mass effect on the left ventricle; (C) T1 pre-gadolinium exhibiting hemorrhage (white areas) along posterior lateral margin of tumor; (D) multifocal bihemispheric disease

1.1.4. Treatment of glioblastoma

1.1.4.1. Conventional therapy

GB has one of the poorest survival rates of any malignant brain tumor. Such poor survival rate contributes disproportionately to cancer mortality and morbidity. The first step in GB management is surgical excision of the brain lesion [26]. This excision makes it possible to make the histological diagnosis through the anatomo-pathological examination of the operative specimen, which is also the first step of the GB management. Currently, the complementary reference treatment after surgical resection of a GB is a protocol described by Stupp et al [16,31], combining adjuvant radiotherapy and TMZ (**Figure 3**). This protocol includes:

- *Primary phase:* Multiple sessions of 2 Gy each 5 days in a week for a period of 6 weeks to reach a total dose of 60 Gy along with a daily dose of TMZ administered orally at a dose of 75 mg/m²/day.
- *Treatment break:* a break in the treatment for a period of 4 weeks

- **Secondary phase:** Six cycles consisting of 150-200 mg/m²/day for 5 days during each 28-day cycle.

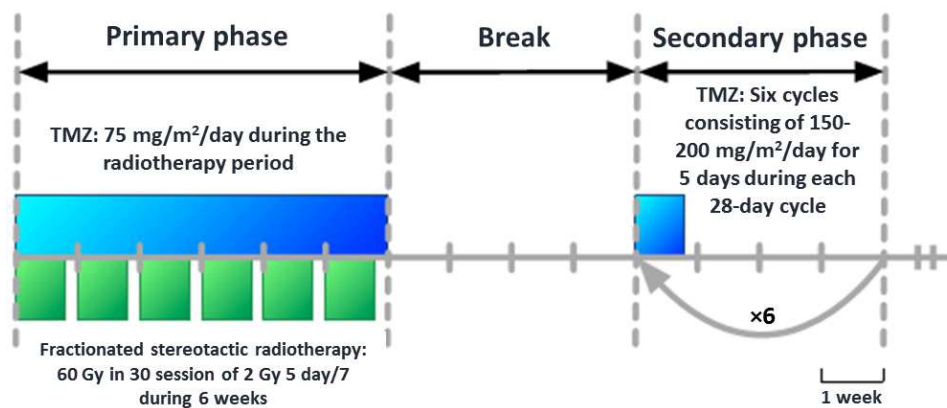


Figure 3: Schematic representation of radiotherapy plus concomitant and adjuvant TMZ for GB

As it is reported, median survival after diagnosis with GB is nearly 12 months, and this survival period raises to almost 14.6 months when patients are treated with the protocol validated by Stupp et al. [16,31].

Another therapeutic option in the management of GB is the employment of local therapies. Gliadel[®], comprised of carmustine implants placed within the surgical resection cavity, is the only local treatment of GB which is commercially available. Randomized controlled trials have demonstrated a significant increase in survival of carmustine implant-treated patients, showing an overall survival increase of 2.3 months [32,33]. It is reported that combination of Stupp protocol and carmustine implants can increase overall survival for 3.4 months [34]. This study also demonstrated that although the postoperative complication rate is higher with the use of carmustine implants, this has no negative impact on patient survival. Moreover, it is possible to employ antiangiogenic treatments, such as the most famous one which is bevacizumab (Avastin[®]), an antibody directed against vascular endothelial growth factor (VEGF). Bevacizumab was approved for the treatment of patients with recurrent GB in a number of countries, including the United States [35]. European authorities refused approval on the grounds of insufficient evidence for improved overall survival time [36]. Recently, it is shown that in patients with GB who received bevacizumab after the failure of standard care, including radiotherapy, TMZ and also lomustine, progression-free survival (PFS) time was 3.5 months, suggesting an increase in

comparison to the outcomes of standard therapy [37]. However the median overall survival was not increased [37], indicating that it is not efficacious enough.

In general, the results of conventional therapies are not satisfactory and the tumor typically recurs within a few months. This failure can be attributed to the reasons such as: a) inadequate drug delivery across the blood-brain-barrier (BBB); b) the infiltrative nature of GB; c) complicated vascular structure in GB; and, d) the presence of cancer cells resistant to radiotherapy and chemotherapy [7,38]. The latter reason could be as a result of unrestricted growth of resistant cell clones in proximity of the original tumor. Such phenomenon can be stimulated by the high rate of mutagenesis of malignant glial cells, which is augmented by both ionizing radiation and antineoplastic drugs. To overcome these failures, researchers and clinicians are consistently studying novel approaches for treatment of GB in order to enhance the median survival of the patients.

1.1.4.2. Novel strategies in treatment of glioblastoma

Phototherapy is one of the approaches in GB treatment which falls into two main categories: photodynamic therapy (PDT) and photothermal therapy (PTT). PDT as an effective, noninvasive and nontoxic therapeutic modality for cancer was developed over the last century. It is now becoming a more widely used medical tool, having gained regulatory approval for the treatment of various diseases such as cancer and macular degeneration [39,40]. It is a two-step technique in which the delivery of a photosensitizing (PS) drug is followed by irradiation with near-infrared light, infrared light, visible light, UV rays or even X-ray photons [41]. Therefore, activated photosensitizers transfer energy to molecular oxygen, which results in the generation of reactive oxygen species. As a result, this photodynamic pathway activates a cascade of activities, such as apoptotic and necrotic cell death in both the tumor and the neovasculature, leading to a permanent lesion and destruction of GB cells that remain in the healthy tissue. PDT may promote significant tumor regression and extend the lifetime of patients who experience glioma progression [42]. PTT is a treatment regimen involving the irradiation of cancer cells with electromagnetic radiation (VIS-NIR light) to cause thermal damage [43]. PTT in GB treatment remains controversial due to the fact that it is technically difficult to exert a lethal amount of heat to all cell populations within the GB tumor mass. In addition, the heterogeneous

response to different grades of hyperthermia may change the biological nature of the surviving tumor cells [44].

Immunotherapy is another highly regarded strategy for treatment of GB. Researchers believe that it is possible to design immunotherapeutic strategies that counteract GB through inducing, enhancing, or suppressing an immune response in this type of brain tumor. There are multiple immunotherapeutic approaches such as autologous inhibitors of immune checkpoint, cytokine therapy and immunotherapy with dendritic cells, viral therapy, stimulated lymphocytes and tumor or peptide based vaccines, which can be beneficial for treatment of GB. Despite of the advances in development of immunotherapeutic approaches for GB treatment, patient's selection, response monitoring and assessment of clinical outcomes or their possible side effects, are among the multiple problems that need to be solved [45]. In addition, promising preclinical results cannot be easily entered to clinic because of the low relevance of animal models to the human situation. Moreover, setting a maximum tolerable dose in many cases is very challenging. Furthermore, monitoring the immune responses to immunotherapy in animal model is another reported difficulty [26].

Another strategy for GB treatment is employment of nanocarriers for better delivery of the drugs to the tumor cells. In fact, even though many of the available therapeutic agents exhibited promising outcomes in vitro against GB, most were unsuccessful to reproduce such effects, when systemically administered in vivo. The main reason of the limited success is the incapability of the drugs to efficiently traverse the BBB and to penetrate inside the tumor tissue [46]. Over the last few decades, nanocarriers have attracted progressively increasing attention as brain tumor targeted drug delivery systems, because of their capacity to cross the BBB and specifically deliver the therapeutic agents in the tumor tissue. Various nanocarriers have been investigated and reported as potential brain tumor targeted delivery systems [47]. Nanoparticles could be made of different biocompatible materials with different sizes and shapes. It is possible to load the therapeutic agent on or inside them. Therefore, these nanocarriers have been employed to enhance the delivery of different clinically available therapeutic molecules, siRNA, DNA, etc. for pre-clinical research on treatment of GB [48]. Some of these nanocarriers such as gold nanoparticles, albumin-based nanoparticles and nanoliposome, have also entered to clinical trials and most of them are ongoing. Furthermore, the nanocarriers can be tailored to

simultaneously carry both drugs and imaging probes and designed to specifically target molecules of diseased tissues. These nanosystems are called nanotheranostics. Up to now, different nanotheranostics have been developed for benefiting GB treatment [49]. The inorganic nanoparticles could also be utilized not only for drug delivery, but also for diagnostic purposes or hyperthermia therapy. Hyperthermic treatment strategies utilize a magnetic medium such as thermoseeds and magnetic NPs to produce moderate heating in a particular area of the organ where the tumor is located. In addition, nanocarriers have already been employed to increase the GB targeting efficiency for the photosensitive drugs [42]. Overall, treatment of GB through recruitment of nanoparticles is an emerging topic which shows promising sign for their clinical practice in the near future.

Targeting the tumor vessels is another approach for fighting against malignant tumors which has shown promising results up to now. To the fact that vasculature in GB tumor plays an important role in its growth and progression, antiangiogenic therapy has become an important topic for researchers and clinicians.

1.2. Angiogenesis in glioblastoma

Microvascular proliferation is one of the eminent pathological characteristics of GB which distinguishes them from low-grade brain tumors. Hence, the high population of blood vessels in this type of glioma tumor is necessary for its growth and colonization in the brain [50]. The process of formation of new blood vessels from pre-existing blood vessels is termed as angiogenesis [51]. It is well proven that GB tumor growth and its invasion is highly dependent on new vessel formation [52]. In the WHO grading system, endothelial cell proliferation in glioma blood vessels is counted as a key feature of high grade gliomas [53]. The tumors need to be supplied with proper amount of blood in order to grow. Since the growing tumors reach a point at which the existing blood supply is no longer enough to support the necessities of the tumor, it results in a condition in which the tumor is deprived of adequate oxygen supply. This phenomenon is technically called hypoxia. As a result of the hypoxia that control crucial processes associated with tumor aggressiveness such as angiogenesis [54], GB tumor pass through an “angiogenic switch” and increase the release of assorted growth factors to induce the formation of new blood vessels [55]. Such vessel formation results in a complicated vascular structure. The importance of tumor

vasculature in GB growth and progression led to the development of the strategies which attack this vasculature through the agents which inhibit angiogenesis and this strategy is termed as “antiangiogenic therapy”.

1.2.1. Angiogenesis mechanisms

As it is previously described, because of the hypoxia occurrence, GB tumor forms a complicated blood vessel structure through release of specific growth factors. Of these factors, VEGF has a pivotal role in GB angiogenesis to advance tumor growth by interacting with different pathways [56], namely epidermal growth factor (EGF) [57,58], MAPK/ERK, PTEN/p13-kinase/Akt [59], nitric oxide [60], Notch-Delta like ligand 4 (DLL4) [61], tumor necrosis factor α (TNF- α) [62], basic fibroblast growth factor (bFGF) [63,64] and platelet-derived growth factor B (PDGF-B) [64]. The angiopoietins, Ang-1 and Ang-2, are of the other vascular growth factors which have a complex interaction with VEGF through their tyrosine kinase receptors (Tie1 and Tie2). Ang-2 promotes vessel sprouting while VEGF is secreted, but in the absence of VEGF, Ang-2 causes vessel regression [65]. The release of these vascular growth factors, especially in the tumors surrounding the necrotic core, suggests the most probable pathway for stimulating the formation of new blood vessels from pre-existing normal endothelial cells. The mentioned pathway includes both endothelial cell proliferation and enhanced vascular permeability (**Figure 4-B**). Such neovascularization also could be a result of the recruitment of bone marrow-derived endothelial progenitor cells or through mesenchymal or hematopoietic stem cells. Migration of these cells into the tumors through the systemic circulation results in new blood vessel formation (**Figure 4-C**) [66,67]. GB stem cells could also contribute to the formation of tumor blood vessels by differentiating into endothelial cells or pericytes (contractile cells that enclose the endothelial cells of small blood vessels) (**Figure 4-D**) [68–71]. These are the most important pathways that could result in a structurally and functionally abnormal vasculature in GB tumors [72].

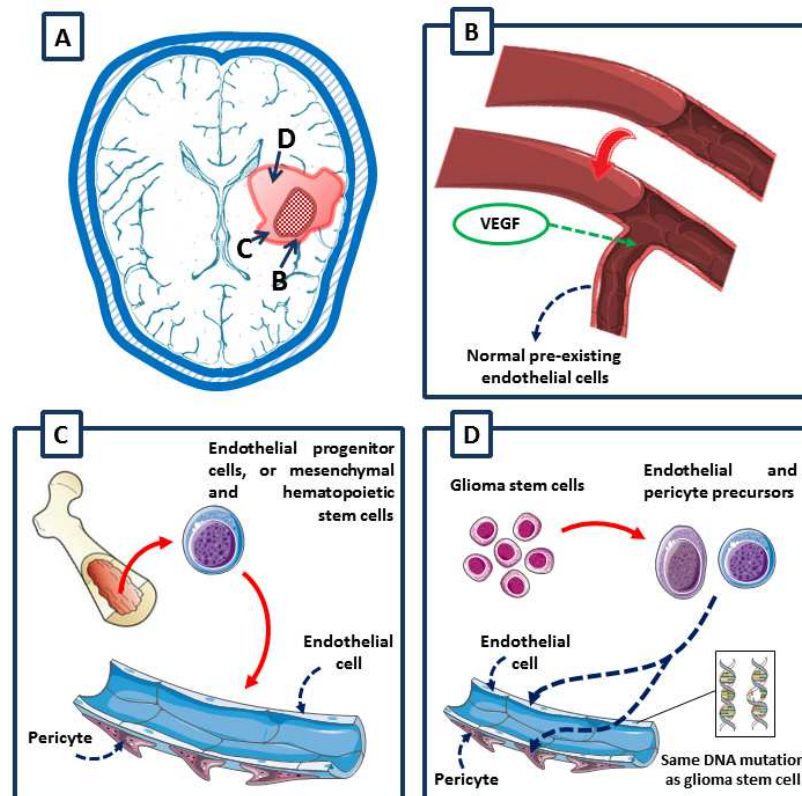


Figure 4. Mostly important pathways for formation of new blood vessels in GB tumor

The resulting vessels are leaky, heterogeneous, serpentine, irregular branching, dilated and saccular with haphazard pattern of interconnection (**Figure 5**). Notably, aberrant morphology in endothelial cells lining is evident. In addition, cells that provide support for the endothelial cells, pericytes, are loosely attached or absent, and the basement membrane is often abnormally thick, and sometimes entirely absent. As a consequence, a spatial and temporal heterogeneity originates in tumor blood flow. In brief, these abnormalities in the vasculature of the tumor cause an anomalous tumor environment in which acidosis, interstitial hypertension and hypoxia take place. Subsequently, paucity of blood supply and interstitial hypertension hamper the delivery of therapeutics in the tumor [73].

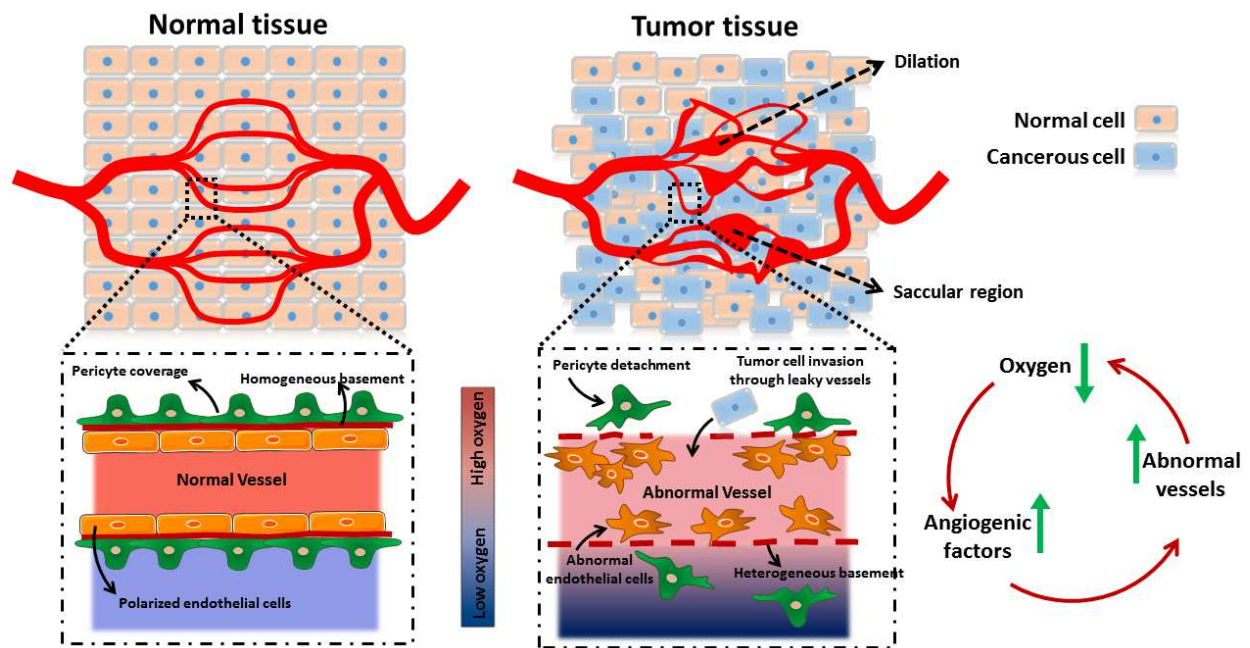


Figure 5. Vasculature in normal tissue and tumor tissue

1.2.2. Antiangiogenic therapy

A number of antiangiogenic agents such as endogenous inhibitors, antibodies, tyrosine kinase inhibitors (TKIs) have already been tested in GB experimental models. Basically, it is hypothesized that antiangiogenic agents result in antitumor effect via induction of apoptosis in endothelial cells, suppression of new blood vessel growth, elimination of small vessels, and reduction in tumor perfusion. These effects leads to a decrease in the supply of oxygen and nutrients necessary for the tumor and it is termed “tumor starvation” [52]. Nevertheless, in the early steps of the treatment, these agents temporarily normalizes the abnormal vasculature in the tumor through decreasing permeability and diameter of blood vessels which contradictorily increases tumor perfusion, diminishes interstitial pressure, and progresses tumor oxygenation [74–76]. Therefore, such condition facilitates sensitization for radiotherapy and leads to elevation of tumor exposure to cytotoxic drugs in chemotherapy (**Figure 6**) [76]. Moreover, it is possible that antiangiogenic therapy stops VEGF-mediated vascular regrowth resulting from exerted injuries in endothelial cells through cytotoxic therapies [77–79]. In addition, antiangiogenic agents may show inherent antitumor activity against GB stem-like cells located in the perivascular niche [80,81]. Furthermore, these agents have the potential to intervene in VEGF-mediated recruitment of tumor-infiltrating VEGFR1+ monocytes [82]. Additionally, antiangiogenic therapy could potentially play a role in raising host immunity through decreasing VEGF-mediated

immune suppression [83], and by that means, enhancing the efficiency of immunotherapy [84].

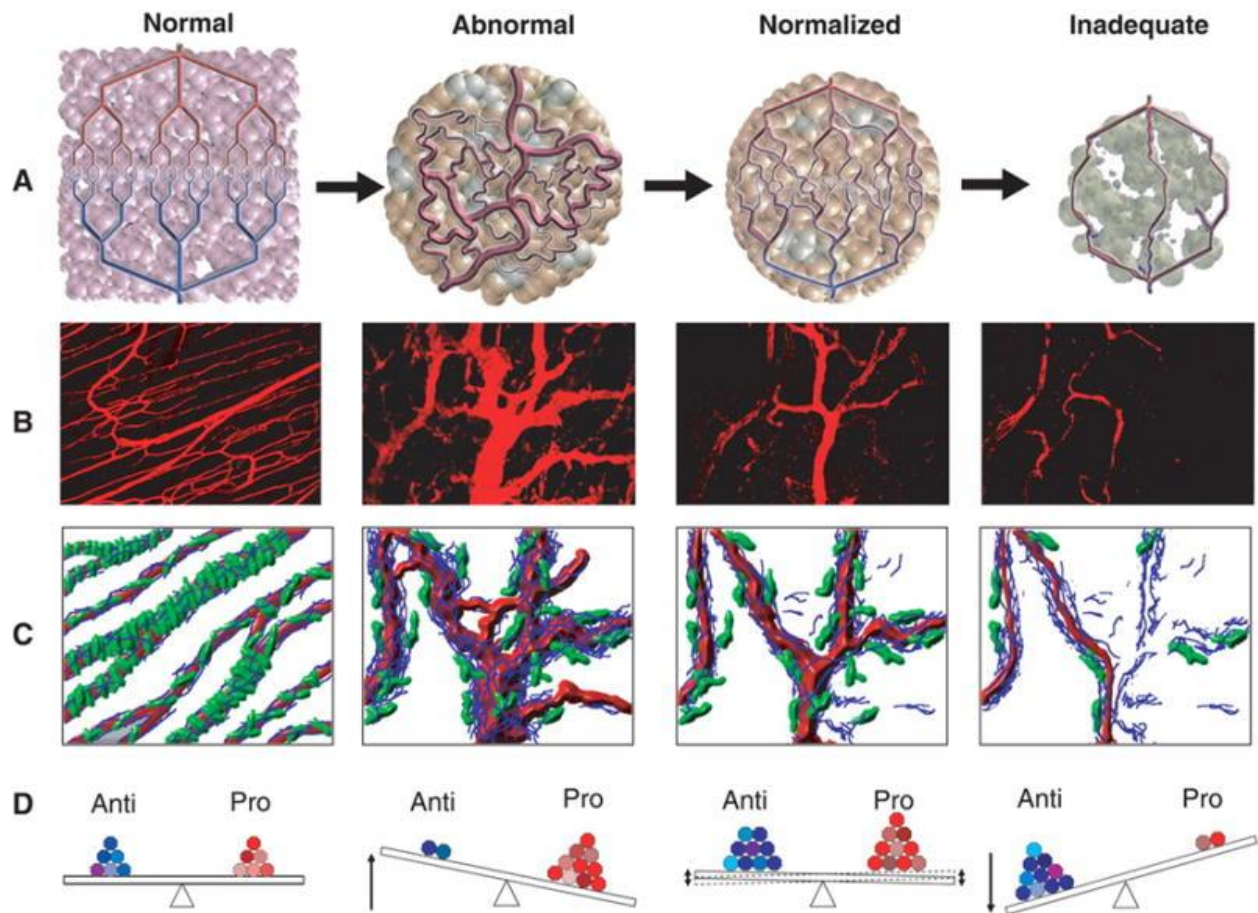


Figure 6: Normalization of tumor vasculature: **(A)** Tumor vasculature naturally has abnormal structure and function. Antiangiogenic therapy transiently reverses the abnormality in both function and tumor vessels. However, continuous antiangiogenic therapy may finally lead to a vasculature that is both inadequate for conveyance of therapeutics or oxygen and resistant to further treatment. **(B)** Patterns of vessel structures before, during and with sustained VEGFR2 blockade. **(C)** The concomitant alteration in basement membrane thickness (blue) and pericyte coverage (green) before, during and with sustained VEGFR2 blockade. **(D)** Alteration in the balance of antiangiogenic and pro-angiogenic factors resulting in the phenotypic changes.

Antiangiogenic agents tested in clinical trials as monotherapy for GB treatment are presented in **Table 2**.

Table 2: Clinical trials of VEGF/VEGFR targeting agents as a monotherapy in GB patients

Type	Agent	Mechanism	Dose	ORR (%)	PFS-6 (%)	OS (median, months)	Ref
Antibodies	Bevacizumab	Humanized anti-VEGF mAb	10mg/kg biweekly	28	43	9.3	[35]
	Aflibercept	Soluble decoy VEGFR	4 mg/kg biweekly	18	7.7	9.8	[85]
Small molecule inhibitors	Pazopanib	VEGFR TKI	800 mg daily	5.7	3	8.8	[86]
	Cediranib	VEGFR TKI	30 mg daily	15.3	16	8.0	[87]
	Nintedanib	VEGFR TKI	200 mg twice a day	0	4	8.1	[88]
	Sunitinib	VEGFR TKI	37.5 mg daily	10	10.4	9.4	[89]
	Vandetanib	VEGFR TKI	300 mg daily	12.5	6.5	6.3	[90]

Abbreviations: *kg*, kilogram; *mAb*, monoclonal antibody; *mg*, milligram; *ORR*, overall radiographic response; *OS*, overall survival; *PFS-6*, progression-free survival at six months; *TKI*, tyrosine kinase inhibitor; *VEGF*, vascular endothelial growth factor; *VEGFR*, vascular endothelial growth factor receptor

As described before, Bevacizumab (Avastin®) is the most commonly utilized antiangiogenic agent for treatment of patients with recurrent GB. It is a recombinant, humanized monoclonal antibody and its half-life is approximately 20 days. In this regard, it is administered every 2 weeks and sometimes every 3 weeks. Bevacizumab binds VEGF and prevents the interaction of VEGF with target receptors VEGFR-1 and VEGFR-2 on the surface of endothelial cells. Neutralizing the biological activity of VEGF reduces tumor angiogenesis, thereby inhibiting tumor growth and vasogenic brain edema [91]. Early studies with bevacizumab in recurrent GB demonstrated radiographic response rates of 28–40% and 6-month progression free survival (PFS-6) rates of 40–50% [92,93]. This compared favorably to previous studies in recurrent GB in which the median PFS-6 was reported as 15% [94]. Although the potential benefits of bevacizumab employment with an optimal dose, a proper schedule and also drug combination have been already better understood, data driven from phase III clinical trials of utilization of bevacizumab in treatment of patients with GB tumors, shows that some GB tumor could be naturally resistant to this therapy [95,96]. Such resistance could be partially attributed to intrinsic insensitivity of the vessels to VEGF inhibition in some GB tumors [97]. Moreover, an antibody like bevacizumab must be administered by intravenous infusion, and it is comprised of large molecular weight protein molecules with limited penetration of the intact BBB. In general, many resistance mechanisms could involve in prevention of antiangiogenic therapy. While the antiangiogenic agents begin inhibiting VEGF signaling, tumor and its

microenvironment secrete alternative pro-angiogenic growth factors to advance VEGF-independent angiogenesis (**Figure 4-D**)[98–100], which may further increase through recruitment of pro-angiogenic myeloid cells, e.g. M2-skewed macrophages, monocytes, granulocytes and myeloid-derived suppressor cells [82,101,102]. In addition, the pericytes which cover the functional vessels may protect endothelial cells against apoptosis induction. Lastly, adaptive resistance has been identified through a transition to a mesenchymal and more invasive tumor phenotype [103–105]. In order to counteract this resistance, TKIs such as sorafenib (SFN) are being explored because of their targeting for several growth factors pathways involved in GB growth and angiogenesis.

1.2.3. Sorafenib as an antiangiogenic drug

SFN (BAY 43-9006, Nexavar®), is a novel diaryl urea compound (a necessary pharmacophore/fragment in producing anticancer molecules to its nearly perfect binding with specific acceptors) which was developed in 1995 [106] and its molecular formula is $C_{21}H_{16}ClF_3N_4O_3$ (**Figure 7**). SFN is considered as an oral anticancer drug that is accepted by the U.S. Food and Drug Administration (FDA) for the purpose of treating unresectable or metastatic hepatocellular carcinoma, advanced renal cell carcinoma and locally metastatic or recurrent, differentiated and progressive thyroid carcinoma refractory to radioactive iodine regimen [107]. It is also being investigated in acute myeloid leukemia and many other solid tumors in children and adults.

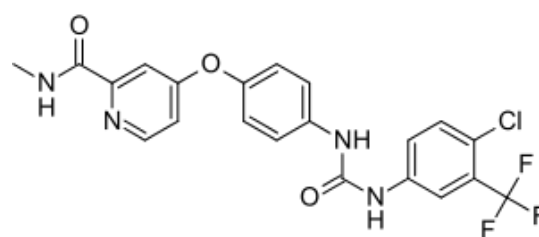


Figure 7: Chemical structure of SFN

SFN is considered as a multikinase inhibitor with inhibitory role on tyrosine kinase receptors including VEGFR-1, -2, -3, PDGFR- β , Flt-3, RET and c-Kit in addition to the RAF serine/threonine kinases (RAF-1, wild-type BRAF and oncogenic B-Raf [V600E]) and the RAS/RAF/MEK/ERK pathway [108]. In contrast, SFN is not active against a kinases like ERK-1, MEK-1, EGFR, HER-2/neu, IGFR-1, c-met, c-yes, PKB, PKA, CDK1/cyclin B, PKC α , PKC γ and PIM-1. In addition, SFN boosts apoptosis in

endothelial cells, pericytes and tumor cells [109,110]. Such suppression leads to a decrease in blood vessel area in the tumor and deprivation of nutrients in cancer cells [106,111]. SFN can also suppress Mcl-1 (myeloid cell leukemia 1) by a MAPK-independent mechanism, which increases the share of apoptosis intrinsic pathway in tumor cells [112,113]. Furthermore, previous studies have mentioned that eukaryotic translation initiation factor 4E (eIF4E) could be involved in SFN-dependent Mcl-1 inhibition [114]. Moreover, SFN improves TRAIL-induced cell death. Such cell death induction happens as a result of decrease in signal transducers, activators of transcription type 3 (STAT3) phosphorylation (Tyr705STAT3), associated proteins Mcl-1, cyclin D1, and survivin in hepatoma cells [115].

1.2.3.1. Sorafenib in treatment of glioblastoma

The activeness of STAT proteins, in particular STAT3, is often raised in a vast variety of solid tumors which is associated with their proliferation and maintenance [116,117]. Therefore, STAT3 has emerged as a favorable molecular target in particular types of solid tumors [118]. In different types of brain tumors, activated STAT3 is expressed. These tumors include both low-grade and high-grade gliomas [119]. It is demonstrated that inhibiting STAT3 signaling pathway results in suppression of proliferation and induction of apoptosis in GB [120,121]. Yang et al. [122], found that SFN leads to induction of apoptosis and inhibition of cell proliferation corresponding to the inhibition of STAT3 signaling in medulloblastomas, the most common type of pediatric malignant primary brain tumor [122]. Referring to these results, the same group found that SFN can also inhibit cell proliferation and induces apoptosis in two primary cell cultures and two established cell lines (U87, U251) of human GB [123]. They reported that SFN effects on GB through inhibition of STAT3 signaling, alongside with the down-regulation of cyclin D, cyclin E and Mcl-1 proteins. These findings suggest that SFN has the potential to be a promising candidate for treatment of GB due to not only attacking angiogenesis, but also targeting the GB cells. Furthermore, it is observed that SFN acts in a synergistic fashion with gamma-radiation to induce GB cell death via the apoptosis pathway. It is also reported that SFN can inhibit two important pathways in GB tumor-initiating cells, MAPK and PI3K/Akt, leading to the block of proliferation and, most of all, the induction of apoptosis via Mcl-1 inhibition [124]. In addition, Siegelin et al. [125], reported that systemic delivery of SFN in orthotopic GB

tumor model in mice was well tolerated, and significantly suppressed intracranial glioma growth via inhibition of cell proliferation, induction of apoptosis and autophagy, and reduction of angiogenesis. Importantly, systemic treatment with SFN was not associated with systemic or organ toxicity, and did not result in animal weight loss throughout treatment and median survival was significantly prolonged in SFN-treated animals in comparison to the control group.

In contrast to the sound preclinical rationale for use of SFN in GB treatment, this antiangiogenic factor does not function efficiently as a monotherapy in clinical trials or in combination with other chemotherapeutics (**Table 3**) [126,127]. These inefficiencies are the reasons that none of these trials has already entered to phase III. However, there are other investigations about applying SFN on metastatic kidney [66] and renal cell carcinoma [67] cancer which have entered phase III.

Table 3: GB treatment with SFN in clinical trials

Intervention or treatment	Phase	Conditions	Status	National Clinical Trials (NCT) Number	Ref
Sorafenib Everolimus	I/II	Brain Tumor Glioblastoma Anaplastic Glioma	Ongoing	NCT01434602	NP*
Sorafenib tosylate Valproic acid Sildenafil citrate	II	Glioblastoma Recurrent Adult Brain Neoplasm Malignant Glioma WHO Grade III Glioma	Ongoing	NCT01817751	NP*
Conventional surgery Sorafenib tosylate Temozolimus	I/II	Adult Giant Cell Glioblastoma Adult Glioblastoma Adult Gliosarcoma Recurrent Adult Brain Tumor	Completed (Apr. 2018)	NCT00329719	NP*
Sorafenib tosylate Erlotinib hydrochloride Tipifarnib Temozolimus	I/II	Adult Giant Cell Glioblastoma Adult Glioblastoma Adult Gliosarcoma Recurrent Adult Brain Tumor	Completed (Dec. 2016)	NCT00335764	NP*
Radiation Therapy Sorafenib Temozolomide	II	Glioblastoma Multiforme	Completed (Sep. 2016)	NCT00544817	[128]
Sorafenib tosylate Erlotinib hydrochloride	II	Adult Giant Cell Glioblastoma Adult Glioblastoma Adult Gliosarcoma Recurrent Adult Brain Tumor	Completed (Avril 2016)	NCT00445588	[129]
Sorafenib tosylate Bevacizumab	II	Brain and Central Nervous System Tumors	Completed (Feb. 2016)	NCT00621686	[130]
Radiation Therapy Sorafenib Temozolomide	I	Glioblastoma Gliosarcoma	Completed (Nov. 2015)	NCT00734526	NP*
Sorafenib	I	Glioblastoma Gliosarcoma Anaplastic Astrocytoma Anaplastic Oligoastrocytoma Anaplastic Oligodendroglioma	Completed (Nov. 2014)	NCT00884416	[131]
Sorafenib tosylate	I	Adult Anaplastic Astrocytoma Adult Anaplastic Oligodendroglioma Adult Giant Cell Glioblastoma Adult Gliosarcoma Recurrent Adult Brain Tumor	Completed (May 2014)	NCT00093613	NP*
Sorafenib Temozolomide	II	Recurrent Glioblastoma Multiforme	Completed (June 2013)	NCT00597493	[132]

NP*: Not published

The poor results obtained from clinical trials in GB may be due, in part, to the route of administration of the SFN. SFN is poorly soluble in water or buffered solution at different pH values (from pH 1.2 to pH 7.4), and in consequence, it is only clinically available in oral tablet formulations. Such oral administration may be efficient for peripheral tumors, such as hepatocellular carcinoma, renal cell carcinoma, and thyroid

cancer, but efficacy may be limited for brain tumors, for which SFN does not penetrate into the brain in sufficient amounts. High systemic doses of this drug are required to obtain effective brain-tumor concentrations but the potentially adverse events associated with the systemic distribution of SFN, such as hand-foot skin reactions, rash, upper and lower gastro-intestinal distress, fatigue, and hypertension often lead to SFN dose reductions or discontinuation [133]. In order to tackle the mentioned problems, novel approaches for efficacious delivery of SFN have been suggested, such as the use of nanosystems.

1.2.3.2 Nanosystems for delivery of sorafenib

The purpose of the use of nanotechnology in pharmacology is, firstly, to protect a therapeutic agent against potential degradation, and secondly to modify the natural distribution of this agent in the body. It is then theoretically possible to direct and accumulate the therapeutic agent at the desired site of action and away from unwanted sites to limit side effects. Nanoparticles have various applications in cancer treatment and more specifically they have been extensively studied in the field of oncology. Up to now, various types of nanoparticle with different shapes, size and surface modifications such as lipid and polymer based nanoparticles, inorganic nanoparticles, hybrid nanoparticles, liposomes and nanoemulsions have been employed for enhancing the delivery of SFN for treatment of different type of cancer models (gastric, breast and liver cancer) (**Figure 8**).

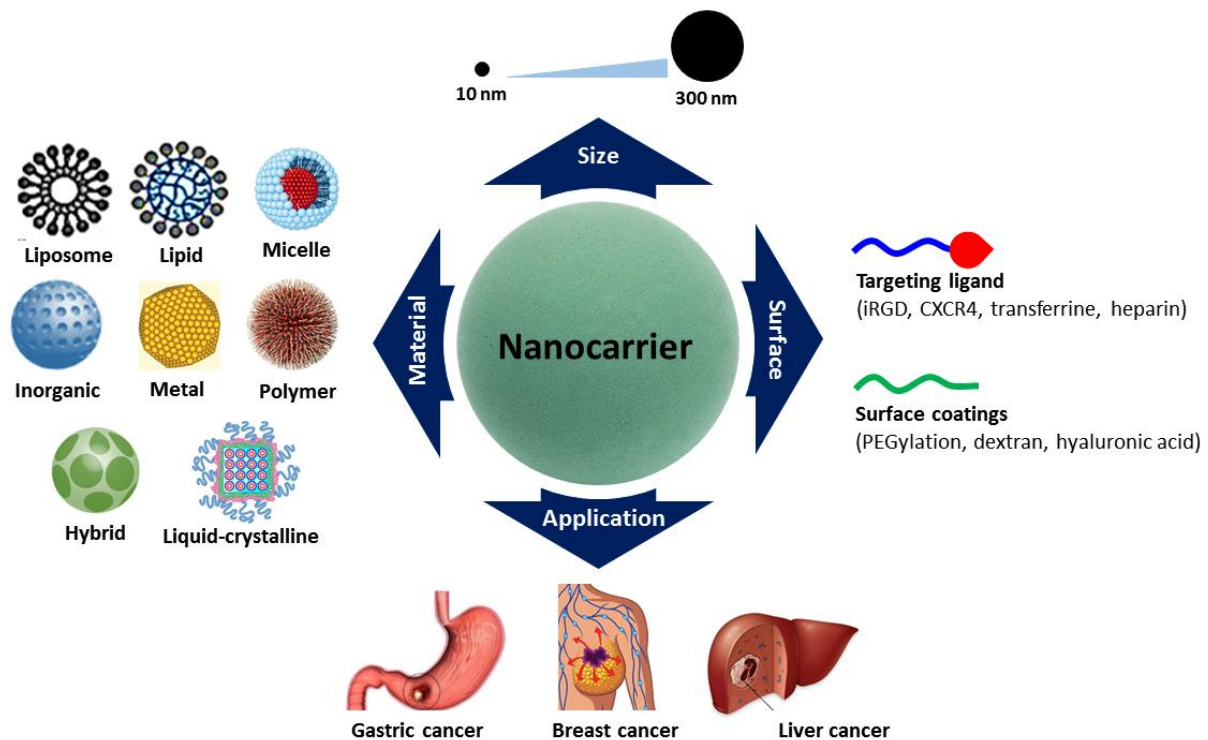


Figure 8: Applied nanocarriers for delivery of SFN

Up to now, the nanosystems developed for enhancing the delivery of SFN have not been employed for treatment of GB tumor. In the current thesis, we selected lipid nanocapsules (LNCs) to encapsulate SFN to their outstanding advantages such as production without using organic solvent and employment of generally recognized as safe (GRAS) excipients. These nanocapsules are highly stable and are generally capable of encapsulating higher amount of drugs in comparison to liposomes and solid lipid nanoparticles [134].

2. Lipid nanocapsules for drug delivery

2.1. Lipid nanocapsule formulation

LNCs are biomimetic lipid-based nanovectors with an approximate size range from 20 to 150 nm which were developed and patented for the first time by Heurtault et al. [135]. The main components of LNC are generally an oily phase, a nonionic surfactant and an aqueous phase. Based on classical LNC [135], the oily phase is triglycerides of capric and caprylic acids which is commercially available under the name of Labrafac™ lipophile WL 1349. Kolliphor® HS 15 is the hydrophilic surfactant which is a derivative of PEG (a mixture of free PEG 660 and PEG 660 hydroxystearate). The aqueous phase contains sodium chloride dissolved in MiliQ® water. Moreover, Lipoid®,

another surfactant, composed of 69% phosphatidylcholine soya bean lecithin, is included into LNC formulation, specifically for obtaining a size between 50 to 100 nm, to noticeably increase LNC stability [136,137]. Based on the applications or limitations, LNCs could also be prepared from other excipients through modification of the classical LNC formulation technique. For example, Transcutol® HP, widely employed in the development of emulsions or microemulsions [138–140] could be utilized as a co-surfactant in the formulation. Consequently, Labrafil® M1944 CS, a hydrophilic oil in which Transcutol® HP is soluble, should be selected and employed as oily phase. Since solubilization of Lipoïd® in Labrafil® M1944 CS is limited, Labrafac™ lipophile WL 1349 should also be added in order to overcome this obstacle [141]. In another example, Labrafac™ lipophile WL 1349 is replaced by glyceryl tricaprilate and formulated as previously described [142]. Interestingly enough, all the utilized components have FDA approvals for oral, topical and parenteral administrations. Each precursor brings an advantageous effect on the final structure of the LNC and its stability which is summarized in **Table 4**.

Table 4: Influence of different factors on the formulation and stability of LNC

Factor	Influence	References
Amount of nonionic surfactant	LNC formulation and stability	[143–145]
Lipophile surfactant	LNC shell rigidity – Freeze drying of the formulation	[137, 146]
Oil proportions	Increasing or decreasing the size	[145]
NaCl	Decreasing phase-inversion temperature (PIT)	[147, 148]
Number of temperature cycles	In favor of LNC formulation – Enhancing the quality of LNC and its homogeneity	[144, 149]

Based on the above mentioned procedure in the patent [135], the LNC formulation process comprises two important steps. The first step is to mix all the components (proportions may vary based on the desired formulation) under magnetic agitation and heating from room temperature to a higher temperature (T_2), beyond the phase-inversion temperature (PIT), to obtain a water in oil (w/o) emulsion. This step is further continued by cooling to a lower temperature (T_1), below the PIT, which forms an oil-in-water (o/w) emulsion. Subsequently, multiple temperature cycles crossing the phase-inversion zone between T_2 and T_1 are applied. The second step is a final quench exerted to the system by abrupt addition of cold water to the mixture at the temperature that hydrophilic-lipophilic balance (HLB) occurs in the nonionic surfactant (**Figure 9**). By addition of cold water to the system, the microemulsion system disentangles in the phase-inversion zone which leads to the formation of stable

nanocapsules. Incidentally, the cyclic heat is normally exerted to the system between 60 to 90 °C at a rate of 4 °C/min [141,148].

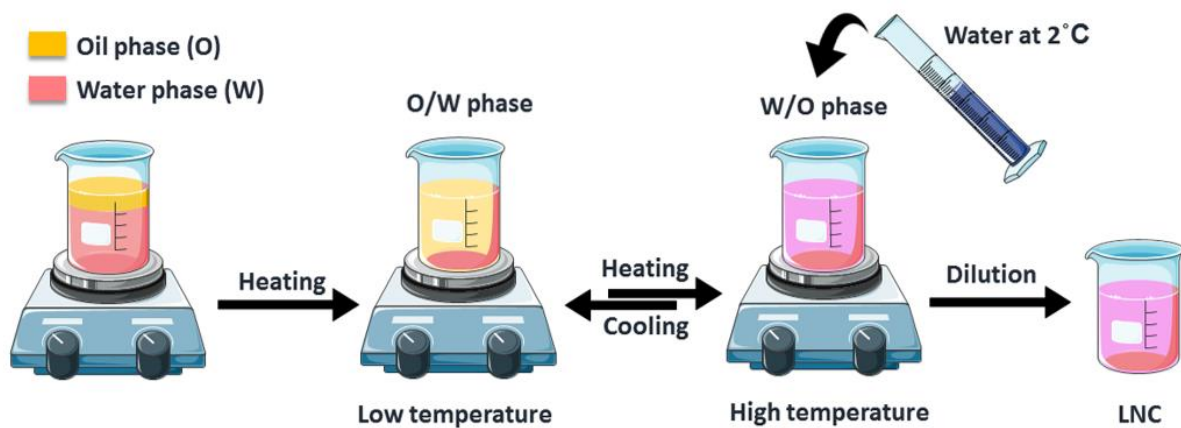


Figure 9: Preparation of LNC formulation based on the phase inversion technique

This process results in production of LNCs with an oily core which is surrounded by a tensioactive and cohesive shell. The shell is a mixture of Lipoid® anchored in the oily phase along with a Kolliphor® decoration which is oriented towards the aqueous phase (**Figure 10-A**) [150]. Although no schematic representation of LNCs incorporating a co-surfactant has been proposed up to now, **Figure 10-B** could illustrates the structure of this kind of LNCs.

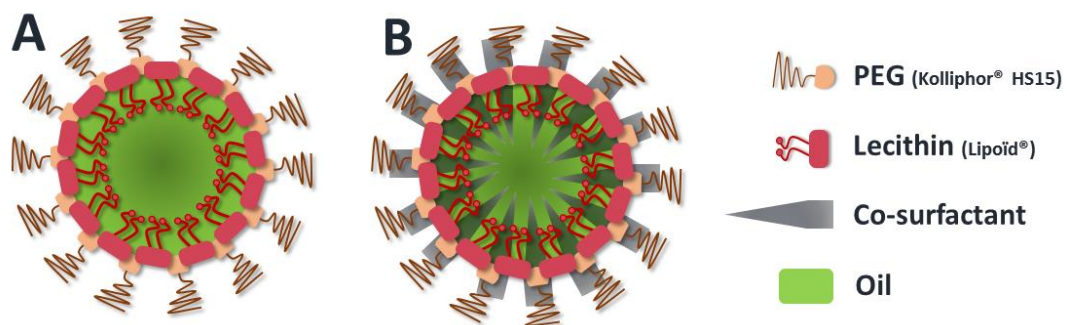


Figure 10: Schematic representation of LNC: (A) Classical LNC, (B) LNC prepared with co-surfactant

2.2. Physical characteristics of lipid nanocapsules

The proportion of components applied in the formulation of LNCs plays a vital role in their particle size and dispersity. The ternary diagram established for classical LNC by Heurtault et al. [145,148], could further elaborate this relation (**Figure 11**). In brief, this diagram is used for optimizing the component proportions. If the proportions of sodium chloride in water and Lipoid® are fixed at 1.75% and 1.5%, a feasibility domain is determined as a parallelogram. This domain in the ternary diagram is approximately

located between 10 to 40% of hydrophilic surfactant, 10 to 25% of oil and 35 to 80% of water. Following the mentioned proportions, if the nanocapsules are formed, their average volume size is in the range of 20 to 150 nm with polydispersity index (PDI) <0.2 which indicates a noticeably narrow dispersion of these nano-objects. Considering the feasibility domain, the size of LNC is greatly under the influence of the percentage of hydrophilic surfactant, Kolliphor®. If this percentage increases, a substantial reduction in average particle size occurs and this is referred to the interaction between triglyceride and water at their surfaces [143]. In contrast, by adding a greater proportion of oil, particle size would increase. In addition, the proportion of water brings no change to the particle size.

It is reported that LNC formation is highly dependent on the heating cycles applied during the preparation process. By increasing the number of cycles, the obtained LNC is more favorable in terms of size and dispersion. Altogether, when the amount of added surfactant decreases, the required number of temperature cycle to stabilize the LNC dispersion increases [144]. Moreover, if the proportions are determined based on the feasibility zone, increasing the number of temperature cycle appears to be unhelpful for enhancing the size and polydispersity of the LNC.

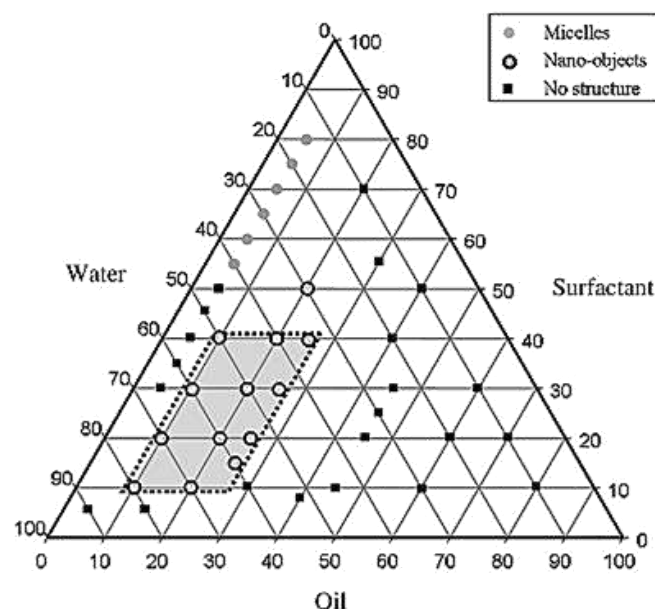


Figure 11: The feasibility zone obtained for formation of classical LNC

Zeta potential is the potential difference existing between the surface of a solid particle immersed in a conducting liquid (e.g. water) and the bulk of the liquid. This is an important factor in LNC stability. LNCs normally have a negative surface charge

resulting from the presence of phospholipid molecules [151] and contribution of PEG dipoles on their membrane [137].

2.3. Therapeutic agent loading and functionalization

Benefiting the advantages of LNCs, there is a great opportunity to encapsulate different kinds of therapeutic agents inside these nanocapsules. Up to now, LNCs showed capability of efficaciously encapsulating hydrophobic drugs such as docetaxel [152], paclitaxel [142], etoposide [153], ferrociphenol [154] or SN38 [141] which provides a pharmacological solution for intravenous or oral administration of therapeutic substances. These nanocapsules are also capable for loading hydrophilic drugs such as fondaparinux¹⁸, doxorubicin hydrochloride, erlotinib hydrochloride, DNA or siRNA through integrating the water-soluble molecule either into lipoplexes in LNCs or through formation of reverse micelle-loaded nanocapsules [155–161]. Up to now, many therapeutic cargoes have been efficiently encapsulated inside LNCs with noticeable encapsulation rates over 90% [134], whereas the encapsulation rate for liposomes is generally about 50% [162]. Incorporation of cargoes to LNCs is performed in two ways, either through encapsulating the hydrophobic drug inside the nanocapsules during the preparation of the LNC formulation or through modifying the shell of the LNCs via a post-insertion technique.

Not only could LNCs be a better option than liposomes in terms of drug encapsulation capacity, but they also outclass liposomes in terms of physical stability. In addition, their remarkably sustained release of the payload is another feature which stands out. For instance, Roger et al. [141] encapsulated SN38 inside LNCs with a size of about 50 nm and they reported that only 7% of SN38 was released after 5 days of in vitro drug release study, while the cumulative release of the same drug from PEGylated nanoliposomes with a size of about 150 nm in the same conditions was reportedly more than 40% [163]. Such feature could be of interest for development of drug delivery systems for different purposes.

Drugs in the form of colloids are susceptible to rapid removal from the blood circulation by the mononuclear phagocyte system (MPS), more specifically through Kuffer cells in liver and macrophage in bone marrow or spleen due to the fact that colloidal particles are considered as foreign bodies [164]. In this regard, the surface of nanoparticles could be decorated with PEG and its derivatives which have been

proven to decrease the opsonization and prolong their half-life while being circulated in the blood [165,166]. Hence, the presence of PEG on the shell of the LNCs at high density raises the half-life of the colloidal system in the bloodstream. In addition, such dense layer of PEG improves passive targeting [167]. While passive targeting is related to half-life of the colloidal system and MPS, active targeting relies on an antibody-based, aptamer-based or ligand-based targeting agent for targeting pathological sites or traversing the biological barriers following a molecular recognition process [168]. The rigidity of the shell in LNCs facilitate their surface modification by a targeting agent [169] or their improvement for a better passive targeting though post-insertion technique [152].

2.4. Application of LNCs in the treatment of glioblastoma

Many studies have been done to investigate the possibility of applying LNCs for a sustained local release of biologically active substances for the treatment of GB. In this regard, various therapeutic cargos have been loaded inside LNCs and they have been tested on heterotopic or orthotopic GB models through different administration routes (**Table 5**).

Table 5: Employment of LNC for the treatment of orthotopic GB model

Encapsulated cargo	Targeting approach	Studied animal	Cell line	Administration route	Findings	Ref
<i>Ferrociphenol</i>	+ER	Fischer rats	9L	CED	Synergistic effect between chemoradiotherapy and external radiotherapy: longer survival times (60%), including 10,5% of long-term survivors (up to 100 days), a statistically substantial raise comparing with groups treated with either of them separately	[170]
	DSPE-mPEG ₂₀₀₀	Fischer rats	9L	IV	Improvement in median survival time compared with the control group (28 vs. 25 days)	[171]

MIAMI cells	Nude mice	U87MG	IC	Improvement in median survival time compared with the control group treated without MIAMI cells (29 vs. 26.5 days)	[172]
DSPE-mPEG ₂₀₀₀	Fischer rats	9L	CED	Surface-functionalized LNC was not capable to increase the median survival time (24 days). The reason was linked to the PEG coating on the LNC which hinders uptake.	[173]
DSPE-mPEG ₂₀₀₀ +HBD	Fischer rats	9L	IC	Hyperosmolar coated-LNC r median survival time of 20% (30 days) compared with both untreated and uncoated-LNC treated groups. Such hyperosmolarity results in shrinkage of endothelial cells and could disrupt the BBB through tight junctions opening.	[173]
NFL	Fischer rats	9L	CED	Decreased median survival time (11 days) in comparison with the untreated group (25 days). Such toxicity had not been previously noticed in the case of untargeted Fc-diOH-loaded LNC (135).	[174]
OX26	Fischer rats	9L	CED	A reduction in median survival time (22 days) compared with the control group (25 days). Such toxicity had not been previously noticed in the case of untargeted Fc-diOH-loaded LNC (135).	[174]
DSPE-mPEG ₂₀₀₀ +OX26	Fischer rats	9L	IC	No significant difference in median survival times in comparison with control group (25 days) (Possibilities: (A) The applied dose was under pharmacological threshold. (B) Limited active targeting which could be because of low antibody coupling on the surface of LNC.	[174]
NFL	Fischer rats	9L	IC	Median survival times significantly increased (44 days)	[174]

Pacitaxel	+ER	Fischer rats	9L	CED	A two-fold increase in median survival time and 10% of long-term survivors (over 106 days) compared with the untreated group. Although, no statistically significant difference with radiotherapy alone suggests dose optimization and/or targeting moiety grafting as a proper approach to further increase the median survival time. [175]
Lauryl-gemcitabine	-	Nude-NMRI mice	U87MG	IT	- LNC in form of injectable hydrogel - Median survival time for the mice treated through IT injection was reportedly 49 days while for the mice treated with drug solution through IV injection was 36 days. Median survival time for the mice without treatment was 24 days. [176]
	-	Nude-NMRI mice	U87MG	A	- LNC in form of injectable hydrogel - Median survival time for the mice treated injection inside the cavity after tumor resection was reportedly 62 days while the mice without treatment was 35.5 days. [176]
Methotrexate	-	Wistar rats	C6	IP	MTX treatment raised CD73 enzyme expression and AMP hydrolysis, resulting in elevation of adenosine production and immunosuppressive capability [177]
¹⁸⁸ Re	CXCR4 Antibody	Scid mice	CXCR4-positive U87MG	CED	In control groups, the median survival time was near to 36 days for both saline solution and blank LNCs, approximately 39 days for CXCR4 antibody-LNCs. Treating the animals with 12G5-LNC ¹⁸⁸ Re resulted in a 50% increase in median survival time compared to the groups treated with CXCR4 antibody-LNCs. Two animals survived more than 100 days. [178]

-	Nude-NMRI mice	Lab1 GB cells*	CED	- Complete distribution all over the tumor and peritumoral region without leakage into the contralateral hemisphere - Median survival time for the treated mice was 56 days while for the untreated mice was 21 days.	[179]
-	Fischer rats	9L	CED	In comparison with control group, 80% increase in median survival time (up to 45 days), and 33% long-term survivors (over 100 days).	[180]
-	Fischer rats	9L	CED and/or SI	SI and CED combination strongly increased median survival time (up to 257%), with an unprecedented rate of long-term survivors, i.e., over 120 days (17 of 24), as a result of tumor eradication observed by MRI. Re-challenge of long-term survivors once again resulted in an enhanced median survival span (148%) and 3 long-term survivors, thereby demonstrating an induced memory antitumor response.	[181]

Abbreviation: SC: subcutaneous; CED: convection-enhanced delivery; IV: intravenous; SI: stereotactic injection; IC: intracarotid; IT: intratumoral; IP: Intra-peritoneal; A: Injection inside the cavity remained after tumor resection; 9L: rat gliosarcoma model; U87MG: experimental human glioma model; F98: rat glioma model; GL261: mouse GB model; MIAMI cells: marrow-isolated adult multilineage inducible cells; DSPE-mPEG₂₀₀₀: 1,2-distearoyl-sn-glycero-3-phosphoethanolamine-polyethylene glycol; P-gp: glycoprotein P; PEG₂₀₀₀-LAA: polyethylene glycol-2-alkyl-lipoamino acid; ER: external radiotherapy; NFL: NFL-TBS.40-63 (cell-penetrating peptide); OX26: OX26 monoclonal antibody; HBD: hypertonic barrier disruption; * Lab1 GB cells obtained from a recurrent GB that relapsed 6 months after treatment of the initial tumor through fractionated radiotherapy (60 Gy).

Table 5 shows that systemic or direct delivery to the brain has been used to deliver drug-loaded LNCs and various approaches have been evaluated for their selective GB targeting.

Systemic LNC delivery: The greatest advantage of using systemic drug-loaded LNCs delivery approaches for GB treatment is their non-invasive nature. The most commonly applied method for administration of LNCs into the body is the intravenous route. As it is mentioned before, this systemic delivery is limited owing to the non-specific uptake of LNCs by the MPS as well as problems in penetrating the BBB. Various factors such as the nature of the components, size, the apparent electrical charge and hydrophilicity of LNCs play a pivotal role in their fate during circulation

[182]. Ideally, these LNCs have to be small, and their surface must be neutral and hydrophilic. It is well proven that a generation of nanoparticles decorated with hydrophilic polymer chains like PEG and its derivatives could provide the colloidal system with a steric repulsion and this effect could lead to their prolonged circulation time in blood stream [165,166]. In the case of LNCs, presence of PEG surfactant on the shell results in prolonged circulation time in blood stream. For example, PEG₁₅₀₀ stearate dramatically increase the plasma elimination half-life time of the nanocapsules up to 5.5 h after intravenous injection into healthy rats, in the way that 20% of total dose was still present after 24 h [183]. In addition, applying other derivatives of PEG such as (DSPE)-PEG₂₀₀₀ or DSPE-PEG₅₀₀₀ resulted in a more prolonged half-life time of over 6 h after intravenous administration [184].

Direct LNC delivery: To overcome the BBB, direct intracranial drug delivery by stereotaxic injection would be considered as a more proficient administration alternative. LNCs can be administered directly into the brain via a bolus injection. This has the advantage of delivering much higher concentrations of drug-loaded LNCs to the brain through bypassing the BBB. However, a major problem is the slower movement of LNCs within the brain owing to limited diffusion coefficients and backflow of the injection. This is because of the naturally packed arrangement of cells in both the gray and white matter microenvironments [185]. Convection-enhanced-delivery (CED) has been employed to overcome these problems. Using an external pressure gradient inducing fluid convection in the brain via a surgically implanted catheter, this method allows a greater volume of distribution to be achieved while being compared with diffusion method alone [186]. Allard et al. [180], treated 9L-bearing rats with a single injection of ¹⁸⁸Re-SSS-labelled LNC by CED and reported an increase in the median survival time about 80% compared to the control group, and 33% of the animals were long-term survivors (over 100 days).

Approaches for selective brain tumor-targeting: Passive and active targeting strategies were used to deliver drug-loaded LNCs. Passive targeting is based on the characteristics of brain tumor tissues such as hyper-vascularization, defective vascular architecture, and a deficient lymphatic drainage system. These features lead to preferential accumulation and retention of LNCs in tumor tissues rather than normal tissues via the EPR effect. In one study, it is reported that the EPR effect is more

pronounced for LNCs which are further decorated by longer PEG chains such as DSPE-PEG₂₀₀₀ due to their longer circulation in comparison to normal LNCs [156]. It should be considered that such EPR effect is not homogenous, in the way that the accumulation of the LNCs deep inside the tumor is more noticeable [174]. Although, higher concentration of PEG could correlate with a prolonged half-life and circulation time, the hydrophilic PEG coating can also hamper interaction between LNCs and the cell, which would be unhelpful for delivery of drug to the tumor.

Despite of the fact that it is possible to prolong the circulation of LNCs in bloodstream, the BBB blocks the entrance of LNCs to the brain site and passive targeting fails for this purpose. Active targeting consists of functionalizing the drug-loaded LNC surface with ligands and antibodies to specifically target the tumor endothelium and tumor-associated antigens (TAA). For example, monoclonal antibody OX26 as covalently grafted on LNCs to target the transferrin receptor (TfR) which is over-expressed on the brain capillary endothelium and surface of GB cells [187]. At 24 h post-injection, the brain concentrations of OX26-LNCs were 2-fold higher than non-targeted LNCs. In another study, Balzeau et al. [188], reported that when paclitaxel-loaded LNCs decorated with a neurofilament derived cell-penetrating peptide (NFL-TBS.40-63) [189], were injected in mice bearing a glioma tumor, they are preferentially targeted to the tumor and reduce its progression. However, these active targeting approaches present limitations because due to the inter-tumor heterogeneity and the inter-patient variability, it is difficult to target all tumor cells.

Another promising strategy for targeting GB is to take advantage of the special tropism of stem cells such as mesenchymal stem cells (MSCs) or neural stem cells (NSCs) for glioma cells. In this regard, various studies employed stem cells as vectors to carry the therapeutic cargo to the tumor site [190]. Our laboratory showed that MSCs or a subpopulation of human MSCs, called “marrow-isolated adult multilineage inducible” (MIAMI) cells were able to employ their endogenous tumor homing activity to distribute ferrociphenol-loaded LNCs in GB after their intratumoral injection (**Figure 12**) [172,190,191].

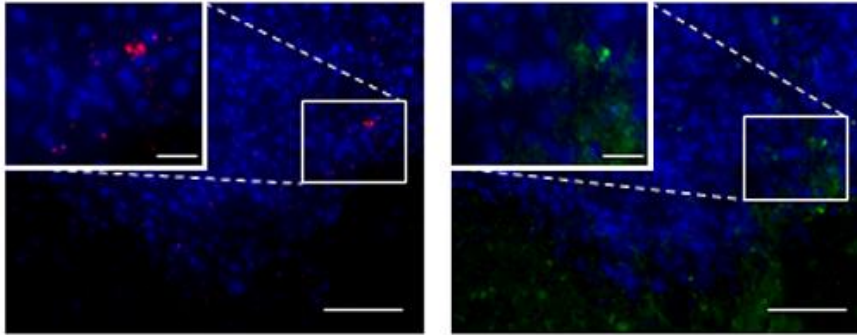


Figure 12. Fluorescent microscopy images of tissues obtained from orthotopic GB tumor in mice after intratumoral injection of MIAMI cells loaded with LNCs after 7 days. The red dots represent MIAMI cells which are labeled with red Y-chromosome and the green fluorescence show coumarin-6 which was encapsulated inside LNCs [190].

In this strategy, the localization of LNCs inside MIAMI cells or MSCs as the vector plays a pivotal role. In case of LNCs, it is assumed that the presence of hydroxystearate-PEG of the Kolliphor[®], which is located on the surface of the nanocapsules, bring a lysosomotropic tendency to the LNCs and therefore disturbs the stability of the lysosome membrane [192].

In general, intracranial administration of therapeutics via CED could lead to higher concentrations in the brain compared to intravenous injection. Although local administration of chemotherapeutic drugs has shown beneficial effects on patients, drawbacks are unfortunately integral with this administration route [193]. Infection, inflammation, seizure, edema and wound healing related problems are of the complications of this method to say the least [194,195]. It is worthy of mention that local administration routes are unlikely to be a logical choice for the drugs which are needed to be administered chronically. On the whole, in previous years, the intranasal pathway, as a non-invasive alternative for the mentioned local administration methods, has been emerging due to the fact that it could be a more safe and efficient way for drug delivery to the brain.

3. Nose-to-brain drug delivery

The intranasal administration route is suggested as a non-invasive approach for delivery of therapeutics directly to the tumor site inside the brain. By benefiting this route of administration, it is possible to bypass the BBB and decrease systemic secondary effects. By this route, pharmacological agents could reach the brain through trigeminal and olfactory nerves. In order to further enhance the nose-to-brain transport

of pharmacological agents, many nanoformulations have been developed. In this section, the aim is to further elaborate on the lipid-based nanoformulations, which enhance the nasal permeability of pharmacological agents to the brain, improve drug delivery at a sustained and slow release rate, protects agents from degradation during the transport, elevate mucoadhesion, and finally enhance nasal transport.

3.1. Intranasal administration

Nose-to-brain transport happens through direct transport of the pharmacological agents or therapeutic tools from the nasal cavity to the brain. This transport is primarily extracellular and transcellular, involving the respiratory and olfactory regions of the nasal cavity. For many years, intranasal administration has been utilized as an alternative for drugs that cannot be taken orally. Through this route, the administered drugs will reach the systemic circulation. It is only a few decades ago that the possibility of intranasal administration for the purpose of drug delivery to the CNS has appealed to researchers and clinicians [196,197]. Through such transport, pharmacological agent can circumvent the BBB during drug delivery and pass into the CNS. Normally, permeability across the BBB is observed for lipophilic molecules with a molecular weight lower than 600 Dalton [198]. Furthermore, the ideal drug partition coefficient between water and octanol (Log P), is reckoned to be 1.5 to 2.7 for an effective transport across the BBB [199]. It is reported that the low rate of permeability across the BBB is related to low levels of pinocytosis and the existence of tight junctions, which is vital for the CNS to retain its homeostasis [200]. In addition, there are also many drug transporters all over the BBB. For instance, the presence of P-glycoprotein (P-gp), hinders the penetration of the pharmacological agents to the CNS [201]. Through bypassing the BBB via intranasal conveyance, the range of therapeutic agents can be expanded to nucleotides, proteins, chemotherapeutics, cells and viral vectors. Furthermore, nose-to-brain delivery of therapeutic agents brings other advantages such as diminishing the risk of systemic secondary effects and hepatic or renal clearance, evasion in the systemic circulation, and the possibility of chronic or repetitive administration. In addition, other advantages such as non-invasiveness, high patient compliance, the possibility for self-administration, and the fast onset of action makes it evident that it should be accepted as an appealing option for the prognosis for GB patients.

3.1.1. Macroscopical anatomy of nasal cavity

For understanding nose-to-brain transport, it is important to firstly comprehend the anatomical structures of the nasal cavity. Therefore, in this section, the important issues around the anatomical organization in the nasal cavity, which is relevant to intranasal transport of therapeutic agents to the central nervous system (CNS), is emphasized. In the beginning, the routes that are responsible for an effectual nose-to-brain transport are elaborated. Then, a more precise look is provided into the anatomical structures that define whether the employed agents can withstand nose-to-brain transport.

3.1.1.1. Olfactory region

The precise mechanisms accounting for nose-to-brain transport have remained an unanswered question, although the olfactory pathway appears to have an important role in this issue. Nearly 10% of the nasal cavity in the human nasal system is considered to be covered by the olfactory region [202]. It is possible for the therapeutic agents to have a rapid access into the CNS through the olfactory nerve fibers located in the olfactory bulb (**Figure 13**). This is the sole direct physical contact between the CNS and the environment [203]. The olfactory pathway starts at the olfactory receptor neurons, located in the olfactory mucosa.

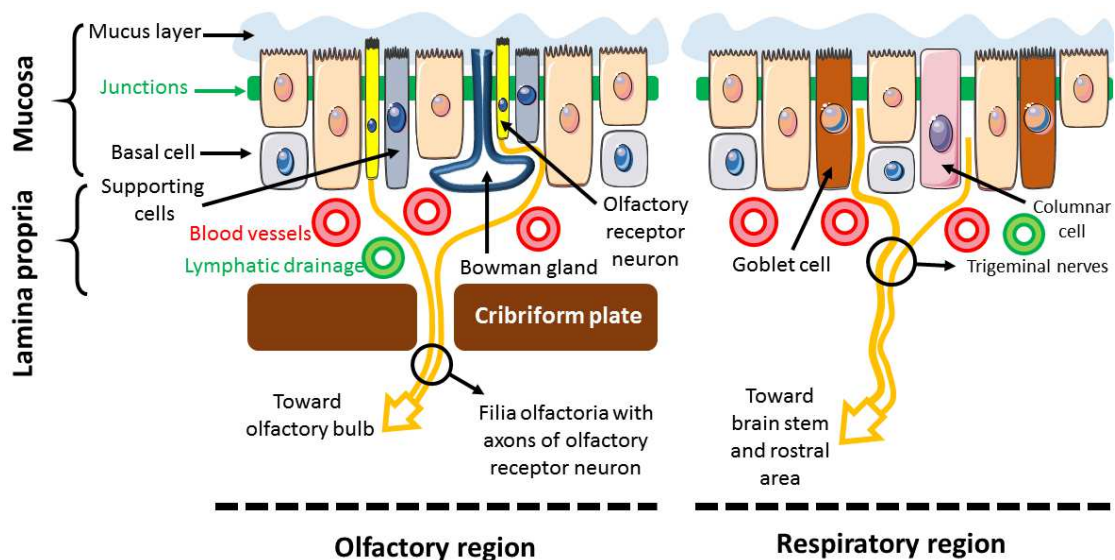


Figure 13: Cellular structure of the olfactory and respiratory mucosa

These cells pick up olfactants and transmit the information to the CNS, mediating the sense of smell [204]. The olfactory receptor neurons are enveloped by microvillar,

basal and supporting cells and all of them are connected by epithelial tight junctions. The olfactory receptor neurons have a continuous activity and they can be constantly replaced by the basal cells which are indeed neural progenitor cells. Such continual replacement of olfactory receptor neurons results in a “leaky” or permeable olfactory mucosa; therefore, such permeability facilitates nose-to-brain transport [205]. From these receptor neurons, axons ramify through the cribriform plate which divides the cranial and nasal cavities, and reaches to mitral cells in the olfactory bulbs. Afterwards, the information received by axons are sent from mitral cells to a couple of regions containing the olfactory tubercle, olfactory nucleus, amygdala, piriform cortex, entorhinal cortex and hypothalamus [206,207]. Hence, through intranasal administration, perineural and intraneural transport is reportedly feasible [208].

3.1.1.2. Respiratory region

Beside the olfactory region, the other vital participant in nose-to-brain transport is considered to be the respiratory region which accounts for 80% to 90% of the nasal cavity in humans. The epithelium layer in this region is crucial for humidifying and warming the inspired air, and for eliminating particles, microorganisms and allergens. This cellular layer is formed out of ciliated and non-ciliated columnar, goblet, and basal cells (**Figure 13**) [209]. Among these cells, the goblet ones secrete mucus which is propelled by the ciliated cells towards the nasopharynx, where it is swallowed or ejected through cough. Projection of the trigeminal nerves abound in the respiratory region. Interestingly, these nerves also facilitate the transport to the brain [208]. The trigeminal nerves are comprised of: (a) the ophthalmic nerve, (b) the maxillary nerve, and (c) the mandibular nerve. Between these three branches, only the ophthalmic and maxillary nerve supply the nerves throughout the nasal passage via the nasal, nasopalatine, and ethmoidal branch [210]. These branches in the respiratory epithelium, enter the brain from two different sites: the cribriform, and the lacerated foramen. By this means, this pathway ends in two entry sites in both the rostral and the caudal brain regions. In brief, when a pharmacological agent is intranasally administered, the agent could move along the olfactory and trigeminal pathways, projecting towards the more rostral and more caudal, regions respectively. Finally, like in the olfactory region, transport to the brain through the nerves in respiratory region is perineuronal and intraneuronal.

3.1.1.3. Other pathways

It is very probable that perineuronal and intraneuronal transport through trigeminal and olfactory nerves plays a major role in the nose-to-brain pathway. Meanwhile, there are some other pathways that might be involved in connecting the nasal cavity to the CNS. The Gruenberg ganglion or the facial nerve are also entrances toward the CNS and might be considered as nose-to-brain pathways [211]. In addition to neural pathways, other routes such as vasculature pathways are also emerging. The vascularization in olfactory region originates from limited branches of the maxillary artery [212]. Drugs which are administered through the intranasal route can reach the systemic circulation through these vessels and cross the BBB for entering the brain site, particularly when the administered drugs are hydrophobic. It is more probable that the molecules are transferred through perivascular regions situated between the adjacent cells from surrounding tissue and the outmost cellular layer of the blood vessels [213]. The mentioned transport pathway originates from diffusion, arterial pulsation and bulk flow. This might account for the quick distribution in the CNS after intranasal administration of the drugs [214]. Involvement of the cerebrospinal fluid in the transport of drug from the nasal cavity to the brain has also been reported, although it is still not well-investigated [215,216]. Transport of intranasally administered substances through lymphatic vessels has also been reported [217].

3.1.2. In-depth overview of transport across epithelial cells in nasal cavity

In this section, the intranasal barriers that need to be surmounted for the applied substances to travel to the brain site are discussed. **Figure 14** schematically illustrates the detailed microscopic view of the way nanoformulations can further improve the nose-to-brain delivery of substances.

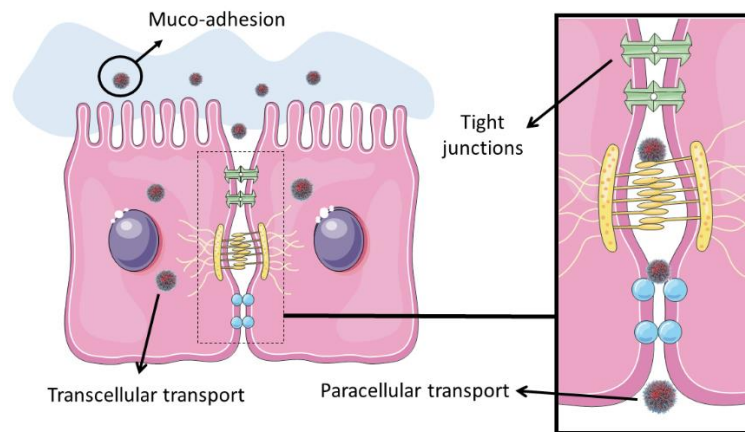


Figure 14: Detailed microscopic view of nanoparticles transport across epithelium cells

3.1.2.1. Nasal Mucosa and Mucus

In general, the very first hurdle that a therapeutic agent will face upon intranasal administration is the layer of mucus spread all over the respiratory and olfactory mucosa. In human, mucus is a multicomponent blend which is secreted by the goblet cells located in mucosa. This mixture is composed of 95% water, 2% mucin, 1% albumin, 1% salt, lactoferrin, lipids, immunoglobulins and lysozyme [218]. The pH of this mixture in the nasal cavity is reported to be neutral or marginally acidic (pH: 5.5 to 6.5) [219]. The cilia propel the mucus cover toward the pharynx. Only the cilia situated on the respiratory mucosa have the potential to relocate the mucus, due to the fact that the cilia on the olfactory mucosa do not have the dynein arms which are essential for movement [220]. The cilia beat rate (1000 beat/min) results in the propulsion of the mucus at 5 mm per min [221]. If a therapeutic agent successfully enters the nasal cavity, mucus is supposedly the initial barrier to traverse before reaching the brain site. Thereafter, the agent could cross the cell transcellularly or paracellularly.

3.1.2.2. Paracellular transport between epithelial cells

When substances are administered intranasally, multiple barriers are faced during penetration and crossing the epithelial cells. Junctions are structures that makes the epithelial cells to be in proximity of each other. These structure are tight junctions, adhering junctions, gap-junctions, and desmosomes [222]. These junctions play a pivotal role in paracellular transport of substances across epithelia since their size is limited. The size of the hydrophilic channel among the epithelial cells is approximately 8 Å [222]. One of the obstacles in paracellular transport across these cells is the

integrity of junctions which normally are not loosened, due to the fact that the olfactory receptor cells are constantly being regenerated and replaced, which renews the entire mucosa [223]. There are some formulations that can momentarily unfasten these junctions and consequently enhance substance permeation [224], which leads to enhance nose-to-brain transport.

3.1.2.3. Transcellular Transport across epithelial cells

It is believed that entities smaller than 20 nm are more probably subjected to paracellular transport across epithelial cells [225]. Thereby, the larger nanomaterials are more likely to be transported transcellularly. Diverse mechanisms, i.e. caveolae-dependent or independent, clathrin-dependent or independent, phagocytosis and micropinocytosis, are suggested in the literature for this type of transport and they are highly dependent on the nature of the applied substance [226]. Materials larger than 200 nm and up to 1000 nm would be internalized through clathrin-mediated endocytosis, while nanosystems with a size of 20-200 nm have a tendency toward caveolae-mediated endocytosis [227]. As it is expected, transcellular transport is slower than paracellular in general, ranging from hours to a couple of days. When materials are introduced to olfactory receptor neurons, consequently they undergo intraneuronal transport following the anterograde direction toward the olfactory bulb [228,229].

3.1.2.4. Axons in olfactory region

The lamina propria is a thin layer of loose areolar connective tissue, just beneath the olfactory mucosal layer. In this region, the various axons of olfactory receptor neurons meet each other and are enveloped by Schwann cells [230]. Naturally, 20 axons are packed in this bundle. One Schwann cell can normally contain 5 to 10 of these bundles, which cumulatively incorporates more than 100 axons. Perineuronal channels with a size of 10 to 15 nm are spotted next to each axons which act as ionic reservoirs. Mesaxons, defined as pores that permit the transport of extracellular fluids, are also found inside this nerve organization. It is reported that transneuronal transport through these axons is very dependent on their size, which in human varies from 100 up to 700 nm [231].

3.2. In vitro models for nasal permeability studies

To study the absorption/permeation of the therapeutic agent through the nasal mucosa, multiple in vitro models have been developed for preclinical screening goals. The advantage of this type of models is mainly the ability to control variables. In addition, it is possible to separate the absorption process from the ulterior distribution and elimination process in vivo. For investigation on therapeutic agent absorption/permeation, artificial membranes, primary cell culture, cell lines and nasal tissue are generally utilized. In this section, these methods are briefly covered.

3.2.1. Artificial membranes

Artificial membrane models have been employed to imitate and predict drug permeation through various biological barriers, such as the BBB, skin, and intestinal mucosa [232–236]. Such models are normally based on a filter-supported lipid membrane system, although different materials have been used as the lipid membrane or the supporting filter. The noticeable limitation of these models is that it is only possible to predict the permeation of therapeutic agents that are majorly transported via transcellular passive diffusion. Therefore, it lacks the possibility to study the paracellular or active transport of the therapeutic agent [237,238]. Thus, the permeation of small hydrophilic substances could be underestimated.

3.2.2. Nasal tissue

Excised nasal tissue

This method is based on excised nasal mucosae obtained from animals, such as cattle, sheep, rabbits and pigs [239–242]. It is reported that the bovine nasal mucosa is similar to the typical respiratory epithelium. However, extracting and preparing excised nasal tissues is very challenging, particularly when wider pieces of fresh tissues are needed. Moreover, stripping the integral tissue from the wall of the nasal cavity is another difficulty which is integral to this method [243].

As it is been reported, there are differences between different animal nasal mucosae, and also between animal and human nasal mucosae [243–245]. To the fact that the junctions shaped between goblet cells or between columnar cells and goblet cells are looser in comparison to the junctions between columnar cells themselves, the proportion of columnar cells and goblet cells, which differs from one type of animal to

the other one, could affect the permeability in the nasal mucosae [243]. Such differences are also evident in the activities of different enzymes. Zhou et al [244], investigated nasal enzyme activities in dogs, rabbits, rats and guinea pigs utilizing nasal tissue homogenates and showed the species variations in the activity of esterases and aminopeptidases. In fact, such species variations exist in all of the excised tissue models from animals.

EpiAirway™

There is another tissue model that can be employed for therapeutic agent permeability studies which is commercially available under the name of EpiAirway™ from MatTek Corporation. This tissue is composed of normal human bronchial/tracheal epithelial cells and it forms a pseudo-stratified, highly differentiated tissue that greatly mimics the epithelial tissue of the respiratory region. There are many studies which have done on nasal drug delivery using EpiAirway™, and it was reported that this tissue is suitable enough for such studies [246–248]. In a comparison with other in vitro models, the benefits of EpiAirway™ are that (a) they can be utilized without any preparation after arrival and (b) they are manufactured out of normal human respiratory epithelial cells and therefore possess a more appropriate differentiation than cancer cell lines. However, to maintain the viability of the manufactured tissue, the total delivery time of EpiAirway™ from the United States of America, where these tissues are prepared, to the receiver should be less than 48 hours. Hence, it might not be practically feasible for many researchers to pre-plan the studies using this kind of tissue. In addition, this model is far more expensive in comparison to other in vitro models.

3.2.3. Primary cell cultures

In general, human primary nasal epithelial cells are acquired from patients during nasal surgery [249,250]. In some cases, the cells are obtained through nasal scraping of healthy candidates [251]. Considering the fact that the nasal cavity is comprised of different divisions and each of these divisions possesses dissimilar constitution and function, the source of the sample can highly influence the features of the primary cell culture model [243]. The respiratory region is considered to be the optimal region for nasal drug absorption. Hence, the samples for extracting primary cell culture are normally collected from this region [245,252].

Several studies have reported that human primary epithelial cells are capable of being cultured into differentiated epithelial cell monolayers which have ciliated nasal cells and mucus secreting goblet cells with tight junctions [249–251,253,254]. Although, the main problem with this model is its restricted access and short-term lifespan. These cells can be subcultured for only 3 or 4 passages without any morphological change in the best case scenario. This behavior in nasal primary cells makes the long-term reproducibility challenging [250,254]. In addition, providing the necessary condition for culturing human primary nasal epithelial cells is quite complicated and expensive, since different proteins such as epidermal growth factor, insulin, transferrin and triiodothyronine should be added in the culture medium [243,250].

3.2.4. Cell lines

In order to cope with some of the limitations of the above mentioned in vitro models, like reproducibility and availability, cultured models founded on cancer cell lines, with prolonged lifespan or maybe immortality, have been of interest. At the moment, RPMI 2650 and Calu-3 cells are the commercially available cell lines that have been employed for human nasal drug delivery researches [255].

RPMI 2650 cell line

The RPMI 2650 cell line was obtained from a human nasal septum squamous cell carcinoma. However, there is no consensus on the permeability and morphology of these cells. The differentiation of these cells has been reported to be low and the cells cannot form a confluent and homogeneous monolayer [243,253,256]. Therefore, this type of cell might not be appropriate as a model for permeation studies. Nevertheless, there is one study that employed the cell line to investigate the permeation of drug-loaded microspheres [257]. The RPMI 2650 cell culture model is however applicable for nasal metabolism researches [255].

Calu-3 cell line

In a comparison to RPMI 2650, the Calu-3 cell line has been well studied. Briefly, these cells are derived from a human bronchial adenocarcinoma. They can form a tight and polarized mucus secreting cell monolayer with apical microvilli [258–261]. Moreover, it has been reported that the monolayer also exhibit cilia at their surface [262,263]. Up to now, these cells have been extensively assessed and employed for pulmonary drug

delivery or transport studies. Although these cells are derived from human bronchia, there is a plethora of studies taking advantage of the features of the Calu-3 cell line to mimic the mucus secreting nasal epithelia in vitro [261,264–273]. For instance, Seki et al. [274], investigated the improving effect of an aminated gelatin (forming a cation by reacting gelatin with ethylenediamine) for the nasal transport of insulin in the Calu-3 cell line model. In another study, Witschi and co-workers employed the Calu-3 cell line to investigate the influence of bioadhesive polymers on the transport of proteins [275]. Similarly, Li et al. [261], utilized this cell line model to evaluate carbopol mediated transport improvement of desmopressin through nasal permeation.

3.3. Lipid-based nanoformulations for nose-to-brain drug delivery

Nanoparticles could enhance nose-to-brain drug delivery, due to the fact that they are capable of protecting the encapsulated drug from chemical and/or biological degradation, and from P-glycoprotein (P-gp) which pumps the drugs (in high doses) out of the cells and thus reducing their cytotoxicity [276]. In addition, retention of bioadhesive nanoparticles on the mucosal regions of the nasal cavity, along with their capability of momentarily opening the tight junctions of the mucosal epithelium (thanks to surfactants utilized in the formulation) participate in the enhancement of nasal drug delivery to the brain [277].

One of the important aspects of nasal nanoformulations is the toxicological and safety profile of the nanoparticles. The prolonged exposure of nanoformulation with the nasal mucosa might result in irritation, damage, ciliotoxicity, epithelial or sub-epithelial toxicity. Such problems could prepare a suitable environment for the growth of bacteria. Furthermore, the nanoformulations for intranasal drug delivery should not cause any damage in the sense of smell and the primary olfactory nerves [278]. This issue is crucial when it comes to intranasal delivery of cytotoxic drugs for the purpose of malignant brain tumor treatment. Up to now, different experimental approaches have been practiced for nose-to-brain delivery of cytotoxic drugs, although these drugs can bring local damages after nasal administration [279]. It suggests that nose-to-brain delivery of drugs for brain tumors treatment necessitates a proper drug carrier that can safeguard the drugs from premature release during the delivery process.

Many colloidal nanocarriers, such as nanoemulsions, vesicular systems, lipid and polymer nanoparticles, have been used for the purpose of nose-to-brain drug delivery [280], although among these nanocarriers, lipid-based nanoparticles are the most promising ones for this goal [281]. Because of their biocompatibility, ease of surface functionalization, stability and cost-effective scale-up, lipid-based nanoparticles have been frequently utilized as nose-to-brain drug delivery system. Up to now, there are multiple accounts on successful intranasal delivery of therapeutic agents for the treatment of various neurodegenerative disorders such as Amyotrophic Lateral Sclerosis, Parkinson's, Alzheimer's and Huntington's diseases, through employment of liposomes [269,282–287] and SLNs [288–294]. Interestingly, the lipid-based nanoparticles also have been utilized for GB treatment via the nasal administration route. For example, Zhuang et al. [295], used folic acid-decorated SLNs for nose-to-brain delivery of miR17. The results showed a rapid delivery of miR17 to the brain of the GB tumor-bearing mice and the nanoparticles were selectively taken up by GL-26 tumor cells. In addition, the authors observed that the mice treated intranasally had delayed brain tumor growth more than the ones in control group. In another study, Khan et al [296], demonstrated that TMZ-encapsulated lipid-based nanoparticles could be delivered intranasally to the brain of Wistar rats, with TMZ penetration in the brain more than two times higher than with the same formulation administered intravenously. Through an *ex vivo* experiment on porcine nasal mucosa, the permeability coefficient and flux for TMZ-encapsulated lipid-based nanoparticles were almost double than those obtained for a TMZ solution. Lipid-based nanoparticles were also used for intranasal delivery of curcumin for GB treatment [297]. It is reported that the lipid-based nanoparticles had an extremely low level of toxicity on astrocytoma-GB cells. In the same study, it is also mentioned that intranasal administration of curcumin loaded lipid-based nanoparticles in rats noticeably increased the presence of curcumin in the CNS, in comparison to a curcumin solution.

One of the important issues in nose-to-brain drug delivery is the fate of the nanocarrier itself. Since the drugs used for GB treatment are cytotoxic, an appropriate nanocarrier for these toxic drugs could be the one that increases the permeability across epithelial barriers while maintaining its nanostructure before reaching the tumor site. Hence, it is of high importance to address this issue in preclinical studies.

Aims and Objectives

The treatment of GB remains difficult so that no contemporary treatments are efficiently curative. While overall mortality rates remain high, recent efforts on understanding of the molecular mechanisms and gene mutations combined with clinical trials are leading to more promising and tailored therapeutic approaches. New studies have thus revealed the path to a new type of therapeutic approach – target therapy – based on the selected targeting of neoplastic cells by means of agents directed against molecular components, whose inhibition is detrimental for tumor development but not for normal tissues. At present, the current idea is that inhibiting both tumor cells and angiogenesis, supporting the oxygen and nutrition delivery to the tumor, would gain better results in GB treatment. Therefore, the single-target therapy is fading in favor of a multitarget approach. The new generation of TKIs, such as SFN, responds to this multitarget approach and represents a potential interest for GB therapy.

In clinical studies in patients with progressive or recurrent GB, SFN treatment has been shown to be of very limited efficacy as a monotherapy or in combination with other chemotherapeutics. This may be due, in part, to the route of administration of the SFN. The poor solubility of SFN strongly limits its application for local treatment and this drug is orally administered in the form of SFN tosylate tablets. Such systemic administration may be efficacious for peripheral tumors but efficacy may be limited for brain tumors, for which SFN does not penetrate into the brain in sufficient amounts due to the presence of the BBB. Increasing the dosage is required to obtain effective brain tumor concentrations but the potentially adverse events associated with the systemic distribution of SFN do not allow it. Therefore, delivery systems for this drug need to be optimized to increase brain-tumor delivery and limit side effects. In this regard, the **first objective** of the current thesis was to reformulate SFN in order to enhance its efficacy. Knowing that LNCs have shown promising results in drug delivery for GB and also the capability of these nanocapsules for encapsulating high doses of hydrophilic drugs, SFN-loaded LNCs were prepared and characterized. Moreover, further studies were conducted to evaluate the efficacy of the prepared formulation on GB and endothelial cells *in vitro*, and after intracranial injection in *in vivo* GB model.

Although intracranial administration of the prepared formulation could help bypassing the BBB, such approach necessitates surgery, thereby it lacks repeatability. An alternative administration route which facilitates both avoiding the BBB and repeatable

administration, is intranasal route. In comparison to intravenous injections, many studies have reported higher brain concentrations from formulations administered intranasally. In this regard, the **second objective** of the current thesis is to find out whether LNCs have the potential to be employed as a suitable nanocarrier for nose-to-brain drug delivery. In this regard, the fate of LNCs with different sizes and matrix components after transport across a model of nasal epithelial barrier was particularly studied.

Chapter 1

Development and characterization of sorafenib-loaded lipid nanocapsules for the treatment of glioblastoma

Scientific context

Even though chemotherapy is an imperative auxiliary treatment for GB, the clinical outcome is commonly restricted because of the specific features of GB, such as the highly abnormal and dysfunctional vasculature. Therefore, drugs with multiple targets could provide a feasible option for the treatment of GB. Among these, SFN is a TKI that could target both GB cells and angiogenesis. Presently, this drug is administered orally using SFN tosylate tablets and the results obtained from clinical trials in patients with GB show that such systemic administration had very limited efficacy. The systemic distribution of SFN is associated with potentially adverse events preventing to increase the dose of this drug. In order to solve this problem, local administration of this drug might result in better outcomes, but SFN is poorly soluble in aqueous medium limiting such administration. In order to overcome this obstacle, SFN was encapsulated in LNCs (SFN-LNCs) which are prepared from regulatory-approved components and through a solvent-free process. Characterization of SFN-LNCs revealed that they had a diameter of 54 ± 1 nm, high encapsulation efficiency ($> 90\%$), and a drug payload of 2.11 ± 0.03 mg/g of LNC dispersion. The *in vitro* release study showed that there is a slow and sustained SFN release up to 20% after 5 days. We observed that the prepared formulation inhibited *in vitro* angiogenesis and the viability of the human U87MG GB cell line similarly to free SFN. Further investigation on the U87MG human GB orthotopic xenograft model revealed that intratumoral administration of SFN-LNCs or free SFN decreased the proportion of proliferating cells in the tumor relative to control groups. For interest, SFN-LNCs were more effective than free SFN in inducing early tumor vascular normalization, characterized by increased tumor blood flow and reduced tumor vessel area. The vascular normalization induced by SFN-LNCs could be used to improve the efficacy of chemotherapy and radiotherapy in the treatment of GB.

Development and characterization of sorafenib-loaded lipid nanocapsules for the treatment of glioblastoma

Anne Clavreul^{1,2*}, Emilie Roger³, Milad Pourbaghi Masouleh^{2,4}, Laurent Lemaire^{3,5}, Clément Tétaud², and Philippe Menei.^{1,2}

¹Département de Neurochirurgie, CHU, Angers, France

²CRCINA, INSERM, Université de Nantes, Université d'Angers, Angers, France

³MINT, UNIV Angers, INSERM 1066, CNRS 6021, Angers, France

⁴Division of Drug Delivery and Tissue Engineering, School of Pharmacy, University of Nottingham

⁵PRISM-IRM, UNIV Angers, Angers, France

* Corresponding author:

Anne Clavreul, Département de Neurochirurgie, CHU, Angers, France

Phone: +33 244 688548; Fax: +33 244 688546; E-mail: anne.clavreul@univ-angers.fr

Contribution: All the formulations, characterizations and analyses are done by Milad Pourbaghi Masouleh.

Abstract

Anticancer agents that target both tumor cells and angiogenesis are of potential interest for glioblastoma (GB) therapy. One such agent is sorafenib (SFN), a tyrosine kinase inhibitor. However, poor aqueous solubility and undesirable side effects limit its clinical application, including local treatment. We encapsulated SFN in lipid nanocapsules (LNCs) to overcome these drawbacks. LNCs are nanocarriers formulated according to a solvent-free process, using only components that have received regulatory approval. SFN-LNCs had a diameter of 54 ± 1 nm, high encapsulation efficiency ($> 90\%$), and a drug payload of 2.11 ± 0.03 mg/g of LNC dispersion. They inhibited *in vitro* angiogenesis and the viability of the human U87MG GB cell line similarly to free SFN. *In vivo* studies showed that intratumoral administration of SFN-LNCs or free SFN in nude mice bearing an orthotopic U87MG human GB xenograft decreased the proportion of proliferating cells in the tumor relative to control groups. SFN-LNCs were more effective than free SFN in inducing early tumor vascular normalization, characterized by increased tumor blood flow and reduced tumor vessel area. These results highlight the potential of LNCs as delivery systems for SFN. The vascular normalization induced by SFN-LNCs could be used to improve the efficacy of chemotherapy and radiotherapy in the treatment of GB.

Keywords: drug delivery; glioblastoma; lipid nanocapsules; sorafenib

Introduction

Glioblastomas (GBs) are the most frequent, aggressive, and fatal type of brain tumor, with a mean five-year survival rate of less than 5% [16,31]. Despite considerable scientific and technological progress, the treatment of GB is still a major challenge.

Signaling pathways initiated by activated receptor tyrosine kinases (RTKs), including those for epidermal growth factor (EGFR), platelet derived growth factor (PDGFR), or vascular-endothelial growth factor (VEGFR), play a key role in the growth, invasiveness, and angiogenesis of this tumor and are attractive therapeutic targets [298–300]. Several drugs directed against RTK signaling pathways have been developed. Sorafenib (Nexavar™, SFN), approved for the treatment of advanced hepatocellular carcinoma, renal cell carcinoma, and thyroid cancer, is one such drug [301]. SFN is a multikinase inhibitor that acts on cell surface RTKs (e.g., VEGFR-2 and VEGFR-3, PDGFR- β , c-kit, and Flt-3) and down-stream intracellular serine/threonine kinases (e.g., Raf-1, wild-type B-Raf, and mutant B-Raf). SFN has demonstrated anti-GB activity in both *in vitro* and *in vivo* models, inhibiting cell proliferation and angiogenesis [123–125]. However, SFN treatment has been shown to have very limited efficacy in patients with progressive or recurrent GB, either as monotherapy or in combination with temozolomide or other targeted drugs, such as erlotinib [126,129,131,302–305]. This may be due, in part, to the route of administration of the SFN. The poor solubility of SFN strongly limits its application for local treatment and this drug is orally administered in the form of SFN tosylate tablets. Such systemic administration may be efficient for peripheral tumors, such as hepatocellular carcinoma, renal cell carcinoma, and thyroid cancer, but efficacy may be limited for brain tumors, for which SFN does not penetrate into the brain in sufficient amounts [306]. High systemic doses of this drug are required to obtain effective brain-tumor concentrations. The systemic distribution of SFN is associated with potentially adverse events, such as hand-foot skin reactions, rash, upper and lower gastrointestinal distress, fatigue, and hypertension [307]. Patient tolerance can be severely limited, which in turn limits the dose and associated patient response. Therefore, delivery systems for this drug need to be optimized to increase brain-tumor delivery and limit side effects. Recently, we used mesenchymal stromal cells (MSCs) to transport SFN to brain tumors [308]. However, despite the potential of MSCs to carry

SFN to brain tumors following intranasal administration, the therapeutic effect was modest, probably due to the pro-tumorigenic properties of the MSCs themselves, which may counteract the action of the released SFN. The use of nanocarriers for tumor delivery and controlled release of SFN could be another alternative. Here, we chose lipid nanocapsules (LNCs) for SFN encapsulation and selective delivery because of the advantages they offer with respect to other types of nanocarriers. These include their production by a phase-inversion process using generally recognized as safe (GRAS) excipients, without the use of organic solvents, their high stability and drug loading capacity (in comparison to liposomes), and the possibility of easy scale-up for their production [134,153]. Modification of the LNC surface, through the grafting of ligands that recognize specific cancer cell receptors, is an additional strategy that could improve the specificity of these nanovectors toward their desired target [188,309,310]. Furthermore, several studies have demonstrated the interest of using LNCs to deliver drugs to glioma tumors [134,174,311,312].

Here, we describe the preparation of SFN-loaded LNCs (SFN-LNCs), which were characterized for size, polydispersity index (PDI), surface charge, drug payload, *in vitro* drug release, and storage stability. Their toxicity toward the U87MG GB cell line and effect on angiogenesis was evaluated *in vitro* and *in vivo*.

Materials and methods

Chemicals

SFN powder was purchased from LC Laboratories (Woburn, USA). Oil solubilizers and excipients were provided by Gattefosse S.A (Saint-Priest, France). Lipoid® S75-3 (soybean lecithin at 70% phosphatidylcholine and 10% phosphatidylethanolamine) and Kolliphor® HS15 (mixture of free polyethylene glycol 660 and polyethylene glycol 660 hydroxystearate) were a gift from Lipoid GmbH (Ludwigshafen, Germany) and BASF (Ludwigshafen, Germany), respectively. NaCl was purchased from Prolabo VWR International (Fontenay-sous-Bois, France). Purified water was obtained from a MilliQ185 System (Millipore, Paris, France). Formic acid, acetic acid, acetonitrile, dimethylsulfoxide (DMSO), methanol, and HPLC-grade tetrahydrofuran (THF) were purchased from Sigma-Aldrich (Saint-Quentin Fallavier, France) and Carlo Erba reagents (Val-de-Reuil, France).

Analytical methods

Analysis of SFN by high-performance liquid chromatography (HPLC-UV)

An HPLC-UV method was used to quantify SFN as previously described [308]. Briefly, HPLC was performed on a Waters modular system (600/717/996/2414) (Waters, Saint-Quentin-en-Yvelines, France) with a SunFire® C18 column (150 × 4.6 mm; 5 µm) at 37°C. SFN was eluted with an isocratic mobile phase (acetonitrile/methanol/1% acetic acid, at a ratio of 35:38:27) at a flow rate of 1 mL/min, with monitoring at 266 nm. The chromatograms were recorded and integrated with Empower 3 software (Waters). The range of linear response was 0.5–32 µg/mL.

Analysis of SFN by liquid chromatography tandem-mass spectrometry (LC-MS/MS)

A specific LC-MS/MS method was previously developed [308]. Briefly, chromatography was performed on a Waters Alliance® 2695 system with an Uptisphere® 5 ODB (150 x 2.0 mm) column, at 25°C, using an isocratic mixture of 0.1% formic acid in water/0.1% formic acid in acetonitrile: 20/80 (v/v) at a flow rate of 0.3 mL/min. Detection was performed using electrospray ionization in positive ion multiple reaction monitoring (MRM) mode with the mass transition, m/z 465 → 270. Quantification was achieved using QuantLynx® (Waters), by comparing the observed peak area ratios of SFN samples with a calibration curve obtained under the same experimental conditions. The calibration curve was linear in the concentration range of 50-1000 ng/mL.

Solubility studies

A screening study was performed to determine the excipients which could solubilize SFN. Ten mg SFN was added to 1 g of excipients. Preparations were vortexed for 5 min, sonicated for 45 min, and centrifuged. Supernatants were extracted and analyzed by HPLC-UV.

LNC formulation

SFN-LNCs were prepared according to the phase-inversion temperature method [313]. SFN was first solubilized in Transcutol® HP (0.7 g) by vortexing for 5 min. Then, Labrafac® WL1349 (0.4 g), Labrafil® M1944CS (1 g) and Lipoïd® S75-3 (150 mg)

were added. The compounds were heated on a hot plate at 80°C, with agitation at 1200 rpm, until the complete solubilization of Lipoïd® S75-3. Once the mixture returned to ambient temperature, the other compounds of the formulation *i.e.*, water, NaCl, and Kolliphor® HS15 (1.8 g, 0.1 g, and 1 g, respectively) were introduced. Three cycles of progressive heating and cooling between 60 and 90°C were then carried out, and at 75°C during the last cycle, an irreversible shock was induced by adding 5 mL 0°C water. Slow magnetic stirring was then applied to the LNC suspension for 5 min at room temperature. The formulation was filtered through a Minisart® 0.2 µm filter (Sartorius, Goettingen, Germany) and stored at 4°C for further characterization. The same procedure was applied to formulate blank LNCs (B-LNCs), from which SFN was omitted.

LNC characterization

Particle size and zeta potential measurements

The size, PDI, and charge distribution of LNCs were measured by dynamic light scattering (DLS) on a Zetasizer® Nano series DTS 1060 (Malvern Instruments S.A., Worcestershire, UK). The PDI was used as a measurement of the size distribution. A PDI value < 0.2 indicates a unimodal size distribution. LNCs were diluted 1:60 (v/v) in deionized water and three consecutive measurements performed.

Encapsulation efficiency and drug loading

Determination of drug loading was carried out by measuring the amount of the remaining SFN in the sample after filtration by Minisart® 0.2 µm filter (Sartorius) using HPLC-UV as described above (filtration of SFN-LNCs results in elimination of the amount of SFN which is free in the solution and not encapsulated inside LNCs). Therefore, three samples were prepared by dissolution of 10 µL filtrated SFN-LNCs in 990 µL 79/20 (v/v) methanol/THF and then filtered through a Millex-LG filter unit (0.2 µm) for HPLC-UV analysis. Experimental SFN loading was determined by calculating the area under the peak at 266 nm as mentioned earlier and expressed in mg of SFN/g of LNC dispersion. Theoretical SFN loading was determined by dividing the quantity of SFN used in preparation of formulation to the final quantity of the prepared formulation. The encapsulation efficiency (%) was determined by dividing the experimental by theoretical drug loading.

Storage stability studies

The stability of SFN-LNC formulations (n = 4) was evaluated after storage at 4°C for four months. Particle size, PDI, zeta potential, and drug payload of the samples were determined after filtration through a Minisart® 0.2 µm filter (Sartorius) as described above.

Evaluation of drug-release profile

We determined the SFN release from nanocapsules by an indirect method. In this regard, the reduction in drug payload was considered as drug release. For this purpose, 1 mL of SFN-LNCs (n = 4) were diluted directly in 170 mL of DPBS (Ozyme, St Quentin-en-Yvelines, France) and incubated at 37°C with shaking. A 1 mL sample was withdrawn from top of the dilution in the container at intervals of 0.5, 1, 2, 3, 8, 24, 48, and 120 h and replaced by 1 mL DPBS. Samples were filtered through a Minisart® filter with 0.2 µm pores (Sartorius), to remove precipitated SFN. Samples were diluted 10 times by 80/20 (v/v) methanol/THF and then filtered through a Millex-LG filter unit (0.2 µm) for LC-MS/MS analysis. The release of SFN from LNCs was determined indirectly, by evaluating SFN loading by the LC-MS/MS method and calculating the reduction in drug loading based on the SFN loading at the start of the experiment. Finally, the cumulative release was calculated by:

Cumulative percentage release (%) = Volume of sample withdrawn (mL)/bath volume (v) × P_(t-1) + P_t

Where P_t is percentage release at time *t* and P_(t-1) is percentage release previous to *t*.

In vitro studies

Cell culture

The human GB cell line U87MG was obtained from the ATCC (LGC Promochem, Molsheim, France) and expanded in DMEM-high glucose medium (DMEM-HG, Ozyme) containing 10% FBS (Fisher Scientific, Illkirch, France) and 1% antibiotics (Sigma-Aldrich). Human umbilical vein endothelial cells (HUVECs) were purchased from Lonza (Verviers, Belgium). Cells were cultured, according to the supplier's

instructions, in endothelial cell growth medium-2 (EGM-2), corresponding to endothelial basal medium-2 (EBM-2), containing the supplements and growth factors of the EGM-2 SingleQuot™ kit (Lonza). U87MG cells and HUVECs were maintained under an atmosphere containing 5% CO₂ (37°C), in a humidified incubator, until reaching 80% confluence.

U87MG viability assay

U87MG (5×10^3 cells/cm²) were plated in 96-well plates. After 48 h, the culture medium was removed, and cells were treated with SFN and SFN-LNCs at concentrations of 0.001 to 100 µM. B-LNCs were also tested with the same excipient concentration as the others. After 96 h, the medium was removed and the plates were stored at -80°C until the assays were carried out. Cell survival was estimated with the CyQUANT® cell proliferation assay kit, according to the manufacturer's instructions (Fisher Scientific).

Endothelial cell tube-formation assay

HUVECs (5×10^4 cells/cm²) were incubated in Corning® Matrigel® basement membrane matrix-coated 96-well plates (VWR International, Fontenay-sous-Bois, France) for 16 h in EGM-2, with or without SFN, B-LNCs, or SFN-LNCs. The formed endothelial tubes were photographed and quantified. The degree of tube formation was assessed by manual counting of the number of tube-like structures in four wells from each condition.

In vivo studies

A scheme for the protocol used in this study is described in Figure S1.

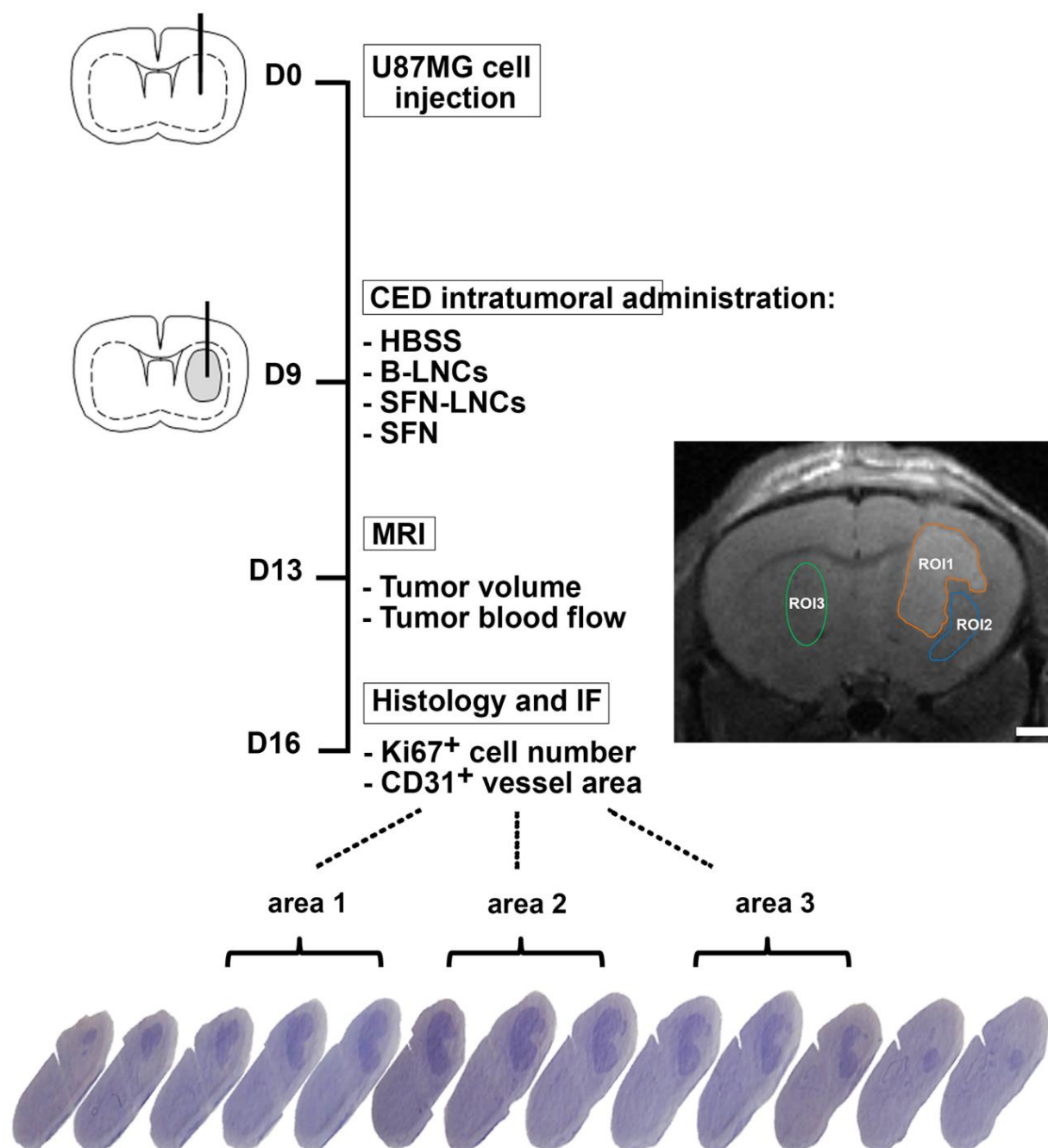


Figure S1: Schematic protocol of the in vivo study. U87MG-bearing mice received HBSS, B-LNCs, SFN-LNCs, or SFN by CED on day 9. Four days later (D13), MRI analyses were performed to follow tumor volume and perfusion. Blood flow was measured in the tumor core (ROI1), the surrounding tissue (ROI2), and in the contralateral striatum (ROI3). On day 16, mice were killed for histological and immunofluorescence analyses. Ki67⁺ cell number and CD31⁺ vessel area were analyzed in three areas of the tumor approximately 400 μ m apart to be representative of the entire tumor.

Intratumoral administration of SFN-LNCs in the U87MG GB model

Female Swiss nude mice (8–10 weeks old) were obtained from Charles River Laboratories (L'Arbresle, France). The protocol was approved by the Committee for the Ethics of Animal Experiments of the "Pays de la Loire" (Permit no. 01785.01). Animals were anesthetized by an intraperitoneal injection of xylazine (13 mg/kg body weight) and ketamine (100 mg/kg body weight) and positioned in a Kopf stereotaxic instrument. On day 0, U87MG cells (5×10^4) in 5 μ L HBSS, with Ca^{2+} and Mg^{2+} , were injected into the right striatum of the mice [coordinates: 2.1 mm lateral to the bregma and 0.5 mm anterior and 3 mm interior to the outer border of the cranium]. On day 9, the mice were assigned to four groups and received an injection by convection-enhanced delivery (CED) (5 μ L; 0.5 μ L/min) at the same coordinates of (a) HBSS with Ca^{2+} and Mg^{2+} ($n = 5$); (b) B-LNCs ($n = 5$); (c) SFN-LNCs ($n = 7$, 3.5 μ g); or (d) SFN ($n = 5$, 3.5 μ g). Tumor volume and perfusion were measured on day 13. Mice were killed on day 16 for the analysis of the number of proliferating Ki67⁺ cells or the area of CD31⁺ vessels in the U87MG tumor. Brains were snap-frozen in liquid nitrogen-cooled isopentane and stored at -80°C . Coronal sections of the brain were cut at 10 μ m intervals and collected on silane-treated slides. For histological analysis, ethanol (95%)/acetic acid (5%)-fixed brain sections were stained with Mayer's hematoxylin solution and permanently mounted.

In vivo measurement of brain tumor volume and perfusion

MRI was performed using a 7T scanner (Biospec 70/20 Avance III, Bruker, Wissembourg, France), equipped with a BGA12S gradient system (675mT/m), under isoflurane anesthesia (1.5-0.5%, O_2 : 0.5 L/min). The body temperature was maintained at 36.5 - 37.5°C with a feedback-regulated heating pad during the entire imaging protocol. Tumor volume was assessed over time using a 1H cryoprobe and rapid acquisition with a relaxation enhancement (RARE) sequence [TR = 3,200 ms; effective echo time (TE_{eff}) = 21.3 ms; acceleration factor = 4; FOV = 2 x 2 cm; matrix 256 x 256; 11 contiguous slices of 0.5 mm, Nex = 1]. Volumes were calculated from manually drawn regions of interest (ROI). Tumor perfusion was assessed by segmented fast imaging with a steady-state precession arterial spin labeling sequence (FISP-ASL), as previously described [314]. Homogeneous radiofrequency excitation was achieved using a proton volume resonator (diameter 87 mm, homogeneous length 80 mm) and signal reception was performed with an actively decoupled phased-

array surface coil (4 channels). Blood flow was measured from two T1 maps acquired once with slice-selective inversion and once with global inversion [315]. A series of 40 gradient echoes were acquired after the inversion pulse to acquire T1 maps (flip angle = 8°, echo time = 1.8 ms, field of view = 18 mm x 18 mm, matrix size = 128 x 128, excitation hermite pulse duration = 800 μ s, inversion hyperbolic secant pulse duration = 15 ms, imaging slice thickness = 1.5 mm, labeling slice thickness = 3.9 mm, with the first echo started 20 ms after the inversion pulse and the duration between each echoes lasting 60 ms). Thirty-two segments were used to fill k-space. A repetition delay of 13 s was introduced after the acquisition of a set of gradient echoes to allow for full relaxation between two inversion pulses. The total measurement time was approximately 14 min. ROIs were manually outlined in the tumor core, the surrounding tissue, and out to the contralateral side of the brain for comparison. Blood flow in these ROIs was calculated using ParaVision 5.1 software (Bruker).

Immunofluorescence

For CD31 and Ki67 expression analyses, brain cryosections were allowed to air dry, rehydrated in DPBS, and fixed by incubation for 10 min in 4% PFA, pH 7.4, at 4°C. Nonspecific binding was blocked by incubating the sections in 4% BSA and 10% normal goat serum in DPBS. The sections were incubated overnight, at 4°C, with isotype controls and primary antibodies against endothelial cells (mouse CD31, BD Biosciences, Le Pont de Claix, France) and proliferative cells (Ki67, Agilent Technologies, Les Ulis, France). The primary antibodies were detected with biotinylated secondary antibodies and the signal was amplified with Alexa Fluor 488 streptavidin (Interchim, Montluçon, France). Nuclei were counterstained with DAPI (Sigma-Aldrich). Cryosections of four mice from each group described above (a, b, c, and d) were analyzed under an Axioscope® 2 fluorescence microscope. CD31⁺ and Ki67⁺ cells were counted with the MetaView computerized image-analysis system in six brain cryosections per mouse, corresponding to three areas of the tumor approximately 400 μ m apart (Figure S1). Five fields per cryosection, at x200 magnification, were randomly selected for each tumor.

Statistics

Results are expressed as the means \pm SEM (standard error of the mean). The Mann–Whitney U-test and the one-way ANOVA-test, followed by Dunnett's multiple comparison post-test, were used for statistical analyses. Differences were considered to be significant if the p-value was < 0.05 .

Results

Production of SFN-LNCs

Solubility studies of SFN

The solubility of SFN in six different excipients (five oils and one co-surfactant) that can be used to formulate LNCs was analyzed at 1% (w/w). SFN was only soluble in Transcutol® HP with a maximum solubilization of 120 mg/g (Table 1).

Table 1: Solubility of SFN in various excipients at 1% (w/w) (S: Soluble, NS: not soluble)

Excipients	Function	Solubility
Transcutol® HP	Co-surfactant	S
Labrafil® M1944CS	Oil	NS
Peceol™	Oil	NS
Labrafac® WL1349	Oil	NS
Captex® 8000	Oil	NS
Oleic acid $\geq 99\%$	Oil	NS

Formulation of SFN-LNCs

Based on the solubility of SFN in Transcutol® HP and the previous results of Roger *et al.* (2011), a mixture of Labrafac® CC, Labrafil® M1944CS, and Lipoid® S75-3 was used to formulate LNCs. B-LNCs had a mean diameter of 49 ± 1 nm and a narrow size distribution (PDI = 0.11) (Table 2).

We assessed the physicochemical characteristics of SFN-LNCs (filtration, peak number, particle size, and PDI) as a function of the amount of SFN (15, 20, 30, 50 and 84 mg) solubilized in Transcutol® HP (0.7 g). The formulations became increasingly difficult to filter as the quantity of SFN increased and showed a greater and heterogeneous size distribution (Table S1). We set the amount of SFN used in the formulation to 20 mg based on these observations. The resulting SFN-LNCs had

physicochemical properties similar to those of B-LNCs and a drug payload of 2.11 mg/g of LNC dispersion with an encapsulation efficiency > 90% (Table 2).

Table 2: Characterization of B-LNCs (n = 6) and SFN-LNCs (n = 17)

Sample	Size (nm)	PDI	Zeta Potential (mV)	Drug payload (mg/g)	Encapsulation Efficiency (%)
B-LNCs	49 ± 1	0.11 ± 0.01	-7.9 ± 0.4	-	-
SFN-LNCs	54 ± 1	0.15 ± 0.01	-7.8 ± 0.6	2.11 ± 0.03	105 ± 1

In vitro release profile

We next assessed the percentage of SFN released from SFN-LNCs into DPBS buffer over time (Figure 1). We observed a burst release of SFN within the first 8 h and the dose reached ~11% of the total SFN. Subsequently, SFN was gradually and sustainably released: ~20% of the initial dose within 120 h.

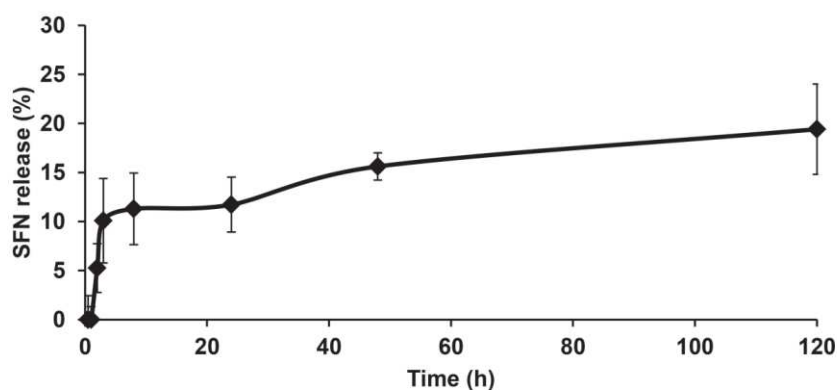


Figure 1: SFN release profile from LNCs in DPBS (n = 4).

Storage stability

SFN-LNCs were physically stable at 2-8°C for at least four months (Table S2). We observed no meaningful change in mean LNC size, pH, or zeta potential. In addition, there was no variation in drug payload after four months.

Table S2: Stability data of SFN-LNCs stored at 2-8°C (size, polydispersity, zeta potential, and drug payload) (n = 4)

Time (day)	Size (nm)	PDI	Zeta potential (mV)	Drug payload (mg/g)
0	54 ± 2	0.14 ± 0.01	-7.4 ± 0.6	2.09 ± 0.03
15	53 ± 2	0.14 ± 0.01	-9.7 ± 1.0	2.24 ± 0.04
30	54 ± 2	0.13 ± 0.01	-9.0 ± 1.5	2.19 ± 0.01
60	55 ± 6	0.13 ± 0.01	-9.6 ± 0.6	2.24 ± 0.02
120	51 ± 2	0.13 ± 0.01	-9.7 ± 1.7	2.22 ± 0.06

In vitro and in vivo effects of SFN-LNCs

Effect of SFN-LNCs on U87MG tumor cells and endothelial tube formation

Neither free SFN nor SFN-LNCs altered the growth of U87MG cells at concentrations below 5 μM (Figure 2a). Above 5 μM , U87MG cell survival decreased, corresponding to an IC_{50} of $7.39 \pm 0.16 \mu\text{M}$ for free SFN, $7.56 \pm 0.07 \mu\text{M}$ for SFN-LNCs AND $>20 \mu\text{M}$ for B-LNCs. The viability of U87MG was unaltered by B-LNCs, except at the highest concentration tested. We examined the antiangiogenic properties of SFN-LNCs using a HUVEC tube-formation assay (Figure 2b, c). Treatment with B-LNCs did not affect EGM-2-induced tube formation, whereas incubation with 5 or 10 μM of SFN-LNCs or SFN markedly and dose-dependently abolished tube formation (Figure 2b, c).

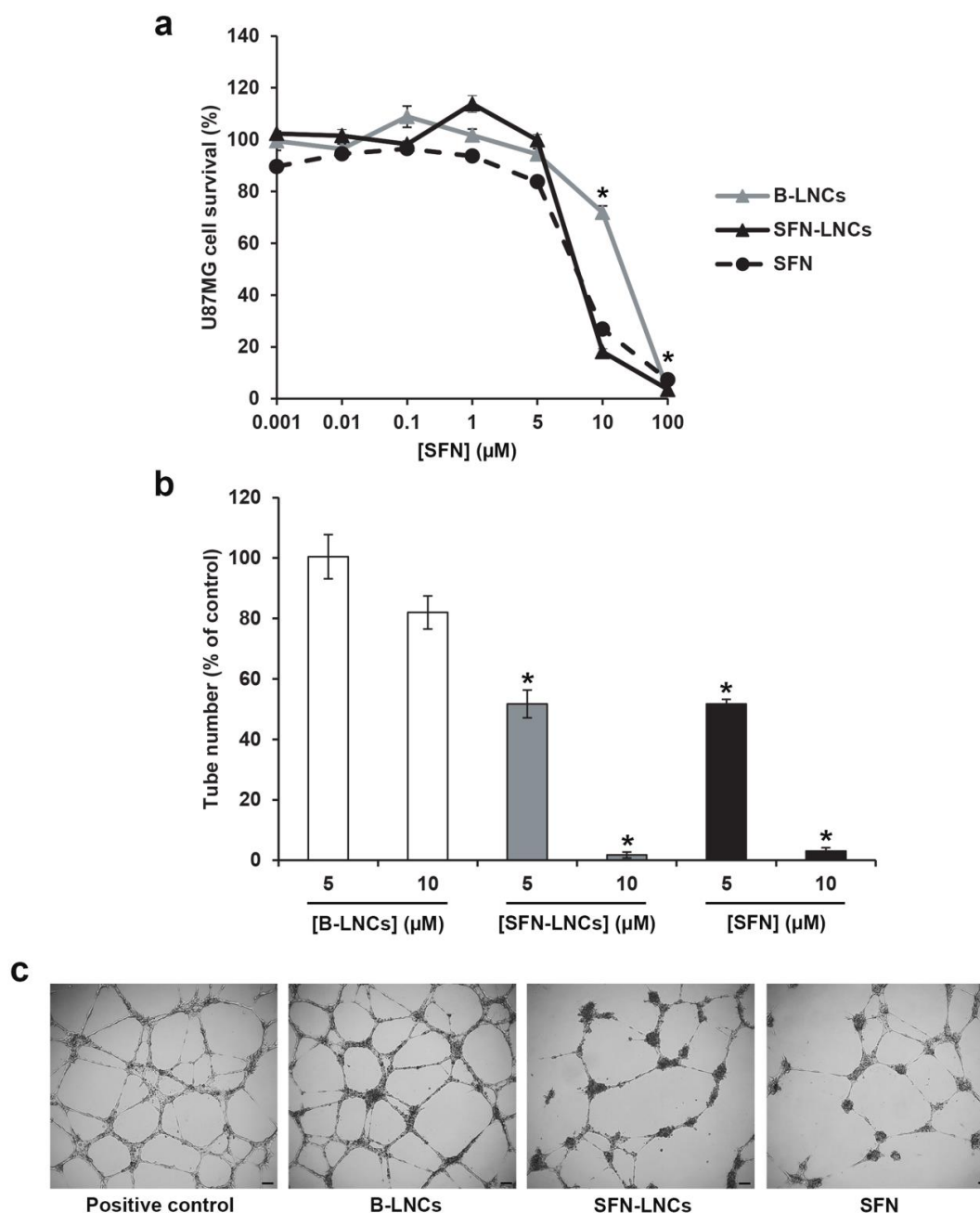


Figure 2: Effect of SFN-LNCs on U87MG tumor cell viability and the ability of HUVECs to form tube-like structures. (a) U87MG cell viability following exposure to various concentrations of B-LNCs, SFN-LNCs, or SFN (0.001–100 μM). Data are expressed as the means \pm SEM ($n = 4$). The results obtained for U87MG cells grown in culture medium alone were considered to correspond to 100% survival ($*P < 0.05$ for B-LNCs, SFN-LNCs or SFN vs culture medium alone, Mann-Whitney U-test). (b) and (c) Formation of tube-like structures by HUVEC following treatment with B-LNCs, SFN-LNCs, or SFN (5 or 10 μM). (b) Angiogenesis was quantified by manually counting the number of tube-like structures. Results are presented as the means \pm SEM. The number of tube-like structures obtained in EGM-2 alone was considered to correspond to 100% ($*P < 0.05$ for SFN-LNCs or SFN vs EGM-2, Mann-Whitney U-test). (c) Representative phase-contrast micrographs of HUVEC tube formation on Matrigel 16 h after treatment with 5 μM B-LNCs, SFN-LNCs, or SFN. The positive control corresponded to EGM-2 medium alone (scale bar = 100 μm).

Evaluation of the intratumoral administration of SFN-LNCs in the orthotopic U87MG GB model

We assessed the effect of intratumoral CED infusion of SFN-LNCs on U87MG growth and angiogenesis as described in Figure S1.

Tumor volume alterations. There was no significant difference in tumor volume between control vehicle-treated groups (HBSS and B-LNCs) and SFN-LNC- or SFN-treated groups four days after administration (HBSS mean = $7.2 \pm 0.6 \text{ mm}^3$, B-LNC mean = $9.1 \pm 0.9 \text{ mm}^3$, SFN-LNC mean = $9.5 \pm 0.9 \text{ mm}^3$, SFN mean = $7.4 \pm 0.7 \text{ mm}^3$, $P > 0.05$) (Figure 3a). The tumor volume was approximately 8 mm^3 . Control vehicle-, SFN-LNC- and SFN-treated-tumors showed the same growth rate between MRI (D13) and histological and immunofluorescence analyses (D16) (data not shown).

Tumor perfusion analyses. We determined tumor perfusion from ASL-MRI perfusion maps to assess tumor microvasculature. For all animals, tumor blood flow (TBF) was reduced with respect to blood flow in the surrounding tissue or contralateral brain tissue (Figure 3b, c). There was a slight increase of blood flow in the tumor core of mice treated with SFN-LNCs relative to that of control vehicle-treated mice and SFN-treated mice (Figure 3b, c) (HBSS mean = $50 \pm 3 \text{ mL}/100 \text{ g}/\text{min}$, B-LNC mean = $51 \pm 2 \text{ mL}/100 \text{ g}/\text{min}$, SFN-LNC mean = $62 \pm 4 \text{ mL}/100 \text{ g}/\text{min}$, SFN mean = $49 \pm 3 \text{ mL}/100 \text{ g}/\text{min}$, $P < 0.05$: SFN-LNC vs HBSS).

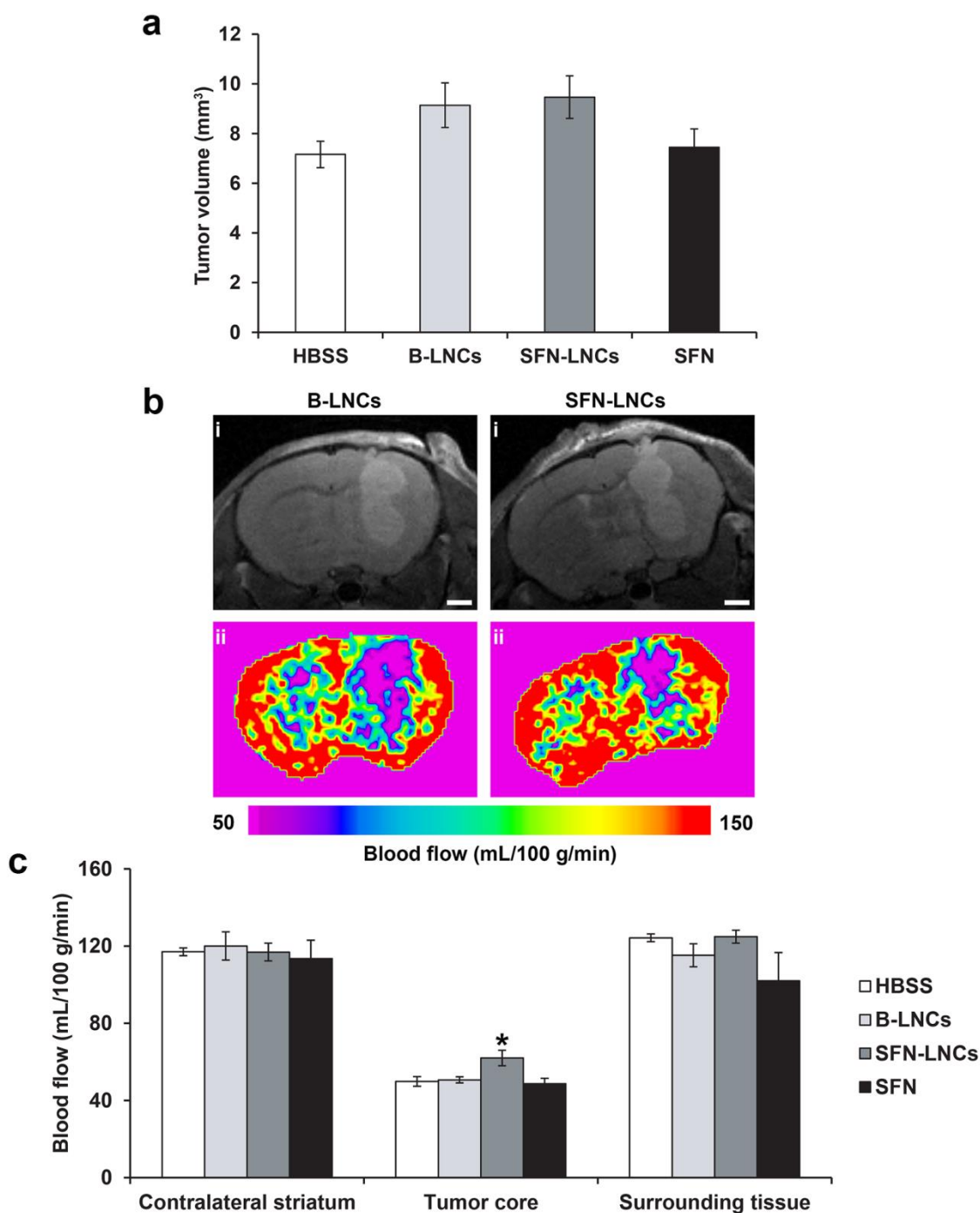


Figure 3: Effect of SFN-LNCs on tumor volume and perfusion in U87MG-bearing mice. (a) Tumor volume distribution in each group, calculated from MRI images four days after treatment (D13). (b) Perfusion MRI images of B-LNC- and SFN-LNC-treated U87MG glioma-bearing mice on day 13. T2-weighted morphological images are shown in the top panels (i), and perfusion maps in the bottom panels (ii). (c) Graph showing blood-flow values in the tumor core, the surrounding tissue, and the contralateral striatum. Blood flow (mL/100 g/min) was measured using the ASL perfusion MRI method (* $P < 0.05$ for SFN-LNCs vs HBSS, one-way ANOVA-test followed by Dunnett's multiple comparison post-test).

Immunofluorescence analyses of proliferative intratumoral Ki67⁺ cells and CD31⁺ vessels. SFN-LNC or SFN treatment decreased the number of intratumoral Ki67⁺ proliferative cells in U87MG-bearing mice relative to control vehicle-treated

groups seven days after administration (Figure 4a, b) (HBSS mean = 671 ± 24 Ki67⁺ cells/mm², B-LNC mean = 629 ± 10 Ki67⁺ cells/mm², SFN-LNC mean = 537 ± 22 Ki67⁺ cells/mm², SFN mean = 556 ± 11 Ki67⁺ cells/mm², $P < 0.05$: SFN-LNC or SFN vs HBSS). SFN-LNC treatment reduced tumor vessel area relative to HBSS, B-LNC or free SFN treatment (Figure 4a, c) (HBSS mean = 130 ± 9 μm^2 , B-LNC mean = 124 ± 6 μm^2 , SFN-LNC mean = 105 ± 5 μm^2 , SFN mean = 128 ± 6 μm^2 , $P < 0.05$: SFN-LNC vs HBSS). Control vehicle-, SFN-LNC- and SFN-treated animals had similar numbers of tumor vessels (data not shown).

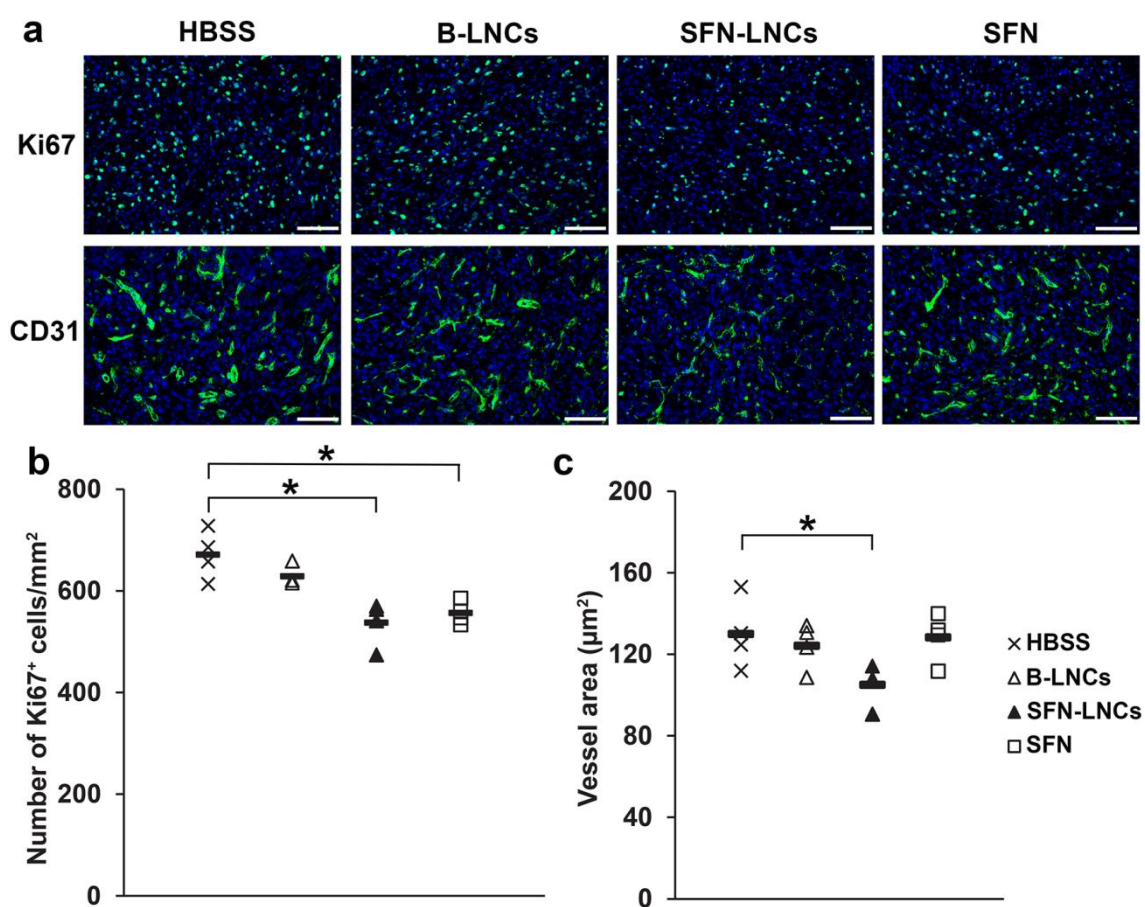


Figure 4: Effect of SFN-LNCs on Ki67⁺ cell number and CD31⁺ vessel area. (a) Immunofluorescence staining for Ki67 and CD31 in the tumor on day 16 in each group of animals (scale bar = 100 μm). (b) and (c) Quantitative results for Ki67 and CD31 immunofluorescence. Results are expressed as the mean number of Ki67⁺ cells per mm² \pm SEM (b) or CD31⁺ vessel area \pm SEM (c) (* $P < 0.05$ vs HBSS, one-way ANOVA-test followed by Dunnett's multiple comparison post-test).

Discussion

SFN has been shown to be a potential targeted molecular therapeutic agent for various solid tumors including GBs. It targets RTKs as well as the RAF/MEK/ERK pathway and thus acts as a combined antiangiogenic and antitumorigenic drug. However, poor

aqueous solubility and undesirable side effects limit the clinical application of SFN, including local treatment. Strategies to overcome these drawbacks need to be implemented. Among such strategies, nanoformulations of SFN might be of interest by combining the intrinsic toxicity of the drug with the nanodelivery approach. Numerous studies have assessed SFN encapsulated or entrapped in various nanocarriers, including polymeric carriers [316–323], lipid-based carriers [320,324–330] and polymer-lipid hybrid nanoparticles [331,332]. These nanocarriers showed promise in liver and gastric cancer models. However, most of these formulations have major drawbacks, such as the presence of organic solvents or toxic compounds, preventing their clinical use. Here, we encapsulated SFN in solvent-free LNCs, which were produced using only GMO-free and GRAS excipients [333–335].

We determined the solubility of SFN in various LNC constituents for their formulation. Among them, only Transcutol® HP was able solubilize SFN. As this compound is a co-surfactant, Labrafac® WL1349 and Labrafil® M1944CS were added to constitute the oily phase of the formulation. SFN-LNCs have a PDI < 0.2, demonstrating the mono-dispersity of the formulation, and the average size was 54 ± 3 nm. The surface charge of SFN-LNCs was negative, favoring the dispersion of LNCs instead of their agglomeration. The encapsulation efficiency of SFN-LNCs was > 90%, indicating that the SFN was highly entrapped within the LNCs. SFN-LNCs were stable for over four months at 4°C, without alteration of their characteristics. After five days in DPBS buffer, approximately 20% of the SFN was released. This low release profile suggests that most of the SFN remained associated with the LNCs, which may be beneficial, as it would allow sufficient time for cells to capture the loaded LNCs. High encapsulation efficiency and slow drug release have also been described for liposomal formulations of SFN [320,327].

SFN-LNCs had a similar cytostatic effect against tumor cells and endothelial cells as free SFN, suggesting that its activity is conserved by LNC encapsulation. We evaluated the *in vivo* effect of SFN-LNCs in nude mice bearing an U87MG human GB orthotopic xenograft after their CED intratumoral administration. We were particularly interested in detecting early vascular changes in response to SFN-LNCs, as endothelial cells are highly sensitive to SFN. We thus performed ASL-MRI, a noninvasive and quantitative technique that measures perfusion by magnetically

labeling water as a freely diffusible endogenous tracer [336], on large established U87MG tumors (approximately 8 μ L). Several studies have already used this technique to evaluate early antiangiogenic treatment responses of brain tumors in humans [337,338], and rodents [339–342]. Blood flow in the tumor core was reduced relative to normal brain tissue, in accordance with the results of Sun *et al.* (2004) [343]. Such impaired blood flow is largely described in GBs, resulting from a dilated, tortuous, disorganized, and leaky vasculature [344–346]. Four days after treatment, we observed an increase in perfusion in the tumor core of animals treated with SFN-LNCs, relative to that in control animals and animals treated with SFN alone. The SFN-LNC treated group showed a TBF value of 62 ± 4 mL/min/100g, whereas the HBSS control group showed a TBF value of 50 ± 3 mL/min/100g. This increase in blood flow was localized only to the tumor core. Blood flow was not altered in the surrounding tissue nor in the contralateral striatum. It is now well established that TBF is dependent on tumor size, irrespective of the type of solid tumor [314,347,348]. Lemaire *et al.* (2016) observed a reduction of approximately 3 mL/min/100g of TBF for every 1 μ L increase in tumor volume. The average tumor size was 9.5 ± 0.9 μ L and 7.2 ± 0.5 μ L for the LNC-SFN treated and HBSS control groups, respectively. Thus, the increase of TBF observed in the LNC-SFN treated group was not due to a decrease in tumor volume. In addition to the increase of perfusion with SFN-LNC treatment, we observed a decrease in tumor vessel area. These data suggest that SFN-LNCs may have normalized abnormal vessel structures, potentially leading to increased blood perfusion. Vessel normalization following treatment with SFN or other tyrosine kinase inhibitors has already been described for various malignancies [74,301,349–351]. We did not observe such vascular changes following the treatment of U87MG-bearing mice with free SFN, highlighting the potential of SFN-LNCs. This may be due to the capacity of LNCs to improve the retention of SFN within the tumor. The prolonged retention of LNCs in brain tumors following intratumoral CED administration was previously shown using LNCs loaded with a lipophilic complex of Rhenium-188 (LNC¹⁸⁸Re-SSS) [181,352]. Seventy percent of the ¹⁸⁸Re-SSS activity was present in the tumor region 24 h after LNC¹⁸⁸Re-SSS injection, whereas free ¹⁸⁸Re-perrhenate was rapidly eliminated in the urine and feces. In addition to the induction of early vascular changes, SFN-LNC-treatment reduced the number of proliferative Ki67⁺ cells in the tumor. We also observed this effect following treatment with free-SFN, probably due to the faster cellular uptake of free SFN by tumor cells than by endothelial cells.

Although SFN-LNCs increased tumor perfusion and reduced tumor vessel area and the number of Ki67⁺ cells, this was not sufficient to modify the growth rate of U87MG tumors. However, the treatment was carried out on large established U87MG tumors to allow perfusion analyses, which required a tumor thickness of 1.5 mm. This condition was not adapted to achieving a therapeutic effect, given the aggressiveness of U87MG tumors (median survival of approximately 24 days following intrastriatal administration of 5×10^4 U87MG cells).

Strategies which improve vascular function in GBs provide a window of opportunity for enhancing the efficacy of chemotherapy or radiotherapy [353]. For example, the delivery of temozolomide in a preclinical intracerebral model of glioma increased after treatment with the angiogenesis inhibitor SU5416, which restored the capillary architecture [354]. Wang *et al.* [355], showed that GB-bearing mice treated with irinotecan in combination with bevacizumab, an antibody to VEGF, survived longer than those treated with irinotecan alone. Thus, the combination of SFN-LNCs with other chemotherapy treatments could be considered to improve efficacy in GB patients.

Conclusion

Here, we demonstrated successful encapsulation of SFN in LNCs by a phase-inversion process, without the use of organic solvents. SFN-LNCs showed *in vitro* cytotoxic activity against human U87MG glioma cells and endothelial cells, similar to that of free SFN. Intratumoral CED administration of SFN-LNCs to U87MG-bearing mice decreased the proportion of proliferating cells and induced an early increase in tumor blood flow, associated with a reduced area of tumor vessels, consistent with the induction of a vascular normalization process. The induction of this process by SFN-LNCs suggests their possible use to enhance the efficacy of chemotherapy or radiotherapy.

Acknowledgements

We are most grateful to the PRISM core facility and, in particular, to Dr. F. Franconi (Rennes-Angers, France) for her technical support. We also thank P. Legras and J. Roux (Service Commun d'Animalerie Hospitalo-Universitaire, Angers, France) and

Nolwenn Lautram (INSERM U1066, Angers, France) for providing facilities and Alex Edelman and Associates for correcting the manuscript.

Funding

This research was supported by grants from the “Fondation de France”, “Ligue Contre le Cancer du Grand-Ouest, Comité Départemental du Maine-et-Loire”, “Association en Avant la Vie”, and the European Commission, Education, Audiovisual and Culture Executive Agency (EACEA), through the NanoFar Erasmus Mundus joint Doctoral program.

Chapter 2

Lipid nanocapsule transport across Calu-3 based model of nasal epithelial barrier

Scientific context

The BBB restricts the transport of potential drugs to the brain site for treatment of malignant brain tumors. One innovative approach to address this challenge is to administer the therapeutics intranasally to noninvasively bypass the BBB. The intranasal route can thus transport drugs directly to the brain from the nasal cavity along the olfactory and trigeminal nerves. Nanosized drug carriers were shown to improve the intranasal delivery of drugs to the brain compared to equivalent drug solution formulations. These nanocarriers firstly should cross nasal epithelial barriers before reaching the brain site. LNCs have shown promising results both in crossing epithelial barriers and also drug delivery to the malignant brain tumors. Therefore, these nanocapsules could be a favorable candidates for nose-to-brain drug delivery. To employ LNCs for this purpose, their integrity after transport across nasal epithelial barrier must be maintained to avoid the release of the cargo before reaching the brain site. The aim of the present study is to investigate the fate of LNCs after their transport across a Calu-3 based nasal epithelial barrier model. We employed Förster Resonance Energy Transfer (FRET) to evaluate the fate of nanocapsules. The results show that nanocapsules enhances the delivery of hydrophobic fluorophore across epithelial barrier; however, the LNCs were degraded. This study shows that LNCs should be redesigned in order to be efficient for nose-to-brain drug delivery.

Lipid nanocapsule transport across Calu-3 based model of nasal epithelial barrier

Milad Pourbaghi Masouleh ^{1,2}; Claudia Conte ^{2,3}; Cynthia Bosquillon ²; Philippe Menei^{1,4}; Snow Stolnik^{2*}

¹ *CRCINA, INSERM, Université de Nantes, Université d'Angers, Angers, France.*

² *Division of Drug Delivery and Tissue Engineering, School of Pharmacy, University of Nottingham, UK.*

³ *Department of Pharmacy, University of Napoli "Federico II", Napoli, Italy.*

⁴ *Département de Neurochirurgie, CHU, Angers, France*

* Corresponding author: snow.stolnik@nottingham.ac.uk

Contribution: All the study is done by Milad Pourbaghi Masouleh.

Abstract

This study investigated the ability of lipid nanocapsules (LNCs) to cross the nasal epithelial barrier, represented by the in vitro cell culture model of Calu-3 monolayers. The LNCs with different matrix component and particle size (30, 50 and 100 nm) were prepared by a low-energy emulsification method. Toxicity studies demonstrated that size and composition of LNCs influenced the viability of Calu-3 cells. Incorporation of a hydrophobic fluorophore, 3,3'-Dioctadecyloxacarbocyanine Perchlorate (DiO) demonstrates that LNCs significantly increased internalization of the fluorophore into the cells, and the transport of the encapsulated material across the epithelial cell monolayer in a size dependent fashion, while the layer integrity remained uncompromised, as judged from transepithelial electrical resistance measurements. The incorporation of a Förster Resonance Energy Transfer (FRET) fluorophore pair (DiO:DiI (1,1'-Dioctadecyl-3,3,3',3'-Tetramethylindocarbocyanine Perchlorate) in an optimized ratio) was used to study the fate of nanocapsules both inside the cells and after transport across the cell monolayer. The confocal microscopy analysis demonstrated as appearance of a FRET donor probe fluorescence inside the cells after 2 and 4 hours, which occurs when the FRET pair is separated, indicating hence that the nanocapsules integrity is affected. Furthermore, co-localization studies point to a possible presence of the nanocapsules inside the lysosomes. The results suggest that the nanocapsules are not intact after transport.

Keywords: Lipid nanocapsules, FRET, Nasal epithelial barrier, Calu-3, Integrity

1. Introduction

Intranasal drug delivery is a systemic drug administration route which has been exploited for many years in treatment of patients [356]. The nasal mucosa allows a rapid and high absorption of therapeutics thanks to: i) a highly vascularized and permeable endothelial membrane [357], ii) the avoidance of first-pass metabolism [358], iii) a large surface area for interaction [359] and iv) ease of accessibility [356]. Lately, the nose-to-brain path has attracted great interest to the passage from the nasal cavity to the brain through the olfactory and trigeminal nerves, bypassing the blood brain barrier and offering quick delivery of drugs from the nose to the brain site [360–363]. Furthermore, intranasal transport is a non-invasive and safe way of drug administration which reportedly has resulted in high patient compliance [364]. However, the amount of drug delivered to the brain through this administration route is less than 1% of quantity of the applied drug. For this reason, the nose-to-brain delivery is therapeutically viable only for highly potent drugs, or if the drug transport is enhanced by using novel drug delivery techniques [365]. In this context, various nanosystems such as nanosuspensions [366], nanoemulsions (NEs) [367], nanostructures [368,369], liposomes [286] and micelles [370] have been applied to enhance the delivery of drugs from the nose to the brain site. The inherent mechanisms exerted by these nanosystems were reported as prolonged retention in the nasal mucosa, improved permeation through epithelium cells, avoidance of enzymatic degradation and by-passing of the P-gp efflux pump [371,372]. Lochhead and Thorne [373] suggested that there are three sequential transport steps essential for a therapeutic substance to be transported to far-reaching sites within the central nervous system (CNS) following intranasal administration: (1) crossing the olfactory or respiratory epithelial barriers located within the nasal passages, (2) conveyance from the nasal mucosa to area of brain entry near the pial brain surface in the cranial compartment (i.e. entrance of peripheral olfactory or trigeminal nerve-associated sections incorporating the delivery pathways), and (3) movement of the therapeutic substance from these entries to other locations of the CNS. As it appears, the first issue that should be addressed for intranasal drug delivery to the brain by nanosystems is the fate of the applied nanocarriers after crossing the nasal epithelial barrier.

Lipid nanocapsules (LNCs) are nano-sized drug carriers obtained through a low-energy emulsification process and can be formulated with 'generally recognized as safe' excipients in absence of organic solvents [334]. Furthermore, LNCs are capable to encapsulate many therapeutics and more specifically hydrophobic drugs [134]. Up to now, LNCs have shown promising results for brain targeting [374] and more specifically for the treatment of malignant brain tumors [172,174,179,191,375–378]. These nanocapsules could be favorable candidates for nose-to-brain drug delivery if they can efficaciously cross nasal epithelial barrier. To date, no investigation has done on behavior of LNCs in transport of cargoes across nasal epithelial barrier, however these nanocapsules have already shown favorable properties for delivery of different hydrophobic drugs such as paclitaxel [142] and SN38 [141] across intestinal epithelial barrier models.

For drug delivery across epithelial barriers, it is crucial to design nanocarriers that are able to be absorbed while maintaining their integrity, and therefore capable to act as stable nanocarriers after crossing the epithelial barriers. Up to now, numerous physicochemical characterisation techniques such as microscopy (TEM, AFM, confocal), spectroscopy (IR, UV, FTIR, NMR) and dynamic light scattering (size and charge analysis) have been used to characterize the overall nanocarrier structure or its individual components, but not their integrity. Therefore, new techniques are necessary to investigate the fate of these nanocarriers. In nanomedicine, the FRET mechanism has been widely employed for several goals, including biosensing, molecular imaging and tracking of drug release as well as nanocarrier degradation [379]. FRET is based on non-radiative energy transfer (long-range, <10 nm, dipole–dipole coupling) from a donor fluorophore in an electronic excited state to a second fluorophore which is the acceptor and has a spectral overlap with the donor emission spectrum and the acceptor absorption spectrum [380]. In this regard, applying the FRET effect in preparation of LNCs offers the possibility to investigate the fate of these nanocapsules after their interaction with cells or the cell microenvironment. Utilizing the FRET effect, Roger et al. [381], demonstrated that glyceryl tricaprilate-based LNCs with size of about 55 nm can cross the intestinal epithelial barrier model while maintaining their integrity. In addition, Groo et al. [382], demonstrated that the same type of LNCs can maintain their integrity after exposure to pig intestinal mucus. Conclusively, these findings show that LNCs could enhance the delivery of

hydrophobic drugs across intestinal epithelial barrier while they maintain their integrity. However, the fate of these nanocarriers after crossing nasal epithelial barrier is still unknown.

In this study, LNC formulations with different particle sizes of 30, 50 and 100 nm, considering the size range appropriate for cellular internalization and transport across epithelial cell monolayers [383], were fabricated. Moreover, in order to find out the behavior of nanocapsule composition on epithelial cell monolayer, three LNC formulations with different matrix components with a size of 50 nm were also prepared. The Calu-3 cell line was selected to prepare a nasal epithelial barrier model which is representative of epithelial cells from respiratory [384] and olfactory [267] regions. Firstly, the toxicity of the nanocapsules on Calu-3 cells were determined. Based on the toxicity results, the prepared formulations were tested on Calu-3 cell monolayer to obtain the transport capability of the nanocapsules. Finally, by using FRET method, we characterized the fate of nanocapsules in both undifferentiated and polarized Calu-3 cells. Intracellular trafficking of nanocapsules was further analyzed by confocal microscopy and lysosomal staining.

2. Materials and methods

2.1. Materials

Methanol (MeOH), tetrahydrofuran (THF) and dimethyl sulfoxide (DMSO) were purchased from Sigma-Aldrich (Poole, UK). Medium chain triglycerides (Labrafac™ lipophile WL 1349), oleoyl polyoxyl-6 glycerides (Labrafil® M1944 CS) and diethylene glycol monoethyl ether (Transcutol® HP) were gifts from Gattefosse S.A (Saint-Priest, France). Glycerol tricaprylate ≥99% was purchase from Sigma-Aldrich (Poole, UK). Lipoïd® S75-3 (soybean lecithin at 70% of phosphatidylcholine and 10% of phosphatidylethanolamine) and Kolliphor® HS15 (a mixture of free polyethylene glycol 660 and polyethylene glycol 660 hydroxystearate) were purchased from Lipoïd GmbH (Ludwigshafen, Germany) and BASF (Ludwigshafen, Germany), respectively. NaCl was purchased from Sigma-Aldrich (Poole, UK). Ultrapure water was obtained from a Milli-Q® Advantage A10 System (Merck Millipore, Darmstadt, Germany). 3,3'-Diocadecyloxacarbocyanine Perchlorate (DiO) and 1,1'-Diocadecyl-3,3,3',3'-Tetramethylindocarbocyanine Perchlorate (DiI) were purchased from Sigma-Aldrich

(Poole, UK). Calu-3 cells were purchased from the American Type Culture Collection (Rockville, MD, USA) and used between passage 30 and 40. Twelve well polycarbonate Transwells® (with 0.4 µm pore size and a surface area of 1.12 cm²) were obtained from Corning Costar (Kennebunk, US). All the cell culture reagents and chemicals were procured from Sigma-Aldrich (Poole, UK). Dulbecco's modified Eagle's medium / Ham's F12 nutrient mixture (DMEM: F12), trypsin/EDTA, antibiotic/antimycotic solution, fetal bovine serum (FBS), L-glutamine, nonessential amino acids (NEAA) and 4-(2-hydroxyethyl)-1-piperazineethanesulfonic acid (HEPES) were purchased from Sigma-Aldrich (Poole, U.K.). Hank's balanced salt solution (HBSS), Triton X-100, 4-(2-hydroxyethyl)-1-piperazineethanesulfonic acid (HEPES), paraformaldehyde, Hoechst (33342) nucleic acid stain, and were also obtained from Sigma-Aldrich. Phosphate buffered saline (PBS) was purchased from Oxoid Ltd. (UK). Lactic dehydrogenase assay (LDH) was obtained from Sigma-Aldrich, and CellTiter 96 AQueous Cell Proliferation Assay (MTS) was obtained from Promega (USA).

2.2. Preparation and characterization of LNC formulations

2.2.1. LNC formulations

Blank LNC: Blank LNC (B-LNC) batches were prepared based on the patent filed by Heurtault et al. [135], through a phase-inversion process [148]. In this method, the PEG-chains of the Kolliphor® HS15, which is one of the surfactants of the LNC, are dehydrated following an increase in temperature. This phenomenon leads to lowering the Hydrophile-Lipophile Balance (HLB) and induces the phase inversion to water in oil emulsion from oil in water emulsion. In order to study the effect of LNC size and matrix component, different LNC batches were prepared (**Table 1**). Briefly, the oily phase (Labrafac™, Labrafil®M1944 CS, Transcutol® HP, and Glyceryl tricaprylate) which could be attributed to the core of lipid nanocapsules were mixed with Lipoid® S75-3, and heated by a hot plate at 80°C under magnetic stirring in order to obtain a homogenous mixture. In the next step, once the ambient temperature of the mixture was recovered, the other compounds of the formulation i.e., water, NaCl and Kolliphor® HS15 were introduced. Thereafter, the heating cycles were performed between 60 and 90°C with a gradient of 4°C/min while the system was quenched (addition of ice-cold water which irreversibly shocks the system) at the temperature which phase-inversion happens in each batch (71°C for L30, 72°C for L50, 75°C for

L50, 75°C for T50 and 72°C for C50) by adding the determined amount of 0°C Milli-Q® water during the third cycle. Finally, the agitation of 1200 rpm was provided until the solution reached the room temperature. At last, the LNC formulation was filtered utilizing Minisart® 0.2µm filter (Sartorius, Goettingen, Germany) (see chapter 1, 2.1. Lipid nanocapsule formulation).

Table 1: Amount of different excipients for preparation of different batches of lipid nanocapsules

Formulation	L30	L50	L100	T50	C50
Labrafac™ (mg)	846	1028	1209	400	-
Labrafil®M1944 CS (mg)	-	-	-	1000	-
Transcutol® HP (mg)	-	-	-	700	-
Glyceryl tricaprilate (mg)	-	-	-	-	1200
Lipoid® S75-3 (mg)	75	75	75	150	65
Kolliphor® HS15 (mg)	1934	850	484	1000	1000
NaCl (mg)	103	90	157	100	75
Water at 25°C (µL)	2055	296	3143	1800	1800
Water at 0°C (mL)	12.5	12.5	12.5	5	5.8

DiO loaded LNC: In order to encapsulate the DiO inside the LNC (DiO-LNC), the same procedure was applied. Firstly, a stock solution of DiO in DCM at a concentration of 33.9 mM was prepared. Then, 65 µL of this solution was added to the oily compartment of the formulation, and gently mixed for 20 minutes at room temperature. In order to eliminate DCM from the system, the mixtures, while being stirred, were water-bathed at 60°C for 1 hour and the rest of the steps for preparation of LNC formulations were taken as mentioned before. Finally, DiO-LNC formulations were dialyzed at 4°C (10 kDa cut-off, Spectra/Por®, Spectrum® Labs) overnight, filtered again and kept at 4°C.

FRET loaded LNC: DiO and Dil were selected as the FRET fluorophore pair [380,385]. Firstly, to find the ideal FRET-LNC, L50 formulations with different weight ratios of DiO to Dil (DiO:Dil) (w:w) were prepared. In this regard, stock solutions of DiO in DCM (1.13 mM) and Dil in DCM (1.07 mM) were prepared. Then, different volumes of these solutions were added to the oily compartment in order to have a DiO:Dil ratio of 2:1, 1:1, 1:2, 1:5 and 1:10 (w:w). The rest of the steps were taken as it was described for DiO-LNC. The final FRET-LNC formulations were prepared based on the best resulting DiO:Dil ratio with sixteen times more concentrated stock solutions of fluorophore in DCM.

2.2.2. Characterization of LNC formulations

The hydrodynamic diameter, polydispersity index (PDI) and zeta potential of LNC batches were determined at intensity in the range 10^4 – 10^6 counts/s and measurements were performed at 25 °C on 90° angle on a Zetasizer Nano ZS (Malvern Instruments Ltd.). The samples were diluted 1:60 (v:v) in Mili-Q water in order to assure optimal scattered intensity on the detector.

2.2.3. Fluorescence measurement

The experiments with DiO-LNC were assessed by fluorescence spectroscopy using an Infinite M200 plate reader (Tecan, Switzerland) at excitation slit width of 5 nm, an emission slit width of 5 nm and an integration time of 0.5 s, at $\lambda_{ex}/\lambda_{em}$ 484/529 nm. Quantification of DiO was calculated by means of standard calibration curves derived from a mixture of DiO-DMSO stock solution/THF/MeOH for control sample and DiO-MeOH stock solution/LNC/THF/MeOH for LNC samples. Fluorescence spectra were recorded on a (Varian Cary Eclipse, UK). Emission spectra were collected from 470 to 600 nm with a 1 nm increment. An excitation slit width of 5 nm, an emission slit width of 5 nm and an integration time of 0.5 s were applied. FRET ratio (was calculated according to the following equation below:

$$FRET\ ratio = \frac{I_A}{I_D + I_A}$$

where I_D and I_A are the maxima of fluorescence intensity of the donor (502 nm) and acceptor (568 nm), respectively. For the experiments done with L50 to find the optimum DiO:Dil ratio, I_A was considered as the maximum of fluorescence at the second peak (acceptor) (**Method S2**).

2.3. Cell Studies

2.3.1. Calu-3 Cell culture

Calu-3 cells were cultured in Dulbecco's modified Eagle's medium/Ham's F12 nutrient mixture (DMEM: F12) 1:1 completed with 10% v/v of fetal bovine serum (FBS, non USA origin and sterile filtered), 1% v/v of 2 mM L-glutamine, 1% v/v of penicillin-

streptomycin antibiotic solution and 1% v/v of non-essential amino acids. The cells were maintained at 37 °C in a humidified CO₂ atmosphere, the medium was changed every alternative day and cells were subcultured weekly using 0.22% (v/v) EDTA/0.25% (v/v) trypsin solution.

For the purpose of preparing air-liquid interface Calu-3 cell monolayer, cells were seeded at a density of 1 x 10⁵ cells/cm² on Transwells® and incubated overnight. Then the medium was removed from the apical and basolateral chamber which followed by adding 500 µL of the medium in the basolateral chamber and the cells were grown at an air-liquid interface using culture conditions as described previously [258]. The culture medium in the basolateral chamber (500 µL) was changed every two days. Cell layer integrity and tight junction formation was assessed by periodic measurements of transepithelial electrical resistance (TEER), conducted using an EVOM epithelial voltohmmeter (World Precision Instruments, Stevenage, UK). Finally, cells were used for studies after 14 days of culture only if the TEER value was above 500 Ω.cm².

2.3.2. LNC cytotoxicity studies

The effect of B-LNC formulations on cell metabolic activity was determined employing the CellTiter 96 AQueous (MTS) cell proliferation assay kit. The cells were seeded onto 96-well plates in a total volume of 150 µL of culture medium at a number of 1×10⁴ cells/well and incubated for 48 hours prior to the study. Culture medium was removed and replaced with 150 µL of LNC suspensions diluted in HBSS-10 mM HEPES (HBSS-HEPES) at different concentrations of LNC matrix component (0.001 to 5 mg/ml (LNC/HBSS-HEPES)) (**Method S1**) for 4 hours. Cells incubated with HBSS-HEPES or with Triton X-100 (0.2% v/v in HBSS) were used as negative and positive control, respectively. After this interval, LNC formulation samples were removed and cells were washed two times with PBS. Thereafter, 100 µL of culture medium was added into each well, followed by 20 µL of the MTS reagent. After 2h of incubation, MTS absorbance was measured at 490 nm by a plate reader. Percentage of cell metabolic activity from the MTS assay was calculated employing the following equation:

$$\text{Cell viability (\%)} = \frac{S - T}{H - T} \times 100$$

where S is the absorbance measured from the tested samples, T is the absorbance obtained with Triton X-100, and H is the absorbance observed with HBSS-HEPES.

2.3.3. Evaluation of LNC transport across Calu-3 cell monolayers

Transport studies were conducted on confluent Calu-3 cell monolayer. The culture medium was removed and cells washed two times with PBS (37°C). HBSS-HEPES was applied to both chambers of the Transwells®, and cells equilibrated in this solution for 30 min at 37 °C. HBSS-HEPES in the apical chambers was then replaced with 0.5 mL of DiO-LNC formulations diluted in HBSS-HEPES, at 0.05 mg/mL (LNC/HBSS-HEPES) (**Method S1**) and the basolateral solution was replaced with 1.5 mL of fresh HBSS-HEPES. Nanocapsule transport across the Calu-3 cell monolayer was determined by sampling the basolateral solution at regular time points (every 30 min for 4 h), with the replacement of sampled solution with fresh HBSS. Then, the samples were diluted with THF and then MeOH and finally analyzed by a plate reader. In order to study the effect of treatment on monolayer integrity, TEER value was measured every 1 h until the end of the experiment.

2.3.3.1. LNC association with cells

Following the transport studies, association of LNCs with cells after 4 h of experiment was quantified by measuring the intensity of fluorescence resulting from internalized DiO-LNCs. The remnant from the transport studies were removed from the apical chamber, and cells were washed extensively with ice-cold PBS. The quenching of external fluorescence, which distinguishes internalized from surface-adherent DiO, can be accomplished by applying trypan blue [386,387]. In this regard, the cells were washed with trypan blue (diluted in PBS) and ice-cold PBS. Afterward, the cells were lysed after 20 minutes of incubation with Triton X-100 (0.2% v/v in PBS) [388–390]. The cell lysate from each well was sampled and diluted with tetrahydrofuran THF and then methanol MeOH. The amount of DiO was finally quantified. The lysate of untreated cells was used as the control.

2.3.4. Investigation on integrity of LNC using FRET effect

The stability of the different LNCs in HBSS-HEPES was investigated using the FRET effect. In this regard, FRET-LNCs were diluted with HBSS-HEPES to reach 0.05

mg/mL (LNC/HBSS-HEPES) (**Method S1**) and subsequently 0.5 mL of the dilution was added to the apical chamber of Transwell® and after 2 and 4 h, the FRET ratio was calculated.

The integrity of nanocapsules after exposure to Calu-3 cells was estimated through analyzing the FRET effect. At first, in order to comparatively study the integrity of nanocapsules before and after transport, cell monolayers were treated with different FRET-LNC formulations following the same dilution as above. Samples were collected after 2 and 4 h from the apical and basolateral chamber and directly analyzed by fluorescence spectroscopy. Afterwards, the integrity of the cell-associated nanocapsules was analyzed by fluorescence-activated cell sorting (FACS) measurement. Therefore, the treated cells in previous step were collected and prepared samples were analyzed by FACS. Following the detachment of cells by adding trypsin/EDTA, they were washed multiple times by ice-cold PBS and trypan blue/PBS (4% v:v). The cells were collected by centrifugation at 1500 rpm for 10 min. Finally, 200 μ L paraformaldehyde (4%) and 300 μ L PBS were added to the cell pellet, mixed and kept at 4°C. To compare the effect of polarized and undifferentiated Calu-3 cells on the fate of LNCs, Calu-3 cells were seeded on 24-well plates at the density of 1.9×10^5 cells/well for 3 days, then were treated with 0.5 mL of FRET-LNC formulations with the same dilution as before and finally samples were prepared for FACS analysis using a Beckman Coulter Astrios EQ instrument. A blue laser at 488 nm (λ_{em} : 513/526 nm) and a yellow/green laser at 561 nm (λ_{em} : 579/616 nm) were used as excitation source for the detection of DiO and Dil fluorescence, respectively. For FRET detection, the laser at 488 nm with the emission filter at 576/621 nm was used. 10^4 events/sample were acquired and analyzed with the Kaluza Analysis 1.3 Software [385].

2.3.5. Confocal laser scanning microscopy

Calu-3 cells were seeded on cover slips inside 24-well plates; for uptake study 15×10^4 cells were seeded whereas, to avoid Calu-3 cells clumping and hence obtain better images, 8×10^4 cells per well were seeded for FRET and lysosomal confocal microscopy studies. Following 24 hours growth, cells were washed with HBSS-HEPES and 0.5 mL suspension of LNCs (0.05 mg/mL (LNC/HBSS-HEPES) (**Method S1**) was introduced to each well. After 2 or 4 hours, cells were washed twice with HBSS-HEPES

and fixed by adding 0.2 mL paraformaldehyde (4%) and 0.2 mL PBS for 10 min at room temperature. The nucleus was stained by adding Hoechst stain (1 $\mu\text{g}/\text{mL}$) and lysosomes were stained with LysoTracker Red DND-99 (L-Red) (red, λ_{ex} 577 nm- λ_{em} 590 nm) (Sigma, UK) (100 nM) for 1 hour. Confocal imaging was performed using a Zeiss LSM 700 Confocal Laser Scanning Microscope equipped with Argon (488 nm) and HeNe (561, 639 nm) lasers and a 40X/1.2 NA water objective. FRET images were acquired with λ_{ex} 488 nm and spectral filters of 505–530 nm and LP 560 nm for DiO and Dil detections, respectively. Zen 2009 image Software was utilized for image processing.

2.4. Data analysis

Student's t-tests were applied for comparison between two groups GraphPad Prism 7.03 (GraphPad Software, La Jolla, CA, USA). Differences at $p^* < 0.01$ or $p^{**} < 0.001$ were considered as statistically significant.

3. Results

3.1. Development and characterization of LNCs

Table 1 shows compositions of different LNC formulations prepared in this study. In particular, formulations referred to as L30, L50 and L100 (with average particle hydrodynamic diameter around 30, 50 and 100 nm, respectively, **Table 2**), were prepared to study the size effect, with constant composition of the lipid components. The desired particle sizes were achieved by balancing the content of the core forming material and surfactant (i.e increasing the quantity of LabrafacTM and decreasing Kolliphor[®] HS15 content, respectively), as per the ternary diagram [134]. To compare the effect of the composition on LNC behavior in *in vitro* cell model, two additional formulations with an average particle size of approximately 50 nm were prepared following the general protocol; T50 (containing LabrafacTM in addition to Labrafil[®]M1944 CS and Transcutol[®] HP)[141] and C50 (containing only glyceryl tricaprilate) as core materials [142].

Table 2 summarizes characterization of the LNC formulations prepared. The desired sizes of approximately 30, 50 and 100 nm were achieved for specified composition,

with a PDI less than 0.2 and particle size distribution profile indicating relatively homogeneous systems (**Figure S2-A**). All the LNC formulations exhibited a relatively small negative charge, in order of ~ -10 mV in Mili-Q water, indicating the importance of steric stabilization by the surfactants for their colloidal stabilization in the suspensions, as reported previously [148]. Encapsulation of DiO or DiO/Dil pair (FRET-LNC) did not measurably affect the physical characteristics of the LNCs.

Table 2: Physicochemical properties of different batches of LNC formulations

Formulation		L30	L50	L100	T50	C50
B-LNC (N=3) [†]	Size [*] \pm SEM (nm)	28 \pm 3	52 \pm 5	95 \pm 7	45 \pm 4	55 \pm 3
	PDI	0.09	0.04	0.03	0.15	0.06
	Zeta Potential \pm SEM (mV)	-9 \pm 2	-9 \pm 1	-7 \pm 1	-7 \pm 2	-9 \pm 1
Dio-LNC (N=2)	Size \pm SEM (nm)	33 \pm 4	56 \pm 2	99 \pm 7	54 \pm 1	57 \pm 5
	PDI	0.1	0.07	0.06	0.16	0.09
	Zeta Potential \pm SEM (mV)	-9 \pm 1	-7 \pm 2	-5 \pm 2	-5 \pm 3	-8 \pm 3
FRET-LNC (N=1)	Size \pm SD (nm)	32	57	103	56	54
	PDI	0.11	0.09	0.07	0.17	0.12
	Zeta Potential (mV)	-6	-4	-5	-6	-7

^{*}The size of the LNC corresponds to the intensity peak.

[†] Three measurement for each attempt was applied (n=3).

With the view that this study focused on the fate of nanocapsules after internalization into and transport across Calu-3 cell monolayer, DiO and Dil probes combination was selected as FRET pair to enable this analysis [380,385].

Optimizing DiO to Dil ratio using L50 formulation: Initially L50 was selected to encapsulate different Dio:Dil ratio (w:w) in order to optimize the FRET effect (**Method S2** and **Table S5**). As **Figure 1-A** illustrates, the decrease in DiO:Dil ratio results in gradual disappearance of donor peak (DiO) until at 1:10 ratio the only observed peak is emission of acceptor (Dil) with maximum intensity at 568 nm which corresponds to the maximum FRET effect can be obtained among the tested samples (**Figure 1-C**). Knowing the fact that the FRET effect appears once the fluorophores are adjacent to each other, we utilized THF, a strong solvent that can solubilize LNCs, to disassemble the nanocapsule structure and thereafter analyze the FRET effect (**Method S2**). **Figure 1-B** shows that once the 10 μ L of FRET-L50 formulations are solubilized by 10 μ L of THF and further diluted with MeOH, the extent of Dil emission peak at 568 nm

effectively disappeared or was profoundly reduced, with a corresponding increase in DiO emission peak at 502 nm.

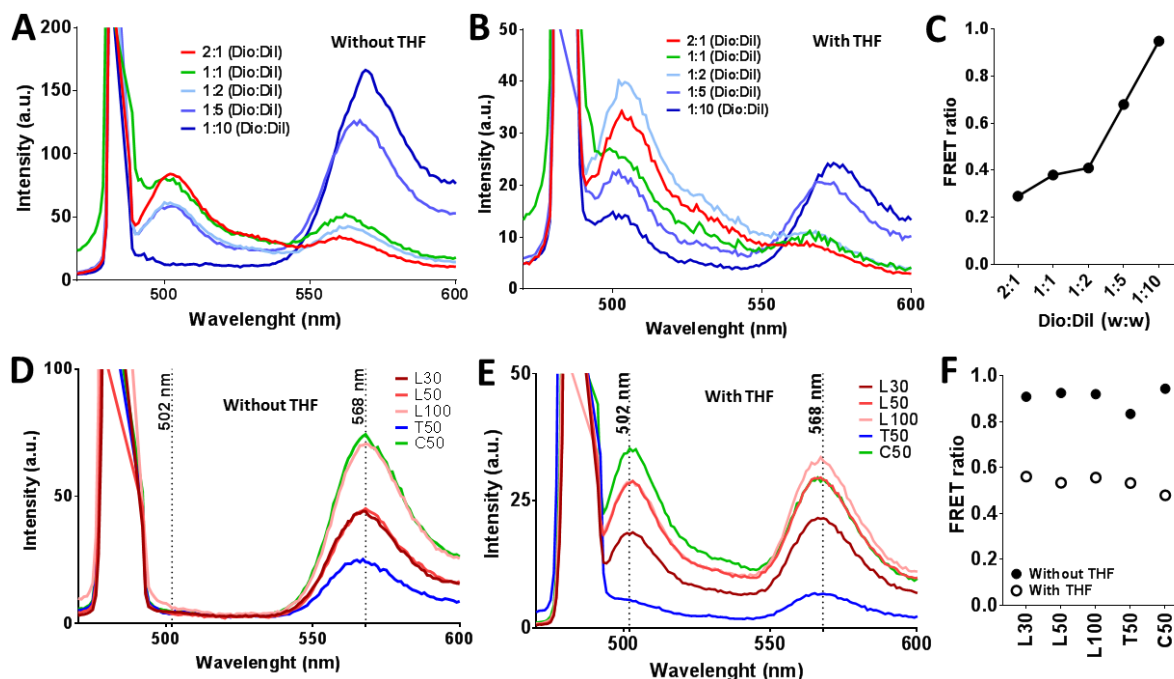


Figure 1: FRET-LNC analyses. **A)** Emission spectra of FRET-L50 formulations with various Dio:Dil ratios (w:w) (diluted with MilliQ water, 1:99 v:v corresponding to FRET-LNC:water), **B)** Emission spectra of FRET-L50 formulations for various Dio:Dil ratios (w:w) (diluted with THF and MeOH, 1:1:98 v:v:v corresponding to FRET-LNC:THF:MeOH), **C)** Evolution of FRET ratio as a function of Dio:Dil (w:w) for the FRET-LNC formulations, **D)** Emission spectra of different FRET-LNC formulations prepared at DiO:Dil ratio of 1:10 (w:w) (diluted with water to 0.05 mg/mL (LNC/HBSS-HEPES)), **E)** Emission spectra of different FRET-LNC formulations prepared at DiO:Dil ratio of 1:10 (w:w) (diluted with 10 μ L of THF and finally diluted with MeOH to reach 0.05 mg/mL (LNC/HBSS-HEPES)). **F)** A comparison between the FRET ratio of FRET-LNC formulations in presence and absence of THF. The samples were excited at λ_{ex} : 484 nm and emission spectra for DiO and FRET effect were collected at λ_{em} : 502 nm and λ_{em} : 568 nm respectively. Dilution procedures are elaborated in **Method S1** and **Method S2**.

Analysis of optimized FRET-LNC formulations: Considering the optimized DiO:Dil at ratio of 1:10 obtained from previous step, FRET-LNC formulations were prepared with sixteen times more concentrated stock solutions of each fluorophore to ensure the proper intensity at lower concentrations that must be applied for cell studies. **Figure 1-D** shows the emission spectra of all the FRET-LNC formulations at concentration of 0.05 mg/mL (LNC/HBSS-HEPES) (**Method S1** and **S2**) after excitation at 484 nm (λ_{ex} for Dio which is the donor). As it can be seen, based on the optimized DiO:Dil ratio, all the energy is transferred to acceptor at 568 nm (λ_{em} for Dil which is the acceptor) and no peak is evident at 502 nm (λ_{em} for DiO which is the donor). When FRET-LNCs were solubilized by THF and further diluted with MeOH to reach the desired concentration, the juxtaposition of DiO and Dil molecules are affected, hence emission peaks at 568

nm (λ_{em} for DiI) which attributed to FRET effect, decreases, resulting in the appearance of an emission peak at 502nm (λ_{em} for DiO which is the donor) (**Figure 1-E**). The results suggests that the prepared FRET-LNC formulations are totally functional in the way that once the FRET pair juxtaposition in nanocapsules is affected by an external factor, the FRET effect noticeably decreases (**Figure 1-E** and **1-F**). Moreover, absence of donor emission (502nm) could benefit FRET confocal imaging (**Figure 1-D**).

3.2. Toxicity studies

Figure 2 shows the effect of different B-LNCs on the cell metabolic activity of Calu-3 cells, as determined by the MTS assay. No cytotoxicity was observed for any of the formulations tested at doses lower than 0.1 mg/mL (LNC/HBSS-HEPES) (**Method S1**). Furthermore, no significant difference between the toxicity behaviors of the formulations was evidenced. In the concentration range 0.1-5 mg/mL (LNC/HBSS-HEPES), metabolic activity of the cells decreases proportionally with an increase in the amount of LNC matrix component per mL of the medium. In particular, by comparing the IC_{50} of LNC formulations, it is noticeable that both size and composition affect the level of toxicity for the concentrations more than 0.1 mg/mL (LNC/HBSS-HEPES). Comparing the IC_{50} of L30, L50, and L100 shows that as the size of the LNC increases, the level of toxicity decreases; IC_{50} for L30, L50 and L100 is 1.19, 2.37 and 5.0 mg/mL (LNC/HBSS-HEPES), respectively, illustrating a clear size dependency of the toxicity. If one considers the LNCs of different compositions at size of 50 nm, IC_{50} for T50 is 0.8 mg/mL, for L50 is 1.19 and for C50 is 2.33 mg/mL (LNC/HBSS-HEPES) pointing to the importance of the nanocapsules composition in toxicity induction in Calu-3 cells.

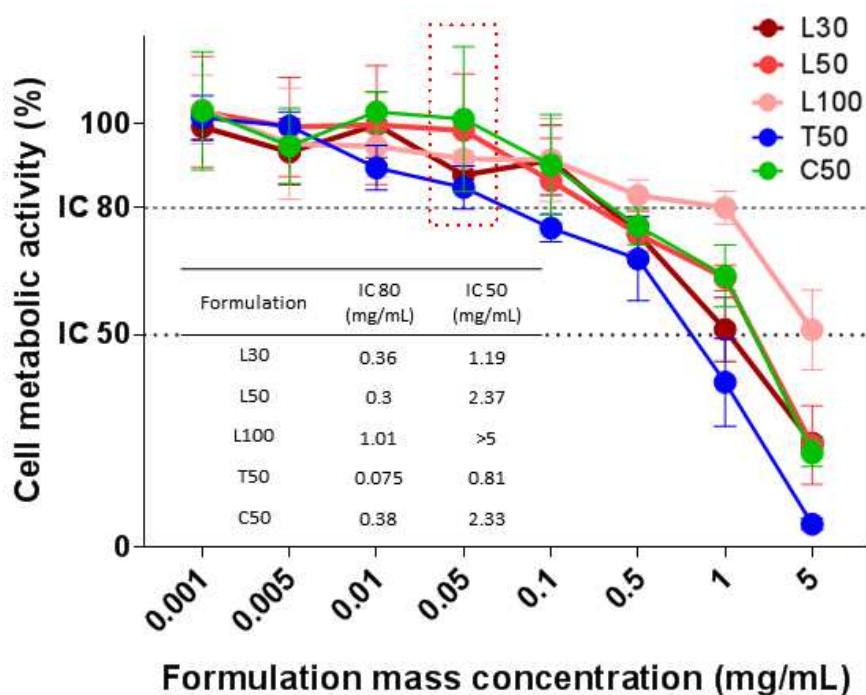


Figure 2: Relative cell metabolic activity (%) as indicated by the MTS assay after incubation of Calu-3 cells with B-LNC formulations in a 4 h experiment at 37°C. B-LNCs were diluted in HBSS:HEPES at different concentrations (**Method S1**). Triton X-100 (TX; 0.2% v/v) was employed as a positive control, and HBSS:HEPES was used as a negative control. Data represents the mean±SEM (N=4, n=4)

The finding suggests that both the size and composition of the nanocapsules play roles in toxicity induction on Calu-3 cells at concentrations higher than 0.1 mg/mL (LNC/HBSS-HEPES), whereas the lower concentrations could be considered as safe. Based on these results, concentration of 0.05 mg/mL (LNC/HBSS-HEPES) was selected as a safe amount of LNC *per* mL of medium (mg/mL) for all preparations tested for the next cell experiments. In fact, cytotoxicity results obtained through LDH assay, a well-known indicator of plasma membrane integrity (**Method S5**), confirmed the safety of the selected concentration.

3.3. Transepithelial transport of LNC

The results of LNC transport across Calu-3 cell monolayers are shown in **Figure 3**. A solution of DiO in DMSO was used as ‘free DiO’ control. Results in **Figure 3-A** demonstrate the ‘free DiO’ which is extensively associated with cells after 4 h of transport study, as would be expected for lipophilic molecules [142].

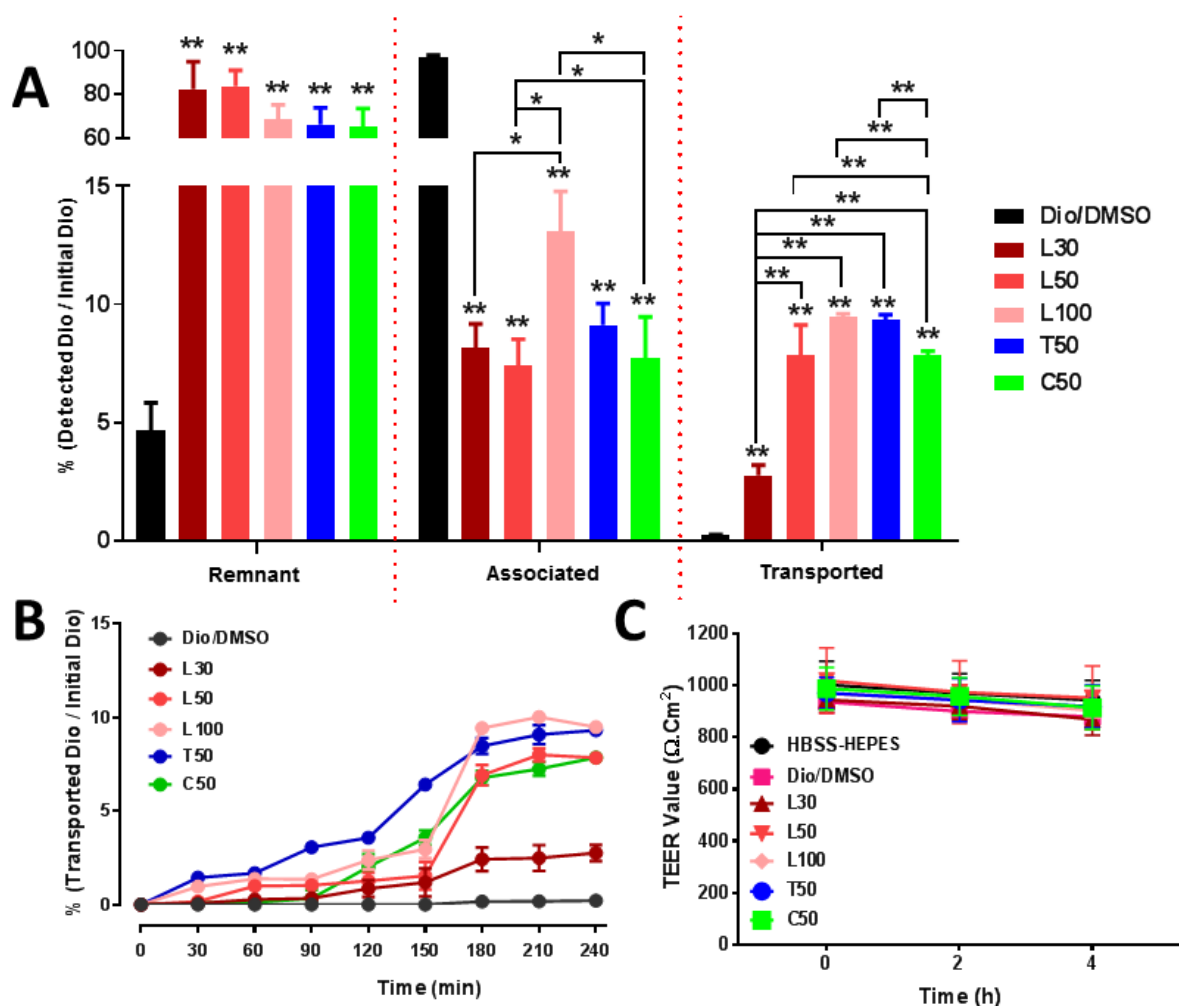


Figure 3: DiO transport study. The Calu-3 cell monolayers were treated with DiO-LNCs at concentration 0.05 mg/mL (LNC/HBSS-HEPES) (**Method S1**) for 4 h. **A**) The percentage of detected DiO to the initial amount of exerted DiO in apical chamber (Detected DiO/Initial DiO (%)) in different stages (Remnant, Associated and Transported) after 4 h, **B**) DiO transport: the percentage of transported DiO to the initial amount of exerted DiO in basolateral chamber (Transported DiO/Initial DiO (%)) by different DiO-LNC formulations (L30, L50, L100, T50 and C50) after each 30 min interval in a 4-h experiment, **C**) TEER value of Calu-3 monolayers during the experiment. The data represents the mean \pm SD deviation (n=4) and a difference of $p < 0.01$ or $p < 0.001$ was considered statistically significant.

Encapsulation of the DiO dye into LNCs completely modified its behavior. All the LNC formulations showed a lower cell association of DiO, relative to free fluorophore, at approximately 7-13 % of the total exerted amount of the initial DiO in each LNC formulation while for 'free Dio' sample, more than 98% of the applied DiO is associated with the Calu-3 cell monolayer. Furthermore, approximately 7-10 % of applied encapsulated amount of DiO in each LNC formulation was translocated from the apical to the basolateral chamber. Comparison of data for L series (30, 50 and 100 nm sized nanocapsules), indicated a statistically significant ($p < 0.001$) size dependent effect on cell association and translocation of DiO whereby, for example, 100 nm nanocapsules showed particularly increased cell association and 30 nm counterparts showed

relatively low DiO translocation across the cell layer. Considering the nanocapsules composition, there is a small significant difference in the cell association and translocated amount of DiO for L50, T50 and C50 series. The data hence demonstrate that particle size effect on Dio association with, and translocation across, the Calu-3 cell layers, although composition of nanocapsules is not a decisive factor.

Figure 3-B displays the profile of DiO transported into the basolateral chamber as a function of time. As expected, no transport of free DiO was detected. It should be mentioned that no specific binding of the DiO to the Transwell® membrane was observed (**Method S4**). Interestingly, the transport profiles for the tested DiO-LNC formulations do not exhibit a linear relationship vs time (**Figure 3-B**), and it was hence not possible to compare the transport for different capsules formulations by calculating the apparent permeability coefficients. One could however observe that between 150 and 180 min, the transport is significantly increased for all tested samples, reaching a plateau 180-240 minutes. The integrity of the cell layers remaining unchanged during the experiment (**Figure 3-C**) eliminates a possibility that the nanocapsules were transported due to a damage to the cell layer or the samples effect on tight junctions.

3.4. Evaluation of LNCs integrity

In this study, FRET was used to investigate whether the nanocapsules retain their integrity during and after their translocation across Calu-3 cell monolayer. Initially FRET-LNC formulations were applied on Transwell® containing no cells for 4 h in the same conditions as the transport experiments to confirm that the FRET ratio is not affected by nanocapsules exposure to the Transwell® membrane (**Figure 4-A**). In addition, a control experiment was conducted to confirm that no significant effect on the lipid nanocapsules occurs when these are exposed to the cell monolayers in the apical chamber (**Figure 4-B**). Results in **Figure 4-C** show that FRET ratio of samples taken from the basolateral chamber. The data clearly demonstrate that after 2 hours the FRET ratio in the basolateral chamber of all the lipid nanocapsules formulations decreased to approximately 50% of the initial value, followed by a further smaller decrease between 2 and 4 h which could be attributed to the faster rate of uptake in comparison to exocytosis. The loss of FRET ratio indicates that LNCs underwent degradation after translocation from apical to basolateral chamber.

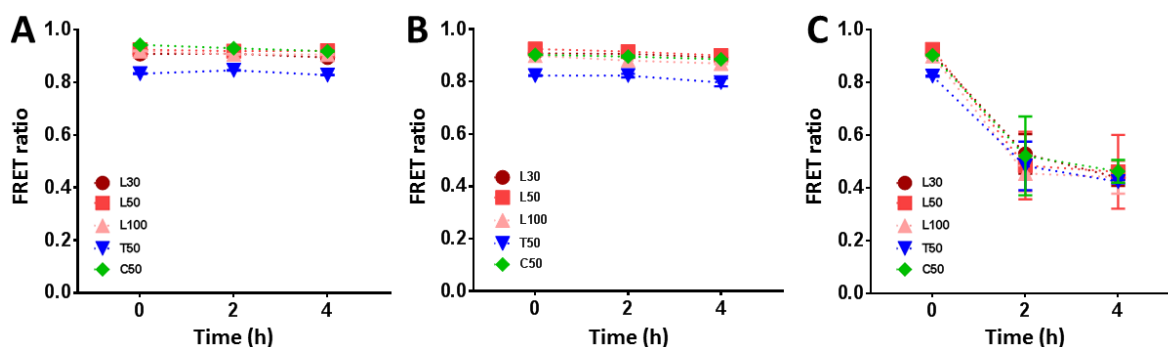


Figure 4: LNC integrity. Variation in FRET effect after exposure of 0.05 mg/mL (LNC/HBSS-HEPES) (**Method S1**) FRET-LNC formulations: **A**) FRET ratio in apical chamber of Transwells® (without cell), **B**) FRET ratio in the apical chamber of Transwell® after treating the Calu-3 cell monolayers with FRET-LNC formulations, **C**) FRET ratio in basolateral chamber of Transwells® after treating the Calu-3 cell monolayers with FRET-LNC formulations. The samples were excited at λ_{ex} : 484 nm and emission spectra for DiO and FRET were collected at λ_{em} : 502 nm (Dio as donor) and λ_{em} : 568 nm (Dil as acceptor), respectively. The data represents the mean \pm SD (n=4).

To further investigate the integrity of nanocapsules inside the Calu-3 cells, FACS measurements and confocal imaging were employed. To optimize the experimental conditions for measuring FRET signals by FACS, we initially set device configuration with the cells treated with DiO-LNC and DiI-LNC formulations individually and in combination, following the method described by Banning et al [391]. Gating was applied to living cells based on forward and sideward scatter (FSC/SSC) and adjusted photomultiplier tube voltages and compensation for DiO and DiI to specifically assess FRET in cells. Therefore, through excitation at 488 nm and employing emission filters at 576/621 nm, FRET was plotted against DiI and a gate was introduced to determine the amount of FRET-positive cells. This gate was adjusted to FRET-negative cells treated with DiI and DiO alone. **Figure 5** compares the FRET ratio for the LNCs exposed to undifferentiated or polarized Calu-3 cells.

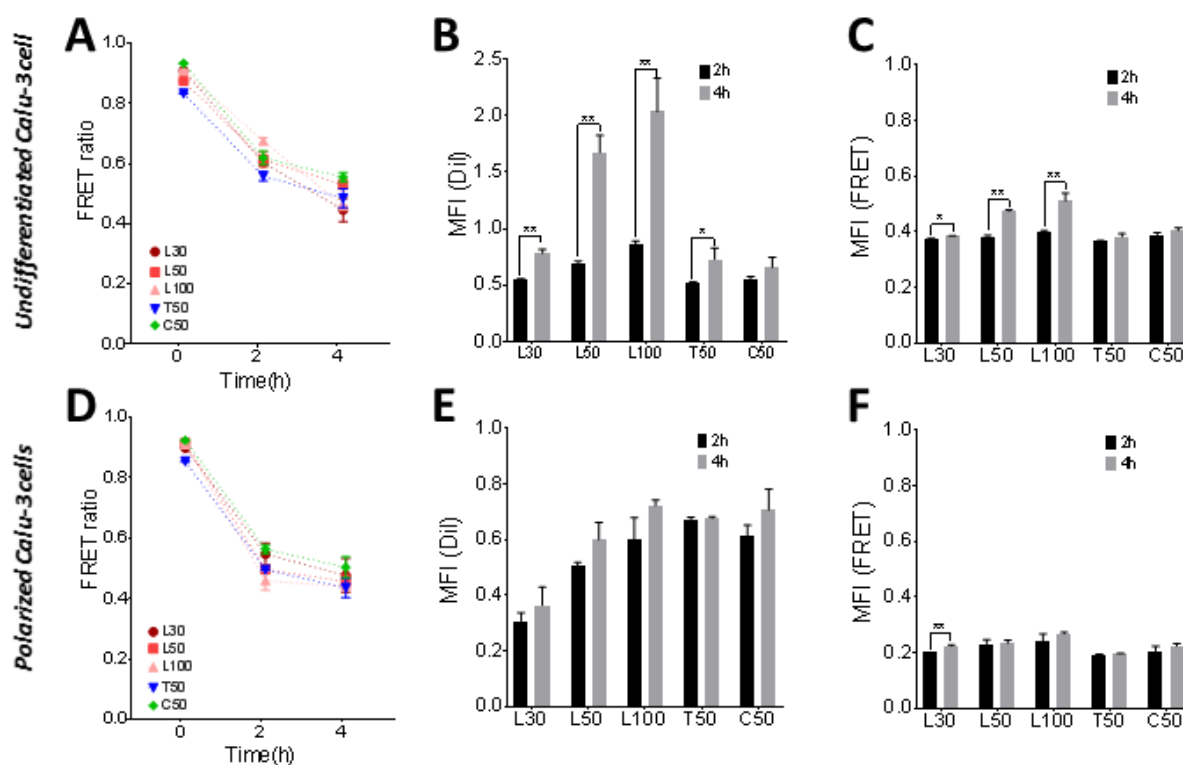


Figure 5: FACS analysis of undifferentiated and polarized Calu-3 cells after treatment with FRET-LNC at concentration of 0.05 mg/mL (LNC/HBSS-HEPES) (**Method S1**) for 2 and 4 h of incubation: **A**) FRET ratio detected in undifferentiated cells after treatment with FRET-LNC formulations, **B**) Dil intensity (MFI) of undifferentiated cells, **C**) FRET intensity (MFI) detected in undifferentiated cells, **D**) FRET ratio detected in polarized cells after treatment with FRET-LNC formulations, **E**) Dil intensity (MFI) of polarized cells, **F**) FRET intensity (MFI) of polarized cells. A blue laser at 488 nm (λ_{em} 513/526 nm) and a yellow/green laser at 561 nm (λ_{em} 579/616 nm) were used as excitation source for the detection of Dio and Dil fluorescence, respectively. For FRET detection, the laser at 488 nm with λ_{em} 576/621 nm was employed. MFI: mean fluorescence intensity. Cells treated with B-LNCs (L30, L50, L100, T50 and C50) was considered as negative control. The data represents the mean \pm SD (n=4) and a difference of $p^* < 0.01$ or $p^{**} < 0.001$ was considered statistically significant.

In both cultured condition (**Figure 5-A** and **5-D**), the FRET ratio dramatically decreases by the 2h time-point, with a further decrease at the 4 h point. This indicates that internalized LNCs underwent degradation in both cell culture conditions. The rate of FRET ratio decrease was higher when LNCs were exposed to undifferentiated cells than cells grown at an air-liquid interface (Calu-3 monolayer). In **Figure 5-B** and **5-E**, the mean fluorescent intensities (MFI) of Dil and FRET of Calu-3 cells after treatment with different LNC formulation for 2 and 4 h, are represented. Through Dil emission analysis (λ_{ex} 561 nm- λ_{em} 579/616 nm), we monitored the uptake rate of LNC in the cells. As the results show, the rate of uptake in undifferentiated cells are higher than polarized cells. Regarding LabrafacTM-based nanocapsules (L30, L50 and L100), the uptake behavior of nanocapsules in both undifferentiated and polarized cells are size dependent and it increases alongside the increase in particle size. Moreover, in

undifferentiated cells, uptake of nanocapsules significantly increases after 4 h ($p < 0.001$), while in case of polarized cells, the increase of uptake after the same time span is not significant. Further comparison between the L50, T50 and C50 reveals that composition of nanocapsules play a major role in uptake rate in undifferentiated cells while for polarized cells, the uptake rate is approximately the same as it was observed before (**Figure 2-A**). Considering the MFI of FRET, we have an indication of the amount of intact nanocapsules internalized by cells. **Figure 5-C** and **5-F** suggest that once the uptake of nanocapsules increases, the FRET intensity, although not significantly in case of polarized Calu-3 cells, increases. The same behavior could be better realized by increase in the population of DiI-positive and FRET-positive cells after 2 and 4 h of incubation, indicating that LNCs uptake and degradation simultaneously happens (**Figure S3**).

The confocal images presented in **Figure 6** show Calu-3 cells incubated with DiO-LNC formulations from different formulations for 2 and 4 h. The images generally show the cell associated presence of DiO green fluorescence at 2 h and 4 h incubation times. The green fluorescence in Z-sections of L100 nanocapsules treated Calu-3 cells after 4 h of incubation shows a punctate perinuclear distribution which implies a lysosomal subcellular localization.

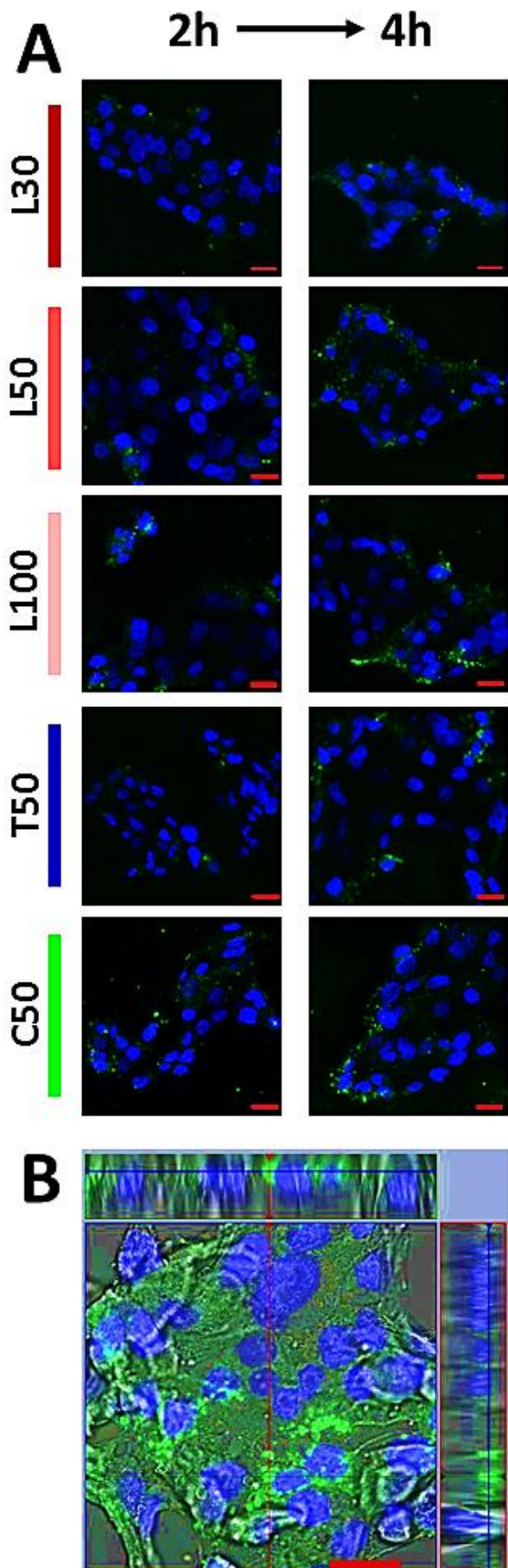
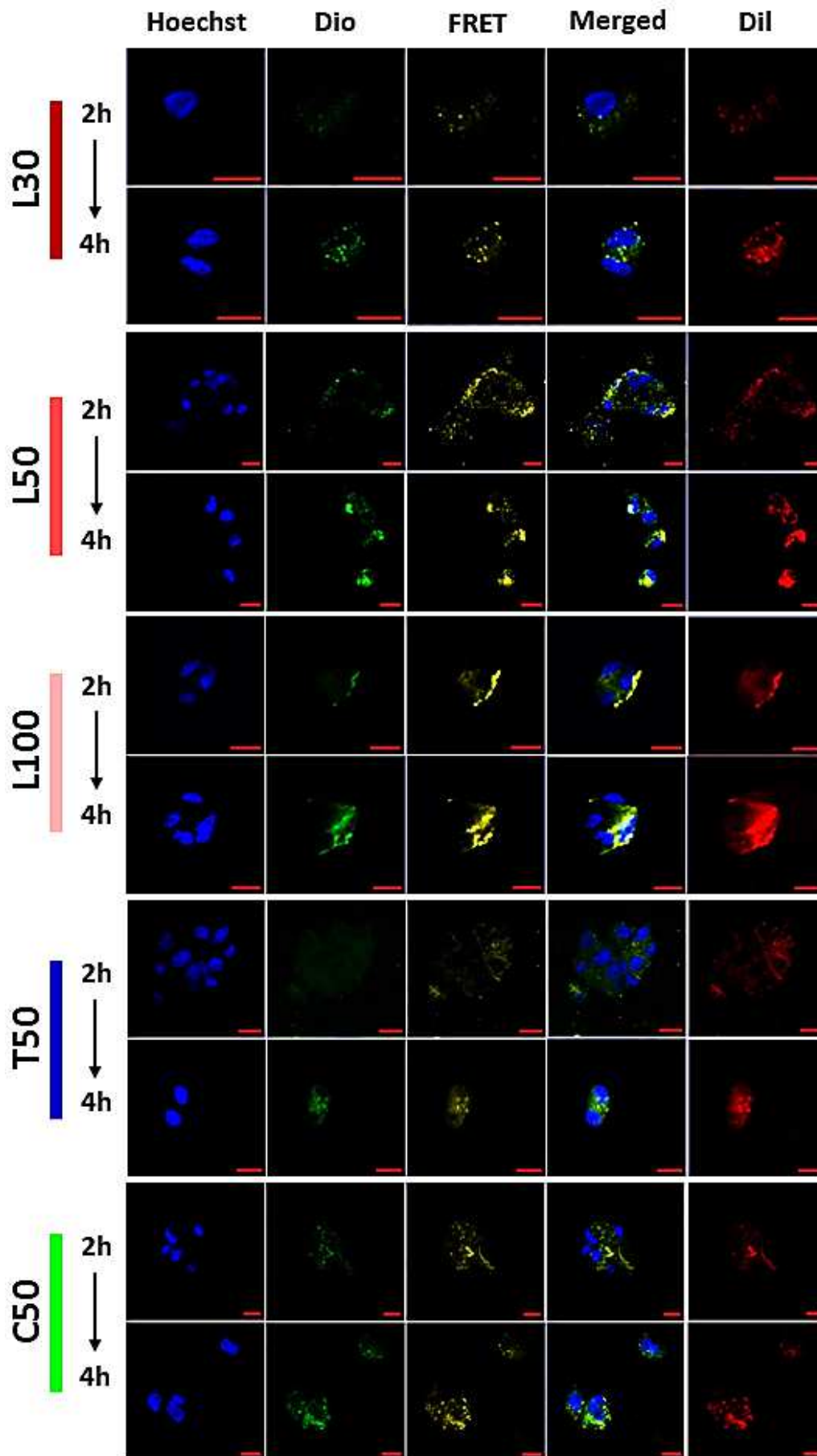


Figure 6: Confocal microscopy images of DiO-LNC formulations uptake by undifferentiated Calu-3 cells. The cells were treated with DiO-LNC formulations at concentration of 0.05 mg/mL (LNC/HBSS-HEPES) (**Method S1**) for 2 and 4h. **A**) 2D images of cellular uptake for different DiO-LNC formulations, **B**) 3D images reconstructed from individual sections ('Z-stacks') taken across the depth of the Calu-3 cells after 4 h of exposure with L100 (40 sections, 0.53 μm thick). The scale bar represents 20 μm . The green signal is DiO and the blue one is for cell nuclei which were labelled with Hoechst.

A panel of images in **Figure 7** shows the confocal images of cell associated DiO, FRET, and Dil fluorescence for tested FRET-LNC formulations on undifferentiated cells. After 2 h of incubation, red fluorescence of Dil, and yellow fluorescence of FRET can be observed in the cells, indicating nanocapsules cellular internalization and their presence in the cells as intact species, although the overall level of fluorescence is generally relatively low. After 4 h, the Dil signal is increased, as well as FRET signal, indicating an increased amount of cell-internalized nanocapsules which is confirmed before by FACS (**Figure 5-B**). By comparing the increase in the intensity of the Dil channel from 2 h to 4 h and considering the results obtained from FACS, we can understand that increase in nanocapsules uptake results in more intense FRET signal (**Figure 5-C**). Considering that the cells were treated with nanocapsules encapsulating the optimal DiO:Dil ratio (**Figure 1-E**), one should not observe green signal of DiO, as the appearance of this color represents the dissociation of FRET pair and hence, at least partial, loss of integrity of the LNCs. All FRET-LNC formulations tested show appearance of green DiO fluorescence suggesting that the nanocapsules integrity is compromised.

Figure 7: FRET confocal microscopy showing the change in FRET signal of FRET-LNC formulations at concentration of 0.05 mg/mL (LNC/HBSS-HEPES) (**Method S1**) exposed to undifferentiated Calu-3 cells for 2 and 4 h. Zen 2009 image Software was utilized for image processing. Different imaging channels are displayed horizontally for each sample (from left to right): Hoechst channel which represents the nuclei (blue), DiO channel (green, λ_{ex} 488 nm- λ_{em} 505–530 nm), FRET channel (yellow, λ_{ex} 488 nm- λ_{em} LP 560 nm), Hoechst, DiO and FRET merged channel, and Dil channel (red, λ_{ex} 543 nm- λ_{em} LP 560 nm). Scale bars in all images are 20 μm .

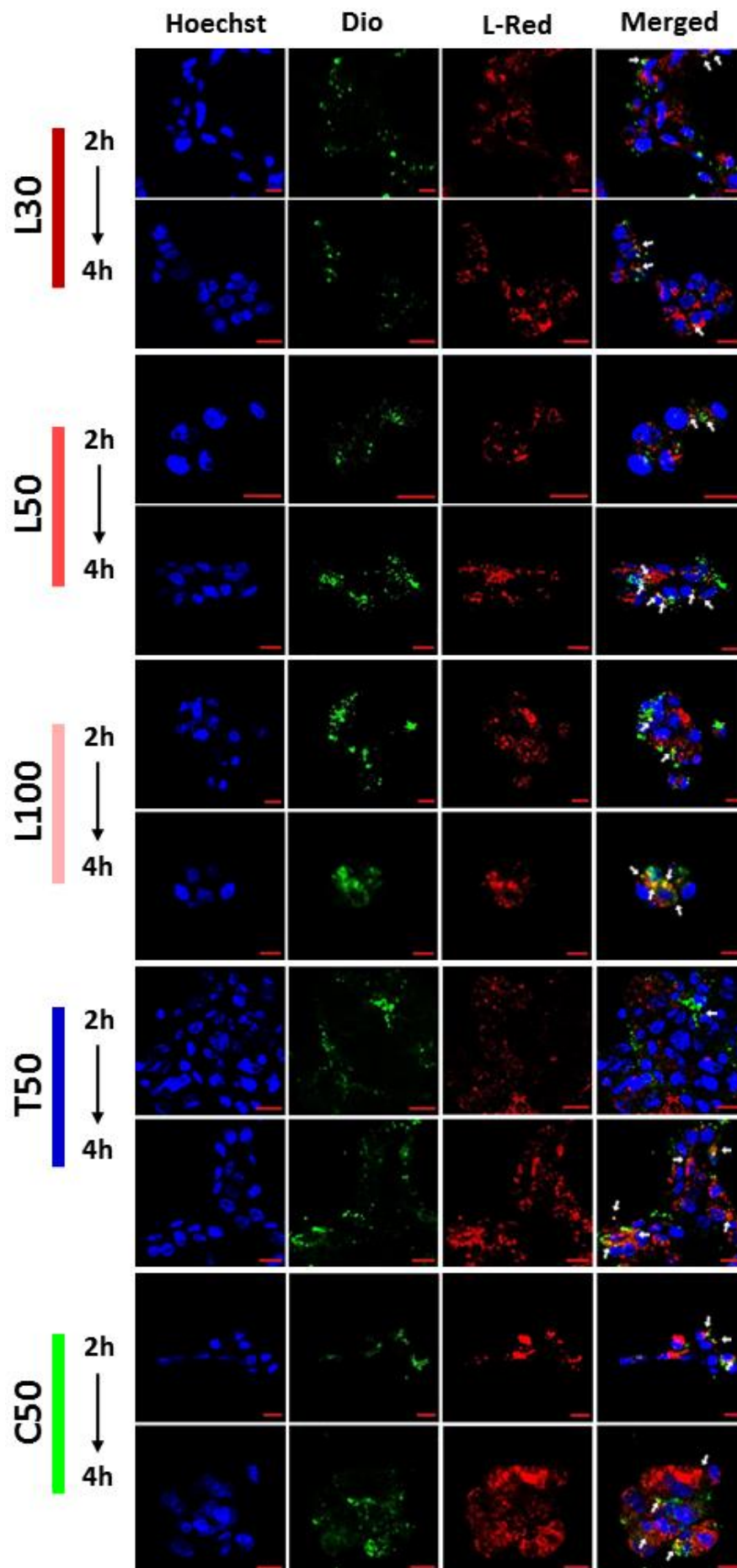
(next page →)



Finally, we investigated a co-localization of encapsulated DiO probe with lysosomal marker (LysoTracker Red DND-99) following undifferentiated Calu-3 cells exposure to Dio-LNC formulations (**Figure 8**).

Figure 8: Confocal microscopy for lysosomal staining representing the localization of DiO-LNCs at concentration of 0.05 mg/mL (LNC/HBSS-HEPES) (**Method S1**) exposed to Calu-3 cells for 2 and 4 h. Zen 2009 image Software was utilized for image processing. Different imaging channels are displayed horizontally for each sample (from left to right): Hoechst channel which represents the nuclei (blue), DiO channel (green, λ_{ex} 488 nm- λ_{em} 505–530 nm), R-red channel (red, λ_{ex} 577 nm- λ_{em} 590 nm), Hoechst, DiO and R-red merged channel. White arrows in “Merged” column shows the DiO and L-Red, representing accumulation of LNCs in lysosomes. Scale bars in all images are 20 μm .

(next page →)



Comparing distribution of green fluorescence, representing Dio, with red, representing lysosomal marker, in the corresponding images (DiO and L-red columns), one can observe similar patterns of color distribution, further confirmed by the presence of yellow-orange color in merged column. The images would hence indicate co-localization of the DiO-containing nanocapsules and lysosomal marker (white arrows), pointing to accumulation, at least a population, of LNCs inside lysosomes. This appears to be the case for all the formulations, evident at both 2 and 4h of incubation (white arrows), although lysosomal accumulation is perhaps less noticeable for L30 than for the other LNC formulations.

4. Discussion

A successful delivery of biologics (high molecular weight compounds such as proteins, microRNA, siRNA, and antibodies) or new classes of small molecular weight compounds with low permeability across nasal epithelial barrier will unlock potential of a non-invasive drug delivery to the brain. In this context, nanocarriers can potentially enhance transepithelial drug delivery by protecting the encapsulated therapeutic agent from biological and/or chemical degradation [276] and by acting as a shuttle to carry the encapsulated material across the nasal epithelial barrier. As previously described, LNCs are nanocarriers which are formulated with 'generally recognized as safe' excipients by a phase-inversion temperature process (a low-energy nano-emulsification method) and have promising use for drug delivery to malignant brain tumors [172,174,179,191,374–378] and also transport of therapeutics across intestinal epithelial barrier [141,142]. Therefore, it is interesting to study potentiality of LNCs for application in nose-to-brain drug delivery. To employ LNCs for the purpose of intranasal drug delivery to the brain, their integrity after transport across nasal epithelial barrier must be maintained to avoid the release of the cargo before reaching the brain site. Here, for the first time, we have studied the fate of different type of LNCs, based on size and matrix component, after crossing a model of nasal epithelial barrier.

In this study, we successfully prepared LNCs from oily core of medium chain triglycerides (Labrafac, Labrafil, or glyceryl tricaprlylate) by encircling a rigid shell of Lipoid® S75-3 (lecithin), which crystallizes, to give an improved physical stability to LNCs, compared to nanoemulsions [134,146]. Regarding Kolliphor® HS15 (PEG (15)-hydroxystearate), it has been suggested previously that Kolliphor® molecules

associate with Labrafac™ core through their lipophilic (hydroxystearate) moiety, and orientating their hydrophilic (polyethylene) chains towards water phase [148]. It is worthy to mention that the liquid state of medium chain triglycerides was maintained after entrapment inside the nanocapsules, thereby the system is comprised of an oily liquid core surrounded by a tensioactive rigid shell made from a mixture of Lipoïd® and Kolliphor® [148]. Knowing that there is a direct correlation between the size of the nanocapsule and the oil amount in the formulation, to study the effect of the particle size on cellular interactions of LNCs, formulations based on Labrafac™ [148] with three different nominal sizes (30, 50 and 100 nm) were prepared (L30, L50 and L100). Furthermore, in order to compare the effect of LNC matrix component on their transport across nasal epithelial barrier, we prepared three different formulations (L50, T50 and C50), of 50 nm. For the preparation of T50, Transcutol® HP, widely employed in the development of emulsions or microemulsions [138–140], was utilized as co-surfactant. Furthermore, Labrafil® M1944 CS, a hydrophilic oil in which Transcutol® HP is soluble, was selected and employed as oily phase. Since solubilization of Lipoïd® in Labrafil® is limited, Labrafac™ was also added in order to overcome this obstacle [141]. For preparation of C50, Labrafac™ was replaced by glyceryl tricaprilate and formulated as previously described [142].

In this work, due to the limitations with primary cell cultures, such as limited subsequent passages [243], we selected Calu-3 cells, which is a ciliated, mucus-secreting cell line and has numerously been employed in preparation of nasal epithelial barrier models [261,264–273]. LNC formulation toxicity, which was measured using MTS cytotoxicity assay, enabled the identification of nontoxic concentrations of nanocapsules, which were used in subsequent experiments. A concentration-dependent effect on cell metabolic activity was observed for LNCs with different sizes and also matrix components (**Figure 2**). The safety of the ideal concentration of LNCs were further validated by LDH assay, a membrane damage indicating assay, to ensure that nanocapsules do not affect the cell membrane (**Method S5**). Knowing the fact that there is a direct relation between the amount of Kolliphor® and toxicity induction in Calu-3 cells [392], our results suggest that the decrease in cell metabolic activity of Calu-3 cells is irrelevant to the amount of Kolliphor® at the concentration of nanocapsules which was introduced to the cells (**Table S1**).

Calu-3 cells were grown at an air-liquid interface on permeable supports to form polarized cell, to investigate the potential of LNC formulations for transporting a hydrophilic agent across the cell monolayer. We observed that nanocapsules facilitate the transport of encapsulated DiO across the cell monolayer to the basolateral chamber. The difference to the behavior of 'free' DiO, where more than 95% of applied dose was associated with the cell monolayer, due to its high lipophilicity, as already demonstrated for other types of hydrophobic drugs [141,142], highlights that drug carriers play a pivotal role in enhancing the drug delivery across epithelial barriers. The transport of DiO from apical chamber to basolateral was found to be dependent on nanocapsules size as the rate of DiO transport increases alongside the increase in the size of nanocapsules, where the highest transepithelial transport of DiO occurred for the largest, 100 nm LNC formulation (**Figure 3-A** and **3-B**). Such behavior was not observed in LNCs with different matrix components

The paracellular transport of agents across epithelial barriers is restricted by the size of the intercellular space and the tightness of junctions present between the epithelial cells which in case of Calu-3 cells is about 8 Å [222]. Furthermore, tight junctions could be opened up by particular constituents and the width of fully opened tight junction is known to be less than 20 nm [393]. The paracellular transport of a nanocarrier could occur once their size and surface modification are suitable. The nominal size of the smallest LNC formulation was around 30 nm which is even larger than the width opened tight junction. Moreover, it has been proven that Kolliphor® (>1mM) could open tight junctions, hence enhancing paracellular transport of agent across Calu-3 cell monolayer [392], but in the current study, final concentration of this surfactant on the surface of nanocapsules is way less than the sufficient amount for resulting in paracellular transport of DiO (**Table S1**). Knowing that measurement of TEER value can be utilized as a marker for disruption of the epithelial monolayer [394] and any decrease in TEER value could reflect an increase of the paracellular permeability [395], we observed no variation in TEER value during the transport study, due to the fact that the transport of LNCs did not affect the TEER value (**Figure 3-C**), hence we can hypothesize that the DiO transport by LNCs was through intracellular trafficking. Further characterization of samples taken from basolateral chamber revealed that the size of the detected nanoparticles noticeably were higher compared to the initial values and the homogeneity as well decreased (**Figure S2-B**). The variation in particle size

and polydispersity could be as a result of agglomeration of nanocapsules, and/or LNC debris and/or cell-derived entities. Such agglomeration could also occur because of the nanocapsule interactions with biomolecules of during the metabolic activity of the cells [396]. Rogers et al. [142], previously reported that transport of tricaprilyn based LNCs (like C50) across Caco-2 cell monolayers could be as a result of transcytosis based on the transmission electron microscopy observations. Therefore, extracellular vesicles could be involved in transport of LNCs. We found that these large particles are detectable after transport in basolateral chamber even for the 'free DiO' sample and it make the idea of transcytosis more probable (**Figure S2-B**).

To achieve one of the primary goals of this study, which is investigation on integrity of LNCs after transport across Calu-3 based nasal epithelial barrier, we firstly optimized FRET-LNC formulations in the way that all the absorbed energy by the donor fluorophore (DiO) transfers to the acceptor one (DiI), thereby the slightest change in the juxtaposition of fluorophore pairs could be detected (**Figure 1**) and efficaciously benefits the FRET imaging. The findings suggest that different types LNCs prepared for this study, cannot maintain their integrity while they are internalized by or transported across Calu-3 cells. We showed that nanocapsules with different sizes and also different compositions maintain their integrity up to 4 h under culture condition with or without presence of cell (**Figure 4-A** and **4-B**), but when they cross the epithelial barrier, the FRET ratio dramatically decreases (**Figure 4-C**). This result suggests that LNCs were subjected to degradation through their passage across Calu-3 cell monolayer because the destruction of LNCs with organic solvents led to the same decrease of the relative FRET ratio (**Figure A**). The results obtained from FACS studies on non-polarized and polarized Calu-3 cells also demonstrated that the FRET ratio in internalized nanocapsules decreases, indicating that intracellular trafficking results in nanocapsule degradation (**Figure 5-A** and **5-D**). As Bastiat et al.[397], demonstrated before, encapsulation of lipophilic carbocyanine dyes (DiO, DiI and DiD) results in their localization inside the surfactant shell of the nanocapsules. Applying their method, we found that the FRET fluorophore pair is inside the shell (**Method S3**). Therefore, we cannot say whether the degradation is attributed to the surface erosion or bulk erosion of nanocapsules [398]. Such estimation necessitates a meticulous study on LNC degradation mechanisms. In addition, intracellular FRET analysis for undifferentiated and polarized cells demonstrated that, although the LNC uptake

behavior is slightly variable, which could be attributed to the density of cells and their differentiation [399], decrease in FRET ratio reduction, which corresponds to degradation of internalized nanocapsules, occurred for all types of LNC formulations following the same pattern (**Figure 5**). Therefore, the FRET imaging of undifferentiated cells could represent the intracellular fate of LNCs internalized by polarized cell monolayer (**Figure 7**). These results further confirms the degradation of nanocapsules inside the cells.

In contrast to our findings, Roger et al. [381], found that tricaprylin based LNCs (like C50) could maintain their integrity after transport across Caco-2 based intestinal epithelial barrier model. Using two complementary techniques, FRET and nanoparticle tracking analysis (NTA), they found that the LNCs are intact after transport and there was not a significant change in their size. Groo et al. [51] have also shown the stability and diffusion of FRET-LNCs in intestinal mucus. The FRET efficiency remained at 78% after 3 h. This slight loss of FRET efficiency (< 25%) was not considered as a sign of LNC destruction but, rather, they reported that an increase of diameter LNCs of 5 nm after as a result of contact with mucus could be the reason for this observation. The difference of results between these studies with ours could be in part due to the employed technique and the barrier characteristics of epithelial cultures. Roger et al. [381], used two lipophilic cyanine dyes (DiD and DiI) bearing the highly hydrophobic tetraphenyl borate (TPB) counterion to achieve an efficient FRET signal. TPB enhances dye solubility in oil and therefore the dye loading capacity. Employment of these TPB-based fluorophores may be more sensitive than the lipophilic carbocyanine dyes we employed to detect integral LNCs. The discrepancy of our results could also be due to the presence of mucus in the Calu-3 cell layer which is absent in Caco-2 cell layer. Indeed, Vllasaliu et al. [400] showed that the presence of mucus notably affect nanoparticle transport across the epithelium.

As previously explained, the rigidity of LNC is due to Lipoid® S75-3 which is composed of two different phospholipids. If this rigid phospholipid-based shell is affected by any transcellular mechanism in nasal epithelial barrier, the nanocapsules could not maintain their integrity. Tagami et al [401], reported that phospholipids are the substrates for phospholipase A2 (PLA2) which is a family of enzymes capable of hydrolyzing phospholipids. Thus, phospholipid based-lipid nanocarriers become leaky

in the presence of PLA2 due to the degradation of phospholipids. PLA2 can cleave the sn-2 position of a phospholipid to generate the lysolipid lysophosphatidylcholine and the fatty acid arachidonic acid [402]. Wadsäter et al. [403], investigated the lipolytic degradation of cubic micellar nanoparticles of soy phosphatidylcholine/glycerol dioleate by PLA2 and reported that it degraded to lysophosphatidylcholine and fatty acids. On one hand, by considering the enzymatic action of PLA2 on phospholipids, the degradation of LNC is inevitable. On the other hand, it is well proven that in epithelial cells, PLA2 is not only prevalently present in the cytosol [404], but also it is highly expressed in the lysosomes of lung cells and are believed to participate in surfactant catabolism [405,406]. Our results show that LNCs are accumulated in both cytosol and lysosome of Calu-3 cells (**Figure 8**), hence degradation of the nanocapsules is unavoidable. Furthermore, there are also other types of lysosomal enzymes that could affect the shell of the nanocapsules such as lecithin:cholesterol acyltransferase [405] or lysosomal acid lipase [407].

5. Conclusion

In this study, interaction of LNC formulations of different sizes and compositions with Calu-3 cells was evaluated. It was shown that these nanocapsules could dramatically enhance the transport of a hydrophobic dye in a size dependent fashion by a transcellular mechanism, while the composition of the LNCs did not affect the transport. FRET studies demonstrated that the integrity of all different types of nanocapsules was affected by the transcellular transport, so that the transported nanocapsules underwent degradation. Intracellular FRET analyses demonstrate that the internalized nanocapsules, accumulated in both cytosol and lysosomes, were degraded. Further investigation is necessary to find out what mechanisms and what enzymatic activity are directly involved in degradation of the nanocapsules and such investigation is integral with a precise understanding about the way LNCs are degraded. Subsequently, a meticulous design of LNCs could be postulated and thus experimented in order to minimize the rate of degradation of the nanocapsules once they are transported across the nasal epithelial barriers.

6. Conflict of interest

The authors declare that there is no conflict of interest.

7. Acknowledgment

The authors are thankful to the supported grant from Culture Executive Agency (EACEA), through the NanoFar Erasmus Mundus joint Doctoral program and would also like to appreciate the invaluable comments of Dr. Anne Clavreul (CHU Angers and University of Angers, France), Dr. Emilie Roger (University of Angers, France), Vijender Panduga and Dr. Robert Cavanagh (School of Pharmacy, University of Nottingham, UK). Dr. Claudia Conte was supported by a fellowship by Associazione Italiana per la Ricerca sul Cancro (AIRC) co-funded by the European Union (iCARE/Marie Curie 2014).

Supplementary Information

Lipid nanocapsules transport across Calu-3 based model of nasal epithelial barrier

Milad Pourbaghi Masouleh ^{1,2}; Claudia Conte ^{2,3}; Cynthia Bosquillon²; Philippe Menei^{1,4}; Snow Stolnik^{2*}

¹ CRCINA, INSERM, Université de Nantes, Université d'Angers, Angers, France.

² Division of Drug Delivery and Tissue Engineering, School of Pharmacy, University of Nottingham, UK.

³ Department of Pharmacy, University of Napoli "Federico II", Napoli, Italy.

⁴ Département de Neurochirurgie, CHU, Angers, France

* Corresponding author: snow.stolnik@nottingham.ac.uk

Content

- Method S1: Dilution of LNC based on formulation mass
- Method S2: FRET-LNC sample preparation for fluorescent spectroscopy analysis:
- Method S3: Incorporation of fluorophore to LNC
- Method S4: DiO binding to membrane filter of Transwell®
- Method S5: LDH assay
- Characterization of different prepared batches of FRET-L50 based on different DiO:Dil ratios
- LNC Size distribution
- Cell population obtained from FACS analyses

Method S1: Dilution of LNC based on formulation mass

To dilute the LNC formulations based on the matrix components that form the nanocapsules, the quantity of the excipients that constructs the nanocapsules (Oils and surfactants), utilized in preparation of formulation, were added and divided by the total quantity of the applied excipients and water (water at 25°C and water at 0°C). Considering the resulted proportion, the desired concentration of the LNC compartments were calculated and diluted by addition of the diluent. This dilution is considered as LNC dilution and its unit is mg/mL (LNC/mL of diluent).

Table S1: Final amount of Kolliphor® in LNC formulations introduced to Calu-3 cells at concentration of 0.05 mg/mL (LNC/HBSS-HEPES)

Formulation	L30	L50	L100	T50	C50
µg	33.9	21.8	13.7	15.4	22.1
µmol	0.035	0.023	0.014	0.016	0.023
µM	0.07	0.045	0.028	0.032	0.046

Method S2: FRET-LNC sample preparation for fluorescent spectroscopy analysis:

FRET-L50 samples: In order to find the best proportion of DiO to Dil for preparation of FRET-LNC formulation, we selected L50 and encapsulated the selected fluorophore pair in the formulation with different Dio to Dil mass (Dio:Dil) ratio (w:w). Once the samples were prepared, filtered, dialyzed overnight and filtered again (as described in LNC formulation section). 10 µL of each sample was diluted with 990 µL of MiliQ water to see the FRET effect (**Figure 1-A**). Knowing the fact that the FRET effect appears once the fluorophores are adjacent to each other, we utilized tetrahydrofuran (THF), a strong solvent that can solubilize LNCs, to disassemble the nanocapsule structure and analyze the FRET effect. For this purpose, 10 µL of each sample was diluted with 10 µL of THF, agitated intensively and followed with addition of 980 µL of MeOH (**Figure 1-B**).

FRET-LNC samples: Considering the selected Dio:Dil ratio (w:w) from the FRET-L50 samples which is 1:10 (w:w), different FRET-LNC batches (FRET-L30, FRET-L50, FRET-L100, FRET-T50 and FRET-C50) was prepared as described before. In order to make sure that FRET-LNC formulations could function efficaciously after dilution to the desired concentration obtained from MTS study (0.05 mg/mL), the samples were

diluted following **Method S1**. To investigate the efficacy the FRET effect after preparation, the prepared LNC formulations were diluted to 0.05 mg/mL by MilliQ water (**Figure 1-D**). Furthermore, the LNC formulations were diluted by addition of 10 μ L of THF, agitated intensively and finally MeOH was added to obtain a concentration of 0.05 mg/mL (**Figure 1-E**).

Method S3: Incorporation of fluorophore to LNC

FRET-LNCs were selected to measure the amount of unassociated fluorophore to LNCs after dialysis and filtration as described before. In this regard, 500 μ L of the different FRET-LNC formulations were filtered by Amicon Ultra-0.5 mL Centrifugal Filter (10 kDa, 10000 rpm, 1h, RT). Consequently, the supernatant was analyzed by fluorescent spectroscopy (λ_{ex} : 484 nm \rightarrow λ_{em} : 502 and 568 nm for DiO and FRET respectively; and, λ_{ex} : 549 nm \rightarrow λ_{em} : 568 nm for Dil).

Table S2: Analysis of supernatant obtained after filtration of FRET-LNC formulation

Ex/Em	FRET-L30	FRET-L50	FRET-L100	FRET-T50	FRET-C50
$\lambda_{ex}/\lambda_{em}$: 484/502	ND	ND	ND	ND	ND
$\lambda_{ex}/\lambda_{em}$: 484/568	ND	ND	ND	ND	ND
$\lambda_{ex}/\lambda_{em}$: 549/568	ND	ND	ND	ND	ND

*ND: Not detected (No peak was detected in the emission spectra).

Lipid transfer experiment

Investigating the association of the DiO and Dil to LNC is a challenging issue. Therefore, based on the transfer of a fluorescent dye from its hosting nanocarrier to a lipophilic compartment, an innovative approach was recently developed by Bastiat et al. [1], to confirm the labeling stability. According to this method, 1 mL of optimized FRET-LNC formulation at concentration of 0.05 mg/mL (LNC/water) (**Method S1**) was mixed with the amount of their oily core (for L30, L50 and L100: LabrafacTM; for T50: LabrafacTM, Labrafil[®] and Transcutol[®]; for C50: Glyceryl tricaprylate) that participate in formation of the nanocapsules at the same concentration. The mixtures were vortexed for 15 s at room temperature, then centrifuged (4000 rpm, 30 min) to separate the lipophilic compartment from nanocapsules. Once complete separation was obtained, a white film remains on top which is the lipophilic compartment, thereby the nanocapsules remain underneath. Therefore, the nanocapsule colloid was carefully

taken out by a syringe and analyzed by fluorescent spectroscopy. **Table S3** shows the FRET ratio of the samples before and after separation:

Table S3: Analysis of supernatant obtained after filtration of FRET-LNC formulation

Condition	FRET-L30	FRET-L50	FRET-L100	FRET-T50	FRET-C50
FRET ratio of original formulation	0.911	0.927	0.913	0.81	0.935
FRET ratio after lipid transfer experiment	0.891	0.909	0.911	0.763	0.916

As the results show, there is not a significant difference before and after separation. Bastiat et al. [1], described that when DiI and DiO are encapsulated in Labrafac™-based LNC, they are trapped in the shell of the nanocapsule, therefore they could not be transferred, even in the presence of an external lipophilic compartment(s). In the prepared FRET-LNC formulations, no significant difference in FRET ratio was observed before and after lipid transfer experiment which agrees with what Bastiat et al. [1] claimed. Regarding T50, the minor loss of FRET ratio could be as a result of Transcutol® which is a co-surfactant and a small proportion of the encapsulated dyes could be transferred to lipophilic compartments by this excipient.

[1] G. Bastiat, C.O. Pritz, C. Roider, F. Fouchet, E. Lignières, A. Jesacher, R. Glueckert, M. Ritsch-Marte, A. Schrott-Fischer, P. Saulnier, J.-P. Benoit, A new tool to ensure the fluorescent dye labeling stability of nanocarriers: A real challenge for fluorescence imaging, *J. Control. Release.* 170 (2013) 334–342. doi:10.1016/j.jconrel.2013.06.014.

Method S4: Dio binding to membrane filter of Transwell®

To study the binding between DiO and membrane filter of Transwell®, the same transport protocol as mentioned before without presence of cells was performed. At the end, the filters were washed with PBS, excised and mediated with THF and methanol. Eventually, the samples were analyzed by a plate reader.

Table S4: DiO quantity associated to the membrane filter of Transwell®

Formulation	Dio-DMSO	Dio-L30	Dio-L50	Dio-L100	Dio-T50	Dio-C50
DiO quantity (ng)	ND*	ND	ND	ND	ND	ND

*ND: Not detected (The results were lower than limit of detection)

Method S5: LDH assay

The LDH assay was employed to assess the cell membrane integrity as a function of the amount of cytoplasmic LDH released into the medium. Calu-3 cells were cultured on 96-well plates at the density of 1×10^4 cells/well for 48 hours before the assay. Then,

the culture medium was removed and cells were washed with PBS before adding 150 μL of LNC suspension in each well (0.05 mg/mL) (**Method S1**). Triton X-100 (0.2% v/v in HBSS) was used to induce LDH release (positive control), whereas HBSS-HEPES was used as negative control. After 4h of incubation, 50 μL of the sample solution was removed from each well, mixed with 150 μL of the LDH reagent and incubated for 25 min at room temperature. Finally, absorbance at 490 nm was measured by the plate reader. Percentage of LDH release from the LNC treated cells was calculated using the equation below:

$$LDH \text{ release } (\%) = \frac{S - H}{T - H} \times 100$$

where S is the absorbance measured from the tested samples, T is the absorbance obtained with Triton X-100, and H is the absorbance observed with HBSS-HEPES.

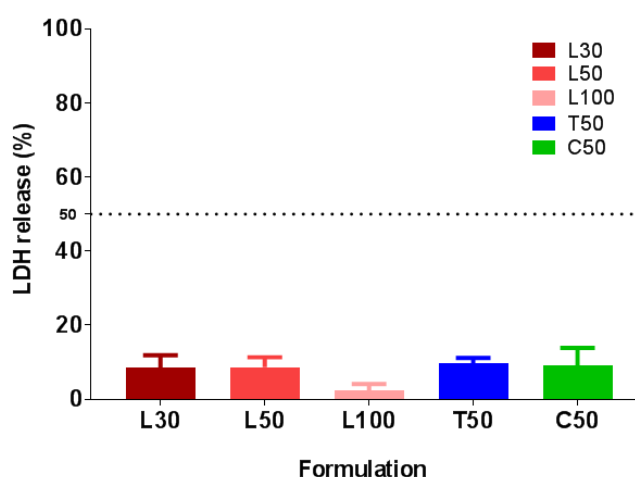


Figure S1: LDH release in the cell culture medium, after incubation of Calu-3 cells with B-LNC formulations at concentration of 0.05 mg/mL (LNC/HBSS-HEPES) (**Method S1**) in a 4 h experiment at 37°C. Triton X-100 (TX; 0.2% v/v) was employed as a positive control, and HBSS:HEPES was used as a negative control. Data represents the mean \pm SEM (N=4, n=4)

● Characterization of different prepared batches of FRET-L50 based on different DiO:Dil ratio

Table S5: Size, PDI and zeta potential of the prepared FRET-L50 batches for optimizing DiO:Dil ratio (n=1)

L50 (DiO:Dil) (w:w)	2:1	1:1	1:2	1:5	1:10
Size ⁺	52	55	53	55	57
Pdl ⁺	0.08	0.09	0.09	0.11	0.1
Zeta ⁺	-7	-7	-5	-6	-8

* The size of the lipid nanocapsules corresponds to the intensity peak.

✦ The batches were measured once, hence SD is not applied.

● LNC Size distribution

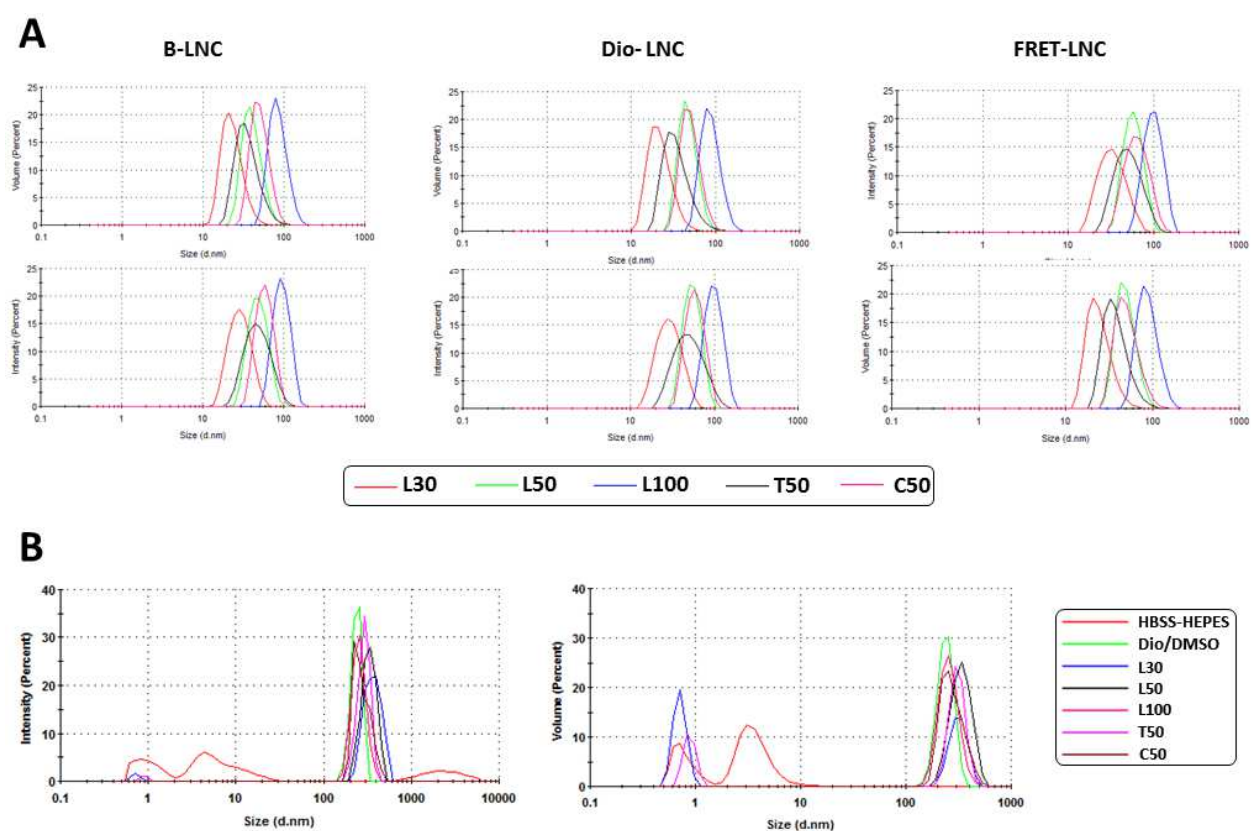


Figure S2: Size distribution of **(A)** a selected batch of each LNC formulation, **(B)** the samples in basolateral chamber after DiO-LNC (at concentration of 0.05 mg/mL (LNC/HBSS-HEPES)) exposure to differentiated Calu-3 cells for 4 h

- Cell population obtained from FACS analyses

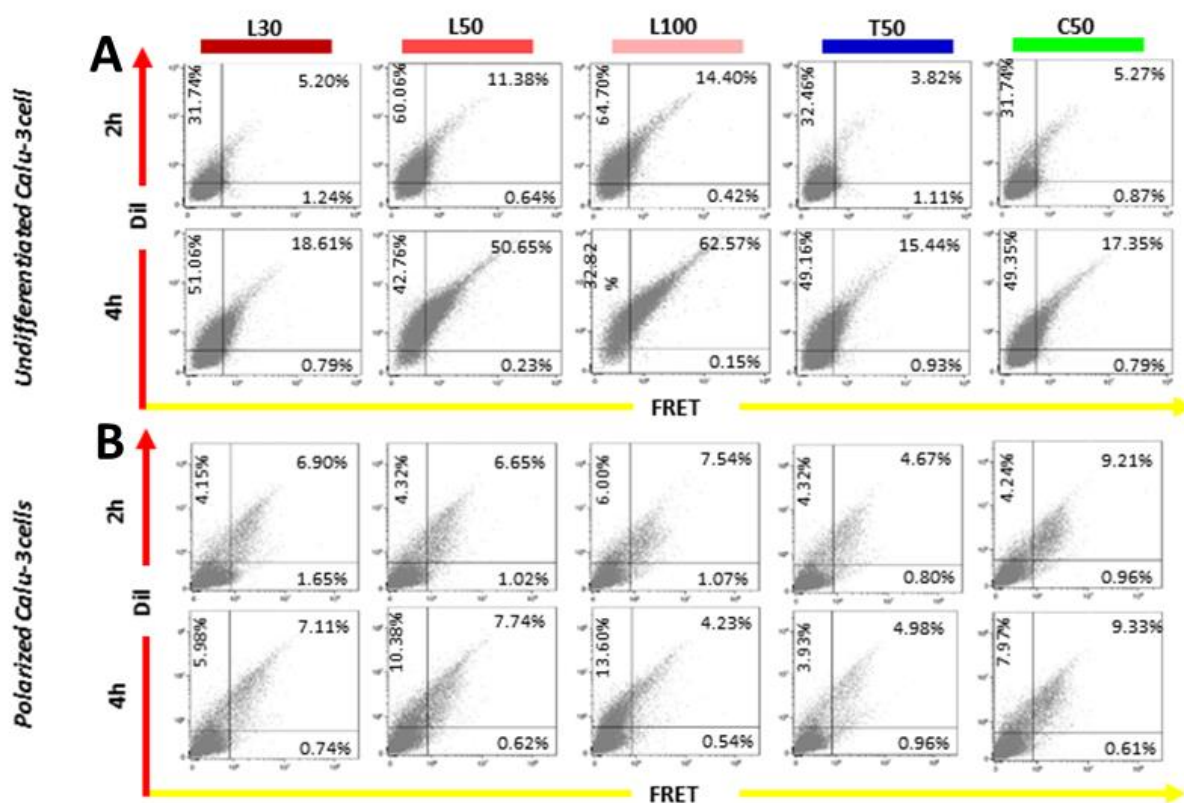


Figure S3: FACS analysis of the polarized or undifferentiated Calu-3 cells after treatment with FRET-LNC at concentration of 0.05 mg/mL (LNC/HBSS-HEPES) (**Method S1**) for 2 and 4 h of incubation: **A**) Comparison between DiI and FRET positive cells in undifferentiated cells, **B**) Comparison between DiI and FRET positive cells in polarized cells. A blue laser at 488 nm (λ_{em} 513/526 nm) and a yellow/green laser at 561 nm (λ_{em} 579/616 nm) were used as excitation source for the detection of DiO and DiI fluorescence, respectively. For FRET detection, the laser at 488 nm with λ_{em} 576/621 nm was employed. Cells treated with B-LNCs (L30, L50, L100, T50 and C50) was considered as negative control. As the figure shows, population of DiI-positive and FRET-positive cells increases after 2 and 4 h, indicating that LNCs uptake and degradation simultaneously happens. The data represents the mean \pm SD (n=4).

General Discussion

GB is the most aggressive, and the most frequent primary tumor of the brain in adults. The standard therapy consists in gross total tumor resection and post-operative adjuvant radiation and chemotherapy [16,31]. The prognosis remains poor, with a mean progression-free survival of 7 months and an average survival of 12 to 15 months. Recurrence occurs 6-7 months after surgery, and in 90% of cases at the margin of the surgical resection [408]. The location of tumor, its high vasculature and motility, and its protection by the BBB make difficult the effectiveness of therapeutic approaches. Over the past decade, angiogenesis has emerged as a leading target of pharmacological development for GB therapy. This development was as a result of the unsatisfactory outcomes with cytotoxic drugs and acknowledging that the substantial pathologic vascularization could make GB potentially susceptible to antiangiogenic therapy [409]. Bevacizumab, a humanized monoclonal antibody against VEGF has increasingly been used in the treatment of recurrent and newly diagnosed GB. Although this agent improves symptoms and allows for reduction in steroid, it has not demonstrated a significant improvement in overall survival compared with standard of care therapy [410].

In general, the major problems that concerns antiangiogenic therapy is mainly the antiangiogenic drug selection, the delivery system and, last but not least, the route of administration.

A smart choice of an antiangiogenic agent is not only based on its potency, but also, the molecular mechanism that it targets. Recently, multitarget antiangiogenic agents have attracted extensive attention in the realm of oncology, as potential therapeutic solutions to malignant tumors [411]. Although the molecular mechanisms that underlie persistent tumorigenesis and treatment resistance in GB are still insufficiently understood, it is well-proven that the growth, the invasion and the angiogenesis of the GB are integral with activation of RTKs [412]. Up to now, various antiangiogenic agents that target the kinase domains of RTKs have been studied in the context of GB and one of them is SFN. Despite its potential in *in vitro* and *in vivo* GB models, efficient outcomes are not reported from the clinical trials of SFN employment as a monotherapy or in combination of other chemotherapeutics for patients with progressive or recurrent GB [126, 129, 131, 132, 303, 306]. The poor results obtained from clinical trials may be due, in part, to the route of administration of the SFN. The poor solubility of SFN strongly limits its application for local treatment and this drug is

orally administered in the form of SFN tosylate tablets. Such systemic administration may be efficient for peripheral tumors, such as hepatocellular carcinoma, renal cell carcinoma, and thyroid cancer, but efficacy may be limited for brain tumors, for which SFN does not penetrate into the brain in sufficient amounts [413]. High systemic doses of this drug are required to obtain effective brain-tumor concentrations but the potentially adverse events associated with the systemic distribution of SFN, such as hand-foot skin reactions, rash, upper and lower gastro-intestinal distress, fatigue, and hypertension do not allow it [414]. In this regard, it is desirable to reformulate this antiangiogenic agent to increase brain-tumor delivery and limit side effects. Up to now, SFN has been encapsulated inside different nanoparticles, but none of these formulations have been tested on GB models. Furthermore, most of these formulations have major drawbacks, such as the presence of organic solvents or toxic compounds, preventing their clinical use. In the current thesis, we selected LNCs to reformulate SFN, and studied the effect of the prepared formulation on *in vitro* and *in vivo* GB models.

LNCs have the ability to encapsulate hydrophobic molecules in their lipid core. Up to now, many cytotoxic molecules have been encapsulated inside these nanocapsules without causing changes in their activity despite the heating steps in the preparation process [134]. In addition, LNC formulations have shown promising results for brain passive and active targeting and an efficacy on *in vivo* GB models [415][172,174,179,191,375–378]. In this regard, the primary goal of this project was to design a LNC formulation that would allow a sustained release of SFN. In general, the determining factor for LNC design is the excipients that participate in solubilization of the drug and the formation of the core of the nanocapsules. Based on the solubility study of SFN in different oily excipients, we found that the ideal one would be Transcutol® HP. To the fact that, after administration, the nanocapsules will have to diffuse through the extracellular space which has been estimated between 35 and 64 nm in diameter [416], the LNC was designed based on the Transcutol® HP with an approximate size of 50 nm (PDI of < 0.2). For finding the optimized SFN-LNCs, different amounts of SFN were encapsulated inside nanocapsules and the formulation with the least changes in characteristics, in comparison to blank LNCs, was selected. This formulation had an encapsulation efficiency of approximately 100%, with a drug payload of 2.11 ± 0.03 mg/g of LNC dispersion. Our findings indicate that LNCs have

superior efficiency over its rival which is liposomes. Indeed, Liu et al [320], produced liposome at size of about 100 nm to encapsulate SFN and even though they obtained the same encapsulation efficiency as ours, the drug loading was 0.05 mg/mL of SFN in liposome solution. It means that LNCs are capable to encapsulate SFN forty times more concentrated than liposomes. Both of these nanocarriers exhibited a much sustained SFN release in PBS medium at pH=7, where after 5 days, near to 20% drug release was observed [320,327]. This release is done in a more controlled way than their polymer counterparts under the above mentioned conditions, so that the release was reported as ~ 40-100% (in 4-5 days) for polymer nanoparticles [318,320,323,332,369-371] and ~ 30% (in 4-5 days) for polymer dendrimers and micelles [420,421]. The low release profile obtained with LNCs suggests that most of the SFN remained associated with the LNCs, which may be beneficial, as it would allow sufficient time for cells to capture the loaded LNCs. SFN-LNCs inhibited *in vitro* angiogenesis and the viability of the human U87MG GB cell line similarly to free SFN, suggesting that its activity is conserved by LNC encapsulation.

We evaluated the *in vivo* effect of SFN-LNCs in nude mice bearing intracerebral U87M tumors after their CED intratumoral administration. Drug administration through CED has the advantage to bypass the BBB and provide sustained drug delivery, leading to enhanced toxicity profiles and diminished dosing frequency [422,423]. The CED administration of LNCs has already been performed successfully on orthotopic GB models to deliver a lipophilic complex of Rhenium-188 (LNC188Re-SSS), ferrociphenol and paclitaxel [170,180,188]. In our study, four days following this local administration approach, we observed that SFN-LNCs increased the tumor blood flow and reduced tumor vessel area in U87MG-bearing mice. These data suggest that SFN-LNCs may have normalized abnormal vessel structures, potentially leading to increased blood perfusion. Vessel normalization following treatment with SFN or other tyrosine kinase inhibitors has already been described for various malignancies [74,87,302,376]. We did not observe such vascular changes following the treatment of U87MG-bearing mice with free SFN, highlighting the potential of SFN-LNCs. This may be due to the capacity of LNCs to improve the retention of SFN within the tumor. The prolonged retention of LNCs in brain tumors following intratumoral CED administration was previously shown using LNCs loaded with LNC188Re-SSS [182,353]. Seventy percent of the 188Re-SSS activity was present in the tumor region 24 h after

LNC¹⁸⁸Re-SSS injection, whereas free ¹⁸⁸Re-perrhenate was rapidly eliminated in the urine and feces. In addition to the induction of vascular changes, SFN-LNC-treatment reduced the number of proliferative Ki67⁺ cells in the tumor but this was not sufficient to modify the growth rate of U87MG tumors. The absence of this effect is probably due to an insufficient dose of SFN-LNCs. Siegelin et al. [125] observed that a daily treatment of U87MG-bearing mice with SFN (100 mg/kg) by intraperitoneal injections resulted in an inhibition of tumor cell proliferation and reduction of angiogenesis with a prolonged survival of mice. We injected only one dose of SFN-LNCs (3.5 µg/mouse), a lower dose than was used in the study of Siegelin et al. corresponding to about 2 mg/mouse/day. A repeated-injection regimen should be planned to increase the injected drug dose and, consequently, to further enhance antitumour efficacy. Despite of the fact that CED offers a number of advantages over conventional drug delivery such as bypass of the BBB, high local concentration of drug, targeted distribution through large brain volumes and minimization of systemic side effects, it remains as an invasive method making a repeated treatment option difficult. In a clinical context, systemic administration of SFN-LNCs could be simpler, less costly and would allow for a chronic treatment. Therefore, it is desirable to find a systemic route for administration of the LNC formulation.

Because of the presence of the BBB, drug delivery to the brain by systemic routes remains challenging to achieve an effective response to treatment [425,426]. In the case of brain tumors, the BBB becomes abnormal [427]. For that reason, the systemic delivery of drugs for treatment of tumors located in the brain may become achievable. Brigger et al. [428], demonstrated that after an intravenous injection of PEG-PHDCA nanoparticles or PHDCA nanoparticles into orthotopic 9L gliosarcoma model in rats, both types of nanoparticles were preferentially accumulated in the tumor, while no accumulation of these nanoparticles was detected for the healthy rats at the intracranial injection of NaCl. However, only a minute fraction of the injected dose was detected in the tumor tissues after 30 minutes of injection (maximal concentration about 0.22% of initial dose per gram of tumor tissues). Hence, although the BBB was disrupted because of the brain tumor, the efficiency of drugs administered by a systemic injection was still minimal by low penetration across this barrier [429]. Furthermore, many solid tumors have a high interstitial fluid pressure, which acts also as a barrier to transcapillary transport and prevents the homogeneous distribution of

therapeutic agent in tumor tissues [430]. In case of LNCs, Huynh et al. [171], reported that a single intravenous injection of ferrociphenol-loaded LNCs, decorated with DSPE-mPEG₂₀₀₀, could dramatically decrease the volume of the subcutaneous 9L gliosarcoma tumor in rats compared to the group treated with drug loaded LNCs without any further surface modification. In contrast, after treatment of orthotopic 9L gliosarcoma-bearing rats by a single intravenous injection of ferrociphenol-loaded LNCs, with or without DSPE-mPEG₂₀₀₀, no significant difference was observed in the median survival times of the rats (27.5 days vs 28 days, respectively). Such DSPE-mPEG₂₀₀₀ surface modification could result in a great accumulation of LNCs in the heterotopic tumor, but this modification is insufficient to allow an effective LNC accumulation in the orthotopic tumor model. For interest, the treatment by intra-carotid injection with ferrociphenol-loaded LNCs coated with a cell-internalizing peptide (NFL-TBS.40–63) that specifically interacts with tubulin-binding sites demonstrated an interesting efficacy that was strengthened by the presence of a long-term survival rat until 44 days after 9L cell implantation [174]. Although intra-carotid injection of drugs results in higher LNC tumor accumulation, this administration route increases the risk of embolism and hemorrhage [431].

LNCs have been proven to be interesting nanocarriers for oral administration [134] and they have already shown promising properties for the oral delivery of poorly water-soluble drugs such as SN38 [141], paclitaxel [142], fondaparinux [157] and miltefosine [432]. These nanocapsules have demonstrated in vitro stability in simulated gastrointestinal media [433] and it has been proven that they can enhance diffusion of therapeutics across the intestinal mucus or the human intestinal epithelium Caco-2 cell model [141,387]. These nanocapsules have never been administered orally for the purpose of drug delivery to orthotopic GB models. Indeed, choosing oral administration route for drug delivery to brain is not an ideal approach because the only way for the drug to reach the brain site is through blood circulation, and therefore the drug would need to cross the BBB. In this regard, this administration route results in low therapeutic levels within the brain tissue and the utilization of higher potency or more concentrated doses may lead to serious toxic side effects [373].

Intranasal administration of LNCs can be considered as a noninvasive and safe alternative delivery way to intravenous or oral administration route. [434]. It has attracted great interest due the delivery passages through the respiratory and olfactory

regions of nasal cavity to the brain, bypassing the BBB and offering fast delivery of drugs from the nose to the brain site [360–363,435]. Up to now, various lipid and polymer nanosystems have been developed to enhance nose-to-brain drug delivery and the inherent mechanisms exerted by them were generally reported as protection of the encapsulated therapeutic agent from biological and/or chemical degradation, prolonged retention in the nasal mucosa, improved permeation through epithelium cells, and bypassing the P-gp efflux pump [277,395,396]. However, there is a paucity of reports about the fate and the integrity of nanosystems after intranasal administration for targeting the brain site, knowing that these parameters play vital roles in the success of the developed delivery system. Lochhead and Thorne [373] suggested that there are three sequential transport steps essential for a therapeutic substance to be transported to far-reaching sites within the brain following intranasal administration: (1) crossing the olfactory or respiratory epithelial barriers located within the nasal passages, (2) delivery from the nasal mucosa to area of brain entry near the pial brain surface in the cranial compartment (i.e. entrance of peripheral olfactory or trigeminal nerve-associated sections incorporating the delivery pathways), and (3) movement of the therapeutic substance from these entries to other locations of brain (**Figure 12**). If the integrity of nanocarriers is conserved after crossing these three sequential transport steps, such nanocarriers are potential to be successful in nose-to-brain drug delivery.

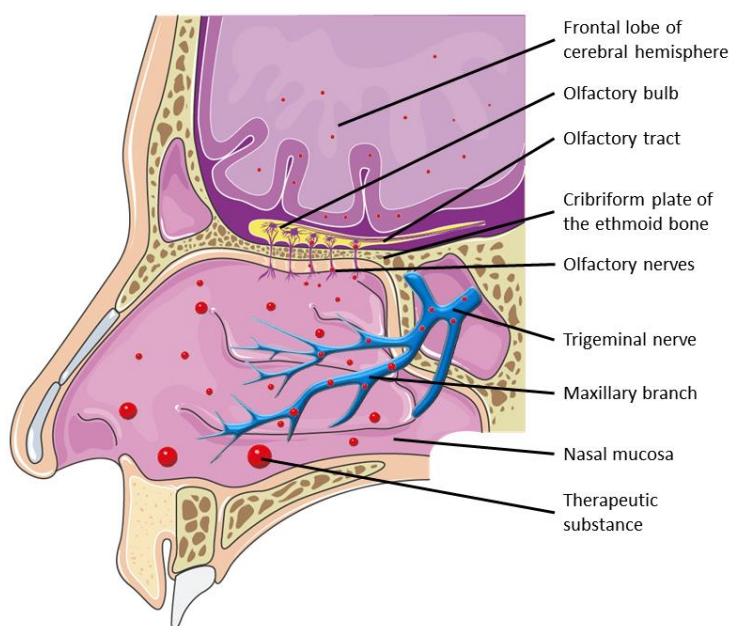


Figure 15: The virtual passages of nose-to-brain delivery

We investigated the fate of different LNCs, based on size (30, 50 and 100 nm) and matrix components (Labrafac™, glyceryl tricaprlylate, or a mixture of Transcutol, Labrafac™ and Labrafil®), after crossing the human airway epithelial cell line Calu-3 monolayer that mimics nasal epithelial barrier. Concerning the selection of a model for pre-clinical studies of nasal administration, *in vitro* cell culture models that closely simulate the physiological conditions of nasal mucosa have emerged as an affordable and efficacious strategy [224,436,437]. In this project, due to the limitations with primary cell cultures, such as limited subsequent passages [243], we selected Calu-3 cells, which is a ciliated, mucus-secreting cell line and has numerously been employed in preparation of nasal mucosa models [261,264–273]. To study LNC transport and permeation through nasal mucosa, we cultured cells on Transwell® at the air interface, which resulted in differentiated cell monolayers and closely resemble that of *in vivo* respiratory mucosa [438]. This model was further validated by measuring the TEER values which is a strong indicator of the tight junction formation and integrity of the cellular barrier before the evaluation for transport of drugs or chemicals [439]. For transport study, we encapsulated DiO, a lipophilic carbocyanine fluorophore, inside LNCs. According to Bastiat et al. [397], using lipophilic carbocyanine dyes (DiO, DiI and DiD) for labeling LNCs is recommended since, unlike other dyes, they remain inside the nanocapsules in the presence of lipid acceptor compartments. We found that employment of LNCs dramatically increased the permeability of DiO across the Calu-3 cell monolayer compared with the 'free DiO'. This result is in agreement with other studies who observed that LNCs improved permeability of paclitaxel [142] or SN38 [141] across the human intestinal epithelium Caco-2 cell model. Our observations revealed that the transport increase of DiO was dependent on size of LNCs with a highest transport obtained for the largest LNCs and it was independent of LNC matrix components. Based on these results, it can be concluded that LNCs could be advantageous nanocarriers for systematic administration. The systematic administration could facilitate repetition of administration for increasing the uptake level of drugs by cancer cells. Therefore through systematic administration of LNCs a therapeutic effect could be achievable.

To use LNCs for the purpose of nose-to-brain delivery of a therapeutic agent, their integrity after transport across the nasal mucosa model must be maintained to avoid the release of the agent before its brain penetration. To investigate the fate of LNCs

after their interaction with the mucosa model, we used the Förster resonance energy transfer (FRET) technique which is the most prevalent fluorescence spectroscopy technique used to observe proximity at the nanoscale level [440]. Briefly, it is based on the interactions between spatially-close (2 to 10 nm) donor and acceptor dye molecules. FRET occurs when the emission spectrum of the donor overlaps with the excitation spectrum of the acceptor. The excitation energy of the donor is transferred to the acceptor whose subsequent emission can be detected. The relative FRET efficiency also called the proximity ratio that characterizes the efficacy of the transfer and that is closely related to the dye proximity is a reliable indicator a preserved nanoscale environment [380,441]. In this study, we used DiO (donor) and Dil (acceptor) as the FRET pair. As it was mentioned before, these carbocyanine dyes locate in the surfactant shell (Lipoïd® and Kolliphore®) around the oil core of the LNCs [397]. We checked that DiO/Dil encapsulated inside LNCs could not interact with another lipophilic compartment which could lead to a FRET signal loss even if the LNCs stayed intact. According to the method of Bastiat et al. [397], the relative FRET efficiency was preserved after mixing dye-loaded LNCs with pure oils indicating the absence of a leakage phenomenon. We observed a decrease of the relative FRET efficiency around 40% after the passage of LNCs across the Calu-3 cell monolayer regardless of size and matrix components. This result suggests that LNCs were subjected to degradation through their passage across Calu-3 cell monolayer because the destruction of LNCs with organic solvents led to a similar decrease of the relative FRET efficiency. In accordance with that, we did not find particles of size corresponding to LNCs. Only large particles were observed which could probably be attributed to extracellular vesicles released by Calu-3 cells since these are also observed after incubation of the cells with 'free DiO'. This degradation seems to happen soon after the capture of LNCs by Calu-3 cells since the analysis of the relative FRET efficiency inside the cells showed the same percent of decrease. To date, studies on transport of integral nanocarriers from nose to brain gave conflicting results. For example, using vertical Franz diffusion chamber or fluorescence microscopy and stereology, Mistry et al. [442,443], did not observe the transport of polystyrene nanoparticles across the excised olfactory tissue irrespective of particle size or surface modification. Ahmad et al. performed *ex vivo* imaging of nasal mucosa, brain and trigeminal nerves 1 h after the intranasal administration of nanoemulsions (NEs) labeled with aggregation-caused quenching (ACQ) probes [95]. They found that

integral NEs can be delivered to the olfactory bulb, but in minute quantity to the brain, whereas the cargoes can be released and permeate into the brain in more amount.

Contrary to our data, an integrity of FRET-LNCs was observed though their transport across the intestinal barrier [381,382]. Roger et al. [381], used two complementary techniques, FRET and nanoparticle tracking analysis (NTA) to analyze the fate of LNCs after their passage across an intestinal epithelium model (Caco-2 cell model). They showed that, after 2 h, the presence of intact FRET-LNCs in the basolateral side of the cell layer corresponding to around 0.3% of the initial quantity of LNCs. Groo et al. [384], have also shown the stability and diffusion of FRET-LNCs in intestinal mucus. The FRET efficiency remained at 78% after 3 h. This slight loss of FRET efficiency (< 25%) was not considered a sign of LNC destruction but, rather, an increase of diameter LNCs of 5 nm after contact with mucus (swelling). The difference of results between these studies with ours could be in part due to the employed technique and the barrier characteristics of epithelial cultures modelling the airway and intestinal mucosa. Roger et al. [381], used two lipophilic cyanine dyes (DiD and DiI) bearing the highly hydrophobic tetraphenyl borate (TPB) counterion to achieve an efficient FRET signal. TPB improves dye solubility in oil and consequently the dye loading capacity. Application of these TPB-based dyes may be more effective than the lipophilic carbocyanine dyes we employed to detect integral LNCs. The discrepancy of our results could also be due to the presence of mucus in the Calu-3 cell layer which is absent in Caco-2 cell layer. Vllasaliu et al. [400] showed that the presence of mucus notably restricts nanoparticle transport across the epithelium.

Knowing that LNCs undergo degradation after transport across mucosa model, it is logical to doubt the success of these nanocarriers for safe delivery of cytotoxic drug from nose to the brain site. To escort SFN-LNCs from nose to the brain site, we tested another alternative by using MSCs which can cross the BBB and display brain tumor tropism after systemic and local administration [154,444–447]. Our laboratory and others have shown that MSCs can deliver chemotherapy drugs to brain tumors without genetic modification [154,172,448–450]. For example, we have shown that MSCs can deliver LNCs containing an organometallic complex (ferrociphenol) in the heterotopic and orthotopic U87MG GB models [154,172]. MSCs were also able to take up and release paclitaxel and to induce cytotoxic damage in GB xenografts [450,451]. Furthermore, similar to what Balyasnikova et al. reported [445], we observed that

MSCs could penetrate the brain from the nasal cavity and infiltrate intracranial glioma xenografts in a mouse model [309] (**Annex 2**). The migration of MSCs may occur through the cribriform plate and into brain tissue via the olfactory and trigeminal pathways [452]. These two clues led us toward employing MSCs as a vehicle for SFN-LNCs that could ameliorate the intranasal delivery of the drug to the brain. Nevertheless, we observed that MSCs could not internalize the SFN-LNC efficiently, while these cells can be primed by SFN alone (**Table 1**) [309].

Table 6: Quantity and percentage of SFN associated with the MSCs after 1 h of incubation with SFN or SFN/LNC (20 μ M)

Sample	SFN content (pg/cell)	SFN uptake (%)
SFN-LNC/MS ¹	0.56 \pm 0.02	2.41 \pm 0.09
SFN /MS ²	8.82 \pm 0.50	37.94 \pm 2.17

¹SFN-LNC/MS¹: the MSC cells primed with SFN-LNC formulation

²SFN /MS²: the MSC cells primed with SFN solution

The results do not follow what we previously described, so that MSCs could internalize ferrociphenol-loaded LNCs (20 pg ferrociphenol/cell and 16% ferrociphenol uptake) [172]. Such discrepancy could be attributed to the lipid components used in the formulation of these two types of loaded LNCs. Ferrociphenol-loaded LNCs were prepared with LabrafacTM, whereas SFN-LNCs were produced with Transcutol[®], owing to the fact that SFN is very poorly soluble in LabrafacTM. The encapsulation of a fluorophore, the DiO, in these two types of LNCs validated our hypothesis, since 80% of the MSCs internalized the LabrafacTM-based LNCs, while the cell internalization was around 3% for the Transcutol[®]-based LNCs (**Figure 2**).

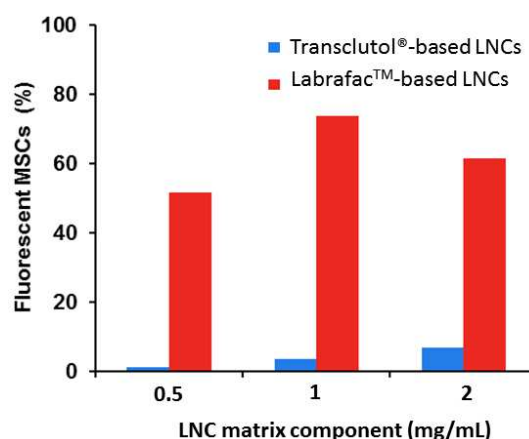


Figure 16: Internalization of LNCs (made of Transclutol[®] or LabrafacTM) by MSCs analyzed using flow cytometry. The nanocapsules were labeled with Dio, which is a hydrophobic fluorophore. The MSCs were incubated for 1 h with different concentrations of each LNC. After washing, the cells were analyzed by flow cytometry and the percentage of Dio-positive cells was determined.

Such dissimilar behavior of MSCs toward internalization of LNCs with different lipid components was out of expectation. The Transcutol[®] that is a co-surfactant might change the surface of LNCs and this could account for the preferential uptake of Labrafac[™]-based LNCs by MSCs.

Following the obtained results, we further continued by directly priming the MSCs with free SFN. Subsequently, we defined the optimal but non-lethal dose of SFN that can be internalized by MSCs. We observed that 80% of MSCs remained viable seven days after priming with SFN. HPLC analysis showed that MSCs were able to release 60% of the drug into the culture medium after 96 h, in a time-dependent manner. The cytostatic activity of the released SFN was entirely conserved, resulting in a significant inhibition of U87MG and endothelial cell proliferation *in vitro*. We further investigated the *in vivo* effect of SFN-primed MSCs on the orthotopic U87MG GB model, following their intranasal administration. SFN-primed MSCs reduced tumor angiogenesis, resulting in a significant decrease of the number of large vessels while no decrease in angiogenesis was observed following the intranasal administration of SFN alone. This highlights the potential value of MSCs as a vector for carrying SFN to the intracerebral tumor following administration via intranasal route. Although antiangiogenic effect was evident, no reduction in tumor size was observed. The absence of effect of therapeutic MSCs on GB growth inhibition could be attributed the insufficient dose of SFN. As described above for SFN-LNCs, we injected only two doses of SFN-primed MSCs (about 5.3 µg/mouse), a lower dose than was used in the study of Siegelin *et al.* corresponding to about 2 mg/mouse/day. The dose of SFN carried by MSCs may be sufficient to have affected endothelial cells, which are four times more sensitive to SFN than U87MG cells but ineffective against U87MG cells *in vivo*. The modest therapeutic effect of MSCs on GB growth inhibition may also be due to the pro-tumorigenic and proangiogenic properties of these cells. Even if the role of MSCs in cancer progression remains a matter of heated debate, increasing numbers of studies are highlighting these properties [454–457]. In line with these studies, we found that the intranasal administration of unprimed MSCs induced a significant increase of the number of small vessels in the U87MG tumor, which was abolished when MSCs were primed with SFN. Different studies indicate that MSCs promote angiogenesis by secreting angiogenic factors, such as VEGF, releasing exosomes, recruiting endothelial progenitors, and/or transdifferentiating into endothelial cells

[458,459]. Even though we did not observe an effect of unprimed MSCs on tumor volume, MSCs are reported to facilitate tumor growth through their secretion of various anti-inflammatory cytokines and proangiogenic factors [455–457]. These data indicate that the pro-tumorigenic and pro-angiogenic properties of MSCs may have limited the action of the released SFN. This calls into question the suitability of MSCs for use in GB therapy and renders it necessary to find methods guaranteeing the safety of this cellular vector after drug delivery.

Conclusions and Future Perspectives

In this thesis work, we described a new formulation for SFN via its encapsulation into LNCs. CED administration of this formulation in U87MG-bearing mice allowed a more efficient retention of SFN within the intracerebral tumor in comparison to free drug. This tumor accumulation decreased the proportion of proliferating cells in the tumor and induced early tumor vascular normalization, characterized by increased tumor blood flow and reduced tumor vessel area. Despite these changes, the growth rate of SFN-LNCs-treated tumors was comparable to control vehicle-treated tumors or SFN-treated tumors. It is considered that strategies which improve vascular function in GB should improve the delivery of other drugs capable of crossing the BBB and this should be associated with an increase in therapeutic activity [73]. For example, pre-clinically, the delivery of TMZ in an intracerebral model of glioma increased after treatment with the angiogenesis inhibitor SU5416 which restored the capillary architecture [354]. Thus, the vascular normalization induced with SFN-LNCs may create a window where blood flow is improved, leading to an opportunity to improve drug delivery for other drugs.

To increase the effectiveness of SFN-LNCs, repeated injections of this formulation are needed. As described above, CED is an invasive method making a repetitive treatment option difficult. In a clinical context, systemic administration of SFN-LNCs would be simpler, less costly and would allow for a chronic treatment. We wanted to use MSCs to perform systemic administration of SFN-LNCs. However, we observed the inability of MSCs to uptake Transcutol[®]-based LNCs while they can uptake free SFN. The understanding of the reasons why MSCs couldn't uptake Transcutol[®]-based LNCs could be interesting but considering the pro-tumorigenic and pro-angiogenic properties of MSCs, we need to find ways of guaranteeing the safety of this cellular vector for clinical use. One possibility would be to use a suicide gene or a small molecule to induce senescence in the MSCs after drug delivery. In parallel, we determined if the intranasal administration of LNCs could be a noninvasive and safe alternative delivery method. We observed that employment of LNCs increased the permeability of the dye across the nasal epithelial barrier model (Calu-3 cell model), but these nanocapsules are degraded after their uptake by the cells. The rigid shell around the core of LNC, which is mainly due to crystallization of Lipoïd[®] [134,146], could not act as a shield against degradation. The degradation of LNCs could be as a result of phospholipase A2 (PLA2) activity, which is prevalent in respiratory epithelial cells [404–406]. It is

reported that PLA2, could result in degradation of cubic micellar nanoparticles which have lecithin in their matrix [403]. In another study, Tagami et al [401], prepared hybrid nanoliposomes which can release a loaded cargo through the PLA2 activity. They have also reported that nanoliposomes made out of mixture of dipalmitoylphosphatidylcholine and cholesterol were not degraded in presence of PLA2. In case that PLA2 is the enzyme that causes degradation of LNCs, nanocapsules should be designed with excipients such as the above mentioned mixture, which are not substrates for this enzyme. Therefore, for nose-to-brain delivery of LNC formulations, it is worth developing nanocapsules which their integrity is not jeopardized by enzymatic activity.

Considering our observations, LNCs are potential nanocarriers for local delivery of antiangiogenic drugs in GB, but it is necessary to redesign these nanocapsules to enhance their efficiency for nose-to brain drug delivery.

References

- [1] F.G. Davis, V. Kupelian, S. Freels, B. McCarthy, T. Surawicz, Prevalence estimates for primary brain tumors in the United States by behavior and major histology groups., *Neuro. Oncol.* 3 (2001) 152–8. <http://www.ncbi.nlm.nih.gov/pubmed/11465395> (accessed March 15, 2018).
- [2] T.F. Cloughesy, W.K. Cavenee, P.S. Mischel, Glioblastoma: From Molecular Pathology to Targeted Treatment, *Annu. Rev. Pathol. Mech. Dis.* 9 (2014) 1–25. doi:10.1146/annurev-pathol-011110-130324.
- [3] P. Giglio, Chemotherapy for Glioblastoma: Past, Present, and Future, in: *Glioblastoma*, Springer New York, New York, NY, 2010: pp. 203–216. doi:10.1007/978-1-4419-0410-2_10.
- [4] Q.T. Ostrom, H. Gittleman, P. Farah, A. Ondracek, Y. Chen, Y. Wolinsky, N.E. Stroup, C. Kruchko, J.S. Barnholtz-Sloan, CBTRUS Statistical Report: Primary Brain and Central Nervous System Tumors Diagnosed in the United States in 2006-2010, *Neuro. Oncol.* 15 (2013) ii1-ii56. doi:10.1093/neuonc/not151.
- [5] H. Loiseau, A. Huchet, M. Rué, A. Cowppli-Bony, I. Baldi, Épidémiologie des tumeurs cérébrales primitives, *Rev. Neurol. (Paris)*. 165 (2009) 650–670. doi:10.1016/j.neurol.2009.04.002.
- [6] A. Brodbelt, D. Greenberg, T. Winters, M. Williams, S. Vernon, V.P. Collins, (UK) National Cancer Information Network Brain Tumour Group, Glioblastoma in England: 2007–2011, *Eur. J. Cancer.* 51 (2015) 533–542. doi:10.1016/j.ejca.2014.12.014.
- [7] D.N. Louis, H. Ohgaki, O.D. Wiestler, W.K. Cavenee, P.C. Burger, A. Jouvet, B.W. Scheithauer, P. Kleihues, The 2007 WHO classification of tumours of the central nervous system., *Acta Neuropathol.* 114 (2007) 97–109. doi:10.1007/s00401-007-0243-4.
- [8] J.A. Schwartzbaum, J.L. Fisher, K.D. Aldape, M. Wrensch, Epidemiology and molecular pathology of glioma, *Nat. Clin. Pract. Neurol.* 2 (2006) 494–503. doi:10.1038/ncpneuro0289.
- [9] R.G.W. Verhaak, K.A. Hoadley, E. Purdom, V. Wang, Y. Qi, M.D. Wilkerson, C.R. Miller, L. Ding, T. Golub, J.P. Mesirov, G. Alexe, M. Lawrence, M. O’Kelly, P. Tamayo, B.A. Weir, S. Gabriel, W. Winckler, S. Gupta, L. Jakkula, H.S. Feiler, J.G. Hodgson, C.D. James, J.N. Sarkaria, C. Brennan, A. Kahn, P.T. Spellman, R.K. Wilson, T.P. Speed, J.W. Gray, M. Meyerson, G. Getz, C.M. Perou, D.N. Hayes, T.C.G.A.R. Cancer Genome Atlas Research Network, Integrated genomic analysis identifies clinically relevant subtypes of glioblastoma characterized by abnormalities in PDGFRA, IDH1, EGFR, and NF1., *Cancer Cell.* 17 (2010) 98–110. doi:10.1016/j.ccr.2009.12.020.
- [10] D.W. Parsons, S. Jones, X. Zhang, J.C.-H. Lin, R.J. Leary, P. Angenendt, P. Mankoo, H. Carter, I.-M. Siu, G.L. Gallia, A. Olivi, R. McLendon, B.A. Rasheed, S. Keir, T. Nikolskaya, Y. Nikolsky, D.A. Busam, H. Tekleab, L.A. Diaz, J. Hartigan, D.R. Smith, R.L. Strausberg, S.K.N. Marie, S.M.O. Shinjo, H. Yan, G.J. Riggins, D.D. Bigner, R. Karchin, N. Papadopoulos, G. Parmigiani, B. Vogelstein, V.E. Velculescu, K.W. Kinzler, An Integrated Genomic Analysis of Human Glioblastoma Multiforme, *Science* (80-.). 321 (2008) 1807–1812.

- doi:10.1126/science.1164382.
- [11] M. Sanson, Y. Marie, S. Paris, A. Idbaih, J. Laffaire, F. Ducray, S. El Hallani, B. Boisselier, K. Mokhtari, K. Hoang-Xuan, J.-Y. Delattre, Isocitrate Dehydrogenase 1 Codon 132 Mutation Is an Important Prognostic Biomarker in Gliomas, *J. Clin. Oncol.* 27 (2009) 4150–4154. doi:10.1200/JCO.2009.21.9832.
- [12] M.E. Hegi, A.-C. Diserens, T. Gorlia, M.-F. Hamou, N. de Tribolet, M. Weller, J.M. Kros, J.A. Hainfellner, W. Mason, L. Mariani, J.E.C. Bromberg, P. Hau, R.O. Mirimanoff, J.G. Cairncross, R.C. Janzer, R. Stupp, *MGMT* Gene Silencing and Benefit from Temozolomide in Glioblastoma, *N. Engl. J. Med.* 352 (2005) 997–1003. doi:10.1056/NEJMoa043331.
- [13] T. Gorlia, M.J. van den Bent, M.E. Hegi, R.O. Mirimanoff, M. Weller, J.G. Cairncross, E. Eisenhauer, K. Belanger, A.A. Brandes, A. Allgeier, D. Lacombe, R. Stupp, Nomograms for predicting survival of patients with newly diagnosed glioblastoma: prognostic factor analysis of EORTC and NCIC trial 26981-22981/CE.3, *Lancet Oncol.* 9 (2008) 29–38. doi:10.1016/S1470-2045(07)70384-4.
- [14] A. Etcheverry, M. Aubry, M. DE Tayrac, E. Vauleon, R. Boniface, F. Guenot, S. Saikali, A. Hamlat, L. Riffaud, P. Menei, V. Quillien, J. Mosser, DNA methylation in glioblastoma: impact on gene expression and clinical outcome., *BMC Genomics.* 11 (2010) 701. doi:10.1186/1471-2164-11-701.
- [15] A. Etcheverry, M. Aubry, A. Idbaih, E. Vauleon, Y. Marie, P. Menei, R. Boniface, D. Figarella-Branger, L. Karayan-Tapon, V. Quillien, M. Sanson, M. de Tayrac, J.-Y. Delattre, J. Mosser, DGKI Methylation Status Modulates the Prognostic Value of *MGMT* in Glioblastoma Patients Treated with Combined Radio-Chemotherapy with Temozolomide, *PLoS One.* 9 (2014) e104455. doi:10.1371/journal.pone.0104455.
- [16] R. Stupp, W.P. Mason, M.J. van den Bent, M. Weller, B. Fisher, M.J.B. Taphoorn, K. Belanger, A.A. Brandes, C. Marosi, U. Bogdahn, J. Curschmann, R.C. Janzer, S.K. Ludwin, T. Gorlia, A. Allgeier, D. Lacombe, J.G. Cairncross, E. Eisenhauer, R.O. Mirimanoff, European Organisation for Research and Treatment of Cancer Brain Tumor and Radiotherapy Groups, National Cancer Institute of Canada Clinical Trials Group, Radiotherapy plus Concomitant and Adjuvant Temozolomide for Glioblastoma, *N. Engl. J. Med.* 352 (2005) 987–996. doi:10.1056/NEJMoa043330.
- [17] A. GUILLAUDEAU, K. DURAND, H. RABINOVITCH-CHABLE, I. POMMEPUY, L. MESTUROUX, S. ROBERT, A. CHAUNAVEL, J.-J. MOREAU, F. LABROUSSE, Adult diffuse gliomas produce mRNA transcripts encoding EGFR isoforms lacking a tyrosine kinase domain, *Int. J. Oncol.* 40 (2012) 1142–1152. doi:10.3892/ijo.2011.1287.
- [18] B. Coulibaly, I. Nanni, B. Quilichini, J. Gaudart, P. Metellus, F. Fina, C. Boucard, O. Chinot, L. Ouafik, D. Figarella-Branger, Epidermal growth factor receptor in glioblastomas: correlation between gene copy number and protein expression, *Hum. Pathol.* 41 (2010) 815–823. doi:10.1016/J.HUMPATH.2009.09.020.
- [19] M. Labussiere, A. Idbaih, X.-W. Wang, Y. Marie, B. Boisselier, C. Falet, S. Paris,

- J. Laffaire, C. Carpentier, E. Criniere, F. Ducray, S. El Hallani, K. Mokhtari, K. Hoang-Xuan, J.-Y. Delattre, M. Sanson, All the 1p19q codeleted gliomas are mutated on IDH1 or IDH2, *Neurology*. 74 (2010) 1886–1890. doi:10.1212/WNL.0b013e3181e1cf3a.
- [20] M.J. Riemenschneider, J.W.M. Jeuken, P. Wesseling, G. Reifenberger, Molecular diagnostics of gliomas: state of the art., *Acta Neuropathol.* 120 (2010) 567–84. doi:10.1007/s00401-010-0736-4.
- [21] R.B. Jenkins, H. Blair, K. V. Ballman, C. Giannini, R.M. Arusell, M. Law, H. Flynn, S. Passe, S. Felten, P.D. Brown, E.G. Shaw, J.C. Buckner, A t(1;19)(q10;p10) Mediates the Combined Deletions of 1p and 19q and Predicts a Better Prognosis of Patients with Oligodendroglioma, *Cancer Res.* 66 (2006) 9852–9861. doi:10.1158/0008-5472.CAN-06-1796.
- [22] D. Kaneshiro, T. Kobayashi, S.T. Chao, J. Suh, R.A. Prayson, Chromosome 1p and 19q Deletions in Glioblastoma Multiforme, *Appl. Immunohistochem. Mol. Morphol.* 17 (2009) 512–516. doi:10.1097/PAI.0b013e3181a2c6a4.
- [23] D. Orringer, D. Lau, S. Khatri, G.J. Zamora-Berridi, K. Zhang, C. Wu, N. Chaudhary, O. Sagher, Extent of resection in patients with glioblastoma: limiting factors, perception of resectability, and effect on survival, *J. Neurosurg.* 117 (2012) 851–859. doi:10.3171/2012.8.JNS12234.
- [24] S.P. Reddy, R. Britto, K. Vinnakota, H. Aparna, H.K. Sreepathi, B. Thota, A. Kumari, B.M. Shilpa, M. Vrinda, S. Umesh, C. Samuel, M. Shetty, A. Tandon, P. Pandey, S. Hegde, A.S. Hegde, A. Balasubramaniam, B.A. Chandramouli, V. Santosh, P. Kondaiah, K. Somasundaram, M.R.S. Rao, Novel Glioblastoma Markers with Diagnostic and Prognostic Value Identified through Transcriptome Analysis, *Clin. Cancer Res.* 14 (2008) 2978–2987. doi:10.1158/1078-0432.CCR-07-4821.
- [25] Y. Jin, W. Xiao, T. Song, G. Feng, Z. Dai, Expression and Prognostic Significance of p53 in Glioma Patients: A Meta-analysis, *Neurochem. Res.* 41 (2016) 1723–1731. doi:10.1007/s11064-016-1888-y.
- [26] M. Davis, Glioblastoma: Overview of Disease and Treatment, *Clin. J. Oncol. Nurs.* 20 (2016) S2–S8. doi:10.1188/16.CJON.S1.2-8.
- [27] P.A. Blissitt, American Association of Neuroscience Nurses, Clinical practice guideline series update: care of the adult patient with a brain tumor., *J. Neurosci. Nurs.* 46 (2014) 367–368. doi:10.1097/JNN.0000000000000088.
- [28] S. V. Ellor, T.A. Pagano-Young, N.G. Avgeropoulos, Glioblastoma: Background, Standard Treatment Paradigms, and Supportive Care Considerations, *J. Law, Med. Ethics.* 42 (2014) 171–182. doi:10.1111/jlme.12133.
- [29] D.R. Johnson, S.E. Fogh, C. Giannini, T.J. Kaufmann, A. Raghunathan, P. V. Theodosopoulos, J.L. Clarke, *Case-Based Review: newly diagnosed glioblastoma*, *Neuro-Oncology Pract.* 2 (2015) 106–121. doi:10.1093/nop/npv020.
- [30] M.C. Chamberlain, Radiographic patterns of relapse in glioblastoma, *J.*

- Neurooncol. 101 (2011) 319–323. doi:10.1007/s11060-010-0251-4.
- [31] R. Stupp, M.E. Hegi, W.P. Mason, M.J. van den Bent, M.J. Taphoorn, R.C. Janzer, S.K. Ludwin, A. Allgeier, B. Fisher, K. Belanger, P. Hau, A.A. Brandes, J. Gijtenbeek, C. Marosi, C.J. Vecht, K. Mokhtari, P. Wesseling, S. Villa, E. Eisenhauer, T. Gorlia, M. Weller, D. Lacombe, J.G. Cairncross, R.-O. Mirimanoff, European Organisation for Research and Treatment of Cancer Brain Tumour and Radiation Oncology Groups, National Cancer Institute of Canada Clinical Trials Group, Effects of radiotherapy with concomitant and adjuvant temozolomide versus radiotherapy alone on survival in glioblastoma in a randomised phase III study: 5-year analysis of the EORTC-NCIC trial, *Lancet Oncol.* 10 (2009) 459–466. doi:10.1016/S1470-2045(09)70025-7.
- [32] J. Perry, A. Chambers, K. Spithoff, N. Laperriere, Gliadel wafers in the treatment of malignant glioma: a systematic review., *Curr. Oncol.* 14 (2007) 189–94. <http://www.ncbi.nlm.nih.gov/pubmed/17938702> (accessed February 14, 2018).
- [33] P. Menei, P. Metellus, E. Parot-Schinkel, H. Loiseau, L. Capelle, G. Jacquet, J. Guyotat, Neuro-oncology Club of the French Society of Neurosurgery, Biodegradable Carmustine Wafers (Gliadel) Alone or in Combination with Chemoradiotherapy: The French Experience, *Ann. Surg. Oncol.* 17 (2010) 1740–1746. doi:10.1245/s10434-010-1081-5.
- [34] A. Gutenberg, C.B. Lumenta, W.E.K. Braunsdorf, M. Sabel, H.M. Mehdorn, M. Westphal, A. Giese, The combination of carmustine wafers and temozolomide for the treatment of malignant gliomas. A comprehensive review of the rationale and clinical experience, *J. Neurooncol.* 113 (2013) 163–174. doi:10.1007/s11060-013-1110-x.
- [35] H.S. Friedman, M.D. Prados, P.Y. Wen, T. Mikkelsen, D. Schiff, L.E. Abrey, W.K.A. Yung, N. Paleologos, M.K. Nicholas, R. Jensen, J. Vredenburgh, J. Huang, M. Zheng, T. Cloughesy, Bevacizumab Alone and in Combination With Irinotecan in Recurrent Glioblastoma, *J. Clin. Oncol.* 27 (2009) 4733–4740. doi:10.1200/JCO.2008.19.8721.
- [36] W. Wick, M. Weller, M. van den Bent, R. Stupp, Bevacizumab and Recurrent Malignant Gliomas: A European Perspective, *J. Clin. Oncol.* 28 (2010) e188–e189. doi:10.1200/JCO.2009.26.9027.
- [37] K.J. Wenger, M. Wagner, S.-J. You, K. Franz, P.N. Harter, M.C. Burger, M. Voss, M.W. Ronellenfitsch, E. Fokas, J.P. Steinbach, O. Bähr, Bevacizumab as a last-line treatment for glioblastoma following failure of radiotherapy, temozolomide and lomustine., *Oncol. Lett.* 14 (2017) 1141–1146. doi:10.3892/ol.2017.6251.
- [38] M. Safari, A. Khoshnevisan, Cancer Stem Cells and Chemoresistance in Glioblastoma Multiform: A Review Article., *J. Stem Cells.* 10 (2015) 271–85. doi:jsc.2015.10.4.271.
- [39] E. Paszko, C. Ehrhardt, M.O. Senge, D.P. Kelleher, J. V. Reynolds, Nanodrug applications in photodynamic therapy, *Photodiagnosis Photodyn. Ther.* 8 (2011) 14–29. doi:10.1016/j.pdpdt.2010.12.001.

- [40] W. Chen, J. Zhang, Using nanoparticles to enable simultaneous radiation and photodynamic therapies for cancer treatment., *J. Nanosci. Nanotechnol.* 6 (2006) 1159–66. <http://www.ncbi.nlm.nih.gov/pubmed/16736782> (accessed June 18, 2018).
- [41] P. Calzavara-Pinton, M. Venturini, R. Sala, Photodynamic therapy: update 2006 Part 1: Photochemistry and photobiology, *J. Eur. Acad. Dermatology Venereol.* 21 (2007) 293–302. doi:10.1111/j.1468-3083.2006.01902.x.
- [42] L.B. de Paula, F.L. Primo, A.C. Tedesco, Nanomedicine associated with photodynamic therapy for glioblastoma treatment., *Biophys. Rev.* 9 (2017) 761–773. doi:10.1007/s12551-017-0293-3.
- [43] P. Rai, S. Mallidi, X. Zheng, R. Rahmanzadeh, Y. Mir, S. Elrington, A. Khurshid, T. Hasan, Development and applications of photo-triggered theranostic agents., *Adv. Drug Deliv. Rev.* 62 (2010) 1094–124. doi:10.1016/j.addr.2010.09.002.
- [44] T. Glaser, I. Han, L. Wu, X. Zeng, Targeted Nanotechnology in Glioblastoma Multiforme., *Front. Pharmacol.* 8 (2017) 166. doi:10.3389/fphar.2017.00166.
- [45] S. Polyzoidis, K. Ashkan, Dendritic cell immunotherapy for glioblastoma, *Expert Rev. Anticancer Ther.* 14 (2014) 761–763. doi:10.1586/14737140.2014.921571.
- [46] X. Ying, H. Wen, W.-L. Lu, J. Du, J. Guo, W. Tian, Y. Men, Y. Zhang, R.-J. Li, T.-Y. Yang, D.-W. Shang, J.-N. Lou, L.-R. Zhang, Q. Zhang, Dual-targeting daunorubicin liposomes improve the therapeutic efficacy of brain glioma in animals, *J. Control. Release.* 141 (2010) 183–192. doi:10.1016/j.jconrel.2009.09.020.
- [47] F. Pourgholi, M. hajivalili, J.-N. Farhad, H.S. Kafil, M. Yousefi, Nanoparticles: Novel vehicles in treatment of Glioblastoma, *Biomed. Pharmacother.* 77 (2016) 98–107. doi:10.1016/j.biopha.2015.12.014.
- [48] R. Karim, C. Palazzo, B. Evrard, G. Piel, Nanocarriers for the treatment of glioblastoma multiforme: Current state-of-the-art, *J. Control. Release.* 227 (2016) 23–37. doi:10.1016/j.jconrel.2016.02.026.
- [49] J. Yao, C.-H. Hsu, Z. Li, T.S. Kim, L.-P. Hwang, Y.-C. Lin, Y.-Y. Lin, Magnetic Resonance Nano-Theranostics for Glioblastoma Multiforme., *Curr. Pharm. Des.* 21 (2015) 5256–66. <http://www.ncbi.nlm.nih.gov/pubmed/26412354> (accessed April 16, 2018).
- [50] I. Fischer, J.P. Gagner, M. Law, E.W. Newcomb, D. Zagzag, Angiogenesis in gliomas: biology and molecular pathophysiology, *Brain Pathol.* 15 (2005) 297–310.
- [51] R.S. Samant, L.A. Shevde, Recent advances in anti-angiogenic therapy of cancer, *Oncotarget.* 2 (2011) 122–134. doi:10.18632/oncotarget.234.
- [52] J. Folkman, Tumor angiogenesis: therapeutic implications, *N Engl J Med.* 285 (1971) 1182–1186. doi:10.1056/nejm197111182852108.
- [53] S. Brem, R. Cotran, J. Folkman, Tumor angiogenesis: a quantitative method for histologic grading, *J Natl Cancer Inst.* 48 (1972) 347–356.

- [54] J. V Joseph, S. Conroy, K. Pavlov, P. Sontakke, T. Tomar, E. Eggens-Meijer, V. Balasubramanian, M. Wagemakers, W.F. den Dunnen, F.A. Kruyt, Hypoxia enhances migration and invasion in glioblastoma by promoting a mesenchymal shift mediated by the HIF1alpha-ZEB1 axis, *Cancer Lett.* 359 (2015) 107–116. doi:10.1016/j.canlet.2015.01.010.
- [55] G. Bergers, L.E. Benjamin, Tumorigenesis and the angiogenic switch, *Nat Rev Cancer.* 3 (2003) 401–410. doi:10.1038/nrc1093.
- [56] K.H. Plate, G. Breier, H.A. Weich, W. Risau, Vascular endothelial growth factor is a potential tumour angiogenesis factor in human gliomas in vivo, *Nature.* 359 (1992) 845–848. doi:10.1038/359845a0.
- [57] C.K. Goldman, J. Kim, W.L. Wong, V. King, T. Brock, G.Y. Gillespie, Epidermal growth factor stimulates vascular endothelial growth factor production by human malignant glioma cells: a model of glioblastoma multiforme pathophysiology, *Mol Biol Cell.* 4 (1993) 121–133.
- [58] M. Ryuto, M. Ono, H. Izumi, S. Yoshida, H.A. Weich, K. Kohno, M. Kuwano, Induction of vascular endothelial growth factor by tumor necrosis factor alpha in human glioma cells. Possible roles of SP-1, *J Biol Chem.* 271 (1996) 28220–28228.
- [59] Y. Yoshino, M. Aoyagi, M. Tamaki, L. Duan, T. Morimoto, K. Ohno, Activation of p38 MAPK and/or JNK contributes to increased levels of VEGF secretion in human malignant glioma cells, *Int J Oncol.* 29 (2006) 981–987.
- [60] M. Saino, T. Maruyama, T. Sekiya, T. Kayama, Y. Murakami, Inhibition of angiogenesis in human glioma cell lines by antisense RNA from the soluble guanylate cyclase genes, GUCY1A3 and GUCY1B3, *Oncol Rep.* 12 (2004) 47–52.
- [61] R.S. Kerbel, Tumor angiogenesis, *N Engl J Med.* 358 (2008) 2039–2049. doi:10.1056/NEJMra0706596.
- [62] S.M. Raza, F.F. Lang, B.B. Aggarwal, G.N. Fuller, D.M. Wildrick, R. Sawaya, Necrosis and glioblastoma: a friend or a foe? A review and a hypothesis, *Neurosurgery.* 51 (2002) 2-12–3.
- [63] R.S. Morrison, J.L. Gross, W.F. Herblin, T.M. Reilly, P.A. LaSala, R.L. Alterman, J.R. Moskal, P.L. Kornblith, D.L. Dexter, Basic fibroblast growth factor-like activity and receptors are expressed in a human glioma cell line, *Cancer Res.* 50 (1990) 2524–2529.
- [64] J.C. Tsai, C.K. Goldman, G.Y. Gillespie, Vascular endothelial growth factor in human glioma cell lines: induced secretion by EGF, PDGF-BB, and bFGF, *J Neurosurg.* 82 (1995) 864–873. doi:10.3171/jns.1995.82.5.0864.
- [65] Y. Reiss, M.R. Machein, K.H. Plate, The role of angiopoietins during angiogenesis in gliomas, *Brain Pathol.* 15 (2005) 311–317.
- [66] A.M. Nakahata, D.E. Suzuki, C.O. Rodini, M.C. Pereira, L. Janjoppi, O.K. Okamoto, Human glioblastoma cells display mesenchymal stem cell features

- and form intracranial tumors in immunocompetent rats, *J Stem Cells*. 5 (2010) 103–111. doi:jsc.2010.5.3.103.
- [67] M.L. Cruceru, M. Neagu, J.B. Demoulin, S.N. Constantinescu, Therapy targets in glioblastoma and cancer stem cells: lessons from haematopoietic neoplasms, *J Cell Mol Med*. 17 (2013) 1218–1235. doi:10.1111/jcmm.12122.
- [68] R. Wang, K. Chadalavada, J. Wilshire, U. Kowalik, K.E. Hovinga, A. Geber, B. Fligelman, M. Leversha, C. Brennan, V. Tabar, Glioblastoma stem-like cells give rise to tumour endothelium, *Nature*. 468 (2010) 829–833. doi:10.1038/nature09624.
- [69] L. Cheng, Z. Huang, W. Zhou, Q. Wu, S. Donnola, J.K. Liu, X. Fang, A.E. Sloan, Y. Mao, J.D. Lathia, W. Min, R.E. McLendon, J.N. Rich, S. Bao, Glioblastoma stem cells generate vascular pericytes to support vessel function and tumor growth, *Cell*. 153 (2013) 139–152. doi:10.1016/j.cell.2013.02.021.
- [70] L. Ricci-Vitiani, R. Pallini, M. Biffoni, M. Todaro, G. Invernici, T. Cenci, G. Maira, E.A. Parati, G. Stassi, L.M. Larocca, R. De Maria, Tumour vascularization via endothelial differentiation of glioblastoma stem-like cells, *Nature*. 468 (2010) 824–828. doi:10.1038/nature09557.
- [71] J. Chen, Y. Li, T.S. Yu, R.M. McKay, D.K. Burns, S.G. Kernie, L.F. Parada, A restricted cell population propagates glioblastoma growth following chemotherapy, *Nature*. 488 (2012) 522–526. doi:10.1038/nature11287.
- [72] R.K. Jain, T. Stylianopoulos, Delivering nanomedicine to solid tumors, *Nat Rev Clin Oncol*. 7 (2010) 653–664. doi:10.1038/nrclinonc.2010.139.
- [73] R.K. Jain, Normalization of tumor vasculature: an emerging concept in antiangiogenic therapy, *Science* (80-.). 307 (2005) 58–62. doi:10.1126/science.1104819.
- [74] T.T. Batchelor, A.G. Sorensen, E. di Tomaso, W.-T. Zhang, D.G. Duda, K.S. Cohen, K.R. Kozak, D.P. Cahill, P.-J. Chen, M. Zhu, M. Ancukiewicz, M.M. Mrugala, S. Plotkin, J. Drappatz, D.N. Louis, P. Ivy, D.T. Scadden, T. Benner, J.S. Loeffler, P.Y. Wen, R.K. Jain, AZD2171, a Pan-VEGF Receptor Tyrosine Kinase Inhibitor, Normalizes Tumor Vasculature and Alleviates Edema in Glioblastoma Patients, *Cancer Cell*. 11 (2007) 83–95. doi:10.1016/j.ccr.2006.11.021.
- [75] A.A.M. Van der Veldt, M. Lubberink, I. Bahce, M. Walraven, M.P. de Boer, H.N.J.M. Greuter, N.H. Hendrikse, J. Eriksson, A.D. Windhorst, P.E. Postmus, H.M. Verheul, E.H. Serné, A.A. Lammertsma, E.F. Smit, Rapid Decrease in Delivery of Chemotherapy to Tumors after Anti-VEGF Therapy: Implications for Scheduling of Anti-Angiogenic Drugs, *Cancer Cell*. 21 (2012) 82–91. doi:10.1016/j.ccr.2011.11.023.
- [76] F. Winkler, S. V Kozin, R.T. Tong, S.S. Chae, M.F. Booth, I. Garkavtsev, L. Xu, D.J. Hicklin, D. Fukumura, E. di Tomaso, L.L. Munn, R.K. Jain, Kinetics of vascular normalization by VEGFR2 blockade governs brain tumor response to radiation: role of oxygenation, angiopoietin-1, and matrix metalloproteinases, *Cancer Cell*. 6 (2004) 553–563. doi:10.1016/j.ccr.2004.10.011.

- [77] D.G. Duda, R.K. Jain, C.G. Willett, Antiangiogenics: The Potential Role of Integrating This Novel Treatment Modality With Chemoradiation for Solid Cancers, *J. Clin. Oncol.* 25 (2007) 4033–4042. doi:10.1200/JCO.2007.11.3985.
- [78] Y. Shaked, R.S. Kerbel, Antiangiogenic Strategies on Defense: On the Possibility of Blocking Rebounds by the Tumor Vasculature after Chemotherapy, *Cancer Res.* 67 (2007) 7055–7058. doi:10.1158/0008-5472.CAN-07-0905.
- [79] D.H. Gorski, M.A. Beckett, N.T. Jaskowiak, D.P. Calvin, H.J. Mauceri, R.M. Salloum, S. Seetharam, A. Koons, D.M. Hari, D.W. Kufe, R.R. Weichselbaum, Blockage of the vascular endothelial growth factor stress response increases the antitumor effects of ionizing radiation., *Cancer Res.* 59 (1999) 3374–8. <http://www.ncbi.nlm.nih.gov/pubmed/10416597> (accessed February 26, 2018).
- [80] C. Calabrese, H. Poppleton, M. Kocak, T.L. Hogg, C. Fuller, B. Hamner, E.Y. Oh, M.W. Gaber, D. Finklestein, M. Allen, A. Frank, I.T. Bayazitov, S.S. Zakharenko, A. Gajjar, A. Davidoff, R.J. Gilbertson, A Perivascular Niche for Brain Tumor Stem Cells, *Cancer Cell.* 11 (2007) 69–82. doi:10.1016/j.ccr.2006.11.020.
- [81] C. Folkins, S. Man, P. Xu, Y. Shaked, D.J. Hicklin, R.S. Kerbel, Anticancer Therapies Combining Antiangiogenic and Tumor Cell Cytotoxic Effects Reduce the Tumor Stem-Like Cell Fraction in Glioma Xenograft Tumors, *Cancer Res.* 67 (2007) 3560–3564. doi:10.1158/0008-5472.CAN-06-4238.
- [82] J.F. de Groot, Y. Piao, H. Tran, M. Gilbert, H.-K. Wu, J. Liu, B.N. Bekele, T. Cloughesy, M. Mehta, H.I. Robins, A. Lassman, L. DeAngelis, K. Camphausen, A. Chen, W. Yung, M. Prados, P.Y. Wen, J. V. Heymach, Myeloid Biomarkers Associated with Glioblastoma Response to Anti-VEGF Therapy with Aflibercept, *Clin. Cancer Res.* 17 (2011) 4872–4881. doi:10.1158/1078-0432.CCR-11-0271.
- [83] M. Terme, S. Pernot, E. Marcheteau, F. Sandoval, N. Benhamouda, O. Colussi, O. Dubreuil, A.F. Carpentier, E. Tartour, J. Taieb, VEGFA-VEGFR Pathway Blockade Inhibits Tumor-Induced Regulatory T-cell Proliferation in Colorectal Cancer, *Cancer Res.* 73 (2013) 539–549. doi:10.1158/0008-5472.CAN-12-2325.
- [84] R.K. Shrimali, Z. Yu, M.R. Theoret, D. Chinnasamy, N.P. Restifo, S.A. Rosenberg, Antiangiogenic Agents Can Increase Lymphocyte Infiltration into Tumor and Enhance the Effectiveness of Adoptive Immunotherapy of Cancer, *Cancer Res.* 70 (2010) 6171–6180. doi:10.1158/0008-5472.CAN-10-0153.
- [85] J.F. de Groot, K.R. Lamborn, S.M. Chang, M.R. Gilbert, T.F. Cloughesy, K. Aldape, J. Yao, E.F. Jackson, F. Lieberman, H.I. Robins, M.P. Mehta, A.B. Lassman, L.M. DeAngelis, W.K.A. Yung, A. Chen, M.D. Prados, P.Y. Wen, Phase II Study of Aflibercept in Recurrent Malignant Glioma: A North American Brain Tumor Consortium Study, *J. Clin. Oncol.* 29 (2011) 2689–2695. doi:10.1200/JCO.2010.34.1636.
- [86] F.M. Iwamoto, K.R. Lamborn, H.I. Robins, M.P. Mehta, S.M. Chang, N.A. Butowski, L.M. DeAngelis, L.E. Abrey, W.-T. Zhang, M.D. Prados, H.A. Fine, Phase II trial of pazopanib (GW786034), an oral multi-targeted angiogenesis

- inhibitor, for adults with recurrent glioblastoma (North American Brain Tumor Consortium Study 06-02), *Neuro. Oncol.* 12 (2010) 855–861. doi:10.1093/neuonc/noq025.
- [87] T.T. Batchelor, P. Mulholland, B. Neyns, L.B. Nabors, M. Campone, A. Wick, W. Mason, T. Mikkelsen, S. Phuphanich, L.S. Ashby, J. DeGroot, R. Gattamaneni, L. Cher, M. Rosenthal, F. Payer, J.M. Jürgensmeier, R.K. Jain, A.G. Sorensen, J. Xu, Q. Liu, M. van den Bent, Phase III Randomized Trial Comparing the Efficacy of Cediranib As Monotherapy, and in Combination With Lomustine, Versus Lomustine Alone in Patients With Recurrent Glioblastoma, *J. Clin. Oncol.* 31 (2013) 3212–3218. doi:10.1200/JCO.2012.47.2464.
- [88] A. Muhic, H.S. Poulsen, M. Sorensen, K. Grunnet, U. Lassen, Phase II open-label study of nintedanib in patients with recurrent glioblastoma multiforme, *J. Neurooncol.* 111 (2013) 205–212. doi:10.1007/s11060-012-1009-y.
- [89] T.N. Kreisl, P. Smith, J. Sul, C. Salgado, F.M. Iwamoto, J.H. Shih, H.A. Fine, Continuous daily sunitinib for recurrent glioblastoma, *J. Neurooncol.* 111 (2013) 41–48. doi:10.1007/s11060-012-0988-z.
- [90] T.N. Kreisl, K.A. McNeill, J. Sul, F.M. Iwamoto, J. Shih, H.A. Fine, A phase I/II trial of vandetanib for patients with recurrent malignant glioma, *Neuro. Oncol.* 14 (2012) 1519–1526. doi:10.1093/neuonc/nos265.
- [91] M.J. Gil-Gil, C. Mesia, M. Rey, J. Bruna, Bevacizumab for the treatment of glioblastoma., *Clin. Med. Insights. Oncol.* 7 (2013) 123–35. doi:10.4137/CMO.S8503.
- [92] J.J. Vredenburgh, A. Desjardins, J.E. Herndon, J. Marcello, D.A. Reardon, J.A. Quinn, J.N. Rich, S. Sathornsumetee, S. Gururangan, J. Sampson, M. Wagner, L. Bailey, D.D. Bigner, A.H. Friedman, H.S. Friedman, Bevacizumab Plus Irinotecan in Recurrent Glioblastoma Multiforme, *J. Clin. Oncol.* 25 (2007) 4722–4729. doi:10.1200/JCO.2007.12.2440.
- [93] T.N. Kreisl, L. Kim, K. Moore, P. Duic, C. Royce, I. Stroud, N. Garren, M. Mackey, J.A. Butman, K. Camphausen, J. Park, P.S. Albert, H.A. Fine, Phase II Trial of Single-Agent Bevacizumab Followed by Bevacizumab Plus Irinotecan at Tumor Progression in Recurrent Glioblastoma, *J. Clin. Oncol.* 27 (2009) 740–745. doi:10.1200/JCO.2008.16.3055.
- [94] E.T. Wong, K.R. Hess, M.J. Gleason, K.A. Jaeckle, A.P. Kyritsis, M.D. Prados, V.A. Levin, W.K.A. Yung, Outcomes and Prognostic Factors in Recurrent Glioma Patients Enrolled Onto Phase II Clinical Trials, *J. Clin. Oncol.* 17 (1999) 2572–2572. doi:10.1200/JCO.1999.17.8.2572.
- [95] O.L. Chinot, W. Wick, T. Cloughesy, Bevacizumab for newly diagnosed glioblastoma., *N. Engl. J. Med.* 370 (2014) 2049. <http://www.ncbi.nlm.nih.gov/pubmed/24860870> (accessed February 26, 2018).
- [96] M.R. Gilbert, E.P. Sulman, M.P. Mehta, Bevacizumab for Newly Diagnosed Glioblastoma, *N. Engl. J. Med.* 370 (2014) 2048–2049. doi:10.1056/NEJMc1403303.

- [97] B. Sitohy, J.A. Nagy, S.-C.S. Jaminet, H.F. Dvorak, Tumor-Surrogate Blood Vessel Subtypes Exhibit Differential Susceptibility to Anti-VEGF Therapy, *Cancer Res.* 71 (2011) 7021–7028. doi:10.1158/0008-5472.CAN-11-1693.
- [98] M. DeLay, A. Jahangiri, W.S. Carbonell, Y.-L. Hu, S. Tsao, M.W. Tom, J. Paquette, T.A. Tokuyasu, M.K. Aghi, Microarray Analysis Verifies Two Distinct Phenotypes of Glioblastomas Resistant to Antiangiogenic Therapy, *Clin. Cancer Res.* 18 (2012) 2930–2942. doi:10.1158/1078-0432.CCR-11-2390.
- [99] O. Casanovas, D.J. Hicklin, G. Bergers, D. Hanahan, Drug resistance by evasion of antiangiogenic targeting of VEGF signaling in late-stage pancreatic islet tumors, *Cancer Cell.* 8 (2005) 299–309. doi:10.1016/j.ccr.2005.09.005.
- [100] K. V Lu, G. Bergers, Mechanisms of evasive resistance to anti-VEGF therapy in glioblastoma, *CNS Oncol.* 2 (2013) 49–65. doi:10.2217/cns.12.36.
- [101] F. Shojaei, X. Wu, X. Qu, M. Kowanz, L. Yu, M. Tan, Y.G. Meng, N. Ferrara, G-CSF-initiated myeloid cell mobilization and angiogenesis mediate tumor refractoriness to anti-VEGF therapy in mouse models, *Proc. Natl. Acad. Sci.* 106 (2009) 6742–6747. doi:10.1073/pnas.0902280106.
- [102] J. de Groot, J. Liang, L.-Y. Kong, J. Wei, Y. Piao, G. Fuller, W. Qiao, A.B. Heimberger, Modulating Antiangiogenic Resistance by Inhibiting the Signal Transducer and Activator of Transcription 3 Pathway in Glioblastoma, *Oncotarget.* 3 (2012) 1036–48. doi:10.18632/oncotarget.663.
- [103] Y. Piao, J. Liang, L. Holmes, V. Henry, E. Sulman, J.F. de Groot, Acquired Resistance to Anti-VEGF Therapy in Glioblastoma Is Associated with a Mesenchymal Transition, *Clin. Cancer Res.* 19 (2013) 4392–4403. doi:10.1158/1078-0432.CCR-12-1557.
- [104] K.V. Lu, J.P. Chang, C.A. Parachoniak, M.M. Pandika, M.K. Aghi, D. Meyronet, N. Isachenko, S.D. Fouse, J.J. Phillips, D.A. Cheresch, M. Park, G. Bergers, VEGF Inhibits Tumor Cell Invasion and Mesenchymal Transition through a MET/VEGFR2 Complex, *Cancer Cell.* 22 (2012) 21–35. doi:10.1016/j.ccr.2012.05.037.
- [105] R. Du, K. V. Lu, C. Petritsch, P. Liu, R. Ganss, E. Passegué, H. Song, S. VandenBerg, R.S. Johnson, Z. Werb, G. Bergers, HIF1 α Induces the Recruitment of Bone Marrow-Derived Vascular Modulatory Cells to Regulate Tumor Angiogenesis and Invasion, *Cancer Cell.* 13 (2008) 206–220. doi:10.1016/j.ccr.2008.01.034.
- [106] A. Gauthier, M. Ho, Role of sorafenib in the treatment of advanced hepatocellular carcinoma: An update, *Hepatol. Res.* 43 (2013) 147–154. doi:10.1111/j.1872-034X.2012.01113.x.
- [107] J. Bruix, M. Sherman, American Association for the Study of Liver Diseases, Management of hepatocellular carcinoma: an update., *Hepatology.* 53 (2011) 1020–2. doi:10.1002/hep.24199.
- [108] S.M. Wilhelm, L. Adnane, P. Newell, A. Villanueva, J.M. Llovet, M. Lynch, Preclinical overview of sorafenib, a multikinase inhibitor that targets both Raf

- and VEGF and PDGF receptor tyrosine kinase signaling, *Mol. Cancer Ther.* 7 (2008) 3129–3140. doi:10.1158/1535-7163.MCT-08-0013.
- [109] S.M. Wilhelm, C. Carter, L. Tang, D. Wilkie, A. McNabola, H. Rong, C. Chen, X. Zhang, P. Vincent, M. McHugh, Y. Cao, J. Shujath, S. Gawlak, D. Eveleigh, B. Rowley, L. Liu, L. Adnane, M. Lynch, D. Auclair, I. Taylor, R. Gedrich, A. Voznesensky, B. Riedl, L.E. Post, G. Bollag, P.A. Trail, BAY 43-9006 Exhibits Broad Spectrum Oral Antitumor Activity and Targets the RAF/MEK/ERK Pathway and Receptor Tyrosine Kinases Involved in Tumor Progression and Angiogenesis, *Cancer Res.* 64 (2004) 7099–7109. doi:10.1158/0008-5472.CAN-04-1443.
- [110] F. Carlomagno, S. Anaganti, T. Guida, G. Salvatore, G. Troncone, S.M. Wilhelm, M. Santoro, BAY 43-9006 Inhibition of Oncogenic RET Mutants, *JNCI J. Natl. Cancer Inst.* 98 (2006) 326–334. doi:10.1093/jnci/djj069.
- [111] R. ERBER, A. THURNHER, A.D. KATSEN, G. GROTH, H. KERGER, H.-P. HAMMES, M.D. MENGER, A. ULLRICH, P. VAJKOCZY, Combined inhibition of VEGF and PDGF signaling enforces tumor vessel regression by interfering with pericyte-mediated endothelial cell survival mechanisms, *FASEB J.* 18 (2004) 338–340. doi:10.1096/fj.03-0271fje.
- [112] C. Yu, L.M. Bruzek, X.W. Meng, G.J. Gores, C.A. Carter, S.H. Kaufmann, A.A. Adjei, The role of Mcl-1 downregulation in the proapoptotic activity of the multikinase inhibitor BAY 43-9006, *Oncogene.* 24 (2005) 6861–6869. doi:10.1038/sj.onc.1208841.
- [113] P. Ulivi, C. Arienti, D. Amadori, F. Fabbri, S. Carloni, A. Tesei, I. Vannini, R. Silvestrini, W. Zoli, Role of RAF/MEK/ERK pathway, p-STAT-3 and Mcl-1 in sorafenib activity in human pancreatic cancer cell lines, *J. Cell. Physiol.* 220 (2009) 214–221. doi:10.1002/jcp.21753.
- [114] M. Rahmani, E.M. Davis, C. Bauer, P. Dent, S. Grant, Apoptosis Induced by the Kinase Inhibitor BAY 43-9006 in Human Leukemia Cells Involves Down-regulation of Mcl-1 through Inhibition of Translation, *J. Biol. Chem.* 280 (2005) 35217–35227. doi:10.1074/jbc.M506551200.
- [115] K.-F. Chen, W.-T. Tai, T.-H. Liu, H.-P. Huang, Y.-C. Lin, C.-W. Shiau, P.-K. Li, P.-J. Chen, A.-L. Cheng, Sorafenib Overcomes TRAIL Resistance of Hepatocellular Carcinoma Cells through the Inhibition of STAT3, *Clin. Cancer Res.* 16 (2010) 5189–5199. doi:10.1158/1078-0432.CCR-09-3389.
- [116] H. Yu, R. Jove, The STATs of cancer — new molecular targets come of age, *Nat. Rev. Cancer.* 4 (2004) 97–105. doi:10.1038/nrc1275.
- [117] E.B. Haura, J. Turkson, R. Jove, Mechanisms of Disease: insights into the emerging role of signal transducers and activators of transcription in cancer, *Nat. Clin. Pract. Oncol.* 2 (2005) 315–324. doi:10.1038/ncponc0195.
- [118] A.K. Pathak, M. Bhutani, A.S. Nair, K.S. Ahn, A. Chakraborty, H. Kadara, S. Guha, G. Sethi, B.B. Aggarwal, Ursolic Acid Inhibits STAT3 Activation Pathway Leading to Suppression of Proliferation and Chemosensitization of Human Multiple Myeloma Cells, *Mol. Cancer Res.* 5 (2007) 943–955. doi:10.1158/1541-

- 7786.MCR-06-0348.
- [119] E. Cattaneo, L. Magrassi, C. De-Fraja, L. Conti, I. Di Gennaro, G. Butti, S. Govoni, Variations in the levels of the JAK/STAT and ShcA proteins in human brain tumors., *Anticancer Res.* 18 (n.d.) 2381–7. <http://www.ncbi.nlm.nih.gov/pubmed/9703883> (accessed February 19, 2018).
- [120] S.O. Rahaman, P.C. Harbor, O. Chernova, G.H. Barnett, M.A. Vogelbaum, S.J. Haque, Inhibition of constitutively active Stat3 suppresses proliferation and induces apoptosis in glioblastoma multiforme cells, *Oncogene.* 21 (2002) 8404–8413. doi:10.1038/sj.onc.1206047.
- [121] A. Iwamaru, S. Szymanski, E. Iwado, H. Aoki, T. Yokoyama, I. Fokt, K. Hess, C. Conrad, T. Madden, R. Sawaya, S. Kondo, W. Priebe, Y. Kondo, A novel inhibitor of the STAT3 pathway induces apoptosis in malignant glioma cells both in vitro and in vivo, *Oncogene.* 26 (2007) 2435–2444. doi:10.1038/sj.onc.1210031.
- [122] F. Yang, T.E. Van Meter, R. Buettner, M. Hedvat, W. Liang, C.M. Kowolik, N. Mepani, J. Mirosevich, S. Nam, M.Y. Chen, G. Tye, M. Kirschbaum, R. Jove, Sorafenib inhibits signal transducer and activator of transcription 3 signaling associated with growth arrest and apoptosis of medulloblastomas, *Mol. Cancer Ther.* 7 (2008) 3519–3526. doi:10.1158/1535-7163.MCT-08-0138.
- [123] F. Yang, C. Brown, R. Buettner, M. Hedvat, R. Starr, A. Scuto, A. Schroeder, M. Jensen, R. Jove, Sorafenib induces growth arrest and apoptosis of human glioblastoma cells through the dephosphorylation of signal transducers and activators of transcription 3., *Mol. Cancer Ther.* 9 (2010) 953–62. doi:10.1158/1535-7163.MCT-09-0947.
- [124] E. Carra, F. Barbieri, D. Marubbi, A. Pattarozzi, R.E. Favoni, T. Florio, A. Daga, Sorafenib selectively depletes human glioblastoma tumor-initiating cells from primary cultures, *Cell Cycle.* 12 (2013) 491–500. doi:10.4161/cc.23372.
- [125] M.D. Siegelin, C.M. Raskett, C.A. Gilbert, A.H. Ross, D.C. Altieri, Sorafenib exerts anti-glioma activity in vitro and in vivo, *Neurosci. Lett.* 478 (2010) 165–170. doi:10.1016/j.neulet.2010.05.009.
- [126] M.R. Hassler, M. Ackerl, B. Flechl, C. Sax, A. Wöhrer, G. Widhalm, K. Dieckmann, J. Hainfellner, M. Preusser, C. Marosi, Sorafenib for patients with pretreated recurrent or progressive high-grade glioma, *Anticancer. Drugs.* 25 (2014) 1. doi:10.1097/CAD.000000000000077.
- [127] L.B. Nabors, J.G. Supko, M. Rosenfeld, M. Chamberlain, S. Phuphanich, T. Batchelor, S. Desideri, X. Ye, J. Wright, S. Gujar, S.A. Grossman, New Approaches to Brain Tumor Therapy (NABTT) CNS Consortium, Phase I trial of sorafenib in patients with recurrent or progressive malignant glioma., *Neuro. Oncol.* 13 (2011) 1324–30. doi:10.1093/neuonc/nor145.
- [128] J.D. Hainsworth, T. Ervin, E. Friedman, V. Priego, P.B. Murphy, B.L. Clark, R.E. Lamar, Concurrent radiotherapy and temozolomide followed by temozolomide and sorafenib in the first-line treatment of patients with glioblastoma multiforme, *Cancer.* 116 (2010) 3663–3669. doi:10.1002/cncr.25275.

- [129] D.M. Peereboom, M.S. Ahluwalia, X. Ye, J.G. Supko, S.L. Hilderbrand, S. Phuphanich, L.B. Nabors, M.R. Rosenfeld, T. Mikkelsen, S.A. Grossman, New Approaches to Brain Tumor Therapy Consortium, NABTT 0502: a phase II and pharmacokinetic study of erlotinib and sorafenib for patients with progressive or recurrent glioblastoma multiforme, *Neuro. Oncol.* 15 (2013) 490–496. doi:10.1093/neuonc/nos322.
- [130] E. Galanis, S.K. Anderson, J.M. Lafky, J.H. Uhm, C. Giannini, S.K. Kumar, T.K. Kimlinger, D.W. Northfelt, P.J. Flynn, K.A. Jaeckle, T.J. Kaufmann, J.C. Buckner, Phase II study of bevacizumab in combination with sorafenib in recurrent glioblastoma (N0776): a north central cancer treatment group trial., *Clin. Cancer Res.* 19 (2013) 4816–23. doi:10.1158/1078-0432.CCR-13-0708.
- [131] A.F. Hottinger, A.B. Aissa, V. Espeli, D. Squiban, N. Dunkel, M.I. Vargas, T. Hundsberger, N. Mach, K. Schaller, D.C. Weber, A. Bodmer, P.-Y. Dietrich, Phase I study of sorafenib combined with radiation therapy and temozolomide as first-line treatment of high-grade glioma, *Br. J. Cancer.* 110 (2014) 2655–2661. doi:10.1038/bjc.2014.209.
- [132] D.A. Reardon, J.J. Vredenburgh, A. Desjardins, K. Peters, S. Gururangan, J.H. Sampson, J. Marcello, J.E. Herndon, R.E. McLendon, D. Janney, A.H. Friedman, D.D. Bigner, H.S. Friedman, H.S. Friedman, Effect of CYP3A-inducing anti-epileptics on sorafenib exposure: results of a phase II study of sorafenib plus daily temozolomide in adults with recurrent glioblastoma., *J. Neurooncol.* 101 (2011) 57–66. doi:10.1007/s11060-010-0217-6.
- [133] J. Chen, A.Y. Sheu, W. Li, Z. Zhang, D.-H. Kim, R.J. Lewandowski, R.A. Omary, L.D. Shea, A.C. Larson, Poly(lactide-co-glycolide) microspheres for MRI-monitored transcatheter delivery of sorafenib to liver tumors, *J. Control. Release.* 184 (2014) 10–17. doi:10.1016/j.jconrel.2014.04.008.
- [134] N.T. Huynh, C. Passirani, P. Saulnier, J.P. Benoit, Lipid nanocapsules: A new platform for nanomedicine, *Int. J. Pharm.* 379 (2009) 201–209. doi:10.1016/j.ijpharm.2009.04.026.
- [135] B. Heurtault, P. Saulnier, J.-P. Benoit, J.-E. Proust, B. Pech, J. Richard, Lipid nanocapsules, preparation process and use as medicine, US8057823 B2, 2001. <https://www.google.fr/patents/US8057823?dq=WO02688000&hl=en&sa=X&ved=0ahUKEwjliOX8gZzZAhVMDOWKHZalC80Q6AEIKTAA> (accessed February 10, 2018).
- [136] I. Minkov, T. Ivanova, I. Panaiotov, J. Proust, P. Saulnier, Reorganization of lipid nanocapsules at air–water interface, *Colloids Surfaces B Biointerfaces.* 44 (2005) 197–203. doi:10.1016/j.colsurfb.2005.07.001.
- [137] A. Vonarbourg, P. Saulnier, C. Passirani, J.-P. Benoit, Electrokinetic properties of noncharged lipid nanocapsules: Influence of the dipolar distribution at the interface, *Electrophoresis.* 26 (2005) 2066–2075. doi:10.1002/elps.200410145.
- [138] M. Cirri, P. Mura, P.C. Mora, Liquid spray formulations of xibornol by using self-microemulsifying drug delivery systems, *Int J Pharm.* 340 (2007) 84–91. doi:10.1016/j.ijpharm.2007.03.021.

- [139] D.C. Drummond, C.O. Noble, Z. Guo, K. Hong, J.W. Park, D.B. Kirpotin, Development of a highly active nanoliposomal irinotecan using a novel intraliposomal stabilization strategy, *Cancer Res.* 66 (2006) 3271–3277. doi:10.1158/0008-5472.can-05-4007.
- [140] J.S. Woo, T.-S. Kim, J.-H. Park, S.-C. Chi, Formulation and biopharmaceutical evaluation of silymarin using SMEDDS., *Arch. Pharm. Res.* 30 (2007) 82–9.
- [141] E. Roger, F. Lagarce, J.P. Benoit, Development and characterization of a novel lipid nanocapsule formulation of Sn38 for oral administration, *Eur J Pharm Biopharm.* 79 (2011) 181–188. doi:10.1016/j.ejpb.2011.01.021.
- [142] E. Roger, F. Lagarce, E. Garcion, J.-P. Benoit, Lipid nanocarriers improve paclitaxel transport throughout human intestinal epithelial cells by using vesicle-mediated transcytosis, *J. Control. Release.* 140 (2009) 174–181. doi:10.1016/j.jconrel.2009.08.010.
- [143] B. Heurtault, P. Saulnier, B. Pech, J.E. Proust, J.P. Benoit, Properties of polyethylene glycol 660 12-hydroxy stearate at a triglyceride/water interface., *Int. J. Pharm.* 242 (2002) 167–70. <http://www.ncbi.nlm.nih.gov/pubmed/12176240> (accessed February 10, 2018).
- [144] N. Anton, P. Gayet, J.-P. Benoit, P. Saulnier, Nano-emulsions and nanocapsules by the PIT method: An investigation on the role of the temperature cycling on the emulsion phase inversion, *Int. J. Pharm.* 344 (2007) 44–52. doi:10.1016/j.ijpharm.2007.04.027.
- [145] B. Heurtault, P. Saulnier, B. Pech, M.-C. Venier-Julienne, J.-E. Proust, R. Phan-Tan-Luu, J.-P. Benoit, The influence of lipid nanocapsule composition on their size distribution., *Eur. J. Pharm. Sci.* 18 (2003) 55–61. <http://www.ncbi.nlm.nih.gov/pubmed/12554073> (accessed February 10, 2018).
- [146] C. Dulieu, D. Bazile, Influence of lipid nanocapsules composition on their aptness to freeze-drying., *Pharm. Res.* 22 (2005) 285–92. <http://www.ncbi.nlm.nih.gov/pubmed/15783077> (accessed February 25, 2018).
- [147] N. Anton, P. Saulnier, A. Béduneau, J.-P. Benoit, Salting-Out Effect Induced by Temperature Cycling on a Water/Nonionic Surfactant/Oil System, *J. Phys. Chem. B.* 111 (2007) 3651–3657. doi:10.1021/jp0664768.
- [148] B. Heurtault, P. Saulnier, B. Pech, J.E. Proust, J.P. Benoit, A novel phase inversion-based process for the preparation of lipid nanocarriers, *Pharm Res.* 19 (2002) 875–880.
- [149] N. Anton, J.-P. Benoit, P. Saulnier, Design and production of nanoparticles formulated from nano-emulsion templates—A review, *J. Control. Release.* 128 (2008) 185–199. doi:10.1016/j.jconrel.2008.02.007.
- [150] B. Heurtault, P. Saulnier, B. Pech, J.-E. Proust, J.-P. Benoit, Physico-chemical stability of colloidal lipid particles., *Biomaterials.* 24 (2003) 4283–300. <http://www.ncbi.nlm.nih.gov/pubmed/12853260> (accessed February 10, 2018).
- [151] M. Manconi, J. Aparicio, A. Vila, J. Pendás, J. Figueruelo, F. Molina,

- Viscoelastic properties of concentrated dispersions in water of soy lecithin, *Colloids Surfaces A Physicochem. Eng. Asp.* 222 (2003) 141–145. doi:10.1016/S0927-7757(03)00249-8.
- [152] M.N. Khalid, P. Simard, D. Hoarau, A. Dragomir, J.-C. Leroux, Long Circulating Poly(Ethylene Glycol)-Decorated Lipid Nanocapsules Deliver Docetaxel to Solid Tumors, *Pharm. Res.* 23 (2006) 752–758. doi:10.1007/s11095-006-9662-5.
- [153] B. Saliou, O. Thomas, N. Lautram, A. Clavreul, J. Hureauux, T. Urban, J.-P. Benoit, F. Lagarce, Development and in vitro evaluation of a novel lipid nanocapsule formulation of etoposide, *Eur. J. Pharm. Sci.* 50 (2013) 172–180. doi:10.1016/j.ejps.2013.06.013.
- [154] M. Roger, A. Clavreul, N.T. Huynh, C. Passirani, P. Schiller, A. Vessières, C. Montero-Menei, P. Menei, Ferrociphenol lipid nanocapsule delivery by mesenchymal stromal cells in brain tumor therapy, *Int. J. Pharm.* 423 (2012) 63–68. doi:10.1016/j.ijpharm.2011.04.058.
- [155] F. Lagarce, K. Messaoudi, P. Saulnier, K. Boesen, J.-P. Benoit, Anti-epidermal growth factor receptor siRNA carried by chitosan-transacylated lipid nanocapsules increases sensitivity of glioblastoma cells to temozolomide, *Int. J. Nanomedicine.* 9 (2014) 1479. doi:10.2147/IJN.S59134.
- [156] M. Morille, T. Montier, P. Legras, N. Carmoy, P. Brodin, B. Pitard, J.-P. Benoît, C. Passirani, Long-circulating DNA lipid nanocapsules as new vector for passive tumor targeting., *Biomaterials.* 31 (2010) 321–9. doi:10.1016/j.biomaterials.2009.09.044.
- [157] F. Lagarce, R. Alyaa, A. Legras Pierre, A. Tessier-Marteau, O. Thomas, L. Macchi, P. Saulnier, J.-P. Benoit, Oral fondaparinux: use of lipid nanocapsules as nanocarriers and in vivo pharmacokinetic study, *Int. J. Nanomedicine.* 6 (2011) 2941. doi:10.2147/IJN.S25791.
- [158] F. Lagarce, C. Passirani, Nucleic-Acid Delivery Using Lipid Nanocapsules, *Curr. Pharm. Biotechnol.* 17 (2016) 723–727. doi:10.2174/1389201017666160401145206.
- [159] N. Anton, H. Mojzisova, E. Porcher, J.P. Benoit, P. Saulnier, Reverse micelle-loaded lipid nano-emulsions: New technology for nano-encapsulation of hydrophilic materials, *Int. J. Pharm.* 398 (2010) 204–209. doi:10.1016/j.ijpharm.2010.07.039.
- [160] S. Vrignaud, N. Anton, P. Gayet, J.-P. Benoit, P. Saulnier, Reverse micelle-loaded lipid nanocarriers: A novel drug delivery system for the sustained release of doxorubicin hydrochloride, *Eur. J. Pharm. Biopharm.* 79 (2011) 197–204. doi:10.1016/J.EJPB.2011.02.015.
- [161] S. Vrignaud, J. Hureauux, S. Wack, J.-P. Benoit, P. Saulnier, Design, optimization and in vitro evaluation of reverse micelle-loaded lipid nanocarriers containing erlotinib hydrochloride, *Int. J. Pharm.* 436 (2012) 194–200. doi:10.1016/j.ijpharm.2012.06.026.
- [162] P. Wehrlé, Liposomes, in: *Pharm. Galénique Formul. Technol. Pharm.*, Maloine,

- 2007: pp. 241–250.
- [163] F. Atyabi, A. Farkhondehfai, F. Esmaeili, R. Dinarvand, Preparation of pegylated nano-liposomal formulation containing SN-38: In vitro characterization and in vivo biodistribution in mice, *Acta Pharm.* 59 (2009) 133–44. doi:10.2478/v10007-009-0020-0.
- [164] S.M. Moghimi, A.C. Hunter, J.C. Murray, Long-circulating and target-specific nanoparticles: theory to practice., *Pharmacol. Rev.* 53 (2001) 283–318. <http://www.ncbi.nlm.nih.gov/pubmed/11356986> (accessed February 11, 2018).
- [165] S.M. Moghimi, J. Szebeni, Stealth liposomes and long circulating nanoparticles: critical issues in pharmacokinetics, opsonization and protein-binding properties, *Prog. Lipid Res.* 42 (2003) 463–478. doi:10.1016/S0163-7827(03)00033-X.
- [166] V.C. Mosqueira, P. Legrand, J.L. Morgat, M. Vert, E. Mysiakine, R. Gref, J.P. Devissaguet, G. Barratt, Biodistribution of long-circulating PEG-grafted nanocapsules in mice: effects of PEG chain length and density., *Pharm. Res.* 18 (2001) 1411–9. <http://www.ncbi.nlm.nih.gov/pubmed/11697466> (accessed February 11, 2018).
- [167] S. Ballot, N. Noiret, F. Hindré, B. Denizot, E. Garin, H. Rajerison, J.-P. Benoit, 99mTc/188Re-labelled lipid nanocapsules as promising radiotracers for imaging and therapy: formulation and biodistribution, *Eur. J. Nucl. Med. Mol. Imaging.* 33 (2006) 602–607. doi:10.1007/s00259-005-0007-0.
- [168] R. Bazak, M. Hourri, S. El Achy, S. Kamel, T. Refaat, Cancer active targeting by nanoparticles: a comprehensive review of literature, *J. Cancer Res. Clin. Oncol.* 141 (2015) 769–784. doi:10.1007/s00432-014-1767-3.
- [169] B. Ding, P. Chen, Y. Kong, Y. Zhai, X. Pang, J. Dou, G. Zhai, Preparation and evaluation of folate-modified lipid nanocapsules for quercetin delivery, *J. Drug Target.* 22 (2014) 67–75. doi:10.3109/1061186X.2013.839685.
- [170] E. Allard, D. Jarnet, A. Vessières, S. Vinchon-Petit, G. Jaouen, J.-P. Benoit, C. Passirani, Local Delivery of Ferrociphenol Lipid Nanocapsules Followed by External Radiotherapy as a Synergistic Treatment Against Intracranial 9L Glioma Xenograft, *Pharm. Res.* 27 (2010) 56–64. doi:10.1007/s11095-009-0006-0.
- [171] N.T. Huynh, M. Morille, J. Bejaud, P. Legras, A. Vessieres, G. Jaouen, J.-P. Benoit, C. Passirani, Treatment of 9L Gliosarcoma in Rats by Ferrociphenol-Loaded Lipid Nanocapsules Based on a Passive Targeting Strategy via the EPR Effect, *Pharm. Res.* 28 (2011) 3189–3198. doi:10.1007/s11095-011-0501-y.
- [172] A. Clavreul, N. Lautram, F. Franconi, C. Passirani, C. Montero-Menei, P. Menei, C. Tetaud, A. Montagu, A.-L. Laine, A. Vessieres, Targeting and treatment of glioblastomas with human mesenchymal stem cells carrying ferrociphenol lipid nanocapsules, *Int. J. Nanomedicine.* 10 (2015) 1259. doi:10.2147/IJN.S69175.
- [173] N.T. Huynh, C. Passirani, E. Allard-Vannier, L. Lemaire, J. Roux, E. Garcion, A. Vessieres, J.-P. Benoit, Administration-dependent efficacy of ferrociphenol lipid nanocapsules for the treatment of intracranial 9L rat gliosarcoma, *Int. J. Pharm.*

- 423 (2012) 55–62. doi:10.1016/j.ijpharm.2011.04.037.
- [174] A.-L. Laine, N.T. Huynh, A. Clavreul, J. Balzeau, J. Béjaud, A. Vessieres, J.-P. Benoit, J. Eyer, C. Passirani, Brain tumour targeting strategies via coated ferrociphenol lipid nanocapsules, *Eur. J. Pharm. Biopharm.* 81 (2012) 690–693. doi:10.1016/j.ejpb.2012.04.012.
- [175] S. Vinchon-Petit, D. Jarnet, A. Paillard, J.-P. Benoit, E. Garcion, P. Menei, In vivo evaluation of intracellular drug-nanocarriers infused into intracranial tumours by convection-enhanced delivery: distribution and radiosensitisation efficacy, *J. Neurooncol.* 97 (2010) 195–205. doi:10.1007/s11060-009-0012-4.
- [176] C. Bastiancich, J. Bianco, K. Vanvarenberg, B. Ucakar, N. Joudiou, B. Gallez, G. Bastiat, F. Lagarce, V. Pr at, F. Danhier, Injectable nanomedicine hydrogel for local chemotherapy of glioblastoma after surgical resection, *J. Control. Release.* 264 (2017) 45–54. doi:10.1016/j.jconrel.2017.08.019.
- [177] F. Figueir , C.P. de Oliveira, L.S. Bergamin, L. Rockenbach, F.B. Mendes, E.H.F. Jandrey, C.E.J. Moritz, L.F. Pettenuzzo, J. S evigny, S.S. Guterres, A.R. Pohlmann, A.M.O. Battastini, Methotrexate up-regulates ecto-5'-nucleotidase/CD73 and reduces the frequency of T lymphocytes in the glioblastoma microenvironment, *Purinergic Signal.* 12 (2016) 303–312. doi:10.1007/s11302-016-9505-8.
- [178] D. S eh edic, I. Chourpa, C. T etaud, A. Griveau, C. Loussouarn, S. Avril, C. Legendre, N. Lepareur, D. Wion, F. Hindr , F. Davodeau, E. Garcion, Locoregional Confinement and Major Clinical Benefit of ¹⁸⁸Re-Loaded CXCR4-Targeted Nanocarriers in an Orthotopic Human to Mouse Model of Glioblastoma, *Theranostics.* 7 (2017) 4517–4536. doi:10.7150/thno.19403.
- [179] A. Cikankowitz, A. Clavreul, C. T etaud, L. Lemaire, A. Rousseau, N. Lepareur, D. Dabli, F. Bouchet, E. Garcion, P. Menei, O. Couturier, F. Hindr , Characterization of the distribution, retention, and efficacy of internal radiation of ¹⁸⁸Re-lipid nanocapsules in an immunocompromised human glioblastoma model, *J. Neurooncol.* 131 (2017) 49–58. doi:10.1007/s11060-016-2289-4.
- [180] E. Allard, F. Hindre, C. Passirani, L. Lemaire, N. Lepareur, N. Noiret, P. Menei, J.-P. Benoit, ¹⁸⁸Re-loaded lipid nanocapsules as a promising radiopharmaceutical carrier for internal radiotherapy of malignant gliomas, *Eur. J. Nucl. Med. Mol. Imaging.* 35 (2008) 1838–1846. doi:10.1007/s00259-008-0735-z.
- [181] C. Vanpouille-Box, F. Lacoeyille, C. Belloche, N. Lepareur, L. Lemaire, J.-J. LeJeune, J.-P. Beno t, P. Menei, O.F. Couturier, E. Garcion, F. Hindr , Tumor eradication in rat glioma and bypass of immunosuppressive barriers using internal radiation with ¹⁸⁸Re-lipid nanocapsules, *Biomaterials.* 32 (2011) 6781–6790. doi:10.1016/j.biomaterials.2011.05.067.
- [182] A. Vonarbourg, C. Passirani, P. Saulnier, J.-P. Benoit, Parameters influencing the stealthiness of colloidal drug delivery systems, *Biomaterials.* 27 (2006) 4356–4373. doi:10.1016/j.biomaterials.2006.03.039.
- [183] A. B eduneau, P. Saulnier, N. Anton, F. Hindr , C. Passirani, H. Rajerison, N.

- Noiret, J.-P. Benoit, Pegylated Nanocapsules Produced by an Organic Solvent-Free Method: Evaluation of their Stealth Properties, *Pharm. Res.* 23 (2006) 2190–2199. doi:10.1007/s11095-006-9061-y.
- [184] D. Hoarau, P. Delmas, S. David, E. Roux, J.-C. Leroux, Novel Long-Circulating Lipid Nanocapsules, *Pharm. Res.* 21 (2004) 1783–1789. doi:10.1023/B:PHAM.0000045229.87844.21.
- [185] C. Nicholson, E. Syková, Extracellular space structure revealed by diffusion analysis., *Trends Neurosci.* 21 (1998) 207–15. <http://www.ncbi.nlm.nih.gov/pubmed/9610885> (accessed June 19, 2018).
- [186] M.A. Vogelbaum, Convection enhanced delivery for the treatment of malignant gliomas: symposium review, *J. Neurooncol.* 73 (2005) 57–69. doi:10.1007/s11060-004-2243-8.
- [187] A. Béduneau, P. Saulnier, F. Hindré, A. Clavreul, J.-C. Leroux, J.-P. Benoit, Design of targeted lipid nanocapsules by conjugation of whole antibodies and antibody Fab' fragments, *Biomaterials.* 28 (2007) 4978–4990. doi:10.1016/j.biomaterials.2007.05.014.
- [188] J. Balzeau, M. Pinier, R. Berges, P. Saulnier, J.-P. Benoit, J. Eyer, The effect of functionalizing lipid nanocapsules with NFL-TBS.40-63 peptide on their uptake by glioblastoma cells, *Biomaterials.* 34 (2013) 3381–3389. doi:10.1016/j.biomaterials.2013.01.068.
- [189] A. Bocquet, R. Berges, R. Frank, P. Robert, A.C. Peterson, J. Eyer, Neurofilaments Bind Tubulin and Modulate Its Polymerization, *J. Neurosci.* 29 (2009) 11043–11054. doi:10.1523/JNEUROSCI.1924-09.2009.
- [190] M. Roger, A. Clavreul, M.-C. Venier-Julienne, C. Passirani, L. Sindji, P. Schiller, C. Montero-Menei, P. Menei, Mesenchymal stem cells as cellular vehicles for delivery of nanoparticles to brain tumors, *Biomaterials.* 31 (2010) 8393–8401. doi:10.1016/j.biomaterials.2010.07.048.
- [191] M. Roger, A. Clavreul, N.T. Huynh, C. Passirani, P. Schiller, A. Vessieres, C. Montero-Menei, P. Menei, Ferrociphenol lipid nanocapsule delivery by mesenchymal stromal cells in brain tumor therapy, *Int J Pharm.* 423 (2012) 63–68. doi:10.1016/j.ijpharm.2011.04.058.
- [192] A. Paillard, F. Hindré, C. Vignes-Colombeix, J.-P. Benoit, E. Garcion, The importance of endo-lysosomal escape with lipid nanocapsules for drug subcellular bioavailability, *Biomaterials.* 31 (2010) 7542–7554. doi:10.1016/j.biomaterials.2010.06.024.
- [193] Y. Mardor, Y. Roth, Z. Lidar, T. Jonas, R. Pfeffer, S.E. Maier, M. Faibel, D. Nass, M. Hadani, A. Orenstein, J.S. Cohen, Z. Ram, Monitoring response to convection-enhanced taxol delivery in brain tumor patients using diffusion-weighted magnetic resonance imaging., *Cancer Res.* 61 (2001) 4971–3. <http://www.ncbi.nlm.nih.gov/pubmed/11431326> (accessed February 14, 2018).
- [194] D.R. Groothuis, The blood-brain and blood-tumor barriers: a review of strategies for increasing drug delivery., *Neuro. Oncol.* 2 (2000) 45–59.

- <http://www.ncbi.nlm.nih.gov/pubmed/11302254> (accessed February 14, 2018).
- [195] R.H. Bobo, D.W. Laske, A. Akbasak, P.F. Morrison, R.L. Dedrick, E.H. Oldfield, Convection-enhanced delivery of macromolecules in the brain., *Proc. Natl. Acad. Sci. U. S. A.* 91 (1994) 2076–80. <http://www.ncbi.nlm.nih.gov/pubmed/8134351> (accessed February 14, 2018).
- [196] M.T. Shipley, Transport of molecules from nose to brain: transneuronal anterograde and retrograde labeling in the rat olfactory system by wheat germ agglutinin-horseradish peroxidase applied to the nasal epithelium., *Brain Res. Bull.* 15 (1985) 129–42. <http://www.ncbi.nlm.nih.gov/pubmed/3840049> (accessed February 14, 2018).
- [197] R.G. Thorne, C.R. Emory, T.A. Ala, W.H. Frey, Quantitative analysis of the olfactory pathway for drug delivery to the brain., *Brain Res.* 692 (1995) 278–82. <http://www.ncbi.nlm.nih.gov/pubmed/8548316> (accessed February 14, 2018).
- [198] L. Illum, Transport of drugs from the nasal cavity to the central nervous system., *Eur. J. Pharm. Sci.* 11 (2000) 1–18. <http://www.ncbi.nlm.nih.gov/pubmed/10913748> (accessed February 14, 2018).
- [199] H. Pajouhesh, G.R. Lenz, Medicinal chemical properties of successful central nervous system drugs, *NeuroRX.* 2 (2005) 541–553. doi:10.1602/neurorx.2.4.541.
- [200] T.S. Reese, M.J. Karnovsky, Fine structural localization of a blood-brain barrier to exogenous peroxidase., *J. Cell Biol.* 34 (1967) 207–17. <http://www.ncbi.nlm.nih.gov/pubmed/6033532> (accessed February 14, 2018).
- [201] D.S. Miller, Regulation of P-glycoprotein and other ABC drug transporters at the blood–brain barrier, *Trends Pharmacol. Sci.* 31 (2010) 246–254. doi:10.1016/j.tips.2010.03.003.
- [202] D.E. Hornung, Nasal Anatomy and the Sense of Smell, in: *Tast. Smell*, KARGER, Basel, 2006: pp. 1–22. doi:10.1159/000093747.
- [203] B. Jansson, E. Björk, Visualization of In Vivo Olfactory Uptake and Transfer Using Fluorescein Dextran, *J. Drug Target.* 10 (2002) 379–386. doi:10.1080/1061186021000001823.
- [204] D.A. Leopold, The relationship between nasal anatomy and human olfaction, *Laryngoscope.* 98 (1988) 1232–1238. doi:10.1288/00005537-198811000-00015.
- [205] M. Caggiano, J.S. Kauer, D.D. Hunter, Globose basal cells are neuronal progenitors in the olfactory epithelium: a lineage analysis using a replication-incompetent retrovirus., *Neuron.* 13 (1994) 339–52. <http://www.ncbi.nlm.nih.gov/pubmed/8060615> (accessed February 15, 2018).
- [206] P.-M. Lledo, G. Gheusi, J.-D. Vincent, Information Processing in the Mammalian Olfactory System, *Physiol. Rev.* 85 (2005) 281–317. doi:10.1152/physrev.00008.2004.
- [207] S.T. Carmichael, M.-C. Clugnet, J.L. Price, Central olfactory connections in the

- macaque monkey, *J. Comp. Neurol.* 346 (1994) 403–434. doi:10.1002/cne.903460306.
- [208] T.P. Crowe, M.H.W. Greenlee, A.G. Kanthasamy, W.H. Hsu, Mechanism of intranasal drug delivery directly to the brain, *Life Sci.* 195 (2018) 44–52. doi:10.1016/j.lfs.2017.12.025.
- [209] B.W. Jafek, Ultrastructure of human nasal mucosa., *Laryngoscope.* 93 (1983) 1576–99. <http://www.ncbi.nlm.nih.gov/pubmed/6645759> (accessed February 15, 2018).
- [210] F. Bojsen-Møller, Demonstration of terminalis, olfactory, trigeminal and perivascular nerves in the rat nasal septum, *J. Comp. Neurol.* 159 (1975) 245–256. doi:10.1002/cne.901590206.
- [211] S.H. Fuss, M. Omura, P. Mombaerts, The Grueneberg ganglion of the mouse projects axons to glomeruli in the olfactory bulb, *Eur. J. Neurosci.* 22 (2005) 2649–2654. doi:10.1111/j.1460-9568.2005.04468.x.
- [212] J.M. DeSesso, The relevance to humans of animal models for inhalation studies of cancer in the nose and upper airways., *Qual. Assur.* 2 (1993) 213–31. <http://www.ncbi.nlm.nih.gov/pubmed/8137082> (accessed February 15, 2018).
- [213] H. Pollock, M. Hutchings, R.O. Weller, E.T. Zhang, Perivascular spaces in the basal ganglia of the human brain: their relationship to lacunes., *J. Anat.* 191 (Pt 3) (1997) 337–46. <http://www.ncbi.nlm.nih.gov/pubmed/9418990> (accessed February 15, 2018).
- [214] P. Hadaczek, Y. Yamashita, H. Mirek, L. Tamas, M.C. Bohn, C. Noble, J.W. Park, K. Bankiewicz, The “Perivascular Pump” Driven by Arterial Pulsation Is a Powerful Mechanism for the Distribution of Therapeutic Molecules within the Brain, *Mol. Ther.* 14 (2006) 69–78. doi:10.1016/j.ymthe.2006.02.018.
- [215] M. Johnston, A. Zakharov, C. Papaiconomou, G. Salmasi, D. Armstrong, Evidence of connections between cerebrospinal fluid and nasal lymphatic vessels in humans, non-human primates and other mammalian species., *Cerebrospinal Fluid Res.* 1 (2004) 2. doi:10.1186/1743-8454-1-2.
- [216] B.A. Walter, V.A. Valera, S. Takahashi, T. Ushiki, The olfactory route for cerebrospinal fluid drainage into the peripheral lymphatic system, *Neuropathol. Appl. Neurobiol.* 32 (2006) 388–396. doi:10.1111/j.1365-2990.2006.00737.x.
- [217] J.M. Yoffey, C.K. Drinker, THE LYMPHATIC PATHWAY FROM THE NOSE AND PHARYNX: THE ABSORPTION OF DYES., *J. Exp. Med.* 68 (1938) 629–40. <http://www.ncbi.nlm.nih.gov/pubmed/19870807> (accessed February 15, 2018).
- [218] M. Kaliner, Z. Marom, C. Patow, J. Shelhamer, Human respiratory mucus., *J. Allergy Clin. Immunol.* 73 (1984) 318–23. <http://www.ncbi.nlm.nih.gov/pubmed/6366031> (accessed February 16, 2018).
- [219] V. V. Khutoryanskiy, Advances in Mucoadhesion and Mucoadhesive Polymers, *Macromol. Biosci.* 11 (2011) 748–764. doi:10.1002/mabi.201000388.

- [220] D.T. Moran, J.C. Rowley, B.W. Jafek, M.A. Lovell, The fine structure of the olfactory mucosa in man., *J. Neurocytol.* 11 (1982) 721–46. <http://www.ncbi.nlm.nih.gov/pubmed/7143026> (accessed February 16, 2018).
- [221] N.G. Schipper, J.C. Verhoef, F.W. Merkus, The nasal mucociliary clearance: relevance to nasal drug delivery., *Pharm. Res.* 8 (1991) 807–14. <http://www.ncbi.nlm.nih.gov/pubmed/1924131> (accessed February 16, 2018).
- [222] C.M. Van Itallie, J.M. Anderson, Claudins And Epithelial Paracellular Transport, *Annu. Rev. Physiol.* 68 (2006) 403–429. doi:10.1146/annurev.physiol.68.040104.131404.
- [223] H. Altner, I. Altner-Kolnberger, Freeze-fracture and tracer experiments on the permeability of the zonulae occludentes in the olfactory mucosa of vertebrates., *Cell Tissue Res.* 154 (1974) 51–9. <http://www.ncbi.nlm.nih.gov/pubmed/4548378> (accessed February 16, 2018).
- [224] B. Bernocchi, R. Carpentier, I. Lantier, C. Ducournau, I. Dimier-Poisson, D. Betbeder, Mechanisms allowing protein delivery in nasal mucosa using NPL nanoparticles., *J. Control. Release.* 232 (2016) 42–50. doi:10.1016/j.jconrel.2016.04.014.
- [225] J. Brooking, S.S. Davis, L. Illum, Transport of nanoparticles across the rat nasal mucosa., *J. Drug Target.* 9 (2001) 267–79. <http://www.ncbi.nlm.nih.gov/pubmed/11697030> (accessed February 16, 2018).
- [226] S.D. Conner, S.L. Schmid, Regulated portals of entry into the cell, *Nature.* 422 (2003) 37–44. doi:10.1038/nature01451.
- [227] J. Rejman, V. Oberle, I.S. Zuhorn, D. Hoekstra, Size-dependent internalization of particles via the pathways of clathrin- and caveolae-mediated endocytosis., *Biochem. J.* 377 (2004) 159–69. doi:10.1042/BJ20031253.
- [228] H. Baker, R.F. Spencer, Transneuronal transport of peroxidase-conjugated wheat germ agglutinin (WGA-HRP) from the olfactory epithelium to the brain of the adult rat., *Exp. Brain Res.* 63 (1986) 461–73. <http://www.ncbi.nlm.nih.gov/pubmed/3758265> (accessed February 16, 2018).
- [229] R.L. Doty, The olfactory vector hypothesis of neurodegenerative disease: Is it viable?, *Ann. Neurol.* 63 (2008) 7–15. doi:10.1002/ana.21327.
- [230] A.J. de Lorenzo, Electron Microscopy of the Olfactory and Gustatory Pathways, *Ann. Otol. Rhinol. Laryngol.* 69 (1960) 410–420. doi:10.1177/000348946006900210.
- [231] E. Sekerdag, Nasal Physiology and Drug Transport, in: *Nanotechnol. Methods Neurol. Dis. Brain Tumors*, Elsevier, 2017: pp. 93–102. doi:10.1016/B978-0-12-803796-6.00005-8.
- [232] P. Santi, P.L. Catellani, P. Colombo, C. Ringard-Lefebvre, C. Barthélémy, A.-M. Guyot-Hermann, Partition and transport of verapamil and nicotine through artificial membranes, *Int. J. Pharm.* 68 (1991) 43–49. doi:10.1016/0378-5173(91)90125-8.

- [233] C. Zhu, L. Jiang, T.-M. Chen, K.-K. Hwang, A comparative study of artificial membrane permeability assay for high throughput profiling of drug absorption potential., *Eur. J. Med. Chem.* 37 (2002) 399–407. <http://www.ncbi.nlm.nih.gov/pubmed/12008054> (accessed February 18, 2018).
- [234] K. Sugano, N. Takata, M. Machida, K. Saitoh, K. Terada, Prediction of passive intestinal absorption using bio-mimetic artificial membrane permeation assay and the paracellular pathway model., *Int. J. Pharm.* 241 (2002) 241–51. <http://www.ncbi.nlm.nih.gov/pubmed/12100852> (accessed February 18, 2018).
- [235] L. Di, E.H. Kerns, K. Fan, O.J. McConnell, G.T. Carter, High throughput artificial membrane permeability assay for blood-brain barrier., *Eur. J. Med. Chem.* 38 (2003) 223–32. <http://www.ncbi.nlm.nih.gov/pubmed/12667689> (accessed February 18, 2018).
- [236] S. CARRARA, V. REALI, P. MISIANO, G. DONDIO, C. BIGOGNO, Evaluation of in vitro brain penetration: Optimized PAMPA and MDCKII-MDR1 assay comparison, *Int. J. Pharm.* 345 (2007) 125–133. doi:10.1016/j.ijpharm.2007.05.057.
- [237] E.H. Kerns, L. Di, S. Petusky, M. Farris, R. Ley, P. Jupp, Combined Application of Parallel Artificial Membrane Permeability Assay and Caco-2 Permeability Assays in Drug Discovery, *J. Pharm. Sci.* 93 (2004) 1440–1453. doi:10.1002/jps.20075.
- [238] * Manfred Kansy, and Frank Senner, K. Gubernator, Physicochemical High Throughput Screening: Parallel Artificial Membrane Permeation Assay in the Description of Passive Absorption Processes, (1998). doi:10.1021/JM970530E.
- [239] P.M. Reardon, C.H. Gochoco, K.L. Audus, G. Wilson, P.L. Smith, In vitro nasal transport across ovine mucosa: effects of ammonium glycyrrhizinate on electrical properties and permeability of growth hormone releasing peptide, mannitol, and lucifer yellow., *Pharm. Res.* 10 (1993) 553–61. <http://www.ncbi.nlm.nih.gov/pubmed/8483838> (accessed February 18, 2018).
- [240] H. Kubo, K.-I. Hosoya, H. Natsume, K. Sugibayashi, Y. Morimoto, In vitro permeation of several model drugs across rabbit nasal mucosa, *Int. J. Pharm.* 103 (1994) 27–36. doi:10.1016/0378-5173(94)90200-3.
- [241] C. Wadell, E. Björk, O. Camber, Nasal drug delivery--evaluation of an in vitro model using porcine nasal mucosa., *Eur. J. Pharm. Sci.* 7 (1999) 197–206. <http://www.ncbi.nlm.nih.gov/pubmed/9845806> (accessed February 18, 2018).
- [242] M.C. Schmidt, D. Simmen, M. Hilbe, P. Boderke, G. Ditzinger, J. Sandow, S. Lang, W. Rubas, H.P. Merkle, Validation of Excised Bovine Nasal Mucosa as In Vitro Model to Study Drug Transport and Metabolic Pathways in Nasal Epithelium††Data adopted from yet unpublished parts of the Ph.D. theses of Günter Ditzinger, Steffen Lang, and M. Christiane Schmidt, *J. Pharm. Sci.* 89 (2000) 396–407. doi:10.1002/(SICI)1520-6017(200003)89:3<396::AID-JPS10>3.0.CO;2-F.
- [243] Merkle, Ditzinger, Lang, Peter, Schmidt, In vitro cell models to study nasal mucosal permeability and metabolism., *Adv. Drug Deliv. Rev.* 29 (1998) 51–79.

- <http://www.ncbi.nlm.nih.gov/pubmed/10837580> (accessed February 18, 2018).
- [244] Xin Hua Zhou, Alain Li Wan Po, Comparison of enzyme activities of tissues lining portals of absorption of drugs: Species differences, *Int. J. Pharm.* 70 (1991) 271–283. doi:10.1016/0378-5173(91)90291-U.
- [245] Dahl, Mygind, Anatomy, physiology and function of the nasal cavities in health and disease., *Adv. Drug Deliv. Rev.* 29 (1998) 3–12. <http://www.ncbi.nlm.nih.gov/pubmed/10837577> (accessed February 18, 2018).
- [246] N. V. Chemuturi, P. Hayden, M. Klausner, M.D. Donovan, Comparison of Human Tracheal/Bronchial Epithelial Cell Culture and Bovine Nasal Respiratory Explants for Nasal Drug Transport Studies, *J. Pharm. Sci.* 94 (2005) 1976–1985. doi:10.1002/jps.20404.
- [247] A.K. Leonard, A.P. Sileno, C. MacEvelly, C.A. Foerder, S.C. Quay, H.R. Costantino, Development of a novel high-concentration galantamine formulation suitable for intranasal delivery, *J. Pharm. Sci.* 94 (2005) 1736–1746. doi:10.1002/jps.20389.
- [248] S.-C. Chen, K. Eiting, K. Cui, A.K. Leonard, D. Morris, C.-Y. Li, K. Farber, A.P. Sileno, M.E. Houston, P.H. Johnson, S.C. Quay, H.R. Costantino, Therapeutic utility of a novel tight junction modulating peptide for enhancing intranasal drug delivery, *J. Pharm. Sci.* 95 (2006) 1364–1371. doi:10.1002/jps.20510.
- [249] U. Werner, T. Kissel, Development of a human nasal epithelial cell culture model and its suitability for transport and metabolism studies under in vitro conditions., *Pharm. Res.* 12 (1995) 565–71. <http://www.ncbi.nlm.nih.gov/pubmed/7596993> (accessed February 18, 2018).
- [250] J.-W. Yoo, Y.-S. Kim, S.-H. Lee, M.-K. Lee, H.-J. Roh, B.-H. Jhun, C.-H. Lee, D.-D. Kim, Serially passaged human nasal epithelial cell monolayer for in vitro drug transport studies., *Pharm. Res.* 20 (2003) 1690–6. <http://www.ncbi.nlm.nih.gov/pubmed/14620527> (accessed February 18, 2018).
- [251] N. LOPEZ-SOUZA, P.C. AVILA, J.H. WIDDICOMBE, Polarized cultures of human airway epithelium from nasal scrapings and bronchial brushings, *Vitr. Cell. Dev. Biol. - Anim.* 39 (2003) 266. doi:10.1290/1543-706X(2003)039<0266:PCOHAE>2.0.CO;2.
- [252] M. UGWOKE, R. AGU, N. VERBEKE, R. KINGET, Nasal mucoadhesive drug delivery: Background, applications, trends and future perspectives, *Adv. Drug Deliv. Rev.* 57 (2005) 1640–1665. doi:10.1016/j.addr.2005.07.009.
- [253] U. Werner, T. Kissel, In-vitro cell culture models of the nasal epithelium: a comparative histochemical investigation of their suitability for drug transport studies., *Pharm. Res.* 13 (1996) 978–88. <http://www.ncbi.nlm.nih.gov/pubmed/8842033> (accessed February 18, 2018).
- [254] M.-K. Lee, J.-W. Yoo, H. Lin, Y.-S. Kim, D.-D. Kim, Y.-M. Choi, S.-K. Park, C.-H. Lee, H.-J. Roh, Air-Liquid Interface Culture of Serially Passaged Human Nasal Epithelial Cell Monolayer for *In Vitro* Drug Transport Studies, *Drug Deliv.* 12 (2005) 305–311. doi:10.1080/10717540500177009.

- [255] S. Dimova, M.E. Brewster, M. Noppe, M. Jorissen, P. Augustijns, The use of human nasal in vitro cell systems during drug discovery and development, *Toxicol. Vitro*. 19 (2005) 107–122. doi:10.1016/j.tiv.2004.07.003.
- [256] A. De Fraissinette, R. Brun, H. Felix, J. Vonderscher, A. Rummelt, Evaluation of the human cell line RPMI 2650 as an in vitro nasal model., *Rhinology*. 33 (1995) 194–8. <http://www.ncbi.nlm.nih.gov/pubmed/8919210> (accessed February 19, 2018).
- [257] S. Harikarnpakdee, V. Lipipun, N. Sutanthavibul, G.C. Ritthidej, Spray-dried mucoadhesive microspheres: preparation and transport through nasal cell monolayer., *AAPS PharmSciTech*. 7 (2006) E12. doi:10.1208/pt070112.
- [258] C.I. Grainger, L.L. Greenwell, D.J. Lockley, G.P. Martin, B. Forbes, Culture of Calu-3 Cells at the Air Interface Provides a Representative Model of the Airway Epithelial Barrier, *Pharm. Res*. 23 (2006) 1482–1490. doi:10.1007/s11095-006-0255-0.
- [259] K.A. Foster, M.L. Avery, M. Yazdanian, K.L. Audus, Characterization of the Calu-3 cell line as a tool to screen pulmonary drug delivery., *Int. J. Pharm.* 208 (2000) 1–11. <http://www.ncbi.nlm.nih.gov/pubmed/11064206> (accessed February 19, 2018).
- [260] N.R. Mathias, J. Timoszyk, P.I. Stetsko, J.R. Megill, R.L. Smith, D.A. Wall, Permeability Characteristics of Calu-3 Human Bronchial Epithelial Cells: In Vitro - In Vivo Correlation to Predict Lung Absorption in Rats, *J. Drug Target*. 10 (2002) 31–40. doi:10.1080/10611860290007504.
- [261] L. Li, N.R. Mathias, C.L. Heran, P. Moench, D.A. Wall, R.L. Smith, Carbopol-mediated paracellular transport enhancement in Calu-3 cell layers, *J. Pharm. Sci.* 95 (2006) 326–335. doi:10.1002/jps.20541.
- [262] I. Pezron, R. Mitra, D. Pal, A.K. Mitra, Insulin aggregation and asymmetric transport across human bronchial epithelial cell monolayers (Calu-3)., *J. Pharm. Sci.* 91 (2002) 1135–46. <http://www.ncbi.nlm.nih.gov/pubmed/11948552> (accessed February 19, 2018).
- [263] B.I. Florea, M.L. Cassara, H.E. Junginger, G. Borchard, Drug transport and metabolism characteristics of the human airway epithelial cell line Calu-3., *J. Control. Release*. 87 (2003) 131–8. <http://www.ncbi.nlm.nih.gov/pubmed/12618029> (accessed February 19, 2018).
- [264] D. Teijeiro-Osorio, C. Remuñán-López, M.J. Alonso, New Generation of Hybrid Poly/Oligosaccharide Nanoparticles as Carriers for the Nasal Delivery of Macromolecules, *Biomacromolecules*. 10 (2009) 243–249. doi:10.1021/bm800975j.
- [265] Y. Wang, M. Li, S. Qian, Q. Zhang, L. Zhou, Z. Zuo, B. Lee, M. Toh, T. Ho, Zolpidem Mucoadhesive Formulations for Intranasal Delivery: Characterization, In Vitro Permeability, Pharmacokinetics, and Nasal Ciliotoxicity in Rats, *J. Pharm. Sci.* 105 (2016) 2840–2847. doi:10.1016/j.xphs.2016.03.035.
- [266] T. Qin, Y. Yin, X. Wang, H. Liu, J. Lin, Q. Yu, Q. Yang, Whole inactivated avian

- Influenza H9N2 viruses induce nasal submucosal dendritic cells to sample luminal viruses via transepithelial dendrites and trigger subsequent DC maturation, *Vaccine*. 33 (2015) 1382–1392. doi:10.1016/j.vaccine.2015.01.022.
- [267] L. Zhang, S. Du, Y. Lu, C. Liu, Z. Tian, C. Yang, H. Wu, Z. Wang, Puerarin transport across a Calu-3 cell monolayer – an in vitro model of nasal mucosa permeability and the influence of paeoniflorin and menthol, *Drug Des. Devel. Ther.* Volume 10 (2016) 2227–2237. doi:10.2147/DDDT.S110247.
- [268] M. Amoako-Tuffour, P. Yeung, R. Agu, Permeation of losartan across human respiratory epithelium: An in vitro study with Calu-3 cells, *Acta Pharm.* 59 (2009) 395–405. doi:10.2478/v10007-009-0038-3.
- [269] X. Zheng, X. Shao, C. Zhang, Y. Tan, Q. Liu, X. Wan, Q. Zhang, S. Xu, X. Jiang, Intranasal H102 Peptide-Loaded Liposomes for Brain Delivery to Treat Alzheimer’s Disease, *Pharm. Res.* 32 (2015) 3837–3849. doi:10.1007/s11095-015-1744-9.
- [270] Y. Ye, Y. Xu, W. Liang, G.P.H. Leung, K.-H. Cheung, C. Zheng, F. Chen, J.K.W. Lam, DNA-loaded chitosan oligosaccharide nanoparticles with enhanced permeability across Calu-3 cells, *J. Drug Target.* 21 (2013) 474–486. doi:10.3109/1061186X.2013.766885.
- [271] M.B. Pearce, A. Jayaraman, C. Pappas, J.A. Belser, H. Zeng, K.M. Gustin, T.R. Maines, X. Sun, R. Raman, N.J. Cox, R. Sasisekharan, J.M. Katz, T.M. Tumpey, Pathogenesis and transmission of swine origin A(H3N2)v influenza viruses in ferrets., *Proc. Natl. Acad. Sci. U. S. A.* 109 (2012) 3944–9. doi:10.1073/pnas.1119945109.
- [272] R.J. Verheul, N. Hagenaaars, T. van Es, E.V.B. van Gaal, P.H.J.L.F. de Jong, S. Bruijns, E. Mastrobattista, B. Slütter, I. Que, J.G.M. Heldens, H. van den Bosch, H.L. Glansbeek, W.E. Hennink, W. Jiskoot, A step-by-step approach to study the influence of N-acetylation on the adjuvanticity of N,N,N-trimethyl chitosan (TMC) in an intranasal nanoparticulate influenza virus vaccine, *Eur. J. Pharm. Sci.* 45 (2012) 467–474. doi:10.1016/j.ejps.2011.10.001.
- [273] A.S. Tulbah, H.X. Ong, L. Morgan, P. Colombo, P.M. Young, D. Traini, Dry powder formulation of simvastatin, *Expert Opin. Drug Deliv.* 12 (2015) 857–868. doi:10.1517/17425247.2015.963054.
- [274] T. Seki, H. Kanbayashi, T. Nagao, S. Chono, M. Tomita, M. Hayashi, Y. Tabata, K. Morimoto, Effect of aminated gelatin on the nasal absorption of insulin in rats., *Biol. Pharm. Bull.* 28 (2005) 510–4. <http://www.ncbi.nlm.nih.gov/pubmed/15744079> (accessed February 19, 2018).
- [275] C. Witschi, R.J. Mersny, In vitro evaluation of microparticles and polymer gels for use as nasal platforms for protein delivery., *Pharm. Res.* 16 (1999) 382–90. <http://www.ncbi.nlm.nih.gov/pubmed/10213368> (accessed February 26, 2018).
- [276] A. Mistry, S. Stolnik, L. Illum, Nanoparticles for direct nose-to-brain delivery of drugs, *Int. J. Pharm.* 379 (2009) 146–157. doi:10.1016/j.ijpharm.2009.06.019.
- [277] A.D. Kulkarni, Y.H. Vanjari, K.H. Sancheti, V.S. Belgamwar, S.J. Surana, C. V.

- Pardeshi, Nanotechnology-mediated nose to brain drug delivery for Parkinson's disease: a mini review, *J. Drug Target.* 23 (2015) 775–788. doi:10.3109/1061186X.2015.1020809.
- [278] N. Haffejee, J. Du Plessis, D.G. Müller, C. Schultz, A.F. Kotzé, C. Goosen, Intranasal toxicity of selected absorption enhancers., *Pharmazie.* 56 (2001) 882–8. <http://www.ncbi.nlm.nih.gov/pubmed/11817176> (accessed February 21, 2018).
- [279] M. van Woensel, N. Wauthoz, R. Rosière, K. Amighi, V. Mathieu, F. Lefranc, S.W. van Gool, S. de Vleeschouwer, Formulations for Intranasal Delivery of Pharmacological Agents to Combat Brain Disease: A New Opportunity to Tackle GBM?, *Cancers (Basel).* 5 (2013) 1020–48. doi:10.3390/cancers5031020.
- [280] K. Phukan, M. Nandy, R.B. Sharma, H.K. Sharma, Nanosized Drug Delivery Systems for Direct Nose to Brain Targeting: A Review., *Recent Pat. Drug Deliv. Formul.* 10 (2016) 156–64. <http://www.ncbi.nlm.nih.gov/pubmed/26996366> (accessed February 21, 2018).
- [281] O. Gartziandia, S.P. Egusquiaguirre, J. Bianco, J.L. Pedraz, M. Igartua, R.M. Hernandez, V. Préat, A. Beloqui, Nanoparticle transport across in vitro olfactory cell monolayers, *Int. J. Pharm.* 499 (2016) 81–89. doi:10.1016/j.ijpharm.2015.12.046.
- [282] J. Wattanatho, W. Phachonpai, A. Pripem, S. Suthiparin, J. Wattanathorn, W. Phachonpai, A. Pripem, S. Suthiparinyanont, Intranasal Administration of Quercetin Liposome Decreases Anxiety-like Behavior and Increases Spatial Memory, *Am. J. Agric. Biol. Sci.* 2 (2007) 31–35. doi:10.3844/ajabssp.2007.31.35.
- [283] M.M. Migliore, R. Ortiz, S. Dye, R.B. Campbell, M.M. Amiji, B.L. Waszczak, Neurotrophic and neuroprotective efficacy of intranasal GDNF in a rat model of Parkinson's disease, *Neuroscience.* 274 (2014) 11–23. doi:10.1016/j.neuroscience.2014.05.019.
- [284] T. Tong-Un, S. Muchimapura, W. Phachonpai, J. Wattanathorn, T. Tong-Un, S. Muchimapura, W. Phachonpai, J. Wattanathorn, Nasal Administration of Quercetin Liposomes Modulate Cognitive Impairment and Inhibit Acetylcholinesterase Activity in Hippocampus, *Neurosci. Int.* 2010, Vol. 1, Page 21. 1 (2010) 21–27. doi:10.3844/AMJNSP.2010.21.27.
- [285] K. Arumugam, G. Subramanian, S. Mallayasamy, R. Averineni, M. Reddy, N. Udupa, A study of rivastigmine liposomes for delivery into the brain through intranasal route, *Acta Pharm.* 58 (2008) 287–97. doi:10.2478/v10007-008-0014-3.
- [286] Z.-Z. Yang, Y.-Q. Zhang, Z.-Z. Wang, K. Wu, J.-N. Lou, X.-R. Qi, Enhanced brain distribution and pharmacodynamics of rivastigmine by liposomes following intranasal administration, *Int. J. Pharm.* 452 (2013) 344–354. doi:10.1016/j.ijpharm.2013.05.009.
- [287] W. Li, Y. Zhou, N. Zhao, B. Hao, X. Wang, P. Kong, Pharmacokinetic behavior and efficiency of acetylcholinesterase inhibition in rat brain after intranasal

- administration of galanthamine hydrobromide loaded flexible liposomes, *Environ. Toxicol. Pharmacol.* 34 (2012) 272–279. doi:10.1016/j.etap.2012.04.012.
- [288] A.M. Fatouh, A.H. Elshafeey, A. Abdelbary, Intranasal agomelatine solid lipid nanoparticles to enhance brain delivery: formulation, optimization and *in vivo* pharmacokinetics., *Drug Des. Devel. Ther.* 11 (2017) 1815–1825. doi:10.2147/DDDT.S102500.
- [289] A.M. Fatouh, A.H. Elshafeey, A. Abdelbary, Agomelatine-based *in situ* gels for brain targeting via the nasal route: statistical optimization, *in vitro*, and *in vivo* evaluation, *Drug Deliv.* 24 (2017) 1077–1085. doi:10.1080/10717544.2017.1357148.
- [290] S. Patel, S. Chavhan, H. Soni, A.K. Babbar, R. Mathur, A.K. Mishra, K. Sawant, Brain targeting of risperidone-loaded solid lipid nanoparticles by intranasal route, *J. Drug Target.* 19 (2011) 468–474. doi:10.3109/1061186X.2010.523787.
- [291] E. Esposito, R. Cortesi, M. Drechsler, J. Fan, B.M. Fu, L. Calderan, S. Mannucci, F. Boschi, C. Nastruzzi, Nanoformulations for dimethyl fumarate: Physicochemical characterization and *in vitro* / *in vivo* behavior, *Eur. J. Pharm. Biopharm.* 115 (2017) 285–296. doi:10.1016/j.ejpb.2017.04.011.
- [292] R. Bhatt, D. Singh, A. Prakash, N. Mishra, Development, characterization and nasal delivery of rosmarinic acid-loaded solid lipid nanoparticles for the effective management of Huntington's disease, *Drug Deliv.* 22 (2015) 931–939. doi:10.3109/10717544.2014.880860.
- [293] E. Muntimadugu, R. Dhommatti, A. Jain, V.G.S. Challa, M. Shaheen, W. Khan, Intranasal delivery of nanoparticle encapsulated tarenflurbil: A potential brain targeting strategy for Alzheimer's disease, *Eur. J. Pharm. Sci.* 92 (2016) 224–234. doi:10.1016/j.ejps.2016.05.012.
- [294] P. Chandra Bhatt, P. Srivastava, P. Pandey, W. Khan, B.P. Panda, Nose to brain delivery of astaxanthin-loaded solid lipid nanoparticles: fabrication, radio labeling, optimization and biological studies, *RSC Adv.* 6 (2016) 10001–10010. doi:10.1039/C5RA19113K.
- [295] X. Zhuang, Y. Teng, A. Samykutty, J. Mu, Z. Deng, L. Zhang, P. Cao, Y. Rong, J. Yan, D. Miller, H.-G. Zhang, Grapefruit-derived Nanovectors Delivering Therapeutic miR17 Through an Intranasal Route Inhibit Brain Tumor Progression., *Mol. Ther.* 24 (2016) 96–105. doi:10.1038/mt.2015.188.
- [296] A. Khan, S.S. Imam, M. Aqil, A. Ahad, Y. Sultana, A. Ali, K. Khan, Brain Targeting of Temozolomide via the Intranasal Route Using Lipid-Based Nanoparticles: Brain Pharmacokinetic and Scintigraphic Analyses, *Mol. Pharm.* 13 (2016) 3773–3782. doi:10.1021/acs.molpharmaceut.6b00586.
- [297] R.G. Madane, H.S. Mahajan, Curcumin-loaded nanostructured lipid carriers (NLCs) for nasal administration: design, characterization, and *in vivo* study, *Drug Deliv.* 23 (2014) 1–9. doi:10.3109/10717544.2014.975382.
- [298] R. Chen, A.L. Cohen, H. Colman, Targeted Therapeutics in Patients With High-

- Grade Gliomas: Past, Present, and Future, *Curr. Treat. Options Oncol.* 17 (2016) 42. doi:10.1007/s11864-016-0418-0.
- [299] L. Lin, J. Cai, C. Jiang, Recent Advances in Targeted Therapy for Glioma, *Curr. Med. Chem.* 24 (2017) 1365–1381. doi:10.2174/0929867323666161223150242.
- [300] J.J. Miller, P.Y. Wen, Emerging targeted therapies for glioma, *Expert Opin. Emerg. Drugs.* 21 (2016) 441–452. doi:10.1080/14728214.2016.1257609.
- [301] S. Wilhelm, C. Carter, M. Lynch, T. Lowinger, J. Dumas, R.A. Smith, B. Schwartz, R. Simantov, S. Kelley, Discovery and development of sorafenib: a multikinase inhibitor for treating cancer, *Nat. Rev. Drug Discov.* 5 (2006) 835–844. doi:10.1038/nrd2130.
- [302] R.B. Den, M. Kamrava, Z. Sheng, M. Werner-Wasik, E. Dougherty, M. Marinucchi, Y.R. Lawrence, S. Hegarty, T. Hyslop, D.W. Andrews, J. Glass, D.P. Friedman, M.R. Green, K. Camphausen, A.P. Dicker, A phase I study of the combination of sorafenib with temozolomide and radiation therapy for the treatment of primary and recurrent high-grade gliomas., *Int. J. Radiat. Oncol. Biol. Phys.* 85 (2013) 321–8. doi:10.1016/j.ijrobp.2012.04.017.
- [303] E.Q. Lee, J. Kuhn, K.R. Lamborn, L. Abrey, L.M. DeAngelis, F. Lieberman, H.I. Robins, S.M. Chang, W.K.A. Yung, J. Drappatz, M.P. Mehta, V.A. Levin, K. Aldape, J.E. Dancey, J.J. Wright, M.D. Prados, T.F. Cloughesy, M.R. Gilbert, P.Y. Wen, Phase I/II study of sorafenib in combination with temsirolimus for recurrent glioblastoma or gliosarcoma: North American Brain Tumor Consortium study 05-02, *Neuro. Oncol.* 14 (2012) 1511–1518. doi:10.1093/neuonc/nos264.
- [304] D.A. Reardon, J.J. Vredenburgh, A. Desjardins, K. Peters, S. Gururangan, J.H. Sampson, J. Marcello, J.E. Herndon, R.E. McLendon, D. Janney, A.H. Friedman, D.D. Bigner, H.S. Friedman, H.S. Friedman, Effect of CYP3A-inducing anti-epileptics on sorafenib exposure: results of a phase II study of sorafenib plus daily temozolomide in adults with recurrent glioblastoma., *J. Neurooncol.* 101 (2011) 57–66. doi:10.1007/s11060-010-0217-6.
- [305] F. Zustovich, L. Landi, G. Lombardi, C. Porta, L. Galli, A. Fontana, D. Amoroso, C. Galli, M. Andreuccetti, A. Falcone, V. Zagonel, Sorafenib plus daily low-dose temozolomide for relapsed glioblastoma: a phase II study., *Anticancer Res.* 33 (2013) 3487–94. <http://www.ncbi.nlm.nih.gov/pubmed/23898124> (accessed May 23, 2018).
- [306] S. Agarwal, R. Sane, J.R. Ohlfest, W.F. Elmquist, The role of the breast cancer resistance protein (ABCG2) in the distribution of sorafenib to the brain, *J. Pharmacol. Exp. Ther.* 336 (2011) 223–233. doi:10.1124/jpet.110.175034.
- [307] M.S. Brose, C.T. Frenette, S.M. Keefe, S.M. Stein, Management of sorafenib-related adverse events: a clinician's perspective, *Semin. Oncol.* 41 Suppl 2 (2014) S1–S16. doi:10.1053/j.seminoncol.2014.01.001.
- [308] A. Clavreul, M. Pourbaghi-Masouleh, E. Roger, N. Lautram, C.N. Montero-Menei, P. Menei, Human mesenchymal stromal cells as cellular drug-delivery vectors for glioblastoma therapy: a good deal?, *J. Exp. Clin. Cancer Res. CR.*

- 36 (2017) 135. doi:10.1186/s13046-017-0605-2.
- [309] A. Béduneau, P. Saulnier, J.-P. Benoit, Active targeting of brain tumors using nanocarriers, *Biomaterials*. 28 (2007) 4947–4967. doi:10.1016/j.biomaterials.2007.06.011.
- [310] S. Hirsjärvi, C. Belloche, F. Hindré, E. Garcion, J.-P. Benoit, Tumour targeting of lipid nanocapsules grafted with cRGD peptides, *Eur. J. Pharm. Biopharm. Off. J. Arbeitsgemeinschaft Fur Pharm. Verfahrenstechnik e.V.* 87 (2014) 152–159. doi:10.1016/j.ejpb.2013.12.006.
- [311] E. Garcion, A. Lamprecht, B. Heurtault, A. Paillard, A. Aubert-Pouessel, B. Denizot, P. Menei, J.-P. Benoît, A new generation of anticancer, drug-loaded, colloidal vectors reverses multidrug resistance in glioma and reduces tumor progression in rats, *Mol. Cancer Ther.* 5 (2006) 1710–1722. doi:10.1158/1535-7163.MCT-06-0289.
- [312] G. Lollo, M. Vincent, G. Ullio-Gamboa, L. Lemaire, F. Franconi, D. Couez, J.-P. Benoit, Development of multifunctional lipid nanocapsules for the co-delivery of paclitaxel and CpG-ODN in the treatment of glioblastoma, *Int. J. Pharm.* 495 (2015) 972–980. doi:10.1016/j.ijpharm.2015.09.062.
- [313] B. Heurtault, P. Saulnier, B. Pech, J.-E. Proust, J.-P. Benoit, A novel phase inversion-based process for the preparation of lipid nanocarriers., *Pharm. Res.* 19 (2002) 875–80. <http://www.ncbi.nlm.nih.gov/pubmed/12134960> (accessed February 10, 2018).
- [314] L. Lemaire, J. Nel, F. Franconi, G. Bastiat, P. Saulnier, Perfluorocarbon-Loaded Lipid Nanocapsules to Assess the Dependence of U87-Human Glioblastoma Tumor pO₂ on In Vitro Expansion Conditions, *PLoS One*. 11 (2016) e0165479. doi:10.1371/journal.pone.0165479.
- [315] F. Kober, I. Iltis, M. Izquierdo, M. Desrois, D. Ibarrola, P.J. Cozzone, M. Bernard, High-resolution myocardial perfusion mapping in small animals in vivo by spin-labeling gradient-echo imaging, *Magn. Reson. Med.* 51 (2004) 62–67. doi:10.1002/mrm.10676.
- [316] E.F. Craparo, C. Sardo, R. Serio, M.G. Zizzo, M.L. Bondi, G. Giammona, G. Cavallaro, Galactosylated polymeric carriers for liver targeting of sorafenib, *Int. J. Pharm.* 466 (2014) 172–180. doi:10.1016/j.ijpharm.2014.02.047.
- [317] D.-Y. Gao, T.-T. Lin, Y.-C. Sung, Y.C. Liu, W.-H. Chiang, C.-C. Chang, J.-Y. Liu, Y. Chen, CXCR4-targeted lipid-coated PLGA nanoparticles deliver sorafenib and overcome acquired drug resistance in liver cancer, *Biomaterials*. 67 (2015) 194–203. doi:10.1016/j.biomaterials.2015.07.035.
- [318] Y.-J. Li, M. Dong, F.-M. Kong, J.-P. Zhou, Folate-decorated anticancer drug and magnetic nanoparticles encapsulated polymeric carrier for liver cancer therapeutics, *Int. J. Pharm.* 489 (2015) 83–90. doi:10.1016/j.ijpharm.2015.04.028.
- [319] T.-T. Lin, D.-Y. Gao, Y.-C. Liu, Y.-C. Sung, D. Wan, J.-Y. Liu, T. Chiang, L. Wang, Y. Chen, Development and characterization of sorafenib-loaded PLGA

- nanoparticles for the systemic treatment of liver fibrosis, *J. Control. Release.* 221 (2016) 62–70. doi:10.1016/j.jconrel.2015.11.003.
- [320] J. Liu, B. Boonkaew, J. Arora, S.H. Mandava, M.M. Maddox, S. Chava, C. Callaghan, J. He, S. Dash, V.T. John, B.R. Lee, Comparison of Sorafenib-Loaded Poly (Lactic/Glycolic) Acid and DPPC Liposome Nanoparticles in the in Vitro Treatment of Renal Cell Carcinoma, *J. Pharm. Sci.* 104 (2015) 1187–1196. doi:10.1002/jps.24318.
- [321] Y. Liu, J. Yang, X. Wang, J. Liu, Z. Wang, H. Liu, L. Chen, In vitro and in vivo evaluation of redox-responsive sorafenib carrier nanomicelles synthesized from poly (acrylic acid) -cystamine hydrochloride-D- α -tocopherol succinate, *J. Biomater. Sci. Polym. Ed.* 27 (2016) 1729–1747. doi:10.1080/09205063.2016.1236883.
- [322] Y.-C. Yang, J. Cai, J. Yin, J. Zhang, K.-L. Wang, Z.-T. Zhang, Heparin-functionalized Pluronic nanoparticles to enhance the antitumor efficacy of sorafenib in gastric cancers, *Carbohydr. Polym.* 136 (2016) 782–790. doi:10.1016/j.carbpol.2015.09.023.
- [323] L. Zhang, F. Gong, F. Zhang, J. Ma, P. Zhang, J. Shen, Targeted therapy for human hepatic carcinoma cells using folate-functionalized polymeric micelles loaded with superparamagnetic iron oxide and sorafenib in vitro, *Int. J. Nanomedicine.* 8 (2013) 1517–1524. doi:10.2147/IJN.S43263.
- [324] S. Benizri, L. Ferey, B. Alies, N. Mebarek, G. Vacher, A. Appavoo, C. Staedel, K. Gaudin, P. Barthélémy, Nucleoside-Lipid-Based Nanocarriers for Sorafenib Delivery, *Nanoscale Res. Lett.* 13 (2018) 17. doi:10.1186/s11671-017-2420-2.
- [325] M.L. Bondì, C. Botto, E. Amore, M.R. Emma, G. Augello, E.F. Craparo, M. Cervello, Lipid nanocarriers containing sorafenib inhibit colonies formation in human hepatocarcinoma cells, *Int. J. Pharm.* 493 (2015) 75–85. doi:10.1016/j.ijpharm.2015.07.055.
- [326] A. Grillone, E.R. Riva, A. Mondini, C. Forte, L. Calucci, C. Innocenti, C. de Julian Fernandez, V. Cappello, M. Gemmi, S. Moscato, F. Ronca, R. Sacco, V. Mattoli, G. Ciofani, Active Targeting of Sorafenib: Preparation, Characterization, and In Vitro Testing of Drug-Loaded Magnetic Solid Lipid Nanoparticles, *Adv. Healthc. Mater.* 4 (2015) 1681–1690. doi:10.1002/adhm.201500235.
- [327] L. Mo, J.G. Song, H. Lee, M. Zhao, H.Y. Kim, Y.J. Lee, H.W. Ko, H.-K. Han, PEGylated hyaluronic acid-coated liposome for enhanced in vivo efficacy of sorafenib via active tumor cell targeting and prolonged systemic exposure, *Nanomedicine Nanotechnology, Biol. Med.* 14 (2018) 557–567. doi:10.1016/j.nano.2017.12.003.
- [328] Y. Xiao, Y. Liu, S. Yang, B. Zhang, T. Wang, D. Jiang, J. Zhang, D. Yu, N. Zhang, Sorafenib and gadolinium co-loaded liposomes for drug delivery and MRI-guided HCC treatment, *Colloids Surf. B. Biointerfaces.* 141 (2016) 83–92. doi:10.1016/j.colsurfb.2016.01.016.
- [329] S. Yang, B. Zhang, X. Gong, T. Wang, Y. Liu, N. Zhang, In vivo biodistribution, biocompatibility, and efficacy of sorafenib-loaded lipid-based nanosuspensions

- evaluated experimentally in cancer, *Int. J. Nanomedicine*. 11 (2016) 2329–2343. doi:10.2147/IJN.S104119.
- [330] Z. Zhang, B. Niu, J. Chen, X. He, X. Bao, J. Zhu, H. Yu, Y. Li, The use of lipid-coated nanodiamond to improve bioavailability and efficacy of sorafenib in resisting metastasis of gastric cancer, *Biomaterials*. 35 (2014) 4565–4572. doi:10.1016/j.biomaterials.2014.02.024.
- [331] J. Zhang, J. Hu, H.F. Chan, M. Skibba, G. Liang, M. Chen, iRGD decorated lipid-polymer hybrid nanoparticles for targeted co-delivery of doxorubicin and sorafenib to enhance anti-hepatocellular carcinoma efficacy, *Nanomedicine Nanotechnology, Biol. Med.* 12 (2016) 1303–1311. doi:10.1016/j.nano.2016.01.017.
- [332] J. Zhang, T. Wang, S. Mu, L.D. Olerile, X. Yu, N. Zhang, Biomacromolecule/lipid hybrid nanoparticles for controlled delivery of sorafenib in targeting hepatocellular carcinoma therapy, *Nanomedicine (Lond)*. 12 (2017) 911–925. doi:10.2217/nnm-2016-0402.
- [333] J. Hureauux, F. Lagarce, F. Gagnadoux, A. Clavreul, J.-P. Benoit, T. Urban, The adaptation of lipid nanocapsule formulations for blood administration in animals, *Int. J. Pharm.* 379 (2009) 266–269. doi:10.1016/j.ijpharm.2009.05.033.
- [334] J. Hureauux, F. Lagarce, F. Gagnadoux, M.-C. Rousselet, V. Moal, T. Urban, J.-P. Benoit, Toxicological Study and Efficacy of Blank and Paclitaxel-Loaded Lipid Nanocapsules After *i.v.* Administration in Mice, *Pharm. Res.* 27 (2010) 421–430. doi:10.1007/s11095-009-0024-y.
- [335] G. Le Roux, H. Moche, A. Nieto, J.-P. Benoit, F. Nessler, F. Lagarce, Cytotoxicity and genotoxicity of lipid nanocapsules, *Toxicol. Vitr. an Int. J. Publ. Assoc. with BIBRA*. 41 (2017) 189–199. doi:10.1016/j.tiv.2017.03.007.
- [336] A.C. Silva, S.G. Kim, M. Garwood, Imaging blood flow in brain tumors using arterial spin labeling, *Magn. Reson. Med.* 44 (2000) 169–173.
- [337] J.B. Andre, S. Nagpal, D.S. Hippe, A.C. Ravanpay, H. Schmiedeskamp, R. Bammer, G.J. Palagallo, L. Recht, G. Zaharchuk, Cerebral Blood Flow Changes in Glioblastoma Patients Undergoing Bevacizumab Treatment Are Seen in Both Tumor and Normal Brain, *Neuroradiol. J.* 28 (2015) 112–119. doi:10.1177/1971400915576641.
- [338] S. Fellah, N. Girard, O. Chinot, P.J. Cozzzone, V. Callot, Early evaluation of tumoral response to antiangiogenic therapy by arterial spin labeling perfusion magnetic resonance imaging and susceptibility weighted imaging in a patient with recurrent glioblastoma receiving bevacizumab, *J. Clin. Oncol. Off. J. Am. Soc. Clin. Oncol.* 29 (2011) e308-311. doi:10.1200/JCO.2010.32.6082.
- [339] R. Rajendran, W. Huang, A.M.Y. Tang, J.M. Liang, S. Choo, T. Reese, H. Hentze, S. van Boxtel, A. Cliffe, K. Rogers, B. Henry, K.H. Chuang, Early detection of antiangiogenic treatment responses in a mouse xenograft tumor model using quantitative perfusion MRI, *Cancer Med.* 3 (2014) 47–60. doi:10.1002/cam4.177.

- [340] R.A. Towner, M. Ihnat, D. Saunders, A. Bastian, N. Smith, R.K. Pavana, A. Gangjee, A new anti-glioma therapy, AG119: pre-clinical assessment in a mouse GL261 glioma model, *BMC Cancer*. 15 (2015) 522. doi:10.1186/s12885-015-1538-9.
- [341] T.J. Yun, H.R. Cho, S.H. Choi, H. Kim, J.-K. Won, S.-W. Park, J.-H. Kim, C.-H. Sohn, M.H. Han, Antiangiogenic Effect of Bevacizumab: Application of Arterial Spin-Labeling Perfusion MR Imaging in a Rat Glioblastoma Model, *AJNR. Am. J. Neuroradiol.* 37 (2016) 1650–1656. doi:10.3174/ajnr.A4800.
- [342] J. Ziegler, A. Bastian, M. Lerner, L. Bailey-Downs, D. Saunders, N. Smith, J. Sutton, J.D. Battiste, M.A. Ihnat, A. Gangjee, R.A. Towner, AG488 as a therapy against gliomas, *Oncotarget*. 8 (2017) 71833–71844. doi:10.18632/oncotarget.18284.
- [343] Y. Sun, N.O. Schmidt, K. Schmidt, S. Doshi, J.B. Rubin, R. V. Mulkern, R. Carroll, M. Ziu, K. Erkmén, T.Y. Poussaint, P. Black, M. Albert, D. Burstein, M.W. Kieran, Perfusion MRI of U87 brain tumors in a mouse model, *Magn. Reson. Med.* 51 (2004) 893–899. doi:10.1002/mrm.20029.
- [344] Y. Boucher, M. Leunig, R.K. Jain, Tumor angiogenesis and interstitial hypertension, *Cancer Res.* 56 (1996) 4264–4266.
- [345] V.P. Chauhan, T. Stylianopoulos, Y. Boucher, R.K. Jain, Delivery of molecular and nanoscale medicine to tumors: transport barriers and strategies, *Annu. Rev. Chem. Biomol. Eng.* 2 (2011) 281–298. doi:10.1146/annurev-chembioeng-061010-114300.
- [346] R.K. Jain, Normalizing tumor vasculature with anti-angiogenic therapy: a new paradigm for combination therapy, *Nat Med.* 7 (2001) 987–989. doi:10.1038/nm0901-987.
- [347] S.H. Hwang, J. Cha, K. Jo, Y.H. Jeong, H. Kim, A. Cho, W.J. Kang, M. Yun, Correlation of tumor size and metabolism with perfusion in hepatocellular carcinoma using dynamic contrast enhanced CT and F-18 FDG PET-CT, *J. Nucl. Med.* 56 (2015) 1330–1330.
- [348] F. Kallinowski, K.H. Schlenger, S. Runkel, M. Kloes, M. Stohrer, P. Okunieff, P. Vaupel, Blood flow, metabolism, cellular microenvironment, and growth rate of human tumor xenografts, *Cancer Res.* 49 (1989) 3759–3764.
- [349] T.T. Batchelor, E.R. Gerstner, K.E. Emblem, D.G. Duda, J. Kalpathy-Cramer, M. Snuderl, M. Ancukiewicz, P. Polaskova, M.C. Pinho, D. Jennings, S.R. Plotkin, A.S. Chi, A.F. Eichler, J. Dietrich, F.H. Hochberg, C. Lu-Emerson, A.J. Iafrate, S.P. Ivy, B.R. Rosen, J.S. Loeffler, P.Y. Wen, A.G. Sorensen, R.K. Jain, Improved tumor oxygenation and survival in glioblastoma patients who show increased blood perfusion after cediranib and chemoradiation., *Proc. Natl. Acad. Sci. U. S. A.* 110 (2013) 19059–64. doi:10.1073/pnas.1318022110.
- [350] A.C. Navis, A. Bourgonje, P. Wesseling, A. Wright, W. Hendriks, K. Verrijp, J.A.W.M. van der Laak, A. Heerschap, W.P.J. Leenders, Effects of dual targeting of tumor cells and stroma in human glioblastoma xenografts with a tyrosine kinase inhibitor against c-MET and VEGFR2, *PLoS One*. 8 (2013)

- e58262. doi:10.1371/journal.pone.0058262.
- [351] A.G. Sorensen, K.E. Emblem, P. Polaskova, D. Jennings, H. Kim, M. Ancukiewicz, M. Wang, P.Y. Wen, P. Ivy, T.T. Batchelor, R.K. Jain, Increased survival of glioblastoma patients who respond to antiangiogenic therapy with elevated blood perfusion, *Cancer Res.* 72 (2012) 402–407. doi:10.1158/0008-5472.CAN-11-2464.
- [352] A. Cikankowitz, A. Clavreul, C. Tétaud, L. Lemaire, A. Rousseau, N. Lepareur, D. Dabli, F. Bouchet, E. Garcion, P. Menei, O. Couturier, F. Hindré, Characterization of the distribution, retention, and efficacy of internal radiation of ¹⁸⁸Re-lipid nanocapsules in an immunocompromised human glioblastoma model, *J. Neurooncol.* 131 (2017) 49–58. doi:10.1007/s11060-016-2289-4.
- [353] R.K. Jain, Normalization of tumor vasculature: an emerging concept in antiangiogenic therapy, *Science.* 307 (2005) 58–62. doi:10.1126/science.1104819.
- [354] J. Ma, S. Li, K. Reed, P. Guo, J.M. Gallo, Pharmacodynamic-mediated effects of the angiogenesis inhibitor SU5416 on the tumor disposition of temozolomide in subcutaneous and intracerebral glioma xenograft models., *J. Pharmacol. Exp. Ther.* 305 (2003) 833–9. doi:10.1124/jpet.102.048587.
- [355] W. Wang, W. Sivakumar, S. Torres, N. Jhaveri, V.P. Vaikari, A. Gong, A. Howard, E.B. Golden, S.G. Louie, A.H. Schönthal, F.M. Hofman, T.C. Chen, Effects of convection-enhanced delivery of bevacizumab on survival of glioma-bearing animals, *Neurosurg. Focus.* 38 (2015) E8. doi:10.3171/2015.1.FOCUS14743.
- [356] A. Pires, A. Fortuna, G. Alves, A. Falcão, Intranasal drug delivery: how, why and what for?, *J. Pharm. Pharm. Sci.* 12 (2009) 288–311.
- [357] M. Morishita, K. Park, *Biodrug delivery systems : fundamentals, applications and clinical development*, Informa Healthcare USA, 2010.
- [358] S. Türker, E. Onur, Y. Ozer, Nasal route and drug delivery systems., *Pharm. World Sci.* 26 (2004) 137–42.
- [359] P.G. Djupesland, Nasal drug delivery devices: characteristics and performance in a clinical perspective—a review, *Drug Deliv. Transl. Res.* 3 (2013) 42–62. doi:10.1007/s13346-012-0108-9.
- [360] B. Wang, W.Y. Feng, M. Wang, J.W. Shi, F. Zhang, H. Ouyang, Y.L. Zhao, Z.F. Chai, Y.Y. Huang, Y.N. Xie, H.F. Wang, J. Wang, Transport of Intranasally Instilled Fine Fe₂O₃ Particles into the Brain: Micro-distribution, Chemical States, and Histopathological Observation, *Biol. Trace Elem. Res.* 118 (2007) 233–243. doi:10.1007/s12011-007-0028-6.
- [361] X. Wang, N. Chi, X. Tang, Preparation of estradiol chitosan nanoparticles for improving nasal absorption and brain targeting, *Eur. J. Pharm. Biopharm.* 70 (2008) 735–740. doi:10.1016/j.ejpb.2008.07.005.
- [362] Y.-Y. Wang, S.K. Lai, J.S. Suk, A. Pace, R. Cone, J. Hanes, Addressing the

- PEG Mucoadhesivity Paradox to Engineer Nanoparticles that “Slip” through the Human Mucus Barrier, *Angew. Chemie Int. Ed.* 47 (2008) 9726–9729. doi:10.1002/anie.200803526.
- [363] M.I. Alam, S. Baboota, A. Ahuja, M. Ali, J. Ali, J.K. Sahni, A. Bhatnagar, Pharmacoscintigraphic evaluation of potential of lipid nanocarriers for nose-to-brain delivery of antidepressant drug, *Int. J. Pharm.* 470 (2014) 99–106. doi:10.1016/j.ijpharm.2014.05.004.
- [364] F. Malerba, F. Paoletti, S. Capsoni, A. Cattaneo, Intranasal delivery of therapeutic proteins for neurological diseases, *Expert Opin. Drug Deliv.* 8 (2011) 1277–1296. doi:10.1517/17425247.2011.588204.
- [365] L. Illum, Is nose-to-brain transport of drugs in man a reality?, *J. Pharm. Pharmacol.* 56 (2004) 3–17. doi:10.1211/0022357022539.
- [366] Bhavna, S. Md, M. Ali, R. Ali, A. Bhatnagar, S. Baboota, J. Ali, Donepezil nanosuspension intended for nose to brain targeting: In vitro and in vivo safety evaluation, *Int. J. Biol. Macromol.* 67 (2014) 418–425. doi:10.1016/j.ijbiomac.2014.03.022.
- [367] T.K. Vyas, A.K. Babbar, R.K. Sharma, A. Misra, Intranasal mucoadhesive microemulsions of zolmitriptan: Preliminary studies on brain-targeting, *J. Drug Target.* 13 (2005) 317–324. doi:10.1080/10611860500246217.
- [368] A.S. Joshi, H.S. Patel, V.S. Belgamwar, A. Agrawal, A.R. Tekade, Solid lipid nanoparticles of ondansetron HCl for intranasal delivery: development, optimization and evaluation, *J. Mater. Sci. Mater. Med.* 23 (2012) 2163–2175. doi:10.1007/s10856-012-4702-7.
- [369] O. Gartzandia, E. Herran, J.L. Pedraz, E. Carro, M. Igartua, R.M. Hernandez, Chitosan coated nanostructured lipid carriers for brain delivery of proteins by intranasal administration, *Colloids Surfaces B Biointerfaces.* 134 (2015) 304–313. doi:10.1016/j.colsurfb.2015.06.054.
- [370] T. Kanazawa, F. Akiyama, S. Kakizaki, Y. Takashima, Y. Seta, Delivery of siRNA to the brain using a combination of nose-to-brain delivery and cell-penetrating peptide-modified nano-micelles, *Biomaterials.* 34 (2013) 9220–9226. doi:10.1016/j.biomaterials.2013.08.036.
- [371] H. Zhang, C.-W. Lin, M.D. Donovan, Correlation between nasal membrane permeability and nasal absorption rate., *AAPS PharmSciTech.* 14 (2013) 60–3. doi:10.1208/s12249-012-9884-2.
- [372] M. Dahlin, B. Jansson, E. Björk, Levels of dopamine in blood and brain following nasal administration to rats., *Eur. J. Pharm. Sci.* 14 (2001) 75–80.
- [373] J.J. Lochhead, R.G. Thorne, Intranasal delivery of biologics to the central nervous system, *Adv. Drug Deliv. Rev.* 64 (2012) 614–628. doi:10.1016/j.addr.2011.11.002.
- [374] D. Carradori, P. Saulnier, V. Pr at, A. des Rieux, J. Eyer, NFL-lipid nanocapsules for brain neural stem cell targeting in vitro and in vivo, *J. Control.*

- Release. 238 (2016) 253–262. doi:10.1016/j.jconrel.2016.08.006.
- [375] P. Resnier, S. David, N. Lautram, G.J.-R. Delcroix, A. Clavreul, J.-P. Benoit, C. Passirani, EGFR siRNA lipid nanocapsules efficiently transfect glioma cells in vitro, *Int. J. Pharm.* 454 (2013) 748–755. doi:10.1016/j.ijpharm.2013.04.001.
- [376] A. Griveau, J. Bejaud, S. Anthiya, S. Avril, D. Autret, E. Garcion, Silencing of miR-21 by locked nucleic acid–lipid nanocapsule complexes sensitize human glioblastoma cells to radiation-induced cell death, *Int. J. Pharm.* 454 (2013) 765–774. doi:10.1016/j.ijpharm.2013.05.049.
- [377] C. Bastiancich, K. Vanvarenberg, B. Ucar, M. Pitorre, G. Bastiat, F. Lagarce, V. Pr at, F. Danhier, Lauroyl-gemcitabine-loaded lipid nanocapsule hydrogel for the treatment of glioblastoma, *J. Control. Release.* 225 (2016) 283–293. doi:10.1016/j.jconrel.2016.01.054.
- [378] A. B duneau, F. Hindr e, A. Clavreul, J.-C. Leroux, P. Saulnier, J.-P. Benoit, Brain targeting using novel lipid nanovectors, *J. Control. Release.* 126 (2008) 44–49. doi:10.1016/j.jconrel.2007.11.001.
- [379] N.-T. Chen, S.-H. Cheng, C.-P. Liu, J.S. Souris, C.-T. Chen, C.-Y. Mou, L.-W. Lo, Recent advances in nanoparticle-based F rster resonance energy transfer for biosensing, molecular imaging and drug release profiling., *Int. J. Mol. Sci.* 13 (2012) 16598–623. doi:10.3390/ijms131216598.
- [380] T.O. McDonald, P. Martin, J.P. Patterson, D. Smith, M. Giardiello, M. Marcello, V. See, R.K. O'Reilly, A. Owen, S. Rannard, Multicomponent Organic Nanoparticles for Fluorescence Studies in Biological Systems, *Adv. Funct. Mater.* 22 (2012) 2469–2478. doi:10.1002/adfm.201103059.
- [381] E. Roger, J.-C. Gimel, C. Bensley, A.S. Klymchenko, J.-P. Benoit, Lipid nanocapsules maintain full integrity after crossing a human intestinal epithelium model, *J. Control. Release.* 253 (2017) 11–18. doi:10.1016/j.jconrel.2017.03.005.
- [382] A.C. Groo, F. Lagarce, P. Saulnier, J.-C. Gimel, J. Gravier, C. Ailhas, J.-P. Benoit, Fate of paclitaxel lipid nanocapsules in intestinal mucus in view of their oral delivery, *Int. J. Nanomedicine.* 8 (2013) 4291. doi:10.2147/IJN.S51837.
- [383] A.M. Bannunah, D. Vilasaliu, J. Lord, S. Stolnik, Mechanisms of Nanoparticle Internalization and Transport Across an Intestinal Epithelial Cell Model: Effect of Size and Surface Charge, *Mol. Pharm.* 11 (2014) 4363–4373. doi:10.1021/mp500439c.
- [384] C. Bosquillon, M. Madlova, N. Patel, N. Clear, B. Forbes, A Comparison of Drug Transport in Pulmonary Absorption Models: Isolated Perfused rat Lungs, Respiratory Epithelial Cell Lines and Primary Cell Culture, *Pharm. Res.* 34 (2017) 2532–2540. doi:10.1007/s11095-017-2251-y.
- [385] C. Conte, F. Mastrotto, V. Taresco, A. Tchoryk, F. Quaglia, S. Stolnik, C. Alexander, Enhanced uptake in 2D- and 3D- lung cancer cell models of redox responsive PEGylated nanoparticles with sensitivity to reducing extra- and intracellular environments, *J. Control. Release.* 277 (2018) 126–141.

- doi:10.1016/j.jconrel.2018.03.011.
- [386] S. Sahlin, J. Hed, I. Rundquist, Differentiation between attached and ingested immune complexes by a fluorescence quenching cytofluorometric assay., *J. Immunol. Methods.* 60 (1983) 115–24.
- [387] E.S. Van Amersfoort, J.A. Van Strijp, Evaluation of a flow cytometric fluorescence quenching assay of phagocytosis of sensitized sheep erythrocytes by polymorphonuclear leukocytes, *Cytometry.* 17 (1994) 294–301. doi:10.1002/cyto.990170404.
- [388] J. Davda, V. Labhasetwar, Characterization of nanoparticle uptake by endothelial cells., *Int. J. Pharm.* 233 (2002) 51–9.
- [389] S. Sundaram, S.K. Roy, B.K. Ambati, U.B. Kompella, Surface-functionalized nanoparticles for targeted gene delivery across nasal respiratory epithelium, *FASEB J.* 23 (2009) 3752–3765. doi:10.1096/fj.09-129825.
- [390] H.L. Wong, R. Bendayan, A.M. Rauth, H.Y. Xue, K. Babakhanian, X.Y. Wu, A Mechanistic Study of Enhanced Doxorubicin Uptake and Retention in Multidrug Resistant Breast Cancer Cells Using a Polymer-Lipid Hybrid Nanoparticle System, *J. Pharmacol. Exp. Ther.* 317 (2006) 1372–1381. doi:10.1124/jpet.106.101154.
- [391] C. Banning, J. Votteler, D. Hoffmann, H. Koppensteiner, M. Warmer, R. Reimer, F. Kirchhoff, U. Schubert, J. Hauber, M. Schindler, A Flow Cytometry-Based FRET Assay to Identify and Analyse Protein-Protein Interactions in Living Cells, *PLoS One.* 5 (2010) e9344. doi:10.1371/journal.pone.0009344.
- [392] S. Shubber, D. Vllasaliu, C. Rauch, F. Jordan, L. Illum, S. Stolnik, Mechanism of Mucosal Permeability Enhancement of CriticalSorb® (Solutol® HS15) Investigated In Vitro in Cell Cultures, *Pharm. Res.* 32 (2015) 516–527. doi:10.1007/s11095-014-1481-5.
- [393] K. Sonaje, E.-Y. Chuang, K.-J. Lin, T.-C. Yen, F.-Y. Su, M.T. Tseng, H.-W. Sung, Opening of Epithelial Tight Junctions and Enhancement of Paracellular Permeation by Chitosan: Microscopic, Ultrastructural, and Computed-Tomographic Observations, *Mol. Pharm.* 9 (2012) 1271–1279. doi:10.1021/mp200572t.
- [394] C.H. Pedemonte, Inhibition of Na(+)-pump expression by impairment of protein glycosylation is independent of the reduced sodium entry into the cell., *J. Membr. Biol.* 147 (1995) 223–31.
- [395] M. Haghi, P.M. Young, D. Traini, R. Jaiswal, J. Gong, M. Bebawy, Time- and passage-dependent characteristics of a Calu-3 respiratory epithelial cell model, *Drug Dev. Ind. Pharm.* 36 (2010) 1207–1214. doi:10.3109/03639041003695113.
- [396] A. Elder, S. Vidyasagar, L. DeLouise, Physicochemical factors that affect metal and metal oxide nanoparticle passage across epithelial barriers, *Wiley Interdiscip. Rev. Nanomedicine Nanobiotechnology.* 1 (2009) 434–450. doi:10.1002/wnan.44.

- [397] G. Bastiat, C.O. Pritz, C. Roider, F. Fouchet, E. Lignières, A. Jesacher, R. Glueckert, M. Ritsch-Martel, A. Schrott-Fischer, P. Saulnier, J.-P. Benoit, A new tool to ensure the fluorescent dye labeling stability of nanocarriers: A real challenge for fluorescence imaging, *J. Control. Release.* 170 (2013) 334–342. doi:10.1016/j.jconrel.2013.06.014.
- [398] R. Dinarvand, N. Sepehri, S. Manoochehri, H. Rouhani, F. Atyabi, Polylactide-co-glycolide nanoparticles for controlled delivery of anticancer agents., *Int. J. Nanomedicine.* 6 (2011) 877–95. doi:10.2147/IJN.S18905.
- [399] L. Vila, A. García-Rodríguez, C. Cortés, A. Velázquez, N. Xamena, A. Sampayo-Reyes, R. Marcos, A. Hernández, Effects of cerium oxide nanoparticles on differentiated/undifferentiated human intestinal Caco-2 cells, *Chem. Biol. Interact.* 283 (2018) 38–46. doi:10.1016/j.cbi.2018.01.018.
- [400] D. Vllasaliu, R. Fowler, M. Garnett, M. Eaton, S. Stolnik, Barrier characteristics of epithelial cultures modelling the airway and intestinal mucosa: A comparison, *Biochem. Biophys. Res. Commun.* 415 (2011) 579–585. doi:10.1016/j.bbrc.2011.10.108.
- [401] T. Tagami, Y. Ando, T. Ozeki, Fabrication of liposomal doxorubicin exhibiting ultrasensitivity against phospholipase A 2 for efficient pulmonary drug delivery to lung cancers, *Int. J. Pharm.* 517 (2017) 35–41. doi:10.1016/j.ijpharm.2016.11.039.
- [402] M. Murakami, I. Kudo, Phospholipase A2., *J. Biochem.* 131 (2002) 285–92. <http://www.ncbi.nlm.nih.gov/pubmed/11872155> (accessed May 12, 2018).
- [403] M. Wadsäter, J. Barauskas, F. Tiberg, T. Nylander, The lipolytic degradation of highly structured cubic micellar nanoparticles of soy phosphatidylcholine and glycerol dioleate by phospholipase A 2 and triacylglycerol lipase, *Chem. Phys. Lipids.* (2017). doi:10.1016/j.chemphyslip.2017.11.011.
- [404] E.A. Dennis, J. Cao, Y.-H. Hsu, V. Magrioti, G. Kokotos, Phospholipase A 2 Enzymes: Physical Structure, Biological Function, Disease Implication, Chemical Inhibition, and Therapeutic Intervention, *Chem. Rev.* 111 (2011) 6130–6185. doi:10.1021/cr200085w.
- [405] A. Glukhova, V. Hinkovska-Galcheva, R. Kelly, A. Abe, J.A. Shayman, J.J.G. Tesmer, Structure and function of lysosomal phospholipase A2 and lecithin:cholesterol acyltransferase, *Nat. Commun.* 6 (2015) 6250. doi:10.1038/ncomms7250.
- [406] B.P. Hurley, B.A. McCormick, Multiple roles of phospholipase A2 during lung infection and inflammation., *Infect. Immun.* 76 (2008) 2259–72. doi:10.1128/IAI.00059-08.
- [407] T. Zhao, X. Ding, H. Du, C. Yan, Lung Epithelial Cell-Specific Expression of Human Lysosomal Acid Lipase Ameliorates Lung Inflammation and Tumor Metastasis in *Lipa*(-/-) Mice., *Am. J. Pathol.* 186 (2016) 2183–2192. doi:10.1016/j.ajpath.2016.04.014.
- [408] K. Petrecca, M.-C. Guiot, V. Panet-Raymond, L. Souhami, Failure pattern

- following complete resection plus radiotherapy and temozolomide is at the resection margin in patients with glioblastoma, *J. Neurooncol.* 111 (2013) 19–23. doi:10.1007/s11060-012-0983-4.
- [409] T.T. Batchelor, D.A. Reardon, J.F. de Groot, W. Wick, M. Weller, Antiangiogenic therapy for glioblastoma: current status and future prospects., *Clin. Cancer Res.* 20 (2014) 5612–9. doi:10.1158/1078-0432.CCR-14-0834.
- [410] A. Desjardins, What is the optimal use of bevacizumab in glioblastoma?, *Nat. Rev. Neurol.* 11 (2015) 429–430. doi:10.1038/nrneurol.2015.127.
- [411] A. Petrelli, S. Giordano, From single- to multi-target drugs in cancer therapy: when aspecificity becomes an advantage., *Curr. Med. Chem.* 15 (2008) 422–32. <http://www.ncbi.nlm.nih.gov/pubmed/18288997> (accessed May 22, 2018).
- [412] J.R.D. Pearson, T. Regad, Targeting cellular pathways in glioblastoma multiforme, *Signal Transduct. Target. Ther.* 2 (2017) 17040. doi:10.1038/sigtrans.2017.40.
- [413] S. Agarwal, R. Sane, J.R. Ohlfest, W.F. Elmquist, The Role of the Breast Cancer Resistance Protein (ABCG2) in the Distribution of Sorafenib to the Brain, *J. Pharmacol. Exp. Ther.* 336 (2011) 223–233. doi:10.1124/jpet.110.175034.
- [414] M.S. Brose, C.M. Nutting, B. Jarzab, R. Elisei, S. Siena, L. Bastholt, C. de la Fouchardiere, F. Pacini, R. Paschke, Y.K. Shong, S.I. Sherman, J.W.A. Smit, J. Chung, C. Kappeler, C. Peña, I. Molnár, M.J. Schlumberger, DECISION investigators, Sorafenib in radioactive iodine-refractory, locally advanced or metastatic differentiated thyroid cancer: a randomised, double-blind, phase 3 trial, *Lancet.* 384 (2014) 319–328. doi:10.1016/S0140-6736(14)60421-9.
- [415] J. Aparicio-Blanco, A.-I. Torres-Suárez, Glioblastoma Multiforme and Lipid Nanocapsules: A Review., *J. Biomed. Nanotechnol.* 11 (2015) 1283–311. <http://www.ncbi.nlm.nih.gov/pubmed/26295134> (accessed February 8, 2018).
- [416] R.G. Thorne, C. Nicholson, In vivo diffusion analysis with quantum dots and dextrans predicts the width of brain extracellular space, *Proc. Natl. Acad. Sci.* 103 (2006) 5567–5572. doi:10.1073/pnas.0509425103.
- [417] Z.-B. Zhao, J. Long, Y.-Y. Zhao, J.-B. Yang, W. Jiang, Q.-Z. Liu, K. Yan, L. Li, Y.-C. Wang, Z.-X. Lian, Adaptive immune cells are necessary for the enhanced therapeutic effect of sorafenib-loaded nanoparticles, *Biomater. Sci.* 6 (2018) 893–900. doi:10.1039/C8BM00106E.
- [418] X. Sheng, T. Huang, J. Qin, Q. Li, W. Wang, L. Deng, A. Dong, Preparation, pharmacokinetics, tissue distribution and antitumor effect of sorafenib-incorporating nanoparticles in vivo, *Oncol. Lett.* 14 (2017) 6163–6169. doi:10.3892/ol.2017.6934.
- [419] M. Cervello, G. Pitarresi, A.B. Volpe, B. Porsio, D. Balasus, M.R. Emma, A. Azzolina, R. Puleio, G.R. Loria, S. Puleo, G. Giammona, Nanoparticles of a polyaspartamide-based brush copolymer for modified release of sorafenib: In vitro and in vivo evaluation, *J. Control. Release.* 266 (2017) 47–56. doi:10.1016/j.jconrel.2017.09.014.

- [420] R.M. Iacobazzi, L. Porcelli, A.A. Lopodota, V. Laquintana, A. Lopalco, A. Cutrignelli, E. Altamura, R. Di Fonte, A. Azzariti, M. Franco, N. Denora, Targeting human liver cancer cells with lactobionic acid-G(4)-PAMAM-FITC sorafenib loaded dendrimers, *Int. J. Pharm.* 528 (2017) 485–497. doi:10.1016/j.ijpharm.2017.06.049.
- [421] S. Sortino, D. Pellosi, F. Moret, A. Fraix, N. Marino, S. Maiolino, E. Gaio, N. Hioka, E. Reddi, F. Quaglia, Pluronic® P123/F127 mixed micelles delivering sorafenib and its combination with verteporfin in cancer cells, *Int. J. Nanomedicine*. Volume 11 (2016) 4479–4494. doi:10.2147/IJN.S103344.
- [422] M.T. Krauze, C.O. Noble, T. Kawaguchi, D. Drummond, D.B. Kirpotin, Y. Yamashita, E. Kullberg, J. Forsayeth, J.W. Park, K.S. Bankiewicz, Convection-enhanced delivery of nanoliposomal CPT-11 (irinotecan) and PEGylated liposomal doxorubicin (Doxil) in rodent intracranial brain tumor xenografts, *Neuro. Oncol.* 9 (2007) 393–403. doi:10.1215/15228517-2007-019.
- [423] T. Inoue, Y. Yamashita, M. Nishihara, S. Sugiyama, Y. Sonoda, T. Kumabe, M. Yokoyama, T. Tominaga, Therapeutic efficacy of a polymeric micellar doxorubicin infused by convection-enhanced delivery against intracranial 9L brain tumor models, *Neuro. Oncol.* 11 (2009) 151–157. doi:10.1215/15228517-2008-068.
- [424] C. Chevreau, A. Le Cesne, I. Ray-Coquard, A. Italiano, A. Cioffi, N. Isambert, Y.M. Robin, C. Fournier, S. Clisant, L. Chaigneau, J.-O. Bay, E. Bompas, E. Gauthier, J.Y. Blay, N. Penel, Sorafenib in patients with progressive epithelioid hemangioendothelioma, *Cancer*. 119 (2013) 2639–2644. doi:10.1002/cncr.28109.
- [425] W.M. Pardridge, The Blood-Brain Barrier: Bottleneck in Brain Drug Development, in: *NeuroRx*, 2005: pp. 3–14.
- [426] W.M. Pardridge, Blood–brain barrier delivery, *Drug Discov. Today*. 12 (2007) 54–61. doi:10.1016/j.drudis.2006.10.013.
- [427] C. Zhan, W. Lu, The Blood-Brain/Tumor Barriers: Challenges and Chances for Malignant Gliomas Targeted Drug Delivery, *Curr. Pharm. Biotechnol.* 13 (2012) 2380–2387. doi:10.2174/138920112803341798.
- [428] I. Brigger, J. Morizet, L. Laudani, G. Aubert, M. Appel, V. Velasco, M.-J. Terrier-Lacombe, D. Desmaële, J. d’Angelo, P. Couvreur, G. Vassal, Negative preclinical results with stealth® nanospheres-encapsulated Doxorubicin in an orthotopic murine brain tumor model, *J. Control. Release*. 100 (2004) 29–40. doi:10.1016/J.JCONREL.2004.07.019.
- [429] U.S. Sharma, A. Sharma, R.I. Chau, R.M. Straubinger, Liposome-mediated therapy of intracranial brain tumors in a rat model., *Pharm. Res.* 14 (1997) 992–8. <http://www.ncbi.nlm.nih.gov/pubmed/9279878> (accessed July 11, 2018).
- [430] C.-H. Heldin, K. Rubin, K. Pietras, A. Ostman, High interstitial fluid pressure - an obstacle in cancer therapy., *Nat. Rev. Cancer*. 4 (2004) 806–13. doi:10.1038/nrc1456.

- [431] S. Joshi, P.M. Meyers, E. Ornstein, Intracarotid delivery of drugs: the potential and the pitfalls., *Anesthesiology*. 109 (2008) 543–64. doi:10.1097/ALN.0b013e318182c81b.
- [432] M.M. Eissa, R.M. El-Moslemany, A.A. Ramadan, E.I. Amer, M.Z. El-Azzouni, L.K. El-Khordagui, Miltefosine Lipid Nanocapsules for Single Dose Oral Treatment of Schistosomiasis Mansonii: A Preclinical Study, *PLoS One*. 10 (2015) e0141788. doi:10.1371/journal.pone.0141788.
- [433] E. Roger, F. Lagarce, J.-P. Benoit, The gastrointestinal stability of lipid nanocapsules, *Int. J. Pharm.* 379 (2009) 260–265. doi:10.1016/j.ijpharm.2009.05.069.
- [434] S. Grassin-Delyle, A. Buenestado, E. Naline, C. Faisy, S. Blouquit-Laye, L.-J. Couderc, M. Le Guen, M. Fischler, P. Devillier, Intranasal drug delivery: An efficient and non-invasive route for systemic administration, *Pharmacol. Ther.* 134 (2012) 366–379. doi:10.1016/j.pharmthera.2012.03.003.
- [435] A.R. Khan, M. Liu, M.W. Khan, G. Zhai, Progress in brain targeting drug delivery system by nasal route, *J. Control. Release*. 268 (2017) 364–389. doi:10.1016/J.JCONREL.2017.09.001.
- [436] M. Matsuho, R. Kubota, S. Asayama, H. Kawakami, Lactoferrin-modified nanoparticles loaded with potent antioxidant Mn-porphyrins exhibit enhanced antioxidative activity in vitro intranasal brain delivery model, *J. Mater. Chem. B*. 5 (2017) 1765–1771. doi:10.1039/C6TB02599D.
- [437] L. Chen, J. Zhu, Y. Li, J. Lu, L. Gao, H. Xu, M. Fan, X. Yang, Enhanced Nasal Mucosal Delivery and Immunogenicity of Anti-Caries DNA Vaccine through Incorporation of Anionic Liposomes in Chitosan/DNA Complexes, *PLoS One*. 8 (2013) e71953. doi:10.1371/journal.pone.0071953.
- [438] R. Fowler, D. Vllasaliu, F.H. Falcone, M. Garnett, B. Smith, H. Horsley, C. Alexander, S. Stolnik, Uptake and transport of B12-conjugated nanoparticles in airway epithelium, *J. Control. Release*. 172 (2013) 374–381. doi:10.1016/j.jconrel.2013.08.028.
- [439] B. Srinivasan, A.R. Kolli, M.B. Esch, H.E. Abaci, M.L. Shuler, J.J. Hickman, TEER measurement techniques for in vitro barrier model systems., *J. Lab. Autom.* 20 (2015) 107–26. doi:10.1177/2211068214561025.
- [440] D.M. Charron, G. Zheng, Nanomedicine development guided by FRET imaging, *Nano Today*. 18 (2018) 124–136. doi:10.1016/J.NANTOD.2017.12.006.
- [441] H. Sahoo, P. Schwille, FRET and FCS-Friends or Foes?, *ChemPhysChem*. 12 (2011) 532–541. doi:10.1002/cphc.201000776.
- [442] A. Mistry, S.Z. Glud, J. Kjems, J. Randel, K.A. Howard, S. Stolnik, L. Illum, Effect of physicochemical properties on intranasal nanoparticle transit into murine olfactory epithelium., *J. Drug Target.* 17 (2009) 543–52. doi:10.1080/10611860903055470.
- [443] A. Mistry, S. Stolnik, L. Illum, Nose-to-Brain Delivery: Investigation of the

- Transport of Nanoparticles with Different Surface Characteristics and Sizes in Excised Porcine Olfactory Epithelium, *Mol. Pharm.* 12 (2015) 2755–2766. doi:10.1021/acs.molpharmaceut.5b00088.
- [444] A. Mangraviti, S.Y. Tzeng, D. Gullotti, K.L. Kozielski, J.E. Kim, M. Seng, S. Abbadi, P. Schiapparelli, R. Sarabia-Estrada, A. Vescovi, H. Brem, A. Olivi, B. Tyler, J.J. Green, A. Quinones-Hinojosa, Non-virally engineered human adipose mesenchymal stem cells produce BMP4, target brain tumors, and extend survival, *Biomaterials.* 100 (2016) 53–66. doi:10.1016/j.biomaterials.2016.05.025.
- [445] I. V Balyasnikova, M.S. Prasol, S.D. Ferguson, Y. Han, A.U. Ahmed, M. Gutova, A.L. Tobias, D. Mustafi, E. Rincón, L. Zhang, K.S. Aboody, M.S. Lesniak, Intranasal Delivery of Mesenchymal Stem Cells Significantly Extends Survival of Irradiated Mice with Experimental Brain Tumors, *Mol. Ther.* 22 (2014) 140–148. doi:10.1038/mt.2013.199.
- [446] S. Pacioni, Q.G. D'Alessandris, S. Giannetti, L. Morgante, V. Coccè, A. Bonomi, M. Buccarelli, L. Pascucci, G. Alessandri, A. Pessina, L. Ricci-Vitiani, M.L. Falchetti, R. Pallini, Human mesenchymal stromal cells inhibit tumor growth in orthotopic glioblastoma xenografts, *Stem Cell Res. Ther.* 8 (2017) 53. doi:10.1186/s13287-017-0516-3.
- [447] S.R. Baglio, D.M. Pegtel, N. Baldini, Mesenchymal stem cell secreted vesicles provide novel opportunities in (stem) cell-free therapy., *Front. Physiol.* 3 (2012) 359. doi:10.3389/fphys.2012.00359.
- [448] L. Li, Y. Guan, H. Liu, N. Hao, T. Liu, X. Meng, C. Fu, Y. Li, Q. Qu, Y. Zhang, S. Ji, L. Chen, D. Chen, F. Tang, Silica Nanorattle–Doxorubicin–Anchored Mesenchymal Stem Cells for Tumor-Tropic Therapy, *ACS Nano.* 5 (2011) 7462–7470. doi:10.1021/nn202399w.
- [449] S. Pacioni, Q.G. D'Alessandris, S. Giannetti, L. Morgante, I. De Pascalis, V. Coccè, A. Bonomi, L. Pascucci, G. Alessandri, A. Pessina, M.L. Falchetti, R. Pallini, Mesenchymal stromal cells loaded with paclitaxel induce cytotoxic damage in glioblastoma brain xenografts, *Stem Cell Res. Ther.* 6 (2015) 194. doi:10.1186/s13287-015-0185-z.
- [450] X. Zhang, S. Yao, C. Liu, Y. Jiang, Tumor tropic delivery of doxorubicin-polymer conjugates using mesenchymal stem cells for glioma therapy, *Biomaterials.* 39 (2015) 269–281. doi:10.1016/j.biomaterials.2014.11.003.
- [451] A. Pessina, A. Bonomi, V. Coccè, G. Invernici, S. Navone, L. Cavicchini, F. Sisto, M. Ferrari, L. Viganò, A. Locatelli, E. Ciusani, G. Cappelletti, D. Cartelli, C. Arnaldo, E. Parati, G. Marfia, R. Pallini, M.L. Falchetti, G. Alessandri, Mesenchymal Stromal Cells Primed with Paclitaxel Provide a New Approach for Cancer Therapy, *PLoS One.* 6 (2011) e28321. doi:10.1371/journal.pone.0028321.
- [452] L. Danielyan, R. Schäfer, A. von Ameln-Mayerhofer, M. Buadze, J. Geisler, T. Klopfer, U. Burkhardt, B. Proksch, S. Verleysdonk, M. Ayturan, G.H. Buniatian, C.H. Gleiter, W.H. Frey, Intranasal delivery of cells to the brain, *Eur. J. Cell Biol.* 88 (2009) 315–324. doi:10.1016/j.ejcb.2009.02.001.

- [453] A. Clavreul, M. Pourbaghi-Masouleh, E. Roger, N. Lautram, C.N. Montero-Menei, P. Menei, Human mesenchymal stromal cells as cellular drug-delivery vectors for glioblastoma therapy: A good deal?, *J. Exp. Clin. Cancer Res.* 36 (2017). doi:10.1186/s13046-017-0605-2.
- [454] L.S. Sherman, M. Shaker, V. Mariotti, P. Rameshwar, Mesenchymal stromal/stem cells in drug therapy: New perspective, *Cytotherapy.* 19 (2017) 19–27. doi:10.1016/j.jcyt.2016.09.007.
- [455] S.M. Ridge, F.J. Sullivan, S.A. Glynn, Mesenchymal stem cells: key players in cancer progression, *Mol. Cancer.* 16 (2017) 31. doi:10.1186/s12943-017-0597-8.
- [456] C. Zhang, S.-J. Yang, Q. Wen, J.F. Zhong, X.-L. Chen, A. Stucky, M.F. Press, X. Zhang, Human-derived normal mesenchymal stem/stromal cells in anticancer therapies., *J. Cancer.* 8 (2017) 85–96. doi:10.7150/jca.16792.
- [457] Y. Shi, L. Du, L. Lin, Y. Wang, Tumour-associated mesenchymal stem/stromal cells: emerging therapeutic targets, *Nat. Rev. Drug Discov.* 16 (2017) 35–52. doi:10.1038/nrd.2016.193.
- [458] A. Bronckaers, P. Hilkens, W. Martens, P. Gervois, J. Ratajczak, T. Struys, I. Lambrichts, Mesenchymal stem/stromal cells as a pharmacological and therapeutic approach to accelerate angiogenesis, *Pharmacol. Ther.* 143 (2014) 181–196. doi:10.1016/j.pharmthera.2014.02.013.
- [459] C. Merino-González, F.A. Zuñiga, C. Escudero, V. Ormazabal, C. Reyes, E. Nova-Lamperti, C. Salomón, C. Aguayo, Mesenchymal Stem Cell-Derived Extracellular Vesicles Promote Angiogenesis: Potencial Clinical Application., *Front. Physiol.* 7 (2016) 24. doi:10.3389/fphys.2016.00024.

Annexes

Annex 1: Publications and communications

Publication (from thesis):

1. M. Pourbaghi Masouleh, C. Conte, C. Bosquillon, P. Menei, S. Stolnik. Lipid nanocapsules transport across Calu-3 based model of nasal epithelial barrier (going to be submitted)
2. A. Clavreul, M. Pourbaghi-Masouleh, P. Menei, *Targeting angiogenesis in glioblastoma with non-viral delivery systems: Where are we?* (going to be submitted)
3. A. Clavreul, E. Roger, M. Pourbaghi Masouleh, L. Lemaire, C. Tétaud, and P. Menei. Development and characterization of sorafenib-loaded lipid nanocapsules for the treatment of glioblastoma. *Drug Delivery*, 25(1), 2018, 1756–1765.
4. A. Clavreul, M. Pourbaghi-Masouleh, E. Roger, N. Lautram, C.N. Montero-Menei, P. Menei, *Human mesenchymal stromal cells as cellular drug-delivery vectors for glioblastoma therapy: A good deal?*, *J. Exp. Clin. Cancer Res.* 36 (2017).

Communication (from thesis):

1. M. P. Masouleh, C. Conte, C. Bosquillon, S. Stolnik. *Lipid Nanocapsule Transport Across Epithelial Barrier: a Förster Resonance Energy Transfer Based Study*, *Innovation for Health*, Rotterdam, NL, 2018. (Oral and Poster)
2. M. P. Masouleh, C. Bosquillon, S. Stolnik. *Lipid nanocapsules transport across Calu-3 cell in vitro model of epithelium*. *Nanofar spring school*, University of Nottingham, Nottingham, UK, 2017. (Poster)
3. M. P. Masouleh, A. Clavreul, E. Roger, P. Menei. *Which types of anti-cancer molecules mesenchymal stem cells can carry to brain tumors?*, Les écoles doctorales (ED) et le Collège doctoral Nantes Atlantique, Université de Nantes, Nantes, France, 2015. (Oral and Poster)
4. M. P. Masouleh, A. Clavreul, E. Roger, P. Menei. *Which types of anti-cancer molecules mesenchymal stem cells can carry to brain tumors?*, *Nanofar autumn school*, Université de Nantes, Nantes, France, 2015. (Poster)
5. M. P. Masouleh, A. Clavreul, E. Roger, C. Bosquillon, S. Stolnik, P. Menei. *Mesenchymal stem cells as cellular vehicles for delivery of drug-loaded nanoparticles to brain tumors via the nasal route*. *Nanofar autumn school*, The Université catholique de Louvain, Brussels, Belgium, 2014. (Oral)

Annex 2: Published article in Journal of Experimental & Clinical Cancer Research

Human mesenchymal stromal cells as cellular drug-delivery vectors for glioblastoma therapy: A good deal?

Contribution: The samples preparation for HPLC and LC-MS/MS, and their characterizations and analyses are done by Milad Pourbaghi Masouleh.

RESEARCH

Open Access



Human mesenchymal stromal cells as cellular drug-delivery vectors for glioblastoma therapy: a good deal?

Anne Clavreul^{1,2*}, Milad Pourbaghi-Masouleh^{2,3}, Emilie Roger⁴, Nolwenn Lautram⁴, Claudia N. Montero-Menei² and Philippe Menei^{1,2}

Abstract

Background: Glioblastoma (GB) is the most malignant brain tumor in adults. It is characterized by angiogenesis and a high proliferative and invasive capacity. Standard therapy (surgery, radiotherapy and chemotherapy with temozolomide) is of limited efficacy. Innovative anticancer drugs targeting both tumor cells and angiogenesis are urgently required, together with effective systems for their delivery to the brain. We assessed the ability of human mesenchymal stromal cells (MSCs) to uptake the multikinase inhibitor, sorafenib (SFN), and to carry this drug to a brain tumor following intranasal administration.

Method: MSCs were primed with SFN and drug content and release were quantified by analytical chemistry techniques. The ability of SFN-primed MSCs to inhibit the survival of the human U87MG GB cell line and endothelial cells was assessed in *in vitro* assays. These cells were then administered intranasally to nude mice bearing intracerebral U87MG xenografts. Their effect on tumor growth and angiogenesis was evaluated by magnetic resonance imaging and immunofluorescence analyses, and was compared with the intranasal administration of unprimed MSCs or SFN alone.

Results: MSCs took up about 9 pg SFN per cell, with no effect on viability, and were able to release 60% of the primed drug. The cytostatic activity of the released SFN was entirely conserved, resulting in a significant inhibition of U87MG and endothelial cell survival *in vitro*. Two intranasal administrations of SFN-primed MSCs in U87MG-bearing mice resulted in lower levels of tumor angiogenesis than the injection of unprimed MSCs or SFN alone, but had no effect on tumor volume. We also observed an increase in the proportion of small intratumoral vessels in animals treated with unprimed MSCs; this effect being abolished if the MSCs were primed with SFN.

Conclusion: We show the potential of MSCs to carry SFN to brain tumors following an intranasal administration. However, the therapeutic effect is modest probably due to the pro-tumorigenic properties of MSCs, which may limit the action of the released SFN. This calls into question the suitability of MSCs for use in GB therapy and renders it necessary to find methods guaranteeing the safety of this cellular vector after drug delivery.

Keywords: Drug delivery, Glioblastoma, Mesenchymal stromal cells, Targeting, Sorafenib

* Correspondence: anne.clavreul@univ-angers.fr

¹Département de Neurochirurgie, CHU, Angers, France

²CRCINA, INSERM, Université de Nantes, Université d'Angers, Angers, France

Full list of author information is available at the end of the article



© The Author(s). 2017 **Open Access** This article is distributed under the terms of the Creative Commons Attribution 4.0 International License (<http://creativecommons.org/licenses/by/4.0/>), which permits unrestricted use, distribution, and reproduction in any medium, provided you give appropriate credit to the original author(s) and the source, provide a link to the Creative Commons license, and indicate if changes were made. The Creative Commons Public Domain Dedication waiver (<http://creativecommons.org/publicdomain/zero/1.0/>) applies to the data made available in this article, unless otherwise stated.

Background

Glioblastoma (GB) is the most common, invasive and aggressive primary brain tumor in humans. Over the last 12 years or so, most patients with GB have been treated with the Stupp protocol [1], consisting of surgical resection followed by radiotherapy with concomitant and adjuvant temozolomide (TMZ) chemotherapy. The efficacy of this treatment is limited, with median overall survival of no more than 15 months [2]. GB treatment is complicated by the high resistance of these tumors to standard chemotherapy agents, the critical role of angiogenesis in their growth and spread and the blood-brain barrier (BBB), which serves as a physiological obstacle to the delivery of drugs to the central nervous system. The development of innovative anticancer drugs targeting both tumor cells and blood vessels is therefore urgently required, together with effective systems for delivering these drugs to the brain.

In recent years, targeted molecular therapies based on the use of inhibitors of several pathways involved in the oncogenic process in GB have emerged [3–5]. Sorafenib (SFN) (Nexavar) is one such inhibitor. It is an oral multikinase inhibitor that targets both cell surface kinase receptors (VEGFR and PDGFR) and downstream intracellular serine/threonine kinases [6] resulting in diverse cellular effects, such as induction of tumor cell apoptosis and autophagy, and reduction of angiogenesis [7–9]. SFN showed efficacy against different solid tumors and is already approved for the treatment of advanced hepatocellular carcinoma, renal cell carcinoma, and thyroid cancer [6]. In clinical studies in patients with progressive or recurrent GB, oral administration of SFN has been shown to be of very limited efficacy as a monotherapy or in combination with TMZ or other targeted drugs, such as erlotinib [10–16]. This lack of efficacy is not restricted to SFN; other drugs fell short of expectations because they penetrated the brain only inefficiently via the BBB or were unable to target tumor cells. Various approaches have been developed to overcome these limitations, including the use of mesenchymal stromal cells (MSCs), which can cross the BBB and display brain tumor tropism after systemic and local administration [17–21]. This property has generated considerable interest in the use of MSCs as treatment vectors for GB [22–25].

MSCs have been genetically modified to overexpress several antitumor factors, such as interleukins, interferons, pro-drugs, oncolytic viruses, anti-angiogenic agents, pro-apoptotic proteins, and growth factor antagonists [26, 27]. Despite promising results in animal models, the genetic manipulation of MSCs for clinical application is not risk-free [28]. We and others have shown that MSCs can deliver chemotherapy drugs to brain tumors without genetic modification [29–33]. For example, we have shown that MSCs can deliver lipid nanocapsules containing an organometallic

complex (ferrociphenol) in the heterotopic and orthotopic U87MG GB models [29, 31]. MSCs were also able to take up and release paclitaxel and to induce cytotoxic damage in GB xenografts [32, 34]. A major concern to use these therapeutic cells is the delivery method. The surgical injection of MSCs directly into the brain is the most frequently used method of delivery. However, this method is invasive making a repeated treatment option difficult. In a clinical context, systemic administration of this therapeutic tool would be simpler, less costly and would allow for a chronic treatment. Intravascular applications of MSCs could be an option but major obstacles are the entrapment and elimination of cells in peripheral organs and the risk of vascular and pulmonary embolization [35, 36]. Intranasal administration of MSCs appears to be a promising noninvasive and safe alternative delivery method to surgical injection or to intravascular administration [37]. Intranasally administered MSCs were able to enter the brain in experimental glioma models [19] as well as in mouse models of Alzheimer's and Parkinson's disease [38] and neonate ischemic brain damage models [39].

In this study, we evaluated the ability of MSCs to take up SFN and target it to the tumor in the orthotopic U87MG GB model, following intranasal administration. We paid particular interest to the effects of SFN-primed MSCs on tumor growth and angiogenesis, through comparisons with the intranasal administration of unprimed MSCs or SFN alone.

Methods

Cell culture and reagents

MSCs were obtained from iliac crest aspirates from a human male post-mortem organ donor (protocol agreed by the French Agency of Biomedicine), and were isolated as previously described [17, 40]. This cell population was expanded by culture in StemMACS™ MSC Expansion Media Kit XF (Miltenyi Biotec, Paris, France) in a humidified incubator at 37 °C, under an atmosphere containing 5% CO₂, until 70% confluence. All experiments were performed with cells between passages 4 and 5.

The human U87MG GB cell line was obtained from the ATCC (LGC Promochem, Molsheim, France). Cells were maintained in Dulbecco's modified eagle medium-high glucose medium (DMEM-HG, Lonza, Verviers, Belgium) containing 10% fetal bovine serum (FBS) (Fisher Scientific, Illkirch, France) and 1% antibiotics (Sigma-Aldrich, St. Quentin Fallavier, France), under an atmosphere containing 5% CO₂ (37 °C), in a humidified incubator, until they reached 80% confluence.

Human umbilical vein endothelial cells (HUVECs) were purchased from Lonza. Cells were cultured according to the supplier's instructions, in endothelial cell growth medium-2 (EGM-2) in a humidified chamber at 37 °C, under an atmosphere containing 5% CO₂.

SFN was purchased from LC Laboratories (Woburn, USA). The stock solution was prepared in DMSO (Sigma-Aldrich), at a concentration of 100 mM. Aliquots were stored at -20°C .

Sensitivity of HUVECs, U87MG and MSCs to SFN

HUVECs and U87MG cells were plated in 96-well plates at densities of 5×10^3 cells/cm² and MSCs were plated at a density of 1×10^4 cells/cm². After 48 h, the culture medium was removed and cells were treated with SFN at concentrations of 0.001 to 100 μM . Four days later, the medium was removed from the wells and the plates were stored at -80°C until their use for assays. Cell survival was estimated with the CyQUANT[®] cell proliferation assay kit, according to the manufacturer's instructions (Fisher Scientific).

Priming of MSCs with SFN

MSCs (4×10^5 cells) were incubated for 1 h at 37°C with 1 mL SFN (20 or 100 μM) in Hank's balanced salt solution (HBSS), with Ca^{2+} and Mg^{2+} (Lonza). At the end of the incubation period, cells were washed twice with HBSS, counted, and used for in vitro and in vivo experiments, as described below.

In vitro characterization of SFN-primed MSCs

SFN content of SFN-primed MSCs

The SFN content of MSCs was measured by high performance liquid chromatography (HPLC) method. SFN-primed MSCs (4×10^5 cells) were suspended in 50 μL H₂O. We then successively added 50 μL tetrahydrofuran and 200 μL methanol. A filtration was performed using a Millex-LG 0.2 μm filter (Millipore, Guyancourt, France) and 10 μL was injected onto the HPLC system. Chromatography was performed with the Waters modular system (600/717/996/2414) (Waters, Saint-Quentin-en-Yvelines, France) on a SunFire[®] C18 column (150 \times 4.6 mm; 5 μm) at 37°C . SFN was eluted with an isocratic mobile phase (acetonitrile/methanol/1% acetic acid, at a ratio of 35:38:27) at a flow rate of 1 mL/min, with monitoring at 266 nm. The chromatograms were recorded and integrated with Empower 3 software (Waters). The range of linear response was 0.5–32 $\mu\text{g}/\text{mL}$.

Viability of SFN-primed MSCs

SFN-primed MSCs were used to seed 96-well plates, and cell survival was estimated one and seven days later, with the CyQUANT[®] cell proliferation assay kit, as described above.

Release of SFN from SFN-primed MSCs

SFN-primed MSCs (3×10^5) were used to seed Transwell[®] inserts with a pore size of 0.4 μm (Millipore) in DMEM-HG supplemented with 10% FBS and 1% antibiotics. We monitored SFN release at different time points, by collecting the

cell-conditioned medium (CM) from the lower compartment at 4, 24, 48, 72 and 96 h. Quantification of SFN in the CM was determined by liquid chromatography tandem-mass spectrometry (LC-MS/MS).

Chromatography was performed with the Waters Alliance[®] 2695 system, with an Uptisphere[®] 5 ODB C18 column (150 \times 2.0 mm) (Interchim, Montluçon, France). The mobile phase consisted of an isocratic mixture of 0.1% formic acid in water/0.1% formic acid in acetonitrile: 20/80 (v/v). The column temperature was set at 25°C and the flow rate was 0.3 mL/min, with a total run time of 10 min. The total HPLC effluent was analyzed in a Quattro[®] Micro triple quadrupole mass spectrometer (Waters). Ionization was achieved by the electrospray method, in positive-ion mode. The mass spectrometer was operated in multiple reaction monitoring (MRM) mode. The (M – H) + m/z transition for SFN was 465 \rightarrow 270. A typical retention time for SFN was 2.3 min. Quantification was achieved with QuantLynx[®] (Waters), by comparing the observed peak area ratios of SFN samples with a calibration curve obtained under the same experimental conditions. The range of the linear response was large, extending from 50 to 1000 ng/mL.

Toxicity of SFN-primed MSCs to U87MG cells and HUVECs

We assessed the in vitro toxicity of SFN-primed MSCs to U87MG cells and HUVECs, by performing coculture experiments in Transwell[®] plates, with inserts with a pore size of 0.4 μm (Millipore). HUVECs and U87MG cells (6×10^3 cells/well) were placed in the lower compartment. After 48 h, we added SFN, or unprimed or SFN-primed MSCs to the upper compartment. Three days later, the inserts were removed and a CyQUANT[®] cell proliferation assay was performed.

In vivo effect of SFN-primed MSCs

U87MG GB model

Female Swiss nude mice (8–10 weeks old) were obtained from Charles River Laboratories (L'Arbresle, France). The protocol was approved by the Committee on the Ethics of Animal Experiments of the "Pays de la Loire" (Permit no. 01785.01). Animals were anesthetized by an intraperitoneal injection of xylazine (13 mg/kg body weight) and ketamine (100 mg/kg body weight) and were positioned in a Kopf stereotaxic instrument. On day 0 (D0), U87MG cells (3×10^4) in 5 μL HBSS with Ca^{2+} and Mg^{2+} were injected into the striatum of mice [coordinates: 2.1 mm lateral to the bregma, 0.5 mm anterior and 3 mm interior to the outer border of the cranium].

Analysis of the distribution of MSCs in the U87MG tumor after their intranasal administration

Intranasal delivery was performed as previously described [19], but with minor modifications. Thirty minutes before

cell administration, anesthetized U87MG tumor-bearing mice (D12) were placed in a supine position and the nasal cavity of each animal was treated with total of 100 U hyaluronidase (Sigma-Aldrich) in the form of four repeated inoculations at two-minute intervals (3 μ L per nostril). We then applied either HBSS with Ca^{2+} and Mg^{2+} , or 6×10^5 MSCs in the same conditions. For analysis of the distribution of MSCs in the U87MG tumor, the animals were killed three or seven days later (D15 and D19, respectively). Brains were snap-frozen in isopentane cooled with liquid nitrogen and stored at -80°C . Coronal sections of the brain were cut at 10 μm intervals and collected on silane-treated slides. MSCs in tumor cryosections were detected by fluorescence in situ hybridization (FISH), with a human Y-chromosome probe, as previously described [34]. The DNA probe was complementary to the highly repetitive human satellite III sequences located close to the centromeric region of the human Y-chromosome DYZ1 locus (CEPY) and was labeled with the SpectrumOrange fluorochrome (Vysis, Abbott Molecular, Rungis, France).

Cryosections of four mice killed at day 15 or day 19 were analyzed under a fluorescence microscope (Axioscope[®] 2 light microscope, Zeiss, Le Pecq, Germany). Y^+ MSCs were counted on nine cryosections per mouse corresponding to the central and peripheral portions of the tumor, with the MetaView computerized image-analysis system (Roper Scientific, Evry, France). About five fields per cryosection, at a magnification of $\times 200$, were randomly selected for each tumor.

Analysis of the effect of SFN-primed MSCs in the orthotopic U87MG GB model

U87MG tumor-bearing mice (D6) were assigned to four groups receiving intranasal injections according to the protocol described above: (a) HBSS with Ca^{2+} and Mg^{2+} ; (b) SFN; (c) unprimed MSCs; (d) SFN-primed MSCs. These injections were repeated on day 10. Seven days later, we measured tumor volume by magnetic resonance imaging (MRI), as previously described [31], and the mice were killed for the analysis of Ki67^+ cells or CD31^+ vessels in the U87MG tumor. The presence of intratumoral Y^+ MSCs in all U87MG tumor-bearing mice treated with unprimed or SFN-primed MSCs was checked by FISH. For CD31 and Ki67 expression analysis, brain cryosections were allowed to dry in air, rehydrated in PBS and fixed by incubation for 10 min in 4% PFA pH 7.4 at 4°C . Nonspecific binding was blocked by incubating the sections in 4% BSA and 10% normal goat serum in PBS. The sections were incubated overnight, at 4°C , with isotype controls and primary antibodies against endothelial cells (mouse CD31 , BD Biosciences, Le Pont de Claix, France) and proliferative cells (Ki67 , Agilent Technologies, Les Ulis, France). The primary antibodies were detected with biotinylated

secondary antibodies and the signal was amplified with streptavidin-FITC (Interchim). Nuclei were counterstained with DAPI (Sigma). Cryosections of four mice from each of the groups described above (a, b, c and d) were analyzed under an Axioscope[®] 2 fluorescence microscope. CD31^+ and Ki67^+ cells were counted with the MetaView computerized image-analysis system in six brain cryosections per mouse corresponding to the central and peripheral portions of the tumor. Five fields per cryosection, at $\times 200$ magnification, were randomly selected for each tumor.

Statistical analysis

Results are expressed as means \pm SEM. The Kruskal–Wallis test was used for statistical analyses. Differences were considered significant if the p -value was < 0.05 .

Results

Effect of SFN on the survival of U87MG cells, HUVECs and MSCs

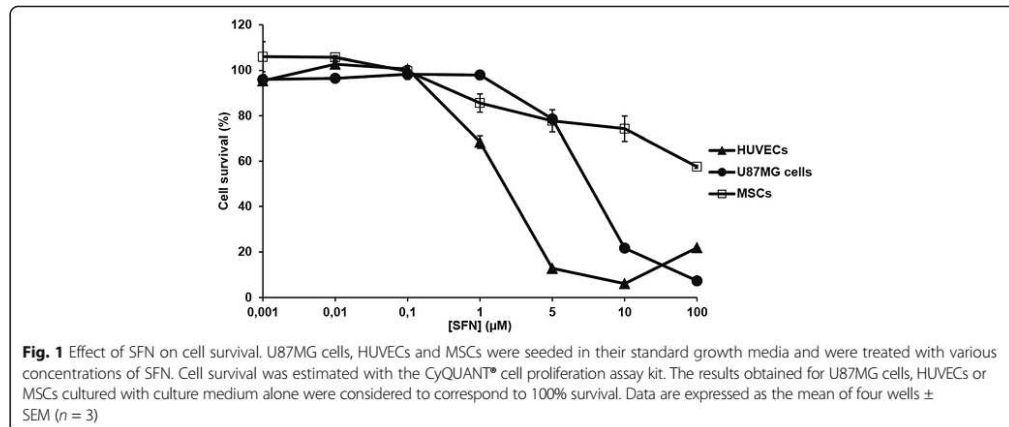
Both U87MG cells and HUVECs displayed dose-dependent survival inhibition when treated for 4 days with SFN (Fig. 1). SFN decreased cell viability with an IC_{50} of $7.39 \pm 0.16 \mu\text{M}$ for U87MG cells and $1.91 \pm 0.19 \mu\text{M}$ for HUVECs. MSCs displayed relative resistance to SFN treatment (about 40% cell death at $100 \mu\text{M}$).

SFN content of SFN-primed MSCs and control of their viability

We defined the dose of SFN that MSCs could carry without deleterious effects on their viability. For this purpose, MSCs (4×10^5) were incubated for 1 h at 37°C with $20 \mu\text{M}$ ($9.2 \mu\text{g/mL}$) or $100 \mu\text{M}$ ($46 \mu\text{g/mL}$). MSCs primed with $20 \mu\text{M}$ and $100 \mu\text{M}$ were carrying 8.8 ± 0.5 and $52.7 \pm 5.0 \text{ pg}$ SFN per cell, respectively (Fig. 2a). The incubation of MSCs with $100 \mu\text{M}$ SFN resulted in a 40% loss of cell viability 1 day after uptake, whereas 80% of MSCs remained viable when incubated with $20 \mu\text{M}$ SFN (Fig. 2b). Seven days after priming, no additional loss of viability was observed in either set of conditions and SFN-primed MSCs retained their capacity to proliferate (data not shown). Given the lower cell viability observed following the incubation of MSCs with $100 \mu\text{M}$ SFN, we decided to prime MSCs with $20 \mu\text{M}$ SFN.

Quantification and toxicity of the SFN released by SFN-primed MSCs

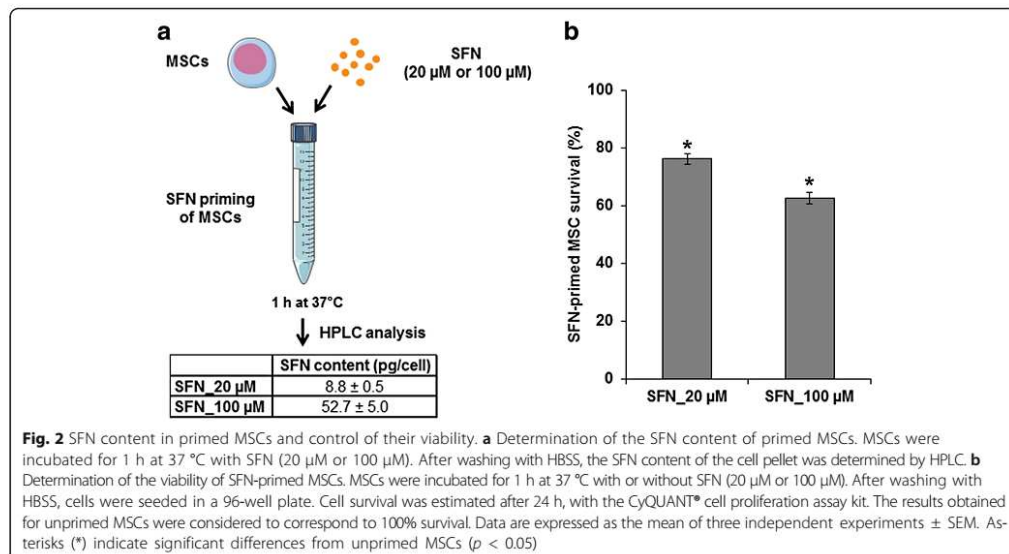
We evaluated the release of SFN over time, by collecting the CM from SFN-primed MSCs 4, 24, 48, 72 and 96 h after priming with SFN ($20 \mu\text{M}$) and analyzing it by LC-MS/MS. We found that about 20% of the SFN was released from SFN-primed MSCs in 4 h, and that 60% of the drug was released in 48 h (Fig. 3a). No further increase was observed for longer incubation

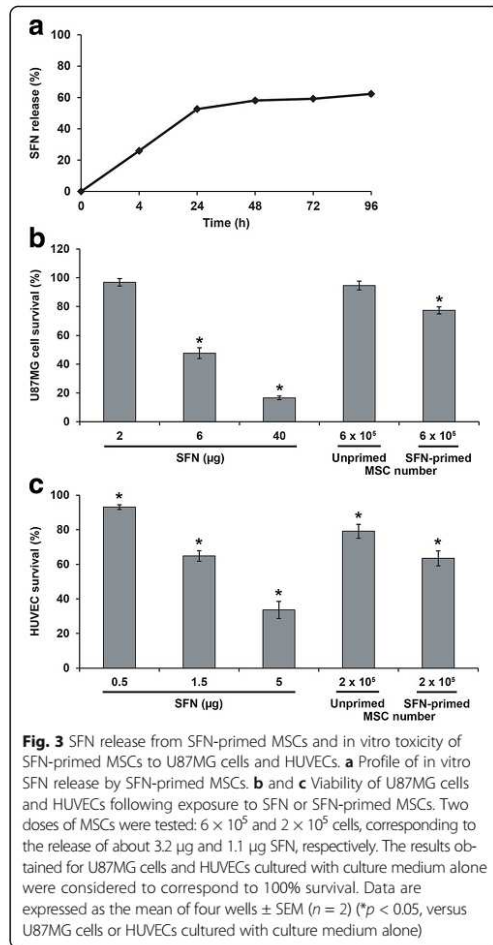


periods. We therefore estimated that about 40% of the SFN was retained by the cells. This result was confirmed in a cytotoxicity assay on U87MG cells and HUVECs (Fig. 3b, c). We found that, after 3 days, 6×10^5 SFN-primed MSCs, corresponding to the release of approximately 3.2 μg SFN, decreased U87MG cell survival by 23%, whereas 6×10^5 unprimed MSCs had no effect on U87MG cell viability (Fig. 3b). This decrease in survival is intermediate between those induced by 2 μg and 6 μg of SFN (Fig. 3b). A similar result was obtained with HUVECs, in which 2×10^5 SFN-primed MSCs,

corresponding to the release of approximately 1.1 μg SFN, decreased cell survival by 37%, a value close to that induced by 1.5 μg SFN (35%) (Fig. 3c).

Analysis of the effects of the intranasal administration of SFN-primed MSCs on U87MG growth and angiogenesis
We first controlled by FISH, the intratumoral distribution of MSCs following intranasal administration in U87MG tumor-bearing mice (D12, tumor volume: $2.9 \pm 0.2 \text{ mm}^3$ estimated by MRI) (n = 8) (Fig. 4a). Three days after intranasal administration of MSCs, we observed MSCs in the





tumor mass and at the border zone between the tumor and the normal parenchyma, consistent with tumor-directed tropism (Fig. 4b). The tumor contained a mean of 157 ± 27 cells/mm² (Fig. 4c). Seven days after intranasal administration, the number of MSCs in the tumor increased to a mean of 403 ± 82 cells/mm² (Fig. 4c). The MSCs were evenly distributed throughout the whole tumor (data not shown). Intranasally administered MSCs were also able to migrate towards smaller U87MG tumors (D6, tumor volume: 1.2 ± 0.1 mm³ estimated by MRI) and this migration was unaffected by priming with SFN (data not shown).

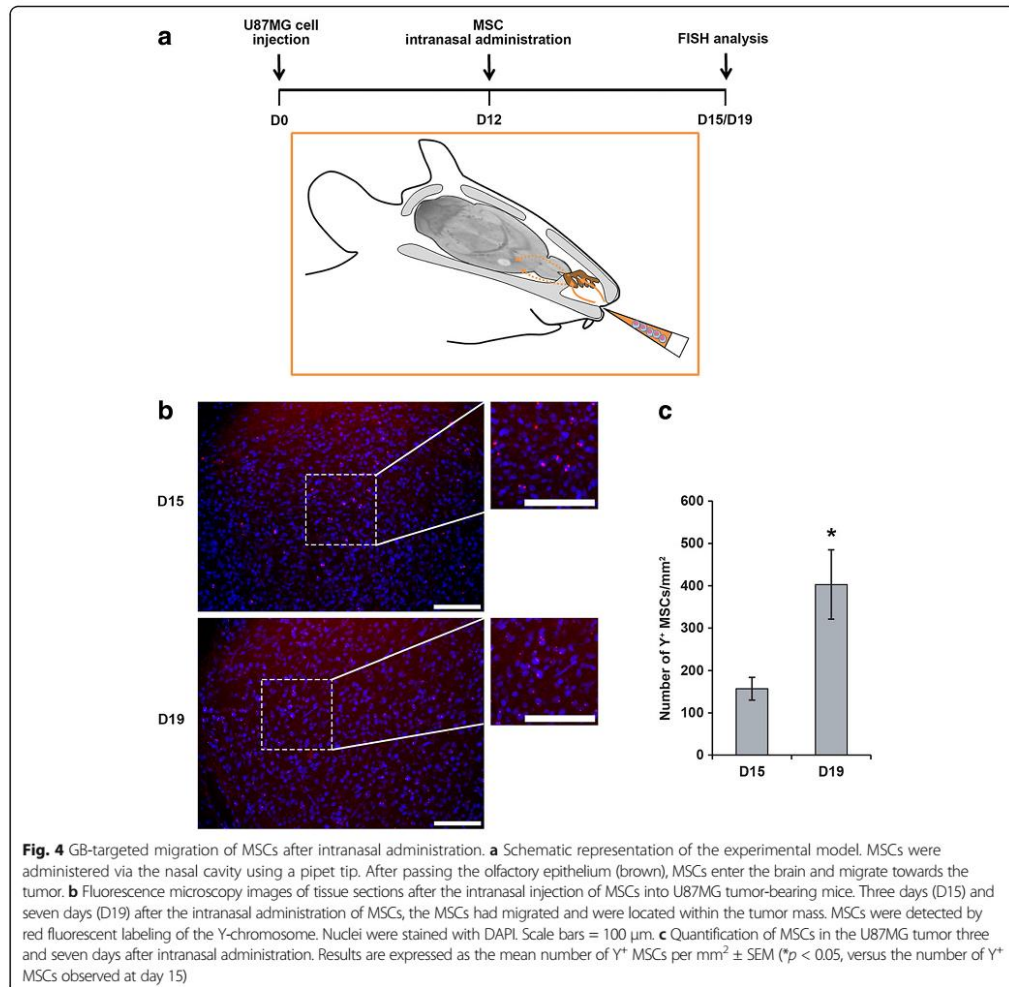
The effect of two intranasal administrations of SFN-primed MSCs was then assessed on U87MG growth and angiogenesis (Fig. 5a). For this purpose, U87MG tumor-

bearing mice were treated on day 6 with SFN, or with unprimed or SFN-primed MSCs, in amounts corresponding to an SFN dose of about 5.3 µg/mouse. This dose caused in vitro U87MG cell and HUVEC mortality rates of close to 40% and 70%, respectively. A control group receiving intranasal administrations of HBSS rather than treatment was also established. This injection protocol was repeated on day 10. Seven days later, we assessed tumor volume, and the numbers of intratumoral Ki67⁺ proliferative cells and CD31⁺ vessels. Intranasal administrations of SFN, or of unprimed or SFN-primed MSCs had no effect on tumor volume (Fig. 5b). There was no significant difference in the number of intratumoral Ki67⁺ cells between control and treated mice (Fig. 5c, d). Nevertheless, mice receiving intranasal administrations of unprimed MSCs had slightly higher levels of angiogenesis: they had significantly more small vessels ($< 100 \mu\text{m}^2$) than mice receiving intranasal administrations of HBSS, SFN or SFN-primed MSCs (Fig. 5c, e). This effect was attenuated by the priming of MSCs with SFN. Furthermore, SFN-primed MSCs induced a significant decrease in the number of large vessels ($> 100 \mu\text{m}^2$) relative to HBSS, SFN and unprimed MSCs (Fig. 5c, e).

Discussion

The best approach to chemotherapy for cancer is to deliver the drug to the tumor microenvironment, to kill tumor cells whilst maintaining the lowest possible level of lethal damage to healthy cells, so as to limit deterioration of the patient's quality of life. Many approaches to achieving this objective have been proposed, including the use of MSCs, which can take up drugs and home to tumors when administered systemically in vivo [41].

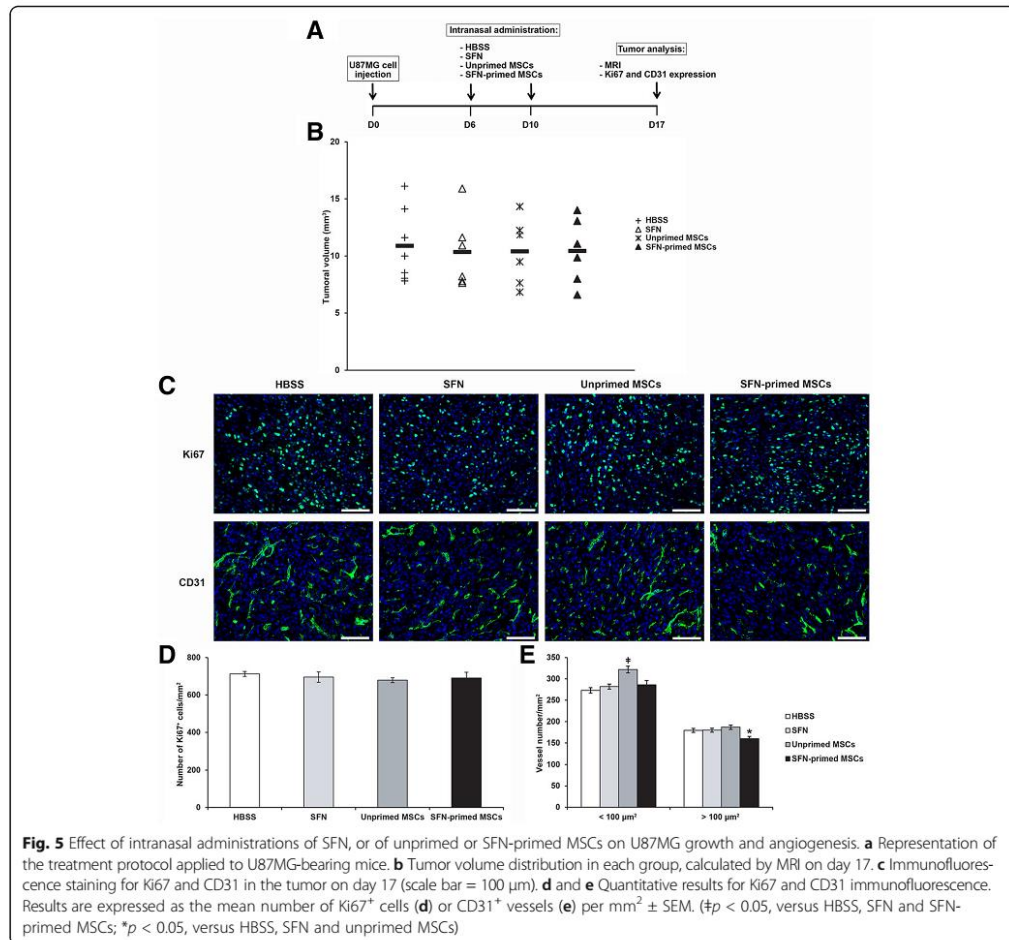
We show here that MSCs can be primed in vitro with SFN, a targeted chemotherapy drug. We showed that a priming concentration of 100 µM SFN caused 40% toxicity in MSCs, whereas a priming concentration of 20 µM was only moderately cytotoxic (about 20%). This concentration was selected to ensure that a sufficient number of MSCs reached the brain tumor after an intranasal delivery. HPLC analysis showed that MSCs primed with 20 µM SFN contained a dose of about 9 pg SFN per cell and were able to release 60% of the drug into the culture medium, in a time-dependent manner. This result is consistent with the findings of Pessina et al. (2011) [34] who estimated that about 25–30% of PTX was retained by PTX-primed MSCs and never released. The cytostatic activity of the released SFN was entirely conserved, resulting in the significant inhibition of U87MG cell and HUVEC proliferation in vitro. The mechanisms by which MSCs excreted SFN did not seem to involve MSC death since 80% of MSCs remained viable seven days after priming with SFN. Further work is required to determine the route by which SFN leaves MSCs, but recent studies have



suggested that MSCs deliver drugs by secreting membrane microvesicles [42, 43].

We investigated the *in vivo* effect of SFN-primed MSCs on the orthotopic U87MG GB model, following their intranasal administration. Intranasal delivery has the advantage over direct intracranial deliver of being noninvasive, making repeated treatment regimens possible. Balyasnikova et al. (2014) [19] showed, with various technical approaches (¹¹¹In-oxine, MRI and bioluminescence imaging), that MSCs could penetrate the brain from the nasal cavity and infiltrate intracranial glioma xenografts in a mouse model. We validated their results with another approach, FISH technique, which can be used for the specific

tracking of male-derived MSCs in female nude mice bearing U87MG tumors, through detection of the Y-chromosome. Three days after the intranasal administration of 6×10^5 MSCs, these cells had accumulated in the U87MG tumor, with a mean of 157 ± 27 cells/mm², and even greater accumulation was observed after seven days. These findings are similar to those of Reitz et al., (2012) [44], who reported a mean accumulation of 54 ± 13 cells/mm² in U87MG tumors five days after the intranasal administration of 3×10^5 neural stem/progenitor cells. The accumulation of MSCs in U87MG was analyzed three days post-MS administration to be sure that a sufficient number of cells could be detected by FISH but part of



MSCs might have reached the tumor as early as 24 h as observed by Balyasnikova et al. (2014) [19]. These same authors analyzed the distribution of MSCs using ¹¹¹In-oxine-labeled MSCs and demonstrated the presence of MSCs in the lung and stomach after intranasal delivery. It is difficult to specify if MSCs accumulate in the brain long-term or if they are cleared out from the brain because the survival time of tumor-bearing animals is short. In our previous study [17], we assessed the fate of MSCs seven days after being injected into intracranial U87MG tumors and compared it to the fate of MSCs injected into the striatum of healthy mice. MSCs did not seem to clear out from the brain. We observed that 20% of MSCs expressed Ki67 proliferation marker in the U87MG environment. In the healthy environment, we found no MSCs

in a proliferative state suggesting that factors produced by the U87MG cells induced MSC proliferation. We observed that MSCs can migrate towards large or small U87MG tumors. This is important in a clinical context because GB is highly invasive with an infiltration that can extend several centimeters deep beyond the radiological limits of the tumor [45]. Furthermore, as previously described for other modified MSCs, the priming of MSCs with SFN did not prevent their migration after intranasal administration [18, 19].

The treatment of U87MG tumor-bearing mice with two intranasal administrations of 6×10^5 SFN-primed MSCs four days apart reduced tumor angiogenesis, resulting in a significant decrease of the number of large vessels. No decrease in angiogenesis was observed

following the intranasal administration of SFN alone, highlighting the potential value of MSCs as a vector for transporting SFN to the intracerebral tumor following administration via this route. We did not observe an effect of SFN-primed MSCs on tumor volume or the proportion of Ki67⁺ cells in the tumor. The absence of this effect is probably due to an insufficient dose of SFN-primed MSCs. Siegelin et al. (2010) [8] observed that a daily treatment of U87MG-bearing mice with SFN (100 mg/kg) by intraperitoneal injections resulted in an inhibition of tumor cell proliferation and reduction of angiogenesis with a prolonged survival of mice. We injected only two doses of SFN-primed MSCs (about 5.3 µg/mouse), a lower dose than was used in the study of Siegelin et al. corresponding to about 2 mg/mouse/day. The dose of SFN carried by MSCs in our study corresponded to an effective dose reducing U87MG cell survival *in vitro*, but was ineffective against U87MG cells *in vivo*. However, it may be sufficient to have affected endothelial cells, which are four times more sensitive to SFN than U87MG cells. The intranasal administration of larger numbers of SFN-primed MSCs may be required for an effect on U87MG growth. However, if we look at global literature data on the use of modified MSCs to treat GB, we notice that the effect of these cells on animal survival is relatively modest, whatever the route of administration and the number of administrations. For example, regarding the intranasal route, Balyanikova et al. (2014) [19] showed that the treatment of irradiated mice bearing intracranial U87-EGFRvIII GB xenografts by four intranasal administrations of 5×10^5 MSCs expressing TNF-related apoptosis inducing ligand at one-week intervals prolonged survival of mice of about ten days compared with irradiated mice treated with control MSCs. Similarly, Mangraviti et al. (2016) [18] observed that the treatment of athymic rats bearing human brain tumor-initiating cells by two intranasal inoculations of 2×10^6 human adipose-derived MSCs (hAMSCs) producing bone morphogenetic protein 4 one week apart induced a 21.4% increase in median survival over that in rats treated with control hAMSCs.

The modest effect of therapeutic MSCs on GB growth inhibition may be due to the pro-tumorigenic and pro-angiogenic properties of these cells. Even if the role of MSCs in cancer progression remains a matter of heated debate, increasing numbers of studies are highlighting these properties [41, 46–48]. In line with these studies, we found that the intranasal administration of unprimed MSCs induced a significant increase of the number of small vessels in the U87MG tumor, which was abolished when MSCs were primed with SFN. Different studies indicate that MSCs promote angiogenesis by secreting angiogenic factors, such as VEGF, releasing exosomes, recruiting endothelial progenitors, and/or transdifferentiating into endothelial cells [49, 50]. The mechanisms

by which SFN inhibited the angiogenic properties of MSCs need to be elucidated. Even though we did not observe an effect of unprimed MSCs on tumor volume or the proportion of Ki67⁺ cells in the U87MG tumor, MSCs are reported to facilitate tumor growth through their secretion of various anti-inflammatory cytokines and proangiogenic factors [41, 46–48]. Furthermore, MSCs can differentiate into cancer-associated fibroblasts (CAFs), which have been described in the stroma of carcinomas and are known to promote tumor growth [46]. In the GB peritumoral environment, we identified MSC-like cells that we named GB-associated stromal cells (GASCs) which have phenotypic and functional properties in common with MSCs and CAFs [51–53]. Like unprimed MSCs, their injection into intracranial U87MG tumors had no effect on tumor volume but promoted angiogenesis with an increase in the number of intratumoral small vessels [52]. Other studies isolated MSC-like cells from GB and these cells were shown to increase angiogenesis, and GB cell proliferation and invasion [54–58]. Consistent with these findings, it has been recently observed that the percentage of GB-associated MSC-like cells is inversely correlated with overall survival, indicating a role for these cells in promoting the aggressive behavior of GB [59, 60]. All these data raise the question if MSCs are interesting candidates as cellular vehicles for the delivery of a therapeutic molecule in a GB context. Even if MSCs have the potential to deliver the therapeutic agent in the tumor, their pro-tumorigenic and pro-angiogenic properties may limit the effect of this agent. We need to find ways of guaranteeing the safety of this cellular vector for clinical use. One possibility would be to use a suicidal gene or a small molecule to induce senescence in the MSCs after drug delivery.

Conclusion

This study demonstrates the capacity of MSCs to carry SFN to GB after their intranasal administration and to decrease angiogenesis. Despite this encouraging result, the anti-angiogenic effect was not enough to affect tumor growth. The pro-tumorigenic and pro-angiogenic properties of MSCs may be responsible for the weakness of the therapeutic effect observed, and the SFN released may not be sufficient to counteract these MSC properties. These findings call into question the suitability of MSCs for use in the cell-based delivery of therapeutic agents for GB treatment.

Abbreviations

FISH: Fluorescence in situ hybridization; GB: Glioblastoma; HUVEC: Human umbilical vein endothelial cell; MRI: Magnetic resonance imaging

Acknowledgements

We thank "la coordination hospitalière des prélèvements d'organes et de tissus" (CHU, Angers, France). We are most grateful to the PRISM core facility and in particular to Dr. F Franconi (Rennes-Angers, France) for her technical

support. We also thank P. Legras and J. Roux (Service commun d'animalerie Hospitalo-Universitaire, Angers, France), Prof. P. Schiller (University of MIAMI, School of Medicine, USA), Dr. L. Lemaire (INSERM U1066, Angers, France), L. Sindji (CRCINA, INSERM U1232, Angers, France), Chloé Appocher and Julie Renaud for providing facilities, and A. Edelman and Associates for correcting the manuscript.

Funding

This research was supported by grants from "Fondation de France", "Ligue contre le Cancer du Grand-Ouest, comité départemental du Maine-et-Loire", "Association en avant la vie" and the European Commission, Education, Audiovisual and Culture Executive Agency (EACEA), through the NanoFar Erasmus Mundus joint Doctoral program.

Authors' contributions

AC and PM developed the idea for the study. AC performed *in vitro* cell experiments and surgical procedures on small animals and wrote the manuscript. MPM, NL and ER performed HPLC and LC-MS/MS analyses. CMM provided human MSCs and contributed in the redaction of the manuscript. All authors read and approved the final manuscript.

Ethics approval and consent to participate

The procedure on animals was approved by the Committee on the Ethics of Animal Experiments of the "Pays de la Loire" (Permit no. 01785.01).

Consent for publication

Not applicable.

Competing interests

The authors declare that they have no competing interests.

Publisher's Note

Springer Nature remains neutral with regard to jurisdictional claims in published maps and institutional affiliations.

Author details

¹Département de Neurochirurgie, CHU, Angers, France. ²CRCINA, INSERM, Université de Nantes, Université d'Angers, Angers, France. ³Division of Drug Delivery and Tissue Engineering, School of Pharmacy, University of Nottingham, Nottingham, UK. ⁴MINT, UNIV Angers, INSERM 1066, CNRS 6021, Université Bretagne Loire, Angers, France.

Received: 20 June 2017 Accepted: 21 September 2017

Published online: 29 September 2017

References

- Stupp R, Mason WP, van den Bent MJ, Weller M, Fisher B, Taphoorn MJB, et al. Radiotherapy plus concomitant and adjuvant temozolomide for glioblastoma. *N Engl J Med*. 2005;352:987–96.
- Stupp R, Hegi ME, Mason WP, van den Bent MJ, Taphoorn MJB, Janzer RC, et al. Effects of radiotherapy with concomitant and adjuvant temozolomide versus radiotherapy alone on survival in glioblastoma in a randomised phase III study: 5-year analysis of the EORTC-NCIC trial. *Lancet Oncol*. 2009;10:459–66.
- Polivka J, Polivka J, Holubec L, Kubikova T, Priban V, Hes O, et al. Advances in Experimental Targeted Therapy and Immunotherapy for Patients with Glioblastoma Multiforme. *Anticancer Res*. 2017;37:21–33.
- Staedtke V, Bai R-Y, Latterra J. Investigational new drugs for brain cancer. *Expert Opin Investig Drugs*. 2016;25:937–56.
- Kang JH, Adamson C. Novel chemotherapeutics and other therapies for treating high-grade glioma. *Expert Opin Investig Drugs*. 2015;24:1361–79.
- Wilhelm S, Carter C, Lynch M, Lowinger T, Dumas J, Smith RA, et al. Discovery and development of sorafenib: a multikinase inhibitor for treating cancer. *Nat Rev Drug Discov*. 2006;5:835–44.
- Carra E, Barbieri F, Marubbi D, Pattarozzi A, Favoni RE, Florio T, et al. Sorafenib selectively depletes human glioblastoma tumor-initiating cells from primary cultures. *Cell Cycle Georget Tex*. 2013;12:491–500.
- Siegelin MD, Raskett CM, Gilbert CA, Ross AH, Altieri DC. Sorafenib exerts anti-glioma activity *in vitro* and *in vivo*. *Neurosci Lett*. 2010;478:165–70.
- Yang F, Brown C, Buettner R, Hedvat M, Starr R, Scuto A, et al. Sorafenib induces growth arrest and apoptosis of human glioblastoma cells through the dephosphorylation of signal transducers and activators of transcription 3. *Mol Cancer Ther*. 2010;9:953–62.
- Peereboom DM, Ahluwalia MS, Ye X, Supko JG, Hilderbrand SL, Phuphanich S, et al. NABTT 0502: a phase II and pharmacokinetic study of erlotinib and sorafenib for patients with progressive or recurrent glioblastoma multiforme. *Neuro-Oncol*. 2013;15:490–6.
- Lee EQ, Kuhn J, Lamborn KR, Abrey L, DeAngelis LM, Lieberman F, et al. Phase III study of sorafenib in combination with temsirolimus for recurrent glioblastoma or gliosarcoma: North American Brain Tumor Consortium study 05-02. *Neuro-Oncol*. 2012;14:1511–8.
- Hottinger AF, Aissa AB, Espeli V, Squiban D, Dunkel N, Vargas MI, et al. Phase I study of sorafenib combined with radiation therapy and temozolomide as first-line treatment of high-grade glioma. *Br J Cancer*. 2014;110:2655–61.
- Den RB, Kamrava M, Sheng Z, Werner-Wasik M, Dougherty E, Marinucci M, et al. A phase I study of the combination of sorafenib with temozolomide and radiation therapy for the treatment of primary and recurrent high-grade gliomas. *Int J Radiat Oncol Biol Phys*. 2013;85:321–8.
- Hassler MR, Ackerl M, Flechl B, Sax C, Wöhrer A, Widhalm G, et al. Sorafenib for patients with pretreated recurrent or progressive high-grade glioma: a retrospective, single-institution study. *Anti-Cancer Drugs*. 2014;25:723–8.
- Zustovich F, Landi L, Lombardi G, Porta C, Galli L, Fontana A, et al. Sorafenib plus daily low-dose temozolomide for relapsed glioblastoma: a phase II study. *Anticancer Res*. 2013;33:3487–94.
- Reardon DA, Vredenburg JJ, Desjardins A, Peters K, Gururangan S, Sampson JH, et al. Effect of CYP3A-inducing anti-epileptics on sorafenib exposure: results of a phase II study of sorafenib plus daily temozolomide in adults with recurrent glioblastoma. *J Neuro-Oncol*. 2011;101:57–66.
- Roger M, Clavreul A, Sindji L, Chassevent A, Schiller PC, Montero-Menei CN, et al. *In vitro* and *in vivo* interactions between glioma and marrow-isolated adult multilineage inducible (MIAMI) cells. *Brain Res*. 2012;1473:193–203.
- Mangraviti A, Tzeng SY, Gullotti D, Kozielski KL, Kim JE, Seng M, et al. Non-virally engineered human adipose mesenchymal stem cells produce BMP4, target brain tumors, and extend survival. *Biomaterials*. 2016;100:53–66.
- Balyasnikova IV, Prasol MS, Ferguson SD, Han Y, Ahmed AU, Gutova M, et al. Intranasal delivery of mesenchymal stem cells significantly extends survival of irradiated mice with experimental brain tumors. *Mol Ther. J. Am. Soc Gene Ther*. 2014;22:140–8.
- Pacioni S, D'Alessandris QG, Giannetti S, Morgante L, Coccè V, Bonomi A, et al. Human mesenchymal stromal cells inhibit tumor growth in orthotopic glioblastoma xenografts. *Stem Cell Res Ther*. 2017;8:53.
- Menon LG, Pratt J, Yang HW, Black PM, Sorensen GA, Carroll RS. Imaging of human mesenchymal stromal cells: homing to human brain tumors. *J Neuro-Oncol*. 2012;107:257–67.
- Binello E, Germano IM. Stem cells as therapeutic vehicles for the treatment of high-grade gliomas. *Neuro-Oncol*. 2012;14:256–65.
- Roger M, Clavreul A, Venier-Julienne M-C, Passirani C, Montero-Menei C, Menei P. The potential of combinations of drug-loaded nanoparticle systems and adult stem cells for glioma therapy. *Biomaterials*. 2011;32:2106–16.
- Bexell D, Svensson A, Bengzon J. Stem cell-based therapy for malignant glioma. *Cancer Treat Rev*. 2013;39:358–65.
- Aleynik A, Gernavage KM, Mourad YS, Sherman LS, Liu K, Gubenko YA, et al. Stem cell delivery of therapies for brain disorders. *Clin Transl Med*. 2014;3:24.
- Bhere D, Shah K. Stem Cell-Based Therapies for Cancer. *Adv Cancer Res*. 2015;127:159–89.
- Namba H, Kawaji H, Yamasaki T. Use of genetically engineered stem cells for glioma therapy. *Oncol Lett*. 2016;11:9–15.
- Zhang X-B, Beard BC, Trobridge GD, Wood BL, Sale GE, Sud R, et al. High incidence of leukemia in large animals after stem cell gene therapy with a HOXB4-expressing retroviral vector. *J Clin Invest*. 2008;118:1502–10.
- Roger M, Clavreul A, Huynh NT, Passirani C, Schiller P, Vessières A, et al. Ferrociphenol lipid nanocapsule delivery by mesenchymal stromal cells in brain tumor therapy. *Int J Pharm*. 2012;423:63–8.
- Li L, Guan Y, Liu H, Hao N, Liu T, Meng X, et al. Silica nanorattle-doxorubicin-anchored mesenchymal stem cells for tumor-tropic therapy. *ACS Nano*. 2011;5:7462–70.
- Clavreul A, Montagu A, Lainé A-L, Tétaud C, Lautram N, Franconi F, et al. Targeting and treatment of glioblastomas with human mesenchymal stem cells carrying ferrociphenol lipid nanocapsules. *Int J Nanomedicine*. 2015;10:1259–71.
- Pacioni S, D'Alessandris QG, Giannetti S, Morgante L, De Pascalis I, Coccè V, et al. Mesenchymal stromal cells loaded with paclitaxel induce cytotoxic damage in glioblastoma brain xenografts. *Stem Cell Res Ther*. 2015;6:194.

33. Zhang X, Yao S, Liu C, Jiang Y. Tumor tropic delivery of doxorubicin-polymer conjugates using mesenchymal stem cells for glioma therapy. *Biomaterials*. 2015;39:269–81.
34. Pessina A, Bonomi A, Coccè V, Invernici G, Navone S, Cavicchini L, et al. Mesenchymal stromal cells primed with paclitaxel provide a new approach for cancer therapy. *PLoS One*. 2011;6:e28321.
35. Fischer UM, Harting MT, Jimenez F, Monzon-Posadas WO, Xue H, Savitz SI, et al. Pulmonary passage is a major obstacle for intravenous stem cell delivery: the pulmonary first-pass effect. *Stem Cells Dev*. 2009;18:683–92.
36. Ramot Y, Steiner M, Morad V, Leibovitch S, Amoyal N, Cesta MF, et al. Pulmonary thrombosis in the mouse following intravenous administration of quantum dot-labeled mesenchymal cells. *Nanotoxicology*. 2010;4:98–105.
37. Danielyan L, Schäfer R, von Arnim-Mayerhofer A, Buaize M, Geisler J, Klopfer T, et al. Intranasal delivery of cells to the brain. *Eur J Cell Biol*. 2009;88:315–24.
38. Danielyan L, Beer-Hammer S, Stolzing A, Schäfer R, Siegel G, Fabian C, et al. Intranasal delivery of bone marrow-derived mesenchymal stem cells, macrophages, and microglia to the brain in mouse models of Alzheimer's and Parkinson's disease. *Cell Transplant*. 2014;23(Suppl 1):S123–39.
39. van Velthoven CTJ, Kavelaars A, van Bel F, Heijnen CJ. Nasal administration of stem cells: a promising novel route to treat neonatal ischemic brain damage. *Pediatr Res*. 2010;68:419–22.
40. D'Ippolito G, Diabira S, Howard GA, Menei P, Roos BA, Schiller PC. Marrow-isolated adult multilineage inducible (MIAMI) cells, a unique population of postnatal young and old human cells with extensive expansion and differentiation potential. *J Cell Sci*. 2004;117:2971–81.
41. Sherman LS, Shaker M, Mariotti V, Rameshwar P. Mesenchymal stromal/stem cells in drug therapy: New perspective. *Cytotherapy*. 2017;19:19–27.
42. Pascucci L, Coccè V, Bonomi A, Ami D, Ceccarelli P, Ciusani E, et al. Paclitaxel is incorporated by mesenchymal stromal cells and released in exosomes that inhibit in vitro tumor growth: a new approach for drug delivery. *J Control Release*. 2014;192:262–70.
43. Del Fattore A, Luciano R, Saracino R, Battafarano G, Rizzo C, Pascucci L, et al. Differential effects of extracellular vesicles secreted by mesenchymal stem cells from different sources on glioblastoma cells. *Expert Opin Biol Ther*. 2015;15:495–504.
44. Reitz M, Demestre M, Sedlák J, Meissner H, Fiebler J, Kim SU, et al. Intranasal delivery of neural stem/progenitor cells: a noninvasive passage to target intracerebral glioma. *Stem Cells Transl Med*. 2012;1:866–73.
45. Lemée J-M, Clavreul A, Menei P. Intratumoral heterogeneity in glioblastoma: don't forget the peritumoral brain zone. *Neuro-Oncol*. 2015;17:1322–32.
46. Ridge SM, Sullivan FJ, Glynn SA. Mesenchymal stem cells: key players in cancer progression. *Mol Cancer*. 2017;16:31.
47. Zhang C, Yang S-J, Wen Q, Zhong JF, Chen X-L, Stucky A, et al. Human-derived normal mesenchymal stem/stromal cells in anticancer therapies. *J Cancer*. 2017;8:85–96.
48. Shi Y, Du L, Lin L, Wang Y. Tumour-associated mesenchymal stem/stromal cells: emerging therapeutic targets. *Nat Rev Drug Discov*. 2017;16:35–52.
49. Bronckaers A, Hilkens P, Martens W, Gervois P, Ratajczak J, Struys T, et al. Mesenchymal stem/stromal cells as a pharmacological and therapeutic approach to accelerate angiogenesis. *Pharmacol Ther*. 2014;143:181–96.
50. Merino-González C, Zuñiga FA, Escudero C, Ormazabal V, Reyes C, Nova-Lamperti E, et al. Mesenchymal Stem Cell-Derived Extracellular Vesicles Promote Angiogenesis: Potential Clinical Application. *Front Physiol*. 2016;7:24.
51. Clavreul A, Etcheverry A, Chassevent A, Quillien V, Avril T, Jourdan M-L, et al. Isolation of a new cell population in the glioblastoma microenvironment. *J Neuro-Oncol*. 2012;106:493–504.
52. Clavreul A, Guette C, Faguer R, Tétaud C, Boissard A, Lemaire L, et al. Glioblastoma-associated stromal cells (GASCs) from histologically normal surgical margins have a myofibroblast phenotype and angiogenic properties. *J Pathol*. 2014;233:74–88.
53. Clavreul A, Etcheverry A, Tétaud C, Rousseau A, Avril T, Henry C, et al. Identification of two glioblastoma-associated stromal cell subtypes with different carcinogenic properties in histologically normal surgical margins. *J Neuro-Oncol*. 2015;122:1–10.
54. Appaix F, Nissou M-F, van der Sanden B, Dreyfus M, Berger F, Issartel J-P, et al. Brain mesenchymal stem cells: The other stem cells of the brain? *World J Stem Cells*. 2014;6:134–43.
55. Kong BH, Shin H-D, Kim S-H, Mok H-S, Shim J-K, Lee J-H, et al. Increased in vivo angiogenic effect of glioma stromal mesenchymal stem-like cells on glioma cancer stem cells from patients with glioblastoma. *Int J Oncol*. 2013;42:1754–62.
56. Lim E-J, Suh Y, Yoo K-C, Lee J-H, Kim I-G, Kim M-J, et al. Tumor-associated mesenchymal stem-like cells provide extracellular signaling cue for invasiveness of glioblastoma cells. *Oncotarget*. 2017;8:1438–48.
57. Hossain A, Gumin J, Gao F, Figueroa J, Shinjima N, Takezaki T, et al. Mesenchymal Stem Cells Isolated From Human Gliomas Increase Proliferation and Maintain Stemness of Glioma Stem Cells Through the IL-6/gp130/STAT3 Pathway. *Stem Cells Dayt Ohio*. 2015;33:2400–15.
58. Svensson A, Ramos-Moreno T, Eberstål S, Scheding S, Bengzon J. Identification of two distinct mesenchymal stromal cell populations in human malignant glioma. *J Neuro-Oncol*. 2017;131:245–54.
59. Shahar T, Rozovski U, Hess KR, Hossain A, Gumin J, Gao F, et al. Percentage of mesenchymal stem cells in high-grade glioma tumor samples correlates with patient survival. *Neuro-Oncol*. 2017;19:660–68.
60. Yoon S-J, Shim J-K, Chang JH, Moon JH, Roh T-H, Sung KS, et al. Tumor Mesenchymal Stem-Like Cell as a Prognostic Marker in Primary Glioblastoma. *Stem Cells Int*. 2016;2016:6756983.

Submit your next manuscript to BioMed Central and we will help you at every step:

- We accept pre-submission inquiries
- Our selector tool helps you to find the most relevant journal
- We provide round the clock customer support
- Convenient online submission
- Thorough peer review
- Inclusion in PubMed and all major indexing services
- Maximum visibility for your research

Submit your manuscript at
www.biomedcentral.com/submit



Annex 3: Curriculum Vitae

Milad Pourbaghi Masouleh

Room A0, Boots Science Building, University Park, Nottingham, NG7 2RD, UK

Mobile: +44 7397 123576

Email: milad.pourbaghimasouleh@nottingham.ac.uk

Google Scholar: <https://scholar.google.co.uk/citations?user=yUnAya0AAAAJ&hl=en>

EDUCATION:

- **University of Nottingham (UK) / University of Angers (France)** Oct 2014-Sep 2018
Ph.D. in Pharmacy/Experimental and Clinical Pharmacology
Thesis: *"Mesenchymal stem cells as cellular vehicles for delivery of drug-loaded nanoparticles to brain tumors via nasal route"*; Supervisors: Dr. Snow Stolnik, Dr. Cynthia Bosquillon (University of Nottingham), Prof. Philippe Menei, Dr. Anne Clavreul (University of Angers)
- **Materials and Energy Research Center (Iran)** Sep 2011-Feb 2014
M.Sc. in Materials Science and Engineering
Thesis: *"Calcium phosphate/polyethylene glycol hybrid nanoparticles for delivery of gentamicin"*; Supervisors: Dr. Saeed Hesaraki, Dr. Ali Zamanian
- **University of Tabriz (Iran)** Sep 2006- Aug 2011
B.Sc. in Materials Science and Engineering
Thesis: *"Optimization of sol-gel technique for coating of hydroxyapatite on metallic substrates using the Taguchi method"*; Supervisor: Dr. Hamed Asgharzadeh

RESEARCH BACKGROUND:

• Drug Delivery:

Skilled in drug delivery nanosystem formulations, more specifically, chemotherapeutic agents:

- Preparation and characterization of **nanosystems for formulating therapeutic agents** (Publication no. 1, 2, 5, 6, 7 and 8)
- Interaction between drug delivery nanosystems and **cellular barriers, intracellular trafficking** of nanoparticles and investigating the integrity of these carriers utilizing **FRET effect** (no. 3)
- **Cellular delivery** of chemotherapeutics, applying **human mesenchymal stromal cells** and tracking the **exosomes** for further analysis of therapeutic cargo delivery, **vehiculating drug loaded nanosystems** using human mesenchymal stromal cells (no. 4)

• Cell-Biomaterial Interaction:

Skilled in design and fabrication of biomaterials for regenerative medicine, more specifically in bone and cartilage tissue engineering:

- **Surface modification and topography analyses** of biomaterials for **controlling the fate of mesenchymal stem cells**, engineering **bioactive surfaces** with instructive properties that were formerly reserved for growth factor to induce mesenchymal stem cells proliferation or osteogenic differentiation (no. 9)
- **Cellular responses** to physical and chemical characteristics of **ion-eluting biomaterials** with different surface topographies (no. 10 and 11)
- Design and fabrication of scaffolds with **unidirectionally aligned pore channels** which incorporate specific **structural and mechanical cues** for **bone cell mechanotransduction** (publication no. 12)
- **Surface modification** of metallic substrates by applying **biocompatible coating** and analyzing the resulted **topography** by **image processing** and various analytical techniques to optimize the preparation procedure (no. 13)
- **Toxicity of nanomaterials** based on their physical and chemical characteristics (no. 6 and 7)

RESEARCH EXPERIENCE:

- **Research Assistant** Oct 2014-
Boots Science Building, University of Nottingham (UK)
Dr. Snow Stolnik
- **Research Assistant** Jun 2017-
The Regional Center for Research in Cancerology and Immunology Nantes/Angers (France)
Prof. Philippe Menei, Prof. Emmanuel Garcion

- **Research Assistant** *Oct 2014-Jun 2017*
INSERM, L'unité Micro et Nanomédecines Biomimétiques (MINT), University of Angers (France)
Prof. Philippe Menei, Prof. Jean-Pierre Benoit
- **Research Internship** *Dec 2013-Sep 2014*
HIV and Drug Demand Reduction Unit, United Nation Office of Drug and Crime (Iran)
Dr. Gelareh Mostashari
- **Research Assistant** *Dec 2011-Sep 2013*
Biomaterials Laboratory, Materials and Energy Research Center (Iran)
Dr. Saeed Hesaraki
- **Research Assistant** *Aug 2010-Aug 2011*
Laboratory of Ceramic Processing, University of Tabriz (Iran)
Dr. Hamed Asgharzadeh

SKILLS and ABILITIES:

- **Cell biology:**
Skilled: 2D and 3D cell culture methods, flow cytometric analyses, FRET analyses, immunostaining, confocal microscopy, various cell and molecular biology techniques, cellular barriers,
- **Formulation:**
Skilled: Drug delivery systems, drug carrier design, theranostics, intracellular trafficking, nanoparticle tracking, drug related kinetics, dosage, solubility studies, separation techniques, surface modification of carriers, nanoemulsions, colloidal nanosystems
- **Materials Science:**
Skilled: Preparation and characterization of biomaterials, scaffolds, nanoparticles, colloidal systems, coating, mechanical tests, surface modification, biodegradation, drug loading
- **Analytical Techniques:**
Skilled: Uv-Vis, fluorescence spectroscopy, FTIR, XRD, DSC, TGA, AFM, SEM, HPLC, LC-MS/MS, DLS
Experienced: Rheometer, TEM, BET
- **Computer Skills:**
Skilled: MS Office, GraphPad, Empower, ChemOffice, Photoshop
Experienced: AutoCAD, MATLAB, Expert Highscore, Muse, HTML/CSS
- **Language skills:**
Excellent oral and written communication skills in English, French and Persian

PUBLICATIONS:

- **Drug Delivery:**
 1. A. Clavreul, M. Pourbaghi-Masouleh, P. Menei, **Targeting angiogenesis in glioblastoma with non-viral delivery systems: Where are we?** (going to be submitted)
 2. A. Clavreul, E. Roger, M. Pourbaghi Masouleh, L. Lemaire, C. Tétaud, and P. Menei. **Development and characterization of sorafenib-loaded lipid nanocapsules for the treatment of glioblastoma** (submitted to Drug Delivery)
 3. M. P. Masouleh, C. Conte, C. Bosquillon, P. Menei, S. Stolnik. **Lipid nanocapsules transport across Calu-3 based model of nasal epithelial barrier** (going to be submitted).
 4. A. Clavreul, M. Pourbaghi-Masouleh, E. Roger, N. Lautram, C.N. Montero-Menei, P. Menei, **Human mesenchymal stromal cells as cellular drug-delivery vectors for glioblastoma therapy: A good deal?**, J. Exp. Clin. Cancer Res. 36 (2017).
 5. M. P. Masouleh, V. Hosseini, M. Pourhaghgouy, M. K. Bakht. **Calcium Phosphate Nanoparticles Cytocompatibility versus Cytotoxicity: a Serendipitous Paradox**. Current Pharmaceutical Designe, 2017, doi: 10.2174/1570163814666170321115007 (In press).
 6. M. Pourbaghi-Masouleh, V. Hosseini. **Amorphous calcium phosphate nanoparticles could function as a novel cancer therapeutic agent by employing a suitable targeted drug delivery platform**. Nanoscale research letters 8 (1), 2013, 1-6.
 7. M. Pourbaghi-Masouleh, S. Hesaraki, A. Zamanian, A. Khanlarkhani. **Gentamicin PEGylated poor crystalline carbonated hydroxyapatite submicron particles**. Materials Letters 113, 2013, 130-133.
 8. M. K. Bakht, M. Sadeghi, M. Pourbaghi-Masouleh, C. Tenreiro. **Scope of nanotechnology-based radiation therapy and thermotherapy methods in cancer treatment**. Current cancer drug targets 12 (8), 2012, 998-1015.

• Cell-Biomaterials Interaction:

9. S. Hesaraki, H. Nazarian, M. Pourbaghi-Masouleh, S. Borhan. **Comparative study of mesenchymal stem cells osteogenic differentiation on low-temperature biomineralized nanocrystalline carbonated hydroxyapatite and sintered hydroxyapatite.** Journal of Biomedical Materials Research Part B: Applied Biomaterials 102, 2014, 108-118.
10. S. Hesaraki, M. Alizadeh, S. Borhan, M. Pourbaghi-Masouleh. **Polymerizable nanoparticulate silica-reinforced calcium phosphate bone cement.** Journal of Biomedical Materials Research Part B: Applied Biomaterials 100, 2012, 1627-1635.
11. A. Pouria, H. Bandegani, M. Pourbaghi-Masouleh, S. Hesaraki, M. Alizadeh. **Physicochemical properties and cellular responses of strontium-doped gypsum biomaterials.** Bioinorganic chemistry and applications, 2012, 2012.
12. M. Pourhaghgouy, A. Zamanian, M. Shahrezaee, M. P. Masouleh. **Physicochemical properties and bioactivity of freeze-cast chitosan nanocomposite scaffolds reinforced with bioactive glass.** Materials Science and Engineering: C 58, 2016, 180-186.
13. M. Pourbaghi-Masouleh, H. Asgharzadeh. **Optimization of sol-gel technique for coating of metallic substrates by hydroxyapatite using the Taguchi method.** Materials Science-Poland 31 (3), 2013, 424-433.

(Citations: 125 / h-index: 6)

PRESENTATIONS:

1. M. P. Masouleh, A. Clavreul, E. Roger, C. Bosquillon, S. Stolnik, P. Menei. **Mesenchymal stem cells as cellular vehicles for delivery of drug-loaded nanoparticles to brain tumors via the nasal route.** Nanofar autumn school, The Université catholique de Louvain, Brussels, Belgium, 2014. (Oral)
2. M. P. Masouleh, A. Clavreul, E. Roger, P. Menei. **Which types of anti-cancer molecules mesenchymal stem cells can carry to brain tumors?** Nanofar autumn school, Université de Nantes, Nantes, France, 2015. (Poster)
3. M. P. Masouleh, A. Clavreul, E. Roger, P. Menei. **Which types of anti-cancer molecules mesenchymal stem cells can carry to brain tumors?** Les écoles doctorales (ED) et le Collège doctoral Nantes Atlantique, Université de Nantes, Nantes, France, 2015. (Oral and Poster)
4. M. P. Masouleh, C. Bosquillon, S. Stolnik. **Lipid nanocapsules transport across Calu-3 cell in vitro model of epithelium.** Nanofar spring school, University of Nottingham, Nottingham, UK, 2017. (Poster)
5. M. P. Masouleh, C. Conte, C. Bosquillon, S. Stolnik. **Lipid Nanocapsule Transport Across Epithelial Barrier: a Förster Resonance Energy Transfer Based Study,** Innovation for Health, Rotterdam, NL, 2018. (Oral and Poster)

AWARDS:

- Erasmus Mundus Scholarship

Sep 2014

Erasmus Mundus Joint Doctorates (EMJD) - NanoFar

Titre : D veloppement de nanocapsules lipidiques pour le traitement anti-angiog nique du glioblastome et  valuation de leur potentiel pour la d livrance de m dicaments au cerveau par voie intranasale

Mots cl s : Glioblastome; Syst mes de d livrance; Anti-angiog nique; Nanocapsule lipidique; Intranasal; Barri re  pith liale; FRET; Nanom decine

R sum  : Le glioblastome (GB), tumeur primitive du cerveau, la plus agressive, et la plus fr quente chez l'adulte, pr sente une prolif ration vasculaire importante. Des agents th rapeutiques innovants ciblant   la fois l'angiog nese et les cellules tumorales sont recherch s, ainsi que des syst mes pour augmenter leur d livrance dans la tumeur c r brale. Un de ces agents est le soraf nib (SFN), un inhibiteur de tyrosine kinase. Sa mauvaise solubilit  aqueuse et ses effets secondaires ind sirables limitent son utilisation. Le premier objectif de cette th se  tait d'encapsuler cet agent dans des nanocapsules lipidiques (NCL) pour contrer ces inconv nients. Nous avons d velopp  des NCL avec une haute efficacit  d'encapsulation du SFN qui inhibaient in vitro l'angiog nese et la viabilit  de la lign e de GB humain U87MG. La d livrance intratumorale de SFN-NCL

chez des souris porteuses d'une tumeur intrac r brale U87MG induit une normalisation vasculaire tumorale pr coce qui pourrait am liorer l'efficacit  de la chimioth rapie et de la radioth rapie. Le second objectif  tait de d finir si la d livrance intranasale de NCL pouvait constituer une voie non-invasive alternative. Nous avons  tudi  via le transfert d' nergie par r sonance de type F rster, le devenir des NCL charg es d'un fluorochrome   travers des monocouches de cellules Calu-3, un mod le de l' pith lium nasal. L'utilisation de NCL augmente le passage du fluorochrome   travers les cellules Calu-3, mais les particules sont rapidement d grad es apr s leur capture. Ces donn es mettent en  vidence que les NCL sont appropri es pour la d livrance locale du SFN mais doivent  tre modifi es pour une d livrance intranasale.

Title : Development of lipid nanocapsules for antiangiogenic treatment of glioblastoma and evaluation of their potential for nose-to-brain drug delivery

Keywords : Glioblastoma; Delivery systems; Anti-angiogenic; Lipid nanocapsules; Intranasal; Epithelial barrier; FRET; Nanomedicine

Abstract : Glioblastoma (GB), the most aggressive, and the most frequent primary tumor of the brain in adults, present a prominent vascular proliferation. Innovative therapeutic agents targeting both angiogenesis and tumor cells are urgently required, along with competent systems for their delivery to the brain tumor. One such agent is sorafenib (SFN), a tyrosine kinase inhibitor. However, poor aqueous solubility and undesirable side effects limit its clinical application. The first objective of this thesis was to encapsulate this drug inside lipid nanocapsules (LNCs) to overcome these drawbacks. We developed LNCs with a high SFN encapsulation efficiency (> 90%) that inhibited in vitro angiogenesis and the viability of the human U87MG GB cell line. Intratumoral delivery of SFN-LNCs in mice bearing

intracerebral U87MG tumors induced early tumor vascular normalization which could be used to improve the efficacy of chemotherapy and radiotherapy in the treatment of GB. The second objective was to define whether intranasal delivery of LNCs could be an alternative non-invasive route. In this regard, we investigated through F rster resonance energy transfer, the fate of dye-loaded LNCs across Calu-3 cell monolayers, a model of the nasal mucosa. We showed that employment of LNCs dramatically increased the delivery of the dye across Calu-3 cell monolayer but they were rapidly degraded after their uptake. These data highlight that LNCs are suitable nanocarriers for the local delivery of SFN but must be redesigned for enhancing their nose-to-brain delivery.